LEHIGH UNIVERSITY.

Final Report

August 1st, 2008 to June 30th, 2012

Agreement No. N00014-08-1-0188

Project Title: Integrated Life-Cycle Framework for Maintenance, Monitoring, and Reliability of Naval Ship Structures

Submitted to
Dr. Paul E. Hess III
Program Officer, Code 331, ONR Ship Systems and Engineering Division,
Office of Naval Research, 875 N. Randolph St., Arlington, VA 22203
Phone: 703-696-9776 Fax: 703-696-0001 E-mail: hessp@onr.navy.mil

Submitted by
Dr. Dan M. Frangopol
Profcssor and Fazlur R. Khan Endowed Chair of Structural Engineering and Architecture,
Department of Civil and Environmental Engineering,
Center for Advanced Technology for Large Structural Systems (ATLSS Center),
Lehigh University, 117 ATLSS Drive, Imbt Labs, Bethlehem, PA 18015-4729
Phone: 610-758-6103 Fax: 610-758-4115 Email: dan.frangopol@lehigh.edu

August 15th, 2012

Table of Contents

1. Abstract

The proper life-cycle management of naval ship structures under uncertainty is best conducted through an integrated and well-coordinated life-cycle framework. This framework can support the rational decision making process and help the planning for future inspection, monitoring, and/or maintenance actions. Additionally, the framework should be capable of modeling the continuous performance deterioration of naval ship structures that occurs due to aging effects as well as different environmental and mechanical stressors. Accordingly, this research project, sponsored by the U.S. Office of Naval Research, was conducted at Lehigh University to build a framework for the probabilistic analysis of ship structures in terms of reliability, redundancy, fatigue, material deterioration, damage detection, monitoring, and inspection optimization.

The work on this project began on August, 1st, 2008 with an intensive literature review and study of the topics related to the performance assessment and monitoring of ship structures. Topics related to ultimate bending strength and fatigue have been covered in this review-study process. Next, the acquired concepts have been investigated, put at work, and new developments have been accomplished. Research work has been performed on four fronts:

1- Bending ultimate strength reliability and monitoring
2- Fatigue reliability and monitoring
3- Cost-effective monitoring planning under uncertainty
4- Optimization of monitoring and inspection strategies.

This report describes the work accomplished by the PI (Dan M. Frangopol) and his co-workers (Nader Okasha, Graduate Research Assistant (Ph.D 2010); Kihyon Kwon, Graduate Research Assistant (Ph.D 2011); Sunyong Kim, Graduate Research Assistant (Ph.D 2011); Alberto Deco, Graduate Research Assistant; Benjin Zhu, Graduate Research Assistant; Duygu Saydam, Graduate Research Assistant; Mohamed Soliman, Graduate Research Assistant; Andre Orcesi, Visiting Research Associate; Paolo Bocchini, Postdoctoral Research Associate; Hao Tian, Visiting Research Scholar) during the period August 1st, 2008 – June, 30th , 2012.

2. Introduction

The objective of this research is the development of an integrated life-cycle framework for maintenance, monitoring and reliability of naval ship structures. The steps of the envisioned framework are described in Fig. 1. In this framework, tools for structural performance assessment and prediction, structural health monitoring (SHM), integration of new information (from SHM and/ or inspection), and optimization of strategies (maintenance, monitoring, … etc.) are required. It is clear that the process begins with the assessment and future prediction of the structural performance. In fact, life-cycle performance assessment is the backbone of the framework. Uncertainty is an integral component in all aspects of this (or any) life-cycle management framework (Frangopol and Okasha 2008). A rational probabilistic methodology is of vital importance for properly treating these uncertainties.

The modeling, assessment, and performance prediction of ship structures over time is by its very nature complex and uncertain. Uncertainty in modeling of structures and randomness in

loading phenomena dictate the use of probabilistic methods in life-cycle analysis. Because models that treat this issue are very sensitive to changes in their input parameters, structural health monitoring (SHM) provides a powerful and needed mechanism to reduce uncertainty, to calibrate, and to improve structural assessment and performance prediction models. Ultimately, optimal decisions are to be made that ensure the continuous safety of structural systems with minimum expected total life-cycle cost. Only a proper integrated probabilistic framework would yield such optimum decisions.

The implementation of the framework described above to ship structures is supported with highly motivating reasons. Randomness in load effects imposed on ship structures in rough seas and highly uncertain complex structural behavior are examples of these motivating reasons. This framework is expected to significantly reduce the risks associated with ship structural performance and reduce the costs required to achieve and maintain an adequate reliability level of ship structures over their service lives.

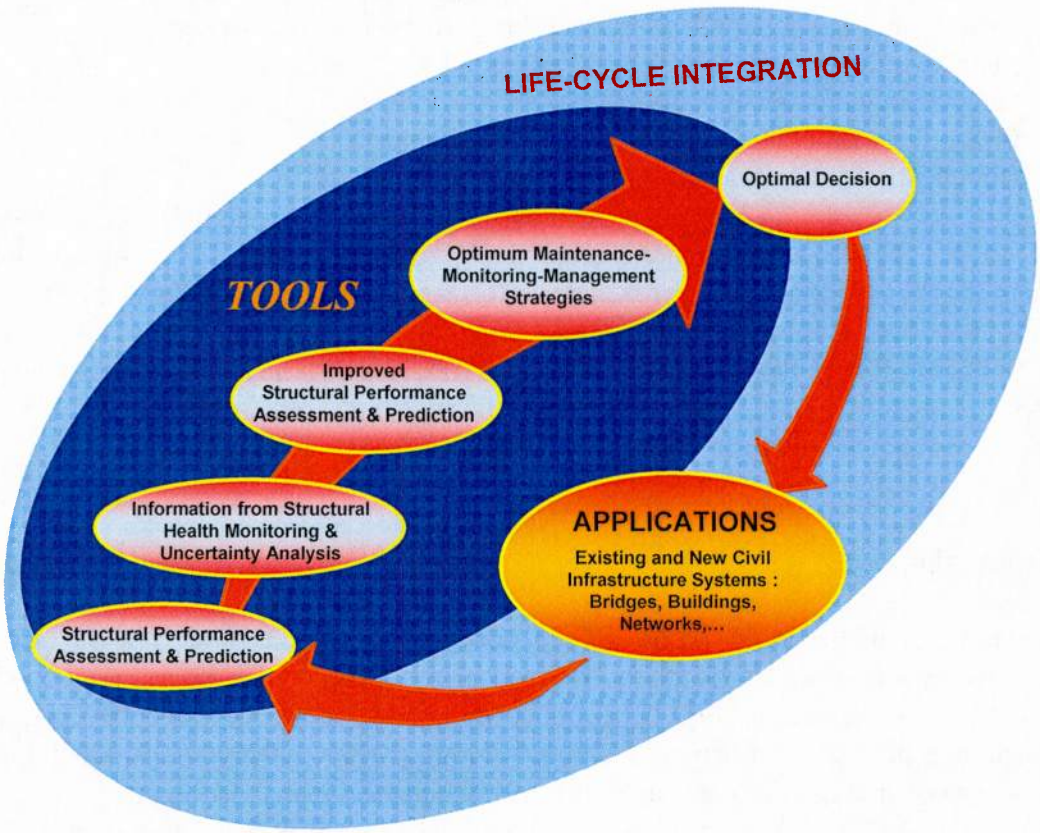

Figure 1. Schematic sketch of a life-cycle integrated management framework

3. Bending ultimate strength reliability and monitoring

A review of the available ship hull ultimate strength analysis methods showed a trade off among these methods in accuracy and computational cost. Since the probabilistic aspects are captured by means of simulation, which require the calculation of the strength a large number of times, a fast and accurate method for analyzing the ship hull is required. In order to obtain this required computational speed and accuracy, a novel deterministic method for the calculation of the ultimate strength of the ship hull is developed. This method is fundamentally based on the original incremental curvature method (Smith 1977). In this method, the ship hull cross section is discretized into elements, each composed of a longitudinal stiffener and its attached plate. Stresses in the hull section are determined using the constitutive models of these elements as found in IACS (2008). The constitutive models take into account the various possible failure modes of stiffened panels. Initial imperfections are also taken into account (Özgüc *et al.* 2006).

For a given curvature, the bending moment of the section is determined in a way similar to that of the rigorous incremental curvature method. However, instead of finding the ultimate strength by incrementing the curvature, the ultimate strength is found by an optimization search algorithm. The curvature is treated as a design variable and the objective is to find the curvature that maximizes the bending moment. The method is shown to be as accurate as the rigorous incremental method but with significantly less computational time. The method is then applied with a Latin hypercube sampling simulation. The output sample is tested against several potential distributions. The parameters of these distributions are found by the maximum likelihood estimate method. Goodness-of-fit tests are performed to determine the best fit distribution. Eventually, the best fit probability distribution of the ultimate strength of the ship hull is provided.

The loading effects that have been considered so far are the still water and wave induced bending moments, and their equations have been found from the IACS (2008). Appropriate corrosion wastage models have been identified and adopted from the literature (Wang et al. 2008, Akpan et al. 2002). These tools have enabled the calculation of the time-variant reliability of ships with respect to the ultimate strength. However, structural redundancy, a subject that attracted a good deal of research in the area of bridges, has been found to the best of our knowledge to be lacking research for ship structures. The treatment of redundancy requires calculation of first failure reliability as well. It was found that the most efficient method to use for the calculation of the first failure flexure strength of ships is Hughes' method (1983). He developed a simple progressive collapse method for the calculation of the ultimate strength of ships based on the assumption that after each stiffened panel fails it has no strength and it sheds its entire loads onto the other stiffened panels. This assumption has no bearing on the calculation of the first failure load since the failure of the first panel is the terminating point in such calculation. The capability of calculating the first failure strength by closed-form solution is the reason for choosing this method, which significantly expedites the simulation process for the reliability calculations.

A program has been developed in MATLAB and linked to other programs to perform the above calculations. The time-variant ultimate reliability of a case study has been conducted and the results are shown in Fig. 2 for the hogging case. Subroutines for the time-variant first failure

reliability and redundancy are included. The program also has the ability to incorporate a set of data provided by a monitoring system.

Developing a procedure for updating the time-variant reliability and redundancy using structural health monitoring is accomplished. It is recognized that numerous monitoring systems for ships exist or have been implemented. Even though the general concepts of the framework are applicable to potentially any monitoring system, the fine details of the procedure will depend on the case study provided. Given that structural reliability is computed based on the resistance of the structure under a given load effect, the first step in this procedure is concerned with the impact of SHM on the structural response aspect. In essence, the simultaneous readings of the strain measured at the provided locations can be used to determine the strain distribution over the cross section and then converted to bending moments using nonlinear constitutive material relationships. Variance of measured bending moment can be found from correlation studies of the different sensor readings. This procedure will enable real-time updating of the structural reliability. In addition, using appropriate statistical analysis, such as statistics of extremes, updating of the reliability for long term prediction is studied.

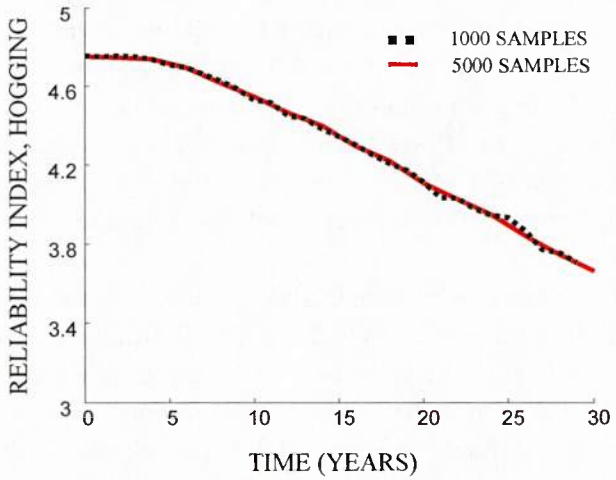

Figure 2. Reliability of the ship hull with respect to ultimate hogging bending moment.

4. Fatigue reliability and monitoring

At present, lifetime assessment and management for naval ship structures is an extremely important issue. Under consideration of potential deterioration mechanisms, fatigue is one of common deterioration processes of vessels. In recent years, a variety of structural health monitoring (SHM) methodologies have been proposed and developed to collect more reliable information for structural performance estimates and reliability prediction for fatigue. However, efficient applications of SHM for assessing time-variant structural reliability are still in their infancy. In addition, finding the most appropriate fatigue detail associated with the defined

category in the SN-Curve Specifications is still an essential challenge. Clearly, integration of SHM concepts and technologies into structural performance assessment and management will assist the preservation of long-term structural performance with optimal maintenance-management actions in a cost-effective manner. For this purpose, this part of the research aims to develop a procedure for fatigue reliability assessment and performance prediction of ship structures that integrates a real-time monitoring system for optimal management of ships and comprises the following tasks: (a) investigation of fatigue detail and potential ship loads for fatigue; (b) time-variant fatigue reliability assessment based on SHM on the component and system levels; and (c) reliability-based life-cycle optimal management of naval ship structures based on SHM.

The potential applications of reliability assessment and performance prediction by using monitoring were first investigated. Based on literature surveys, necessary information was collected in both terms: fatigue resistance (capacity) detail for establishing SN-curve and load effect (demand) during ship operation including low frequency wave-induced, high frequency dynamic (slamming, whipping, springing), and/or still-water loading (Fain and Booth 1979, Munse et al. 1984).

To demonstrate the developed concepts, actual stress history of Sea-Land Mclean (SL-7) was used. The monitoring recorded the complete load history including wave-induced and dynamic stresses in mid-ships, during a five-year period under service on Atlantic and Pacific. Actual monitoring data were converted into the relationship between number of cycles and stress range with average wave period of 7.5 second and interval of 0.5 ksi. Several probability density functions (PDFs) were used to capture uncertainty of ship loading (see Fig. 3(a)). As shown in Fig. 3(b), lifetime fatigue assessment and prediction on the component level were conducted using the following steps: (a) investigating fatigue details of structural members; (b) developing PDFs in loading; (c) estimating mean and standard deviation of equivalent stress range; (d) determining average daily number of cycles and ship operation rate per year; (e) predicting annual cumulative number of cycles; and (f) evaluating fatigue reliability.

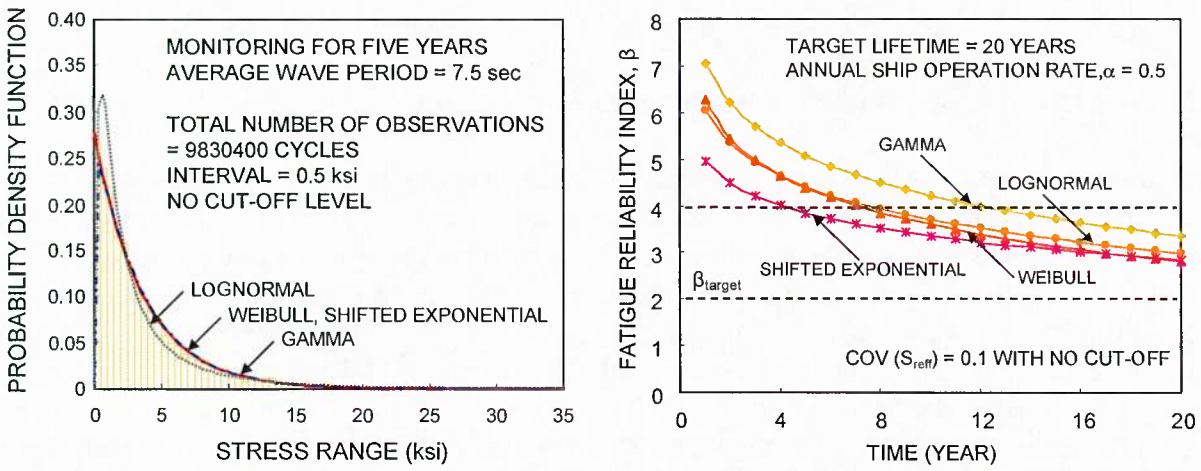

(a) Probability density functions (PDFs) (b) Fatigue reliability

Figure 3. Fatigue reliability assessment and prediction associated with different PDFs

The partial safety factors (PSFs) which contain strength reduction and load amplification factors, were computed to provide a more conservative design SN-curve, especially, to new ship structures where experience is limited (see Fig. 4).

This part of the research is associated with fatigue reliability assessment and performance prediction on the component level based on monitoring. Efficient updating strategies regarding fatigue details of steel or aluminum and potential ship loading conditions can be considered to predict fatigue lifetime more effectively. Consequently, time-variant reliability assessment and prediction can be carried out on the system level as well. The following information is needed to pursue the goals of this research: (a) information on respective structural details (e.g., dimensions, SN categories, geometries); (b) available loading information collected from monitoring (e.g., long-term monitoring data, sensor locations); and (c) necessary requirements of naval ship structures (e.g., expected ship lifetime, target performance level, typical repair options).

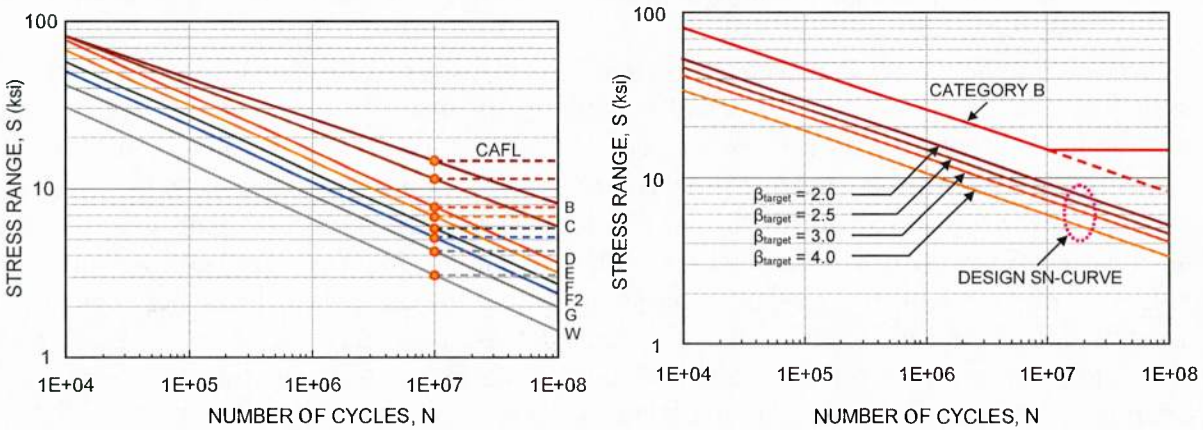

(a) SN-Curve based on BS 5400 (b) Design SN-Curve based on PSFs and β_{target}

Figure 4. SN-Curve of steel ship structures

5. Cost-effective monitoring planning under uncertainty

In order to ensure the structural reliability and extend the service life of deteriorating ship structures, significant efforts related to establishing cost-effective maintenance strategies have to be made. These efforts enable management programs to maintain the required reliabilities and extend the service life of ship structures. The service life can be defined as the expected time period until the structural performance will reach a predefined threshold. Considering uncertainties related to the quantities associated with the structural deterioration, the service life can be predicted as shown in Fig. 5.

Although much effort has been made to assess and predict the structural performance under uncertainty, the reliability assessment using monitoring data has been studied only recently. The application of structural health monitoring (SHM) can have a great potential in cost-effective

maintenance by reduction of uncertainty (Frangopol and Messervey 2007, 2009a, b). The general formulation of the expected life-cycle cost is (Frangopol *et al.* 1997):

$$C_{ET} = C_T + C_{PM} + C_{INS} + C_{REP} + C_F \tag{1}$$

where C_T = initial cost, C_{PM} = the expected cost of routine maintenance, C_{INS} = the expected cost of inspection, C_{REP} = the expected cost of repair, and C_F = the expected cost of failure. If SHM is applied, the expected total cost will be (Frangopol and Messervey 2007)

$$C_{ET,M} = C_T^* + C_{PM}^* + C_{INS}^* + C_{REP}^* + C_F^* + C_M \tag{2}$$

where the superscript * indicates costs in Eq.(1) affected by monitoring, and C_M = expected monitoring cost. The benefit of SHM, B_{MON}, can be captured through a comparison of the expected life-cycle total cost with and without monitoring by subtracting Eq.(1) from Eq.(2). Unless code-driven and using cost as the criterion, monitoring would only be justified if $B_{MON} > 0$, meaning that monitoring is cost-effective.

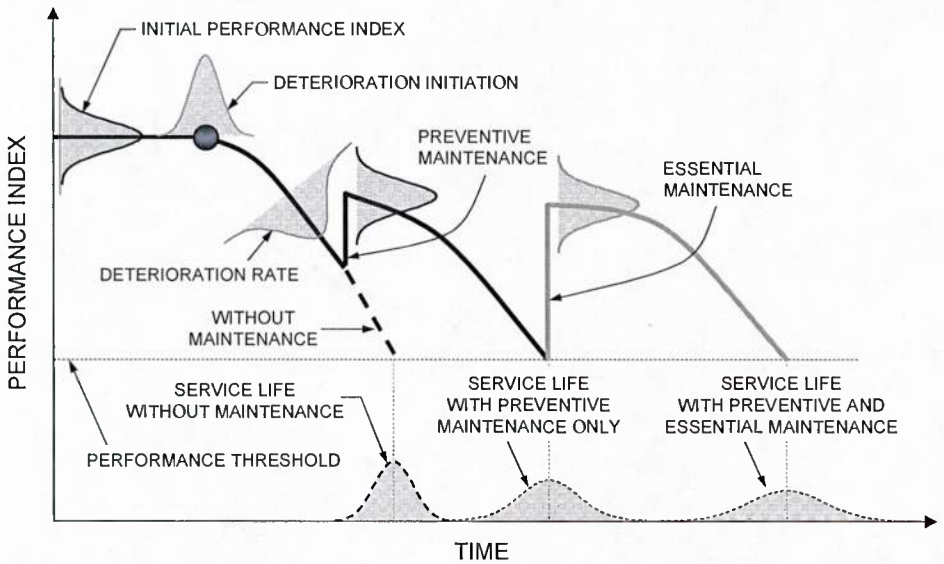

Figure 5. Service life under uncertainty

In order to justify the use of SHM cost-effectively, a bi-objective optimization problem with two conflicting criteria has been formulated and solved. These objectives aim to find an optimum balance between the monitoring costs and the availability of monitoring data for prediction. The availability of monitoring data for prediction can be defined as the probability that the monitoring data can be usable in the future to predict the structural performance. The availability of monitoring data is formulated using a regression function based on the data (Kim and Frangopol, 2009). The expected average availability $E(\overline{A})$ during the period of t days can be derived as:

$$E(\bar{A}) = \frac{t_m}{t}\left[1 - exp\left(-\frac{t}{t_m}\right)\right] \tag{3}$$

If the monitoring cost is proportional to monitoring duration t_m, the total monitoring cost C_{mon} can be determined using the reference monitoring cost C_o during t_o days

$$C_{mon} = \left(\frac{t_m}{t_o} \cdot C_o\right) \cdot \sum_{i=1}^{n}\left(\frac{1}{(1+r_d)^{(i-1)(t+t_m)}}\right) \tag{4}$$

where r_d = daily discount rate of money; and n = total number of monitoring periods over a prescribed investigated time period (in days).

The two conflicting objectives are defined as maximization of the expected average availability defined in Eq. (3) and minimization of the total monitoring cost in Eq. (4). The design variables are monitoring duration t_m and prediction duration t.

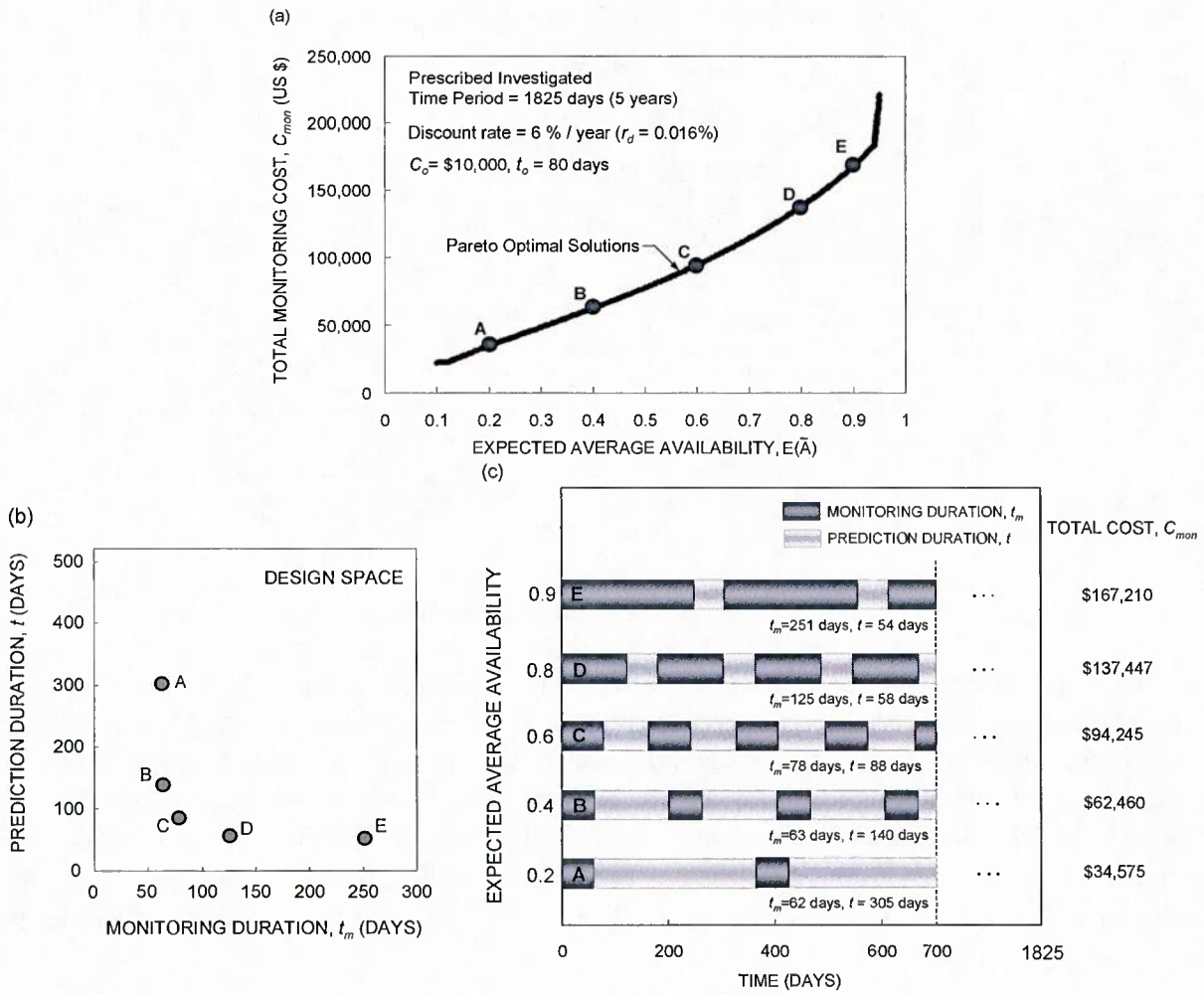

Figure 6. Optimum monitoring plans and required monitoring costs

The proposed approach is illustrated as follows. The two design variables considered, t and t_m, are assumed between 50 days and 500 days, and the prescribed investigated time period is assumed as 1,825 days (*i.e.,* 5 years). It is also assumed that monitoring cost is \$10,000 during 80 days (*i.e.*, C_o = \$10,000 and t_o = 80 days). Through the genetic algorithm with 100 generations, 1,000 Pareto solutions are obtained as shown in Fig. 6a, considering the daily discount rate of money r_d = 0.016 %. The design variables (*i.e.*, monitoring duration t_m and prediction duration t) of five representative solutions A, B, C, D, and E indicated in Fig. 6a are shown in Fig. 6b. Figure 6c shows the associated monitoring schedules and required monitoring costs for each of the five representative solutions. For solution A, the required monitoring duration and prediction duration are t_m = 62 days and t = 305 days, respectively, and the associated monitoring cost during the prescribed investigated time period of 1,825 days is \$34,575 (see Fig. 6c). If $E(\overline{A})$ has to be 0.6 (*i.e.*, solution C), the monitoring duration and prediction duration have to be 78 days and 88 days, respectively, and the expected total monitoring cost has to be \$94,245 (see Fig. 6c). The optimum monitoring planning resulting from the proposed approach, such as in solutions A through E, can be used as an initial monitoring strategy.

6. Optimization of monitoring and inspection strategies

Lifetime functions have been successfully employed in life-cycle performance evaluation of structures (Yang et al. 2004, 2006a,b). The impact of monitoring or inspecting the structure is modeled by an updating of the PDF of time to failure through a Bayesian process. Conditioning on past safe performance affects the future failure probability knowing that the structure survived during the monitoring period. Moreover, the longer the structure is monitored, the more accurate the information is and therefore the more effective the updating is. Visual inspections are subject to greater uncertainties than monitoring. Therefore, the provided information is less accurate and the updating of the PDF of time to failure is less effective. An optimization procedure is used to establish incentive for an efficient monitoring and/or inspection planning. Inspection/monitoring and expected failure costs are minimized simultaneously.

The main objective of structural management systems is to spend the minimum possible amount of financial resources while keeping the structures safe and serviceable. Therefore, the objective of the optimization is to find optimal times and locations for monitoring, and optimal times for inspections when monitoring is not justified. Indeed, some components of the structure might need to be monitored very often and others might only need to be inspected at some times. There are three possible options available for the structural evaluation; namely, to do inspections only, monitoring only, or both. When considering these three strategies individually, the optimal solution can be searched by minimizing both the cumulative owner costs including the evaluation strategy costs (inspection and/or monitoring costs); and minimizing the cumulative expected failure costs at the end of service life. This approach can provide the long term optimum inspection/monitoring schedule for a structure knowing only the survivor function of its components. It is then possible to consider the benefit of monitoring.

An approach for the inspection and monitoring planning for fatigue sensitive details is proposed in this research project. This approach uses the linear elastic fracture mechanics to predict the time dependent crack growth. Next, it finds the optimum inspection and monitoring times which minimizes the damage detection delay simultaneously with minimizing the total inspection and monitoring cost. From the safety point of view, damage detection with less delay will lead to more effective repair actions. However, reducing the delay in the damage detection requires the increase in the number of inspections and/or the inspection qualities. When monitoring is used for damage detection and evaluation, decreasing the damage detection delay would require a corresponding increase in the monitoring duration and/or the number of monitoring actions. This increase in the number or qualities of those actions would require additional financial resources. Therefore, the well-balanced inspection and monitoring scheduling is best performed as a bi-criterion optimization problem with the goals of minimizing both the damage detection delay and the inspection and monitoring cost.

Inputs of the optimization problem include the damage evolution model parameters, inspection and monitoring costs, and qualities of available inspection methods. The output of such optimization problem is in the form of a Pareto-optimal solution set in which each point in the set represents a feasible management plan. Each plan gives the optimum inspection times, inspection quality, monitoring times, and monitoring duration. The solution of such problem considered all the available combinations for a selected combined number of inspection and monitoring actions. Each combination is considered as an individual optimization problem and the final Pareto solution set is obtained by integrating the solutions of all possible combinations. For example, selecting a total number of monitoring and inspections of two will result in four possible combinations, in which two inspections, inspection then monitoring, monitoring then inspection, and two monitoring actions can be performed. These cases are referred to as Case I, Case II, Case III, and Case IV, respectively. The four possible cases along with schematics for the resulting Pareto optimal solution sets are shown in Fig.7

Applying this optimization scheme to the joint between the longitudinal stiffener and the bottom plate of the hull structure results in the Pareto optimal set presented in Fig. 8. Figure 9 shows the combined management plans resulting from the optimization problem in which the design variables (i.e., inspection times, inspection qualities, monitoring times, and monitoring durations) and the corresponding objective function values (i.e., life-cycle cost and expected damage detection delay) are given for selected solutions.

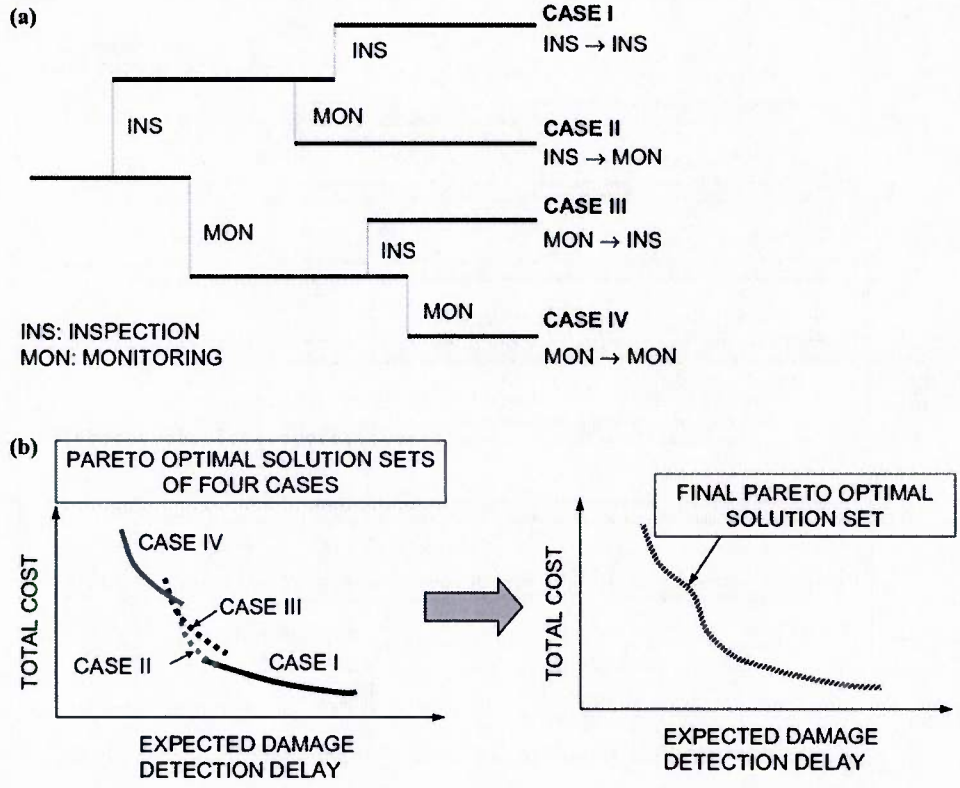

Figure 7. (a) Four possible cases for number of inspections and/or monitorings N = 2; (b) Pareto optimal solution sets associated with the four possible cases, and final Pareto solution set for N = 2.

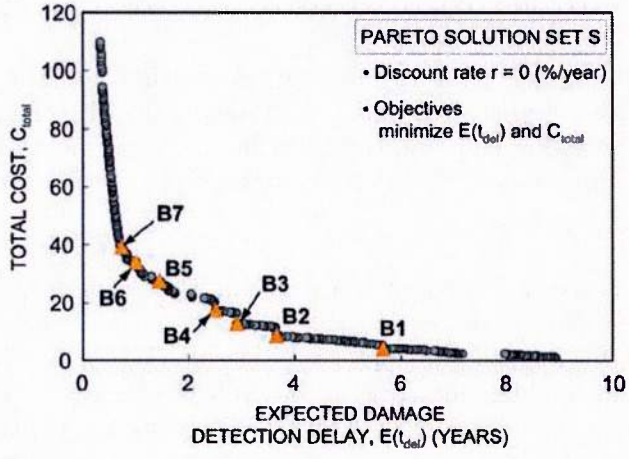

Figure 8. (a) Combined Pareto optimal solution for number of inspections and/or monitorings N = 1, 2, 3, 4, and 5;

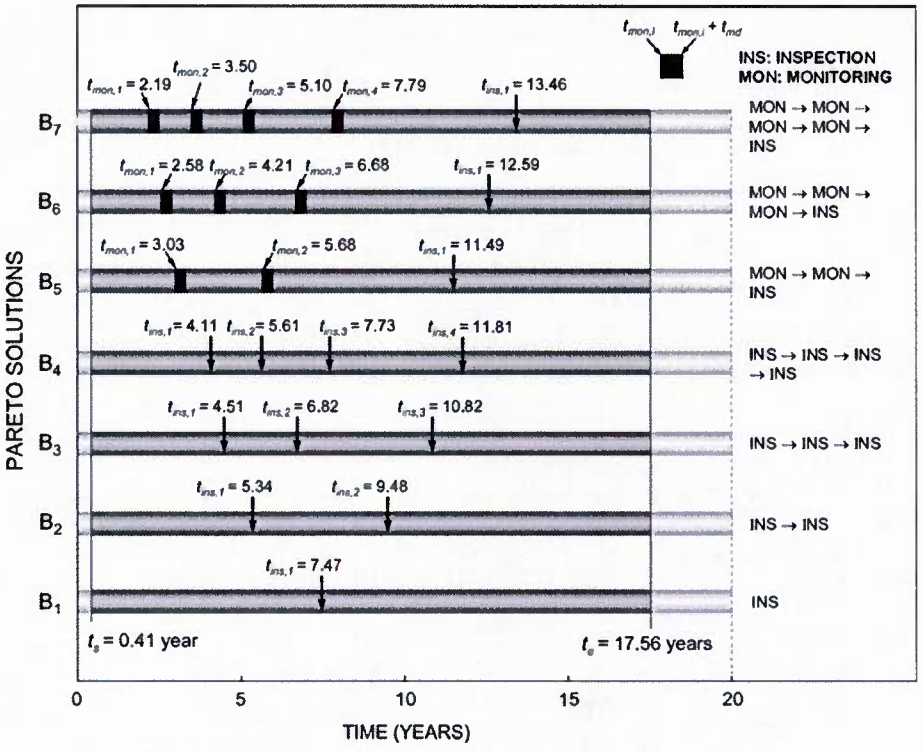

Figure 9. Combined inspection/monitoring plans for solutions $B_1 - B_7$ in Fig.8

Along the research period, several results have been obtained and published in peer-reviewed journals [1-8]. The following sections present a brief summary of these journal papers [1-8] as well as papers presented at the *American Society of Naval Engineers Fleet Maintenance & Modernization Symposium* (FMMS 2011) [8] and the *Eleventh International Conference on Fast Sea Transportation* (FAST 2011) [9].

Efficient method based on optimization and simulation for the probabilistic strength computation of the ship hull (Nader M. Okasha and Dan M. Frangopol. (2010). "Efficient method based on optimization and simulation for the probabilistic strength computation of the ship hull," *Journal of Ship Research,* SNAME). For the full paper see Appendix 1. The abstract is provided below.

The accurate computation of the strength of a ship hull is vital for ensuring its reliability. Taking into account the uncertainties in the material properties and fabrication details requires a probabilistic approach for the determination of the strength of the ship hull. This study proposes an efficient approach for the determination of the probabilistic strength of the ship hull. First, a novel deterministic method for the fast and accurate calculation of the strength of the ship hull is presented. In this method, stresses in the hull section are determined using the constitutive models of the stiffened panels. These models take into account the various possible failure modes and initial imperfections. The ultimate strength is found by an optimization search algorithm. The method is shown to be as accurate as the rigorous incremental curvature method but with significantly less computational time. The method is then applied with a Latin-hypercube sampling simulation, and the output sample is tested against several potential

distributions. The best-fit probability distribution of the ultimate strength of the ship hull is provided.

Time variant redundancy of ship structures (Alberto Decò and Dan M. Frangopol. (2011). "Time variant redundancy of ship structures," *Journal of Ship Research*, SNAME). For the full paper see Appendix II. The abstract is provided below.

An efficient procedure for the computation of the redundancy of ship structures is presented. The changes in the redundancy due to corrosion section loss over time are also studied. Moreover, uncertainties associated with structural geometry, material properties, and loading, are accounted for. In order to calculate the redundancy index, the probability of failure of the first component and the probability of ultimate failure of the whole hull girder must be evaluated. The probability of failure is computed using a hybrid Latin Hypercube - second-order reliability method (SORM) technique. The deterministic analyses during the simulations are conducted using an optimization approach for computing the ultimate bending strength of the whole hull girder and the progressive collapse method for computing the first bending failure.

Integration of structural health monitoring in life-cycle performance assessment of ship structures under uncertainty (Nader M. Okasha, Dan M. Frangopol, and Alberto Decò. (2010). "Integration of structural health monitoring in life-cycle performance assessment of ship structures under uncertainty," *Marine Structures*, Elsevier). For the full paper see Appendix III. The abstract is provided below.

In this paper, an approach for integrating the data obtained from structural health monitoring (SHM) in the life-cycle performance assessment of ship structures under uncertainty is presented. Life-cycle performance of the ship structure is quantified in terms of the reliability with respect to first and ultimate failures and the system redundancy. The performance assessment of the structure is enhanced by incorporating prior design code-based knowledge and information obtained by SHM using Bayesian updating concepts. Advanced modeling techniques are used for the hull strength computations needed for the life-cycle performance analysis. SHM data obtained by testing a scaled model of a Joint High-speed Sealift Ship is used to update its life-cycle performance.

Reliability analysis and damage detection in high speed naval crafts based on structural health monitoring data (by Okasha, N., Frangopol, D.M., Saydam, D., and Salvino, L.W. (2011). "Reliability analysis and damage detection in high speed naval crafts based on structural health monitoring data," *Structural Health Monitoring,* Sage Publication). For the full paper see Appendix IV. The abstract is provided below.

Current and future trends in naval craft design are leaning towards the development of high-speed and high-performance vessels. Lack of information on wave induced loads for these vessels presents a challenge in ensuring their safety that is best tackled with monitoring operational loads and detecting damage via structural health monitoring systems. These monitoring systems, however, require efficient statistical and probabilistic procedures that are able to effectively treat the uncertainties inherent in the massive volumes of collected data and

provide interpretable information regarding the reliability and condition of the craft structure. In this paper, an approach for using Structural Health Monitoring (SHM) data in the reliability analysis and damage detection in high speed naval crafts (HSNCs) under uncertainty is presented. This statistical damage detection technique makes use of vector autoregressive modeling for detection and localization of damage in the ship structure. The methodology is illustrated on an HSNC, HSV-2. Data obtained from seakeeping trials of HSV-2 were treated as the SHM data mentioned above.

Fatigue performance assessment and lifetime prediction of high-speed ship structures based on probabilistic lifetime sea loads (Kwon, K., Frangopol, D.M., and Kim, S. (2010). "Fatigue performance assessment and lifetime prediction of high-speed ship structures based on probabilistic lifetime sea loads," *Structure and Infrastructure Engineering*, Taylor & Francis (in press)). For the full paper see Appendix V. The abstract is provided below.

This paper focuses on estimating probabilistic lifetime sea loads for high-speed ship structures with the aim of assessing their fatigue performance and predicting lifetime from available data. Lifetime performance assessment and prediction for naval ship structures are extremely important issues. In particular, understanding the effect of sea loading on naval high-speed vessels is still a challenge. Potential lifetime load effects including low frequency wave-induced and high frequency slam-induced whipping loadings are investigated in this paper, and lifetime sea loads are estimated by using a probabilistic approach. Clearly, integration of probabilistic sea loads into structural reliability assessment and lifetime prediction will provide a more reliable estimation of the long-term structural performance. Accordingly, this study presents an approach for fatigue reliability evaluation of ship structures based on the estimated lifetime sea loads. Loading information associated with sea states, ship speeds, and relative wave headings are obtained from a Joint High-speed Sealift Ship monohull structural seakeeping trials, while the S-N curves are established based on British Standards.

Optimum inspection planning for minimizing fatigue damage detection delay of ship hull structures (Sunyong Kim and Dan M. Frangopol. (2011). "Optimum inspection planning for minimizing fatigue damage detection delay of ship hull structures," *International Journal of Fatigue*, Elsevier, 33(3):448–459). For the full paper see Appendix VI. The abstract is provided below.

Fatigue is one of the main factors which can produce cracks, and lead to failure of ships. For these structures, damage occurrence and propagation due to fatigue are affected by the action of sea water waves and the sea environment as well as operation, fabrication, and modeling of ship structures under uncertainties. In order to efficiently maintain the safety of ship structures, an optimum inspection plan should be made by considering these uncertainties using a probabilistic approach. In this paper, such an approach is presented and applied to ship hull structures subjected to fatigue. The resulting inspection plan is the solution of an optimization problem based on the minimization of expected fatigue damage detection delay. Damage detection delay will produce the maintenance delay which, in turn, is likely to endanger the serviceability and even the survival of the structure. The formulation of the expected damage detection delay includes uncertainties associated with damage occurrence, propagation,

and detection. The effects of the quality and number of inspections on the optimum inspection planning are investigated. A well-balanced inspection planning is considered as a solution of an optimization problem with two conflicting criteria. This well-balanced inspection planning provides optimum inspection types and times. Furthermore, the cost-effective inspection plans are designed to provide the optimum strategy either by considering a single type or multiple types of inspections.

Probabilistic bicriterion optimum inspection/monitoring planning: Application to naval ships and bridges under fatigue (Sunyong Kim and Dan M. Frangopol. (2012). "Probabilistic bicriterion optimum inspection/monitoring planning: Application to naval ships and bridges under fatigue," *Structure and Infrastructure Engineering*, Taylor & Francis). For the full paper see Appendix VII. The abstract is provided below.

Initiation and propagation of fatigue cracks in steel structures induced by repetitive actions are highly random due to both aleatory and epistemic uncertainties related to material properties, loads, damage, modeling and other factors. For this reason, a probabilistic approach is necessary to predict the fatigue crack growth damage. This study presents a probabilistic approach for combined inspection/monitoring planning for fatigue-sensitive structures considering uncertainties associated with fatigue crack initiation, propagation and damage detection. This combined inspection/monitoring planning is the solution of an optimization formulation, where the objective is minimizing the expected damage detection delay. Furthermore, this formulation is extended to a bicriterion optimization considering the conflicting relation between expected damage detection delay and cost. A set of Pareto solutions is obtained by solving this bicriterion optimisation problem. From this set, a solution can be selected balancing in an optimum manner inspection and monitoring times, quality of inspections, monitoring duration, and number of inspections and monitorings. The proposed approach is applied to a naval ship and a bridge subjected to fatigue.

Integrated life-cycle framework for maintenance, monitoring, and reliability of naval ship structures (Frangopol, D.M., Bocchini, P., Decò, A., Kim, S., Kwon, K., Okasha, N.M., and Saydam, D. (2012). "Integrated life-cycle framework for maintenance, monitoring, and reliability of naval ship structures," *Naval Engineering journal,* Wiley). For the full paper see Appendix VIII. The abstract is provided below.

In the field of Naval Engineering, the use of life-cycle analyses associated with the concept of aging and time-dependent reliability has gained momentum lately. In this regard, the U.S. Office of Naval Research supports a project at Lehigh University focused on the development of an integrated life-cycle framework for ship reliability assessment, redundancy estimation, damage detection, and optimum inspection planning.

This paper presents some of the results obtained at Lehigh University within this project, with emphasis on structural health monitoring and life-cycle analysis under uncertainty.

Life-cycle ship reliability assessment, damage detection, and optimization (Frangopol, D.M., Bocchini, P., Decò, A., Kim, S., Kwon, K., Okasha, N.M., Saydam, D., and Salvino L.W. (2011). "Life-cycle ship reliability assessment, damage detection, and optimization," *Proceedings of the*

Eleventh International Conference on Fast Sea Transportation (FAST 2011), Honolulu, Hawaii, USA, September 26-29 (in press)). For the full paper see Appendix IX. The abstract is provided below.

This paper collects a body of scientific results obtained at Lehigh University, under the sponsorship of the U.S. Office of Naval Research. The aim of the entire research project was to build a general framework for the probabilistic analysis of ship structures in terms of reliability, redundancy, fatigue, material deterioration, damage detection, monitoring, and inspection optimization. Several articles published in international peer-reviewed journals by the first author and his co-workers address the previously mentioned sub-topics. This paper provides an overview of the results, presents the integrated approach that is being developed, and suggests future lines of research.

7. Conclusions

This research project aims to develop an integrated life-cycle framework for maintenance, monitoring and reliability of naval ship structures. The work has begun on August, 1st, 2008. Since then, and through an intensive review and study of the literature, members of the research team have accomplished the necessary understanding of ship structural performance and analysis.

In reference to the envisioned framework described in Fig. 1, the important tools in this framework have been established. Means for effective evaluation of ship life-cycle ultimate and fatigue performance under uncertainty have been developed and program codes were formulated. In addition, methodologies to optimize the scheduling and cost effectiveness of inspection and monitoring have been proposed.

A new optimization-based technique for computing the probabilistic hull strength has been proposed (see Appendix I). The proposed approach treats the moment curvature relationship as a non-linear implicit function to be optimized. Any given curvature is associated with a corresponding flexural capacity that is evaluated by applying the method recommended by IACS. Hence, the value of the curvature, that maximizes its associated bending moment, is found by applying an optimization search algorithm. Indeed, among a large number of discrete values of curvature, in few steps, the flexural capacity is evaluated in order to determine which of such discrete values provides the maximum bending moment. The clear difference is that instead of obtaining a complete moment-curvature curve, only few values are evaluated and the procedure ends when the maximum moment is found. This approach was able to reduce the computational time and to provide results that are as accurate as the ones of the incremental curvature method. This approach was further implemented to evaluate the time dependent redundancy of naval vessels (see Appendix II).

A rational computational platform for inclusion of monitoring and inspection information in the framework has been investigated, by which the predicted performance is updated. Case studies that help generate and test this methodology were analyzed (see Appendices III and IV). Specifically, what is needed are the main characteristics and particulars including geometry,

dimensions of plates and stiffeners, frame spacings at midship, material elasticity and yield strengths, and fatigue details at the sensor locations in addition to tabulated sensor readings for the given ship case study.

It is recognized that numerous monitoring systems for ships exist or have been implemented. Event though the general concepts of the framework should be applicable to potentially any monitoring system, the fine details of the procedure will depend on the case study provided. Given that structural reliability is quantified based on the resistance of the structure and its response to a given load effect, the first step in this process is concerned with the impact of SHM on the structural response aspect. In essence, the simultaneous readings of the strain measured at the provided locations can be converted to bending moments using nonlinear constitutive material relationships. Variance of measured bending moment can be found from correlation studies of the different sensor readings. The procedure enables real-time updating of the structural reliability.

An approach for fatigue reliability assessment and lifetime prediction of high-speed ship structures based on the probabilistic lifetime sea loads estimated from model test data was proposed (see Appendix V). The *S-N* approach to the identified structural details was used to estimate structural capacity in the fatigue reliability evaluation, whereas model test data were used to estimate probabilistic lifetime sea loads in terms of load effects. Under uncertainties associated with fatigue resistance and loading history, two PDFs (i.e., Lognormal, Weibull) were used. The unfiltered (raw) data collected on a scaled JHSS monohull were used to establish stress range bin histogram using peak counting method and to illustrate the proposed approach.

Additionally, inspection and monitoring scheduling for fatigue sensitive naval vessels was investigated. An approach for establishing the inspection schedule which minimizes the expected damage detection delay was proposed (see Appendix VI). Furthermore, the approach was extended to yield the optimum combined inspection and monitoring schedules which simultaneously minimizes the damage detection delay and the total inspection and monitoring costs (see Appendix VII). Appendices VIII and IX provide an overview of the established integrated probabilistic framework.

The journal papers written by the PI and his co-workers collectively deal with four applications. The first one is the HSV-2 high speed naval craft, wave piercing catamaran [2, 4]. The second application is a joint high-speed sealift ship (JHSS) [2, 3, 5]. Data for this application were collected on a scaled down model reported by Devine (2009) in a briefing of the recently completed JHSS monohull and trimaran structural seaways loads test program. The third application is a typical mono-hull tanker section [6,7]. Finally, a sample hull was used to demonstrate the methodology presented in paper [1]. The main research topics that have been addressed are reliability, redundancy, structural health monitoring, fatigue, damage detection, and optimization. In [8, 9], an overview of the probabilistic integrated framework is provided along with the most interesting results obtained throughout the research project.

The matrix in Fig. 10 provides a graphical representation of the topics covered and applications presented by each journal article resulting from this research project.

		HSV-2	JHSS	TANKER	SAMPLE HULL
RELIABILITY		[4]	[3,5]	[2]	[1]
REDUNDANCY				[2]	
SHM		[4]	[3,5]	[6,7]	
FATIGUE			[5]	[6,7]	
DAMAGE DETECTION		[4]		[6,7]	
OPTIMIZATION				[6,7]	[1]
INTERVENTION SCHEDULING	INSPECTION			[6,7]	
	MONITORING			[7]	

Figure 10. Matrix of topics and applications reported in seven journal papers [1-7] resulting from ONR Project N00014-08-1-0188.

[1] Nader M. Okasha and Dan M. Frangopol. Efficient method based on optimization and simulation for the probabilistic strength computation of the ship hull. *Journal of Ship Research*, 54(4):244–256, 2010 (Appendix I).

[2] Alberto Decò, Dan M. Frangopol and Nader M. Okasha, (2011). Time-variant redundancy of ship structures. *Journal of Ship Research*, 55(3):208-219, 2011 (Appendix II).

[3] Nader M. Okasha, Dan M. Frangopol, and Alberto Decò. Integration of structural health monitoring in life-cycle performance assessment of ship structures under uncertainty. *Marine Structures*, 23(3):303–321, 2010 (Appendix III).

[4] Nader M. Okasha, Dan M. Frangopol, Duygu Saydam, and Liming W. Salvino. Reliability analysis and damage detection in high-speed naval craft based on structural health monitoring data. *Structural Health Monitoring*, 10(4): 361-379, 2011 (Appendix IV).

[5] Kihyon Kwon, Dan M. Frangopol, and Sunyong Kim. Fatigue performance assessment and service life prediction of high-speed ship structures based on probabilistic lifetime sea loads. *Structure and Infrastructure Engineering*, in press and already available online, DOI: 10.1080/15732479.2010.524984 (Appendix V).

[6] Sunyong Kim and Dan M. Frangopol. Optimum inspection planning for minimizing fatigue damage detection delay of ship hull structures. *International Journal of Fatigue*, 33(3):448–459, 2011 (Appendix VI).

[7] Sunyong Kim and Dan M. Frangopol. Probabilistic bicriterion optimum inspection/monitoring planning: Application to naval ships and bridges under fatigue. *Structure and Infrastructure Engineering*, 8(10): 912-927, 2012 (Appendix VII).

[8] Dan M. Frangopol, Paolo Bocchini, Alberto Decò, Sunyong Kim, Kihon Kwon, Nader M. Okasha, Duygu Saydam, Integrated life-cycle framework for maintenance, monitoring, and

reliability of naval ship structures, *Naval Engineering Journal*, 124(1): 89-99, 2012 (Appendix VIII).

[9] Dan M. Frangopol, Paolo Bocchini, Alberto Decò, Sunyong Kim, Kihon Kwon, Nader M. Okasha, Duygu Saydam, and Liming W. Salvino. Life-cycle ship reliability assessment, damage detection, and optimization. In *Proceedings of the 11th International Conference on Fast Sea Transportation - FAST 2011*, Honolulu, HI, USA, September 26-29, 2011 (Appendix IX).

8. References

Akpan, U.O., Koko T.S., Ayyub, B. and Dunbar T.E. (2002). Risk assessment of aging ship hull structures in the presence of corrosion and fatigue. Marine structures, 15(3), 211-231.

Deb, K., Pratap, A., Agarwal, S. and Meyarivan, T. (2002). A fast and elitist multiobjective genetic algorithm: NSGA-II. IEEE Transactions on Evolutionary Computation, 6(2), 182-197.

Devine, E.A. (2009). An overview of the recently-completed JHSS Monohull and Trimaran structural seaways loads test program. Naval Surface Warfare Center, Carderock Division (NSWCCD), PowerPoint Briefing, 30 October, 2009.

Fain, R.A. and Booth, E.T. (1979). Results of the first five data years of extreme stress scratch gauge data collected aboard Sea-Land's SL-7's. Ship structure committee (SSC-286).

Frangopol, D.M. and Messervey, T.B. (2007). Risk assessment for bridge decision making. Proceedings of the Fourth Civil Engineering Conference in the Asian Region, CECAR 4, Taipei, Taiwan, June 25-28, 2008 (invited paper); in ASCE Tutorial & Workshop on Quantitative Risk Assessment, Taipei, Taiwan, June 25-28, 37-42.

Frangopol, D.M. and Messervey, T.B. (2009a). Life-cycle cost and performance prediction: Role of structural health monitoring, Chapter 16 in Frontier Technologies for Infrastructure Engineering, S.S., Chen and A.H-S. Ang, eds., Structures and Infrastructures Book Series, Vol. 4, D.M. Frangopol, Book Series Editor, CRC Press/Balkema, Boca Raton, London, New York, Leiden (in press).

Frangopol, D.M. and Messervey, T.B. (2009b). Maintenance principles for civil structures, Chapter 89 in Encyclopedia of Structural Health Monitoring, C. Boller, F-K. Chang, and Y. Fujino, eds., John Wiley & Sons, Vol. 4, 1533-1562.

Frangopol, D.M. and Okasha, N.M. (2008). Life-cycle performance and redundancy of structures, Proceedings of the Sixth International Probabilistic Workshop, C-A. Graubner, H. Schmidt, and D. Proske, eds., Darmstadt, Germany, November 26-27, 2008 (Keynote Lecture), I-14, 2008.

Frangopol, D.M., Lin, K-Y. and Estes, A.C. (1997). Life-cycle cost design of deteriorating structures. Journal of Structural Engineering, ASCE, 123(10), 1390-1401.

Hughes, O.F. (1983). Ship structural design: a rationally-based, computer-aided, optimization approach. Wiley and Sons, New York, 582p.

IACS. (2008). Common structural rules for double hull oil tankers. International Association of Classification Societies. Available from http://www.iacs.org.uk.

Munse, W.H., Wilbur, T.W., Tellalian, M.L., Nicoll, K. and Wilson, K. (1984). Fatigue characterization of fabricated ship details for design. Ship structure committee (SSC-318).

Özgüc, Ö., Das, P.K. and Barltrop, N. (2006). The new simple equations for the ultimate compressive strength of imperfect stiffened plates. Ocean Engineering, Elsevier, 34(7), 970-986.

Smith, C. (1977). Influence of local compressive failure on ultimate longitudinal strength of a ship's hull. Proceedings of the PRADS: International Symposium on Practical Design in Shipbuilding, Tokyo, 18-20.

Wang, G., Leea, A-K Ivanova, L., Lynch, T.J., Serratellaa, C. and Basua R. (2008). A statistical investigation of time-variant hull girder strength of aging ships and coating life. Marine structures, 21(2-3), 240-256.

Yang, S-I, Frangopol, D.M. and Neves, L.C. (2004). Service life prediction of structural systems using lifetime functions with emphasis on bridges. Reliability Engineering & System Safety, Elsevier, 86(1), 39-51.

Yang, S-I, Frangopol, D.M. and Neves, L.C. (2006a). Optimum maintenance strategy for deteriorating structures based on lifetime functions. Engineering Structures, Elsevier, 28(2), 196-206.

Yang, S-I, Frangopol, D.M., Kawakami, Y. and Neves, L.C. (2006b). The use of lifetime functions in the optimization of interventions on existing bridges considering maintenance and failure costs. Reliability Engineering & System Safety, Elsevier, 91(6), 698-705.

9. Bibliography

Ultimate strength reliability and monitoring

Akpan, U.O., Koko T.S., Ayyub, B. and Dunbar T.E. (2002). Risk assessment of aging ship hull structures in the presence of corrosion and fatigue. Marine structures, 15(3), 211-231.

Assakkaf, I.A. (1998). Reliability-based Design of Panels and Fatigue Details of Ship Structures. PhD dissertation, University of Maryland, College Park.

Assakkaf, I.A. and Ayyub, B.M. (2000). Load and resistance factor design approach for fatigue of marine structures. 8th ASCE Specialty Conference on Probabilistic Mechanics and Structural Reliability.

Assakkaf, I.A., Ayyub, B.M. and Mattei, N.J. (2000). Reliability-Based Load and Resistance Factor Design (LRFD) of Hull Structural Components of Surface Ships. Association of Scientists and Engineers, 37th Annual Technical Symposium, ASE.

Atua, K.I. (1998). Reliability-Based Structural Design of Ship Hull Girders and Stiffened Panels. PhD dissertation, University of Maryland, College Park.

Atua, K.I., Assakkaf, I.A. and Ayyub, B.M. (1996). Statistical Characteristics of Strength and Load Random Variables of Ship Structures. Proceedings of the 1996 ASCE Specialty

Conference on Probabilistic Mechanics and Structure Reliability, edited by Frangopol and Grigoriu, August 7-9, 106-109.

Ayala-Uraga, E. and Moan, T. (2007). Time-Variant Reliability Assessment of FPSO Hull Girder With Long Cracks. Journal of Offshore Mechanics and Arctic Engineering, 129, 81-89.

Ayyub, B.M., White G.J. and Purcell E.S. (1989). Estimation of structural service life of ships. Naval engineers journal, 101(3), 156-166.

Ayyub, B.M. and White, G.J. (1987). Reliability-Conditioned Partial Safety Factors. Journal of Structural Engineering, 113(2), 279-294.

Ayyub, B.M. and White, G.J. (1990). Life expectancy assessment of marine structures. Marine Structures, 3, 301-317.

Ayyub, B.M. Assakkaf, I.A., Sikora, J.P., Adamchak, J.C., Atua, K., Melton, W. and Hess, P.E. (2002). Reliability-Based Load and Resistance Factor Design. (LRFD) Guidelines for Hull Girder Bending. Naval Engineers Journal, 114(2), 43-68.

Ayyub, B.M., Assakkaf, I.A., and Atua, K.I. (2000). Reliability-Based Load and Resistance Factor Design (LRFD) of Hull Girders for Surface Ships. Naval Engineers Journal, ASNE, 112(4), 279-296.

Ayyub, B.M., White, G.J., Bell-Wright T.F. and Purcell E.S. (1990). Comparative structural life assessment of patrol boat bottom plating. Naval engineers journal, 102(3), 253-262.

Caldwell, J.B. (1965). Ultimate Longitudinal Strength. Transactions of RINA, 107, 411-430.

Chen, N-Z and Guedes Soares, C. (2007). Longitudinal strength analysis of ship hulls of composite materials under sagging moments. Composite Structures, 77, 36–44.

Chen, N-Z, Sun, H-H and Guedes Soares, C. (2003). Reliability analysis of a ship hull in composite material. Composite Structures, 62, 59–66.

Chen, Y-K., Kutt, L.M., Piaszczyk, C.M. and Bieniek, M.P. (1983). Ultimate Strength of Ship Structures. SNAME Transactions, 91, 149–168.

Dow, R.S., Hugill, R.C., Clark, J.D. and Smith, C.S. (1981). Evaluation of Ultimate Ship Hull Strength. Society of Naval Architects and Marine Engineers, 133–147.

Dowling, P.J., Chatterjee, S., Frieze, P.A. and Moolani, F.M. (1973). Experimental and predicted collapse behaviour of rectangular steel box girders. Proc., Int. Conf. on Steel Box Girder Bridges, P. Cartledge, ed., Institution of Civil Engineers, London, 77–94.

Faulkner, D. (1975). A review of effective plating for use in the analysis of stiffened plating in bending and compression. Journal of ship research, 19(1), 1-17.

Gordo, J.M. and Guedes Soares, C. (1993). Approximate load shortening curves for stiffened plates under uniaxial compression. Integrity of Offshore Structures, EMAS, 189-211.

Gordo, J.M., Guedes Soares, C. and Faulkner, D. (1996). Approximate assessment of the ultimate longitudinal strength of the hull girder. Journal of ship research, 40(1), 60-69.

Guedes Soares, C. and Garbatov, Y. (1999). Reliability of maintained ship hulls subjected to corrosion and fatigue under combined loading. Journal of Constructional Steel Research, 52, 93–115

Guedes Soares, C. and Ivanov, L.D. (1989) Time dependent reliability of the primary ship structure. Reliability engineering & system safety, 26, 59-71.

Guedes Soares, C. and Moan, T. (1985). Uncertainty analysis and code calibration of the primary load effects in ship structures. Structural safety and reliability : proceedings of ICOSSAR '85, the 4th International Conference on Structural Society [sic] and Reliabelity [sic], the International Conference Center Kobe, Kobe, Japan, May 27-29, 1985 / 501-512

Guedes Soares, C. and Teixeira, A.P. (2000). Structural reliability of two bulk carrier designs. Marine Structures, 13(2), 107-128.

Guedes Soares, C., and Doglianib, M. (2000). Probabilistic modelling of time-varying still-water load effects in tankers. Marine structures. 13(2), 129-143.

Guedue Soares, C. and Garbatov, Y. (1997). Reliability assessment of maintained ship hulls with correlated corroded elements - results from three years of testing. Marine structures, 10(8-10), 629-653.

Guo, J.B., Wang, G., Ivanov, L. and Perakis, A.N. (2008). Time-varying ultimate strength of aging tanker deck plate considering corrosion effect. Marine Structures, 21(4), 402-419.

Hansen, A. (1995). Reliability methods for the longitudinal strength of ships. Department of Naval Architecture and Offshore Engineering, Technical University of Denmark.

Hu, Y. and Prusty, B.G. (2007). A new method for oil tanker structure condition monitoring. Ships and offshore structures. Taylor & Francis, 2(4) 371-377.

Hughes, O.F. (1983). Ship structural design: a rationally-based, computer-aided, optimization approach. Wiley and Sons, New York, 582p.

Johnson, A.J. and Taylor, K.V. (1966). Wave induced stresses in ships in service Stresses in service. Proceedings of the second conference arranged on behalf of the Joint British Committee for Stress Analysis, 23-25 March 1966.

Kiykakis, C. (1975). Seakeeping series for cruiser ships. Transactions - The Society of Naval Architects and Marine Engineers.

Kong, C-W, Lee I-C, Kim, C-G and Hong, C-S (1998). Postbuckling and failure of stiffened composite panels under axial compression. Composite Structures, 42, 13-21.

Kutt, L.M., Piazszczyk, C.M., Chen, Y.K. and Lin, D. (1985). Evaluation of the longitudinal ultimate strength of various ship hull configurations. SNAME Transactions, 93, 33-53.

Lacey, P. and Chen, H. (1995). Improved passage planning using weather forecasting, maneuvering guidance, and instrumentation feedback. Marine technology and SNAME news, 1-19.

Little, R.S, Lewis, E.V. and Bailey, F.C. (1971). A statistical study of wave induced bending moments on large oceangoing tanker and bulk carriers. SNAME Transactions, 117–168.

Loseth, R., Sekkeseater, G. and Valsgard, S. (1994). Economics of high tensile steel in ship hulls. Marine Structures, 7, 31–50.

Lua, J. and Hess, P.E. (2006). First-Failure–Based Reliability Assessment and Sensitivity Analysis of a Naval Vessel Under Hogging. Journal of ship research, 50(2), 158-170.

Mansour, A.E. and Hovem, L. (1994). Probability based ship structural analysis. Journal of Ship Research, 38(4), 329-339.

Masaoka, K. and Mansour, A. (2008). Compressive Strength of Stiffened Plates With Imperfections: Simple Design Equations. Journal of ship research, 52(3) 227-237.

Melitz, D.T., Robertson, E.J. and Davison, N.J. (1992). Structural Performance Management of VLCCs - An Owners Approach. Marine technology. 29(4), 250-262.

Miyahara, K., Miyake, R., Abe, N., Kumano, A., Toyota, M. and Nakaji, Y. (2006). Full-scale measurements on hull response of a large-container ship in service. Proceedings of OMAE2006, 25th International Conference on Offshore Mechanics and Arctic Engineering June 4-9, 2006, 283-289.

Muhanna, R.L., Ayyub, B.M. and Bruchman, D.D. (1996). Uncertainty analysis of structural strength of stiffened panels. Naval engineers journal, 108(3) 399-418.

Naar, H. (2006). Ultimate strength of hull girder for passenger ships. PhD Dissertation, Department of Mechanical Engineering Ship Laboratory, Helsinki University of Technology.

Nitta, A., Arai, H. and Maganio, A. (1992). Basis of IACS unified longitudinal strength standard. Marine structures, 5(1), 1-21.

Özgüc, Ö., Das, P.K. and Barltrop, N. (2006). The new simple equations for the ultimate compressive strength of imperfect stiffened plates. Ocean Engineering, Elsevier, 34(7), 970-986.

Paik, J.K. and Frieze, P.A. (2001). Ship structural safety and reliability. Progress in Structural Engineering and Materials, Wiley and Sons, 3(2), 198–210.

Paik, J.K. and Mansour, A.E. (1995). A simple formulation for predicting the ultimate strength of ships. Journal of Marine Science and Technology, 1(1), 52-62.

Paik, J.K. and Seo, J.K. (2005). Ultimate limit state assessment of ship structures. International Conference on Computational Methods in Marine Engineering, MARINE 2005.

Paik, J.K., Kim, D.H. and Bong, H.S. (1992). Deterministic and probabilistic safety evaluation for a new double-hull tanker with transverseless system. Trans SNAME, 100, 173-198.

Paik, J.K., Lee, J.M., Park, Y, Hwang, J.S. and Kim, C.W. (2003). Time-variant ultimate longitudinal strength of corroded bulk carriers. Marine structures, 16(8), 567-600.

Paik, J.K., Thayamballi, A.K., Kim, S.K. and Yang, S.H. (1998). Ship hull ultimate strength reliability considering corrosion. Journal of Ship Research, 42(22), 154-165.

Paik, J.K., Thayamballi, A.K., Che, J.S. and Pedersen, P.T. (1996). Ultimate strength of ship hulls under combined vertical bending, horizontal bending, and shearing forces. Transactions - Society of Naval Architects and Marine Engineers, 104, 31-59.

Qin, S. and Cui, W. (2003). Effect of corrosion models on the time-dependent reliability of steel plated elements. Marine structures, 16(1), 15-34.

Rutherford, S.E. and Caldwell, J.B. (1990). Ultimate Longitudinal Strength of Ships: A Case Study. SNAME Transactions, 98, 441-471.

Sagvolden, G., Pran, K., Vines, L., Torkildsen, H.E. and Wang, G. (2002). Fiber optic system for ship hull monitoring. Optical Fiber Sensors Conference Technical Digest, OFS 2002, vol.1, 435- 438.

Shi, W.B., Thompson, P.A. and Hire, J-CL. (1996). Thermal stress and hull stress monitoring. SNAME Transactions, 104, 61–79.

Shintaku, E., Fujimoto, Y., Hamada, K., and Takeuchi, T. (2000). Study of a simple sensor for stress history measurements of a structural member using a piezoelectric element. Journal of Marine Science Technology, 5, 40–47.

Smith, C. (1977). Influence of local compressive failure on ultimate longitudinal strength of a ship's hull. Proceedings of the PRADS: International Symposium on Practical Design in Shipbuilding, Tokyo, 18-20.

Smith, M.J. and Pegg, N.G. (2003). Automated assessment of Ultimate hull girder strength. Journal of Offshore Mechanics and Arctic Engineering, ASME, 125(3), 211-218.

Sun, H-H and Guedes Soares, C. (2003). Reliability-Based Structural Design of Ship-Type FPSO Units. Transactions of the ASME, Vol. 125, May, 108-113.

Tetsuo, O., Yu, T. and Tomoki, M. (2006). On board measurement of stresses and deflections of a Post-Panamax containership and its feedback to rational design. Marine structures. 19(2-3), 141-172.

Thayamballi, A.K. Chen, Y.K. and Chen, H.H. (1987). Deterministic and Reliability Based Retrospective Strength Assessments of Ocean-going Vessels. Trans. SNAME, 1987, 159-187.

Viner, AC. (1986). Development of ship strength formulations. Proceedings of the International Conference on Advances in Marine Structures, London, Elsevier, 152-173.

Wang, G., Leea, A-K, Ivanova, L., Lynch1, T.J., Serratellaa, C. and Basua, R. (2008). A statistical investigation of time-variant hull girder strength of aging ships and coating life. Marine structures, 21(2-3), 240-256.

Wang, G., Pran, K., Sagvolden, G., Havsgard, G.B., Jensen, A.E., Johnson, G.A. and Vohra, S.T. (2001). Ship hull structure monitoring using fibre optic sensors. Smart material and structures, 10, 472–478.

Ward, G. and Katory, M. (1975). Data on Midship Bending Stresses from Four Ships. The dynamics of Marine vehicles and structures in waves: papers presented at an International Symposium, 1-5 April, 1975. 306-320.

Wirsching, P.H., Ferensic, J. and Thayamballi, A. (1997). Reliability with respect to ultimate strength of a corroding ship hull. Marine structures, 10(7), 501-518.

Witmer, D.J. and Lewis, J.W. (1995). The BP Oil Tanker Structural Monitoring System. Marine technology and SNAME news, 32(4), 277-296.

Xu, J. and Haddara, M.R. (2001). Estimation of wave-induced ship hull bending moment from ship motion measurements. Marine Structures, 14, 593–610.

Yu, H.C., Choi, J.W., Park, G.I., Han, S.Y., Tai, S.C. and Ha, M.K. (2008). Full Scale Measurement of a Large Container Carrier on the Far East - Europe Route. SNAME Annual Meeting & Expo, Technical Program.

Fatigue reliability and monitoring

Andersen, M.R. (1998). Fatigue crack initiation and growth in ship structures. PhD Dissertation, Department of Naval Architecture and Offshore Engineering, Technical University of Denmark, Denmark.

Assakkaf, I.A. and Ayyub, B.M. (2000). Load and resistance factor design approach for fatigue of marine structures. 8th ASCE specialty conference on probabilistic mechanics and structural reliability, PMC2000-169.

Ayyub, B.M., Assakkaf, I.A., Beach, J.E. and Melton, W.M. (2002). Methodology for developing reliability based load and resistance factor design (LRFD) guidelines for ship structures. Naval engineers journal, 114(2), 23-41.

Ayyub, B.M., Assakkaf, I.A., Kihl, D.P. and Siev, M.W. (2002). Reliability-based design guidelines for fatigue of ship structures. Naval engineers journal.

Casella, G., Dogliani, M. and Guedes Soares, C. (1997). Reliability-based design of the primary structure of oil tankers. Journal of offshore mechanics and arctic engineering, 119, 263-269.

Farrar, C.R. and Lieven, N. (2006). Damage prognosis: the future of structural health monitoring. Philosophical transactions of the royal society, 365, 623-632.

Ernesto, H.Z. and Roberto, M.I. (2004). A Bayesian model for the probability distribution of fatigue damage in tubular joints. Journal of offshore mechanics and arctic engineering, 126.

Forristall, G.Z. (1978). On the statistical distribution of wave heights in a storm. Journal of geophysical research, 83(C5).

Jha, A.K. and Winterstein, S.R. (2000). Stochastic fatigue damage accumulation due to nonlinear ship loads. Journal of offshore mechanics and arctic engineering, 122, 253-259

Moan, T. (2003). Marine structures for the future. Centre for offshore research & engineering (CORE) report, 2003-01, National University of Singapore.

Nikolaidis, E., Hughes, O., Ayyub, B.M. and White, G.J. (1993). A methodology for reliability assessment of ship structures. Ship structures symposium, Arlington, Virginia.

Paik, J.K. and Frieze, P.A. (2001). Ship structural safety and reliability. Progress in structural engineering and materials, 3, 198-210.

Paik, J.K., Lee, J.M., Ryu, J.Y., Jang, J.H., Renaud, C. and Hess, P.E. (2006). Mechanical buckling collapse testing on aluminum stiffened plate structures for marine applications. World maritime technology conference (WMTC 2006), London, UK.

Sielski, R.A. (2007). Research needs in aluminum structure. 10th international symposium on practical design of ships and other floating structures, Houston, Texas.

Sikora, J.P., Dinsenbacher, A. and Beach, J.E. (1983). A method for estimating lifetime loads and fatigue lives for swath and conventional monohull ships. Naval engineers journal, 95(3), 63–85.

Guedes Soares, C. and Garbatov, Y. (1999). Reliability of maintained ship hulls subjected to corrosion and fatigue under combined loading. Journal of constructional steel research, 52, 93-115.

Strauss, A., Frangopol, D.M. and Kim, S. (2008). Use of monitoring extreme data for the performance prediction of structures: Bayesian updating. Engineering structures, 30(12), 3654-3666.

Wang, G., Pran, K., Sagvolden, G., Havsgard, G.B., Jensen, A.E., Johnson, G.A. and Vohra, S.T. (2001). Ship hull structure monitoring using fibre optic sensors. Smart materials and structures, 10, 472-478.

Wirsching, P.H. (1998). Fatigue reliability. Progress in structural engineering and materials, 1(2), 200-206.

General

Ang, A. H.-S. and Tang, W.H. (2007). Probability Concepts in Engineering Planning and design, 2nd Edition, John Wiley & Sons.

Deb, K., Pratap, A., Agarwal, S. and Meyarivan, T. (2002). A fast and elitist multiobjective genetic algorithm: NSGA-II. IEEE Transactions on Evolutionary Computation, 6(2), 182-197.

Ditlevsen, O. and Bjerager. P. (1986). Methods of structural systems reliability. Structural Safety, Elsevier, 3(3-4), 195-229.

Ellingwood, B.R. (2005). Risk-informed condition assessment of civil infrastructure: state of practice and research issues. Structure and Infrastructure Engineering, Taylor & Francis, 1(1), 7-18.

Enright, M.P. and Frangopol, D.M. (1999). Condition prediction of deteriorating concrete bridges using Bayesian updating. Journal of structural engineering, 125(10), 1118-1125.

Estes, A.C. and Frangopol, D.M. (2001). Minimum expected cost-oriented optimal maintenance planning for deteriorating structures: application to concrete bridge decks. Reliability Engineering & System Safety, Elsevier, 73, 281-291.

Estes, A.C. and Frangopol, D.M. (1999). Repair optimization of highway bridges using system reliability approach. Journal of Structural Engineering, ASCE, 125(7), 766–775.

Farrar, C.R. and Worden, K. (2007). An introduction to structural health monitoring. Philosophical Transactions of the Royal Society A: Mathematical, Physical and Engineering Sciences, 365(1851), 303-315.

Frangopol, D.M. and Liu, M. (2006). Life-Cycle Cost and Performance of Civil Structures. McGraw-Hill 2006 Yearbook of Science and Technology, McGraw-Hill, New York, 2006, 183-185.

Frangopol, D.M. and Liu, M. (2007). Maintenance and management of civil infrastructure based on condition, safety, optimization and life-cycle cost. Structure and Infrastructure Engineering, Taylor & Francis, 3(1), 29-41.

Frangopol, D.M. and Messervey, T.B. (2007). Risk assessment for bridge decision making. Proceedings of the Fourth Civil Engineering Conference in the Asian Region, CECAR 4, Taipei, Taiwan, June 25-28, 2008 (invited paper); in ASCE Tutorial & Workshop on Quantitative Risk Assessment, Taipei, Taiwan, June 25-28, 37-42.

Frangopol, D.M. and Messervey, T.B. (2009a). Life-cycle cost and performance prediction: Role of structural health monitoring, Chapter 16 in Frontier Technologies for Infrastructure Engineering, S-S, Chen and A.H-S.Ang, eds., Structures and Infrastructures Book Series, Vol. 4, D.M. Frangopol, Book Series Editor, CRC Press/Balkema, Boca Raton, London, New York, Leiden (in press).

Frangopol, D.M. and Messervey, T.B. (2009b). Maintenance principles for civil structures, Chapter 89 in Encyclopedia of Structural Health Monitoring, C. Boller, F-K. Chang, and Y. Fujino, eds., John Wiley & Sons, Vol. 4, 1533-1562.

Frangopol, D.M. and Okasha, N.M. (2008). Life-cycle performance and redundancy of structures, Proceedings of the Sixth International Probabilistic Workshop, C-A. Graubner,

H. Schmidt, and D. Proske, eds., Darmstadt, Germany, November 26-27, 2008 (Keynote Lecture), 1-14, 2008.

Frangopol, D.M., Lin, K-Y. and Estes, A.C. (1997). Life-cycle cost design of deteriorating structures. Journal of Structural Engineering, ASCE, 123(10), 1390-1401.

Gharaibeh, E.S., Frangopol, D.M. and Onoufriou, T. (2002). Reliability-based importance assessment of structural members with applicants to complex structures. Computers and Structures, 80(12), 1113-1131.

Gumbel, E.J. (1958). Statistics of extremes, Columbia University Press, New York.

Hendawi. S. and Frangopol, D.M. (1994). System reliability and redundancy in structural design and evaluation. Structural Safety, Elsevier, 16(1-2), 47-71.

Kong, J.S. and Frangopol, D.M. (2003). Life-cycle reliability-based maintenance cost optimization of deteriorating structures with emphasis on bridges. Journal of Structural Engineering, ASCE, 129(6), 818–828.

Kong, J.S. and Frangopol, D.M. (2005). Probabilistic optimization of aging structures considering maintenance and failure cost. Journal of Structural Engineering, ASCE, 131(4), 600–616.

Moan, T. (2005). Reliability-based management of inspection, maintenance and repair of offshore structures. Structure and Infrastructure Engineering, Taylor & Francis, 1(1), 33-62.

Paik, J.K. and Thayamballi, A.K. (2002). Ultimate strength of ageing ships. Proceedings of the institution of mechanical engineers: Part M, Journal of engineering for the maritime environment, 216.

Selected references from the ship structure committee (SSC) (reports and papers)

Ayyub, B.M., Akpan, U.O., Souza, G.F., Koko, T.S. and Luo, X. (2000). Risk-based life cycle management of ship structures. Ship structure committee (SSC-416).

Chiou, J.W. and Chen, Y.K. (1990). Fatigue prediction analysis validation from SL-7 hatch corner strain data. Ship structure committee (SSC-338).

Donald, J.K. (2007). Fracture mechanics characterization of aluminum alloys for marine structural applications. Ship structure committee (SSC-448).

Fain, R.A. and Booth, E.T. (1979). Results of the first five data years of extreme stress scratch gauge data collected aboard Sea-Land's SL-7's. Ship structure committee (SSC-286).

Hess, P.E., Ayyub, B.M. and Knight, D.E. (2002). Failure definition for structural reliability assessment. Ship structure committee (SSC-420).

Mansour, A. and Thayamballi, A. (1994). Probability-based ship design loads and load combinations. Ship structure committee (SSC-373).

Mansour, A., Wirsching, P.H., Luckett, M., Plumpton, A. et al. (1997). Assessment of reliability of ship structures. Ship structure committee (SSC-398).

Mansour, A., Wirsching, P.H., White, G. and Ayyub, B. (1996). Probability-based ship design implementation of design guidelines for ships: A demonstration. Ship structure committee (SSC-392).

Munse, W.H., Wilbur, T.W., Tellalian, M.L., Nicoll, K. and Wilson, K. (1984). Fatigue characterization of fabricated ship details for design. Ship structure committee (SSC-318).

Selected references from the American Bureau of Shipping (ABS)

ABS (2003). Guide for hull condition monitoring systems.
ABS (2004). Guidance notes on the strength assessment of cargo tank structures beyond 0.4L amidships in oil carriers 150 meters of more in length.
ABS (2004). Guide for buckling and ultimate strength assessment for offshore structures.

Selected references from the international association of classification societies

IACS. (2007). Guidelines for Surveys, Assessment and Repair of Hull Structure – Bulk Carriers. No.76.
IACS. (2008). Common structural rules for double hull oil tankers. International Association of Classification Societies.
IACS. (2007). Requirements Concerning strength of ships.

Appendix I

Nader M. Okasha and Dan M. Frangopol. Efficient method based on optimization and simulation for the probabilistic strength computation of the ship hull. *Journal of Ship Research*, 54(4):244–256, 2010.

Journal of Ship Research, Vol. 54, No. 4, December 2010, pp. 244–256

Efficient Method Based on Optimization and Simulation for the Probabilistic Strength Computation of the Ship Hull

Nader M. Okasha and **Dan M. Frangopol**

Department of Civil & Environmental Engineering, Center for Advanced Technology for Large Structural Systems (ATLSS), Lehigh University, Bethlehem, Pennsylvania

The accurate computation of the strength of a ship hull is vital for ensuring its reliability. Taking into account the uncertainties in the material properties and fabrication details requires a probabilistic approach for the determination of the strength of the ship hull. This study proposes an efficient approach for the determination of the probabilistic strength of the ship hull. First, a novel deterministic method for the fast and accurate calculation of the strength of the ship hull is presented. In this method, stresses in the hull section are determined using the constitutive models of the stiffened panels. These models take into account the various possible failure modes and initial imperfections. The ultimate strength is found by an optimization search algorithm. The method is shown to be as accurate as the rigorous incremental curvature method but with significantly less computational time. The method is then applied with a Latin-hypercube sampling simulation, and the output sample is tested against several potential distributions. The best-fit probability distribution of the ultimate strength of the ship hull is provided.

Keywords: hull form; longitudinal strength; stress analysis; resistance (general)

1. Introduction

Essentially, the overall structure of a ship is a beam—a floating box girder that is internally stiffened and subdivided—in which the decks and bottom structure are flanges and the side shell and any longitudinal bulkheads are webs (Hughes 1983). The maximum value of the hull girder bending moment is the single most important load effect in the analysis and design of ship structures (Hughes 1983). Although a combination of vertical and horizontal bending moments are expected while the ship is in service, the levels of horizontal moments are often small and for practical purposes it may be appropriate to deal only with the vertical bending moment (Guedes Soares & Teixeira 2000). Hull girder vertical bending is referred to as either "hogging" or "sagging" depending on the sense of curvature that it causes (Hughes 1983).

Deterministic methods for calculating the strength of the ship hull are numerous. Even though uncertainties are present in many of the input variables and may have large influence in the strength calculation, the literature lacks studies of the strength analysis of ship hulls that explicitly accounts for these uncertainties and provides means to probabilistically determine the strength of ships. Furthermore, ship structural design has been moving toward probability-based design in recent years (Guedes Soares et al. 1996), stressing the need of treating the strength of ships probabilistically.

A review of the available ship hull strength analysis methods conducted in the next section shows a trade-off among these methods in accuracy and computational cost. Since the probabilistic aspects are captured by means of simulation, which require the calculation of the strength a large number of times, a fast and accurate method for analyzing the ship hull is required. Hess and Lua (2003) used a hybrid simulation-FORM approach to compute the reliability of various ships. However, in their simulation, the rigorous incremental curvature method was used, which can become computationally very expensive when performed repetitively in simulations. This study presents a novel deterministic method for the calculation of the strength of the ship hull, which when performed repetitively in simulations provides a significant

Manuscript received at SNAME headquarters Month xx, xxxx; revised manuscript received Month xx, xxx.

saving in computation time. In this method, the ship hull cross section is discretized into elements, each composed of a longitudinal stiffener and its attached plate. Stresses in the hull section are determined using the constitutive models of these elements. The constitutive models take into account the various possible failure modes of stiffened panels. Initial imperfections are also taken into account. For a given curvature, the bending moment of the section is determined in a way similar to that of the rigorous incremental curvature method. However, instead of finding the ultimate strength by incrementing the curvature, the ultimate strength is found by an optimization search algorithm. The curvature is treated as a design variable, and the objective is to find the curvature that maximizes the bending moment. The method is shown to be as accurate as the rigorous incremental method, but with significantly less computational time.

The method is then applied with a Latin hypercube sampling simulation. The output sample is tested against several potential distributions. The parameters of these distributions are found by the maximum likelihood estimate method. Goodness-of-fit tests are performed to determine the best-fit distribution. Eventually, the best-fit probability distribution of the ultimate strength of the ship hull is provided. For the sake of computational time comparison between methods, all calculations in this paper are performed on the same computer (with Intel Core 2 Duo CPU and E8200 with 2.66 GHz and 3.25 GB of RAM) and with the same software, namely MATLAB (MathWorks 2008a,b).

2. Deterministic methods for the hull strength analysis

The earliest attempt to develop an analytical ultimate strength method including both material yielding and buckling was made by Caldwell (1965). In his model, it was assumed that the entire material in compression has reached its ultimate buckling strength, while full yielding was assumed for the material in tension. The ultimate strength of the material in compression is found using a structural instability strength factor. Faulkner (1975) developed a design method to calculate this reduction factor. Paik and Mansour (1995) further developed the approach to treat the cases where: (a) the yield strengths of the tension flange and the side material are not necessarily the same, (b) the ultimate strengths of the compression flange and the side material are not necessarily the same either, and/or (c) double-hull arrangements are considered. Several similar simple methods have been developed over the years. However, it may not always be the case where the entire cross section reaches its ultimate capacity. The material in the vicinity of the final neutral axis will often remain in the elastic state up to the overall collapse of the hull girder (Paik & Mansour 1995). Accordingly, Paik and Mansour (1995) suggested a simple closed-form solution for the calculation of the ultimate bending moment of the ship hull based on a likely distribution of longitudinal stresses over the hull cross section at the overall collapse state. The stress distribution in the immediate vicinity of the final neutral axis was assumed linear.

Even though the Paik and Mansour (1995) method is fast and with reasonable assumptions, the idealizations made may well affect the accuracy of the results. However, it may be a speedy and convenient alternative to the more accurate and rigorous analytical methods of analysis. The most accurate and most general method is by incremental finite element analysis of the entire hull module (Chen et al. 1983, Kutt et al. 1985), but the computational requirements both in modeling the structure and computing time are too great (Gordo et al. 1996, Hughes 1983). Besides, convergence difficulties are often encountered in the procedure (Smith & Pegg 2003). Alternatively, the idealized structural unit method can be used as an effective tool for nonlinear analysis of large structures (Mansour 1997). The total number of elements and nodal points in this method is much smaller than those associated with the finite element method. However, a good deal of idealizations of the geometric and material nonlinear behavior is involved.

For practical design purposes, Smith (1977) developed a hybrid finite element-incremental curvature method that derives the moment-curvature curve for the complete hull. While this method is based on finite element results for each stiffened panel, Gordo et al. (1996) used simple analytical formulas to model this behavior. The International Association of Classification Societies has integrated this method into its common structural rules (IACS 2008). Özgüç et al. (2006) developed equations to account for initial imperfections in the stiffened panels that can be used with the incremental curvature method. Further details of the rigorous incremental curvature method taking into account initial imperfections are given in the next section.

3. Incremental curvature method

The following is a brief description of the rigorous incremental curvature method based on the guidelines in IACS (2008). In this approach, the ultimate hull girder bending moment capacity is defined as the peak value of the moment curvature curve of the ship cross section. The steps involved in obtaining the moment curvature curve are explained as follows (IACS 2008):

Step 1. Divide the hull girder transverse section into structural elements, that is, longitudinal stiffened panels (one stiffener per element) and hard corners.

Step 2. Derive the stress-strain curves (or so-called load-end shortening curves) for all structural elements.

Step 3. Derive the curvature step size $\Delta\kappa$, which is to be taken as1% of the yield curvature. Determine the elastic neutral axis location. Use it for the first incremental step.

Step 4. For each element, calculate the strain as $\varepsilon_{ij} = \kappa_i (z_j - NA_i)$ corresponding to κ_i, the corresponding stress σ_{ij} (see next section for more details), and hence the force in the element $\sigma_{ij}A_j$, where z_j and A_j are the centroid and area of element j, respectively, and NA_i and κ_i are the neutral axis and curvature at increment i, respectively.

Step 5. Determine the new neutral axis position NA_i by checking the longitudinal force equilibrium over the whole transverse section. Hence, adjust NA_i until the force at increment i is $F_i = \Sigma A_j \sigma_{ij} = 0$.

Step 6. Calculate the corresponding moment by summating the force contributions of all elements as

$$M_i = \sum_j A_j \sigma_{ij} (z_j - NA_i)$$

Step 7. Increase the curvature by $\Delta\kappa$, use the current neutral axis position as the initial value for the next curvature increment and repeat from step 4 until the maximum required curvature, κ_F (given as three times the yield curvature) is reached. The ultimate capacity is the peak value from the M-κ curve. If the peak does not occur in the curve, then κ_F is to be increased until the peak is reached.

Two remarks can be made with respect to the above procedure. First, the elastic portion of the curve can be obtained by scaling the result of the analysis up to the value of the moment at which the first member failure occurs (Hughes 1983) or by using the yield curvature κ_y as given by the IACS formula (IACS 2008)

$$\kappa_y = \frac{M_y}{EI} \tag{1}$$

where M_y is the vertical bending moment given by a linear elastic bending stress of yield in the deck, given as $M_y = S\sigma_y$, where S is elastic section modulus, σ_y is the yield stress, E is the modulus of elasticity, and I is the hull girder moment of inertia. Second, it is noted that the above description does not explain how the neutral axis is to be adjusted in order to achieve equilibrium in step 5 (i.e., it does not provide guidance on an iterative scheme for modified NA_i until $F_i = \Sigma A_j \sigma_{ij} = 0$). A systematic approaching for achieving this equilibrium is given in a later part of this paper. An efficient and fast approach is essential in the probabilistic strength analysis. Further details are given in later sections of this paper.

4. Stress-strain curves including initial imperfections

In order to account for initial imperfections for stiffened panels, the effective width b_E of the panel is multiplied by reduction factors. This approach was first introduced by Guedes Soares (1988). In this paper, formulas proposed by Özgüc et al. (2006) are used as

$$b'_E = b_E R_d R_r R_y R_\tau R_q \tag{2}$$

where b'_E is the imperfect width of stiffened plate, b_E is the effective width of the perfect stiffened plate, R_d is a reduction factor due to initial deflection, R_r is a reduction factor due to welding induced residual stress, R_y is a reduction factor due to yielding, R_τ is a reduction factor due to shear stress, and R_q is a reduction factor due to lateral pressure load. In this study, initial imperfections only due to initial deflection and welding-induced residual stress are considered. The reduction factors that account for these imperfections are expressed as (Özgüc et al. 2006):

$$R_d = 1.0 - 0.2323 f(\lambda) g(\beta) \tag{3}$$

$$f(\lambda) = \begin{cases} 0.015 & \text{for } 0 < \lambda \le 0.35 \\ -1.03 + 2.341\lambda - 1.344\lambda^2 + 0.212\lambda^3 & \text{for } \lambda > 0.35 \end{cases} \tag{4}$$

$$g(\beta) = \begin{cases} 10.818 + 0.204\beta - 5.177\beta^2 & \text{for } 1 < \beta \le 1.5 \\ 4.594 - 0.805\beta + 0.255\beta^2 & \text{for } 1.5 < \beta \le 2.0 \\ 6.404 - 1.847\beta + 0.371\beta^2 & \text{for } 2.0 < \beta \le 2.5 \\ 5.435 - 1.213\beta + 0.202\beta^2 & \text{for } 2.5 < \beta \le 4.0 \end{cases} \tag{5}$$

$$R_r = 1.0 - \left[\frac{\mu}{8.1(\beta - 1.901)^2 + 1} \right] \tag{6}$$

where $\mu = \sigma_r/\sigma_y$ is defined as the normalized welding residual stress, σ_r is the welding residual stress, σ_y is the yield stress, β is the slenderness ratio, and λ is the beam-column slenderness ratio. Expressions for the other reduction factors can be found in Özgüc et al. (2006).

The following is a procedure for generating the stress-strain curves of stiffened panels based on the IACS (2008). The only mode of failure for stiffened panels under tensile load is the elastic-perfectly plastic failure mode. The equation describing the stress-strain curve σ-ε or the elastoplastic failure of these structural elements is

$$\sigma = \Phi \sigma_y \tag{7}$$

where

$$\Phi = \begin{cases} -1 & \text{for } \varepsilon < -1 \\ \varepsilon & \text{for } -1 \le \varepsilon \le 1 \\ 1 & \text{for } \varepsilon > 1 \end{cases} \tag{8}$$

$$\varepsilon = \frac{\varepsilon_E}{\varepsilon_y} \tag{9}$$

$$\varepsilon_y = \frac{\sigma_y}{E} \tag{10}$$

where σ is the element stress, Φ is the edge function, ε is the relative strain, ε_E is the element strain, ε_y is the strain corresponding to yield stress in the element, σ_y is the specified minimum yield stress of the material, and E is the elastic modulus of the material.

The primary modes of failure of a stiffened panel subject to predominantly axial compressive loads are the beam-column buckling, torsional buckling, web local buckling of flanged profiles, and web local buckling of flat bars (IACS 2008). The equation describing the shortening portion of the stress-strain curve for the beam column buckling of stiffeners is

$$\sigma_{CR1} = \Phi \sigma_{C1} \left(\frac{A_s + b_E t}{A_s + st} \right) \tag{11}$$

where

$$\sigma_{C1} = \begin{cases} \frac{\sigma_{E1}}{\varepsilon} & \text{for } \sigma_{E1} \le \frac{\sigma_y}{2}\varepsilon \\ \sigma_y \left(1 - \frac{\sigma_y \varepsilon}{4\sigma_{E1}} \right) & \text{for } \sigma_{E1} > \frac{\sigma_y}{2}\varepsilon \end{cases} \tag{12}$$

$$\sigma_{E1} = \frac{\pi^2 E I_s}{A_E l^2} \tag{13}$$

where A_s is the area of the stiffener without attached plating, s is the plate breadth taken as the spacing between the stiffeners, t is the thickness of attached plating, σ_{C1} is the critical stress, σ_{E1} is the Euler column buckling stress, I_s is the moment of inertia of stiffeners with attached plating of width b_{ES}, which is defined as

$$b_{ES} = \begin{cases} \frac{s}{\beta_p} & \text{for } \beta_p > 1.0 \\ s & \text{for } \beta_p \le 1.0 \end{cases} \tag{14}$$

$$\beta_p = \frac{s}{t} \sqrt{\frac{\varepsilon \sigma_y}{E}} \tag{15}$$

where l_s is the span of stiffener equal to the spacing between the primary support members, and A_E is the area of stiffeners with attached plating of width b_{EP}, which is defined as

$$b_{EP} = \begin{cases} \left(\frac{2.25}{\beta_p} - \frac{1.25}{\beta_P^2} \right) s & \text{for } \beta_p > 1.25 \\ s & \text{for } \beta_p \le 1.25 \end{cases} \tag{16}$$

The equation describing the shortening portion of the stress-strain curve for the torsional buckling of stiffeners is

$$\sigma_{CR2} = \Phi \left(\frac{A_s \sigma_{C2} + st\sigma_{CP}}{A_s + st} \right) \tag{17}$$

where

$$\sigma_{C2} = \begin{cases} \dfrac{\sigma_{E2}}{\varepsilon} & \text{for } \sigma_{E2} \le \dfrac{\sigma_y}{2}\varepsilon \\ \sigma_y\left(1 - \dfrac{\sigma_y \varepsilon}{4\sigma_{E2}}\right) & \text{for } \sigma_{E2} > \dfrac{\sigma_y}{2}\varepsilon \end{cases} \tag{18}$$

$$\sigma_{CP} = \begin{cases} \left(\dfrac{2.25}{\beta_p} - \dfrac{1.25}{\beta_P^2}\right)\sigma_y & \text{for } \beta_p > 1.25 \\ \sigma_y \text{ for } \beta_p \le 1.25 \end{cases} \tag{19}$$

The equation describing the shortening portion of the stress-strain curve for the web local buckling of flanged stiffeners is

$$\sigma_{CR3} = \Phi\left(\frac{b_{EP}t + d_{EW}t_W + b_f t_f}{st + d_w t_W + b_f t_f}\right) \tag{20}$$

where d_w is the depth of the web, t_w is the thickness of the web, b_f is the breadth of the flange, t_f is the thickness of the flange, d_{EW} is the effective depth of the web and is defined as

$$d_{EW} = \begin{cases} \left(\dfrac{2.25}{\beta_W} - \dfrac{1.25}{\beta_W^2}\right)d_w & \text{for } \beta_W > 1.25 \\ d_w \text{ for } \beta_W \le 1.25 \end{cases} \tag{21}$$

$$\beta_W = \frac{d_w}{t_w}\sqrt{\frac{\varepsilon\sigma_y}{E}} \tag{22}$$

The equation describing the shortening portion of the stress-strain curve for the web local buckling of flat bar stiffeners is

$$\sigma_{CR4} = \Phi\left(\frac{st\sigma_{CP} + A_s\sigma_{C4}}{st + A_s}\right) \tag{23}$$

where

$$\sigma_{C4} = \begin{cases} \dfrac{\sigma_{E4}}{\varepsilon} & \text{for } \sigma_{E4} \le \dfrac{\sigma_y}{2}\varepsilon \\ \sigma_y\left(1 - \dfrac{\sigma_y\varepsilon}{4\sigma_{E4}}\right) & \text{for } \sigma_{E4} > \dfrac{\sigma_y}{2}\varepsilon \end{cases} \tag{24}$$

$$\sigma_{E4} = 160{,}000\left(\frac{t_w}{d_w}\right)^2 \tag{25}$$

For each structural element, the stress corresponding to a given element strain is to be taken as the minimum stress value from all applicable stress-strain curves for that element (IACS 2008).

5. Optimization-based ultimate strength calculation

In order to obtain results at least as accurate as the results of the incremental curvature method but with a significant reduction in computing time, a new approach is proposed in this section. In fact, this approach shares most of the features and steps of the incremental curvature method. The distinct difference is that instead of incrementing the curvature to obtain a complete moment-curvature curve, from which the ultimate moment is found, an optimization search algorithm is used with a goal of finding the ultimate moment in a few steps.

In essence, the moment-curvature relation can be viewed as a nonlinear function of a single continuous variable $M(\kappa)$, where the variable is the curvature κ. A value of the curvature κ exists at which the bending moment of the section is maximum. In the sense of optimization, the incremental method is an enumerative search technique in which the curvature variable is discretized to a large number of values at which $M(\kappa)$ is evaluated to determine which of these discrete values gives the maximum moment.

As a result of discretizing the continuous curvature variable, there is always a risk that the true maximum moment lies between two discrete curvature points. Needless to say, this risk is reduced by reducing the size of the increments, in turn increasing the number of discrete curvature points. However, this only comes with a higher computational cost. Furthermore, there is a wide range of search techniques regularly employed in optimization applications that are much more efficient than the enumerative search technique (Arora 2004).

Prior to starting the search process, steps 1 and 2 from the previous section need to be performed. The problem of finding the maximum bending moment of a ship hull cross section may be described by the following single objective nonlinear optimization problem

$$\textit{Given}\text{: Ship section dimensions and material properties} \tag{26a}$$

$$\textit{Find}\text{: } \kappa \tag{26b}$$

$$\textit{To Maximize}\text{: } |M(\kappa)| \tag{26c}$$

$$\textit{Such that}\text{: } \kappa > 0 \text{ (for sagging)} \tag{26d}$$

$$\kappa < 0 \text{ (for hogging)} \tag{26e}$$

Thus, the curvature κ is the design variable and $M(\kappa)$ is the "implicit" objective function to maximize. The objective function is implicit in the sense that its explicit dependence on the design variable is not known (Arora 2004). In fact, for each value of the curvature κ, the function $M(\kappa)$ is evaluated by performing steps 4, 5, and 6 from the previous section.

A choice of the search algorithm needs to be made. MATLAB offers a variety of search algorithms that can be used for optimization applications. In this study, two MATLAB optimization functions are used; namely *fmincon* and *fminbnd*. Among the various algorithms available by *fmincon*, the sequential quadratic programming method is implemented herein. At each major iteration, an approximation is made of the Hessian of the Lagrangian function using a quasi-Newton updating method. This is then used to generate a quadratic programming subproblem whose solution is used to form a search direction for a line search procedure (MathWorks 2008a). On the other hand, the algorithm available by *fminbnd* is not based on derivatives. Instead, it uses the golden-section search and parabolic interpolation. It solves for a local minimum in one dimension within a bounded interval. It is worth mentioning that the order of magnitude of the default tolerance for the design variables in MATLAB is larger than that required for the curvature design variable, which may be as small as 10^{-9}, and has to be reset accordingly.

At each iteration of the search process, the objective function $M(\kappa)$ is evaluated (by performing steps 4, 5, and 6 from the previous section) at least once. Once again, the location of the neutral axis needs to be found in step 5. This requires finding the value of the neutral axis that creates a stress distribution over cross section that satisfies longitudinal force equilibrium. Therefore, the longitudinal force resultant can be understood as a nonlinear function of one variable (i.e., the neutral axis location) and the objective is to find the root of this function. MATLAB offers the ability to do so using the function fzero (MathWorks 2008a). This function uses a combination of bisection, secant, and inverse quadratic interpolation methods. However, this function is only efficient

when the initial trial value provided is near the root. In the case of the incremental curvature method, the initial trial value is used as the neutral axis of the previous increment, which is near the current increment. However, because of the rapid movement of the neutral axis in the inelastic range, it is difficult to guess an initial trial value in the optimization search case since the design points may be far apart. Therefore, a custom subroutine was provided to solve the problem using the Newton-Raphson method for solving nonlinear equations (Arora 2004). In order to add further insurance to the performance of the subroutine against undesired divergence of the solution, a bounding range is specified for the values of the neutral axis. This bound takes values between zero and the depth of the cross section of the ship hull. If the search attempts to cross these bounds, or the number of iterations exceeds a given threshold, a new trial point is drawn randomly from a uniform distribution with parameters zero and the depth of the cross section of the ship hull.

The efficiency and speed of the optimization may well be improved by imposing bounds on the curvature design variable. A reasonable lower bound is the yielding curvature. The value of the maximum curvature specified by the IACS (2008) for the incremental method, (i.e., three times the yield curvature) may be reasonably used as an upper bound. Therefore, the problem becomes a constrained optimization specified as

$$\textit{Given}: \text{ Ship section dimensions and material properties} \quad (27a)$$

$$\textit{Find}: \ \kappa \quad (27b)$$

$$\text{To Maximize: } |M(\kappa)| \quad (27c)$$

$$\textit{Such that}: \ \kappa \leq 3\kappa_y \text{ and } \kappa > \kappa_y \text{ (for sagging)} \quad (27d)$$

$$\kappa \geq -3\kappa_y \text{ and } \kappa < -\kappa_y \text{ (for hogging)} \quad (27e)$$

To illustrate the proposed approach, a large-scale box girder example is investigated using both the curvature incremental method and the optimization approach. This box girder was originally tested experimentally by Dowling et al. (1973) and analytically investigated by others (Gordo & Guedes Soares 1996). Details of the box girder are given in Fig. 1 (Hughes 1983). The upper flange consisted of five in line panels 787 mm in length, the yield stresses of the compression flange, tension flange, web, and stiffeners are 298, 298, 211.6, and 276.5 N/mm^2, respectively, and the moduli of elasticities of these members are 208,500, 208,500, 216,200, and 191,500 N/mm^2, respectively (Hughes 1983). Initial deflections and an initial normalized residual stress ratio of 0.18 are considered (Hughes 1983). A computer program was developed to calculate the ultimate strength of ships using the incremental curvature method described in the previous section and was used to generate the moment curvature curve for the box girder considered. The results are shown in Fig. 2. The maximum sagging bending moment is obtained as the peak of the curve to be 1.52284×10^9 N · mm.

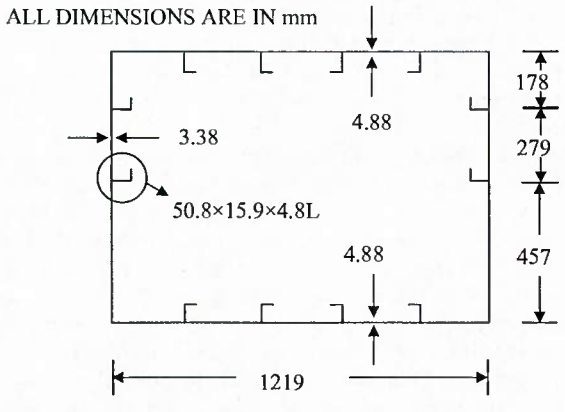

Fig. 1 Midsection of Dowling's box girder model tested in sagging (adapted from Hughes 1983)

The maximum sagging bending moment is now found using both MATLAB functions *fminbnd* and *fmincon*. Figure 3 shows the progress of the iterations in both *fmincon* and *fminbnd* over the moment-curvature curve. The initial design iteration is selected automatically be MATLAB. Note that some iteration results are not shown due to lack of space in the figure. Comparison between the results of the two methods and the incremental curvature method is provided in Table 1.

Table 1 shows that the optimization approaches are able to find the solution much faster than the incremental method approach. It can be seen, however, that the incremental method requires a short amount of time anyway, and thus for a deterministic one-time analysis the speed advantage of using optimization may not be significant. This advantage becomes significant when the strength has to be calculated a large number of times, such as in a simulation, and with systems more complex than the box-girder considered. Table 1 also shows that the optimization requires significantly fewer function evaluations than the incremental method.

It is also clear in Table 1 that *fmincon* requires fewer iterations than *fminbnd* but more function evaluations and longer computational time. This is because derivative-based search algorithms such as the sequential quadratic programming implemented in *fmincon* converge faster to the optimum solution than nonderivative-based algorithms such as the golden section and parabolic interpolation methods used in *fminbnd*. However, the approximation made of the Hessian of the Lagrangian function using a quasi-Newton updating method requires additional function evaluations. Furthermore, *fminbnd* obtained a higher maximum moment than *fmincon*. For a simple convex problem such as finding the peak of a moment

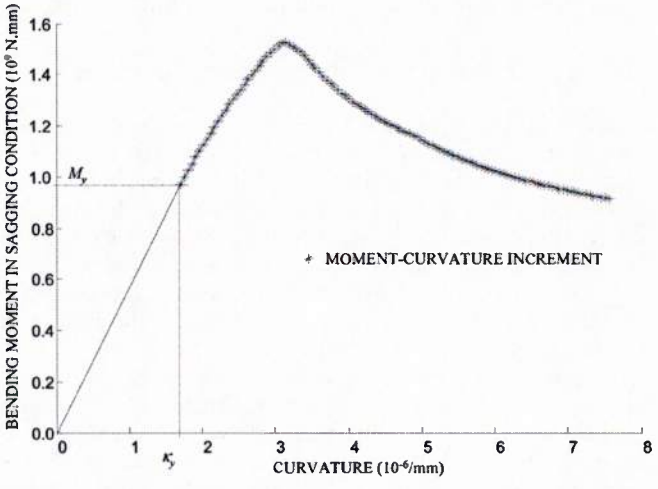

Fig. 2 Results of the incremental method for the box girder model

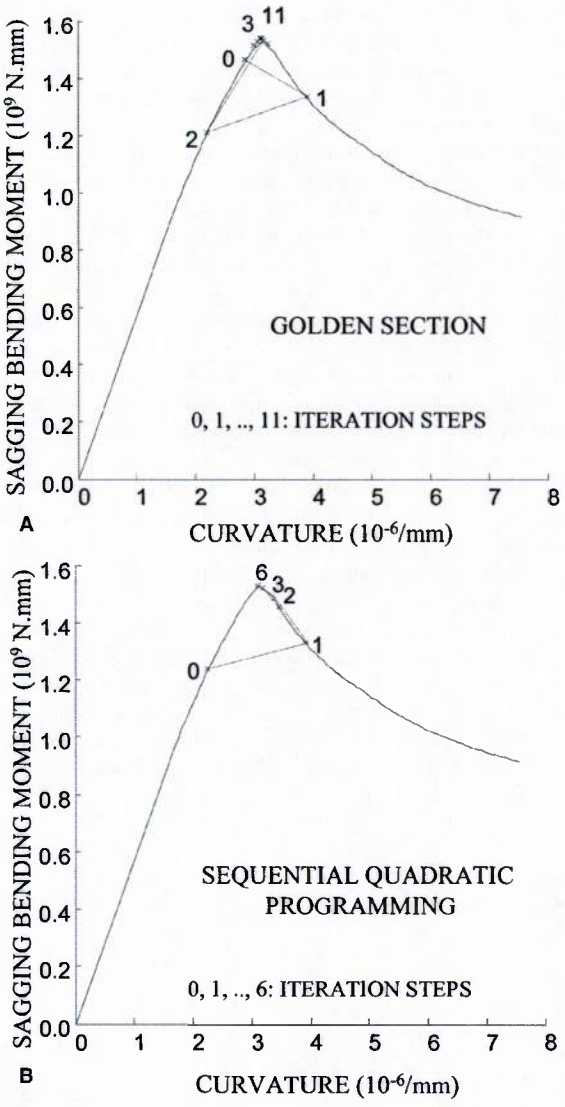

Fig. 3 Results of the optimization method for the box girder model using (A) golden section and (B) sequential quadratic programming

curvature function, a nonderivative-based algorithm such as that used by *fminbnd* is sufficient.

6. Latin-hypercube sampling and distribution fitting

Monte Carlo simulation is routinely used for uncertainty and sensitivity analysis of model outputs in a wide spectrum of scientific disciplines (Morgan & Henrion 1990). Any realistic uncertainty analysis, however, calls for the availability of a representative distribution of such outputs and can become extremely expensive in terms of both time and computer resources in the case of complex models and simple random sampling (Kyriakidis 2005).

McKay et al. (1979) suggested an alternative method of generating random samples that they call Latin hypercube sampling (Stein 1987). It is an intelligent alternative to simple random sampling, and a special case of stratified random sampling, which yields a more representative distribution of model outputs (in terms of smaller sampling variability of their statistics) for the same number of input simulated realizations (Kyriakidis 2005). This sampling technique allows the reduction of the number of necessary samples to reach a certain level of confidence (Neves et al. 2006) and saving both time and computer resources compared with Monte Carlo simulation.

Table 1 Comparison of the incremental method, *fminbnd*, and *fmincon* details for the box girder model

Method	Number of Increments or Iterations	Number of Function Evaluations	Ultimate Sagging Moment (N · mm)	Computation Time (sec)
Incremental method	117	117	1.52284×10^9	1.48
Fminbnd	11	12	1.540738×10^9	0.23
Fmincon	6	19	1.540273×10^9	0.31

Latin hypercube sampling has received numerous developments over the years. Today, various techniques are available (Iman & Conover 1982, Stein 1987, Owen 1994, Olsson et al. 2003). The following is an algorithm for the Latin hypercube sampling of correlated and/or uncorrelated random variables based on Olsson et al. (2003):

1. Generate the $N \times K$ matrix $\mathbf{P}$ where N denotes the required number of realizations and K denotes the number of random variables, in which each of the K columns is a random permutation of 1, .., N. Also generate the $N \times K$ matrix $\mathbf{R}$ of independent random numbers from the uniform (0,1) distribution.
2. Generate the matrix $\mathbf{Y}$ by dividing the elements of $\mathbf{P}$, p_{ij}, by the number of realizations plus 1, and mapping them on the Gaussian distribution with mean zero and standard deviation one as

$$y_{ij} = \Phi_{(0,1)}^{-1}\left(\frac{p_{ij}}{N+1}\right) \tag{28}$$

where $\Phi_{(0,1)}^{-1}$is the inverse of the cumulative standard normal distribution function.

3. Estimate the covariance matrix of $\mathbf{Y}$ and Cholesky decompose it as

$$\overline{\mathbf{L}}\,\overline{\mathbf{L}}^T = \mathrm{cov}(\mathbf{Y}) \tag{29}$$

where $\overline{\mathbf{L}}$ is lower triangular and cov($\mathbf{Y}$) is covariance of $\mathbf{Y}$.

4. Compute a new matrix $\mathbf{Y}^*$ as

$$\mathbf{Y}^* = \mathbf{Y}(\overline{\mathbf{L}}^{-1})^T \tag{30}$$

if the variables are statistically independent and

$$\mathbf{Y}^* = \mathbf{Y}(\overline{\mathbf{L}}^{-1})^T\mathbf{L}^T \tag{31}$$

if they are correlated, where $\mathbf{L}$ is the lower triangular matrix from the Cholesky decomposition of the target correlation matrix.

5. Generate the matrix $\mathbf{P}^*$, where its elements are the ranks of the elements of the columns of $\mathbf{Y}^*$.
6. Generate the matrix $\mathbf{S}$ as

$$\mathbf{S} = \frac{1}{N}(\mathbf{P}^* - \mathbf{R}) \tag{32}$$

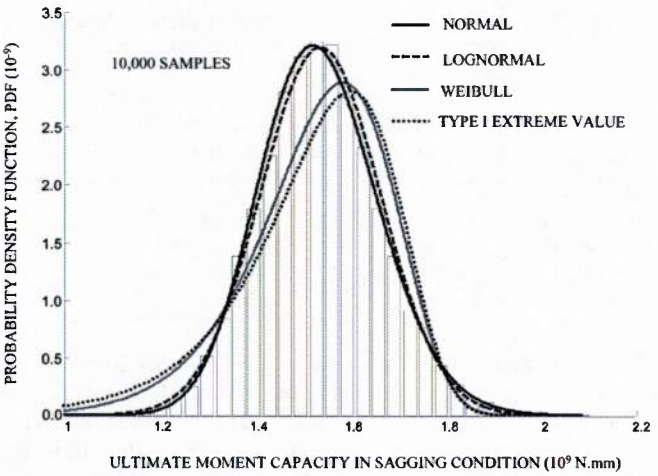

Fig. 4 Probability density function of the maximum sagging bending moment of the box girder model

7. Transform each element of **S** to the respective element of the marginal distribution **X** as

$$x_{ij} = F_{xj}^{-1}(s_{ij}) \tag{33}$$

where F_{xj}^{-1} is the inverse cumulative distribution of random variable x_j. Each vector $x_i = [x_{i1}\, x_{i2} \ldots x_{iK}]$ contains input data for one deterministic computation.

The correlation of the sample will approach the target correlation exactly if the random variables are Gaussian and approximately if the random variables are non-Gaussian. An iterative algorithm may be employed to improve the correlation in the non-Gaussian case (Olsson et al. 2003).

The outcome sample of the bending moment is used to find the most appropriate probability distribution of the strength of the ship hull and its parameters. The distributions considered in this study are the normal, lognormal, Weibull, and Type I extreme value distributions. The maximum likelihood estimate method is used to estimate the pertinent parameters of these probability distributions. This is done using the distribution fitting functions of MATLAB (MathWorks 2008b).

Details of the statistical characterization of the inherent uncertainties associated with material properties and fabrication details can be found in numerous references (Paik & Frieze 2001, Mansour & Hovem 1994, Atua 1998, Atua et al. 1996, Assakkaf 1998, Assakkaf et al. 2000). The details of the strength random variables considered in this study are as follows. The plate thickness t and yield strength σ follow a normal distribution with coefficients of variations (COV) of 0.05 and 0.10, respectively, and the Young's modulus E follows a lognormal distribution with COV of 0.03 (Paik & Frieze 2001). The different components of the ship hull (such as the different stiffeners) potentially have different material properties. However, it is most likely that these components are produced by the same manufacturer. Therefore, in this study, a correlation coefficient of 0.8 is assumed among the random variables (i.e., t, σ, and E) of the components with different material properties.

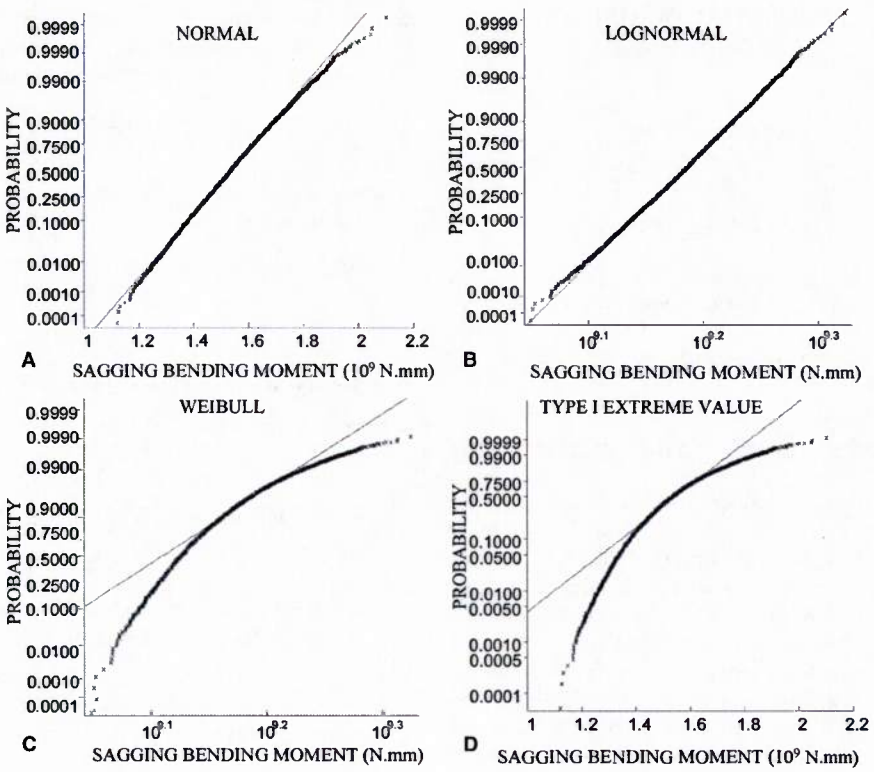

Fig. 5 Probability plots for the maximum sagging bending moment of the box girder model

Table 2 Results of the one-sample Kolmogorov-Smirnov (K-S) test for the maximum sagging moment of the box girder and the maximum likelihood estimates ($\rho = 0.8$)

	Normal	Lognormal	Weibull	Type I Extreme Value
Parameter 1	1.538457×10^9	21.15074	1.596660×10^9	1.601857×10^9
Parameter 2	$1.250356e \times 10^8$	0.08137556	12.47801	1.310436×10^8
K-S statistics	0.0145	0.0089	0.0607	0.0771
P value	0.0289	0.4096	1.7703×10^{-32}	3.7543×10^{-52}
Hypothesis rejected?	Yes	No	Yes	Yes

Table 3 Results of the one-sample Kolmogorov-Smirnov (K-S) test for the maximum sagging moment of the box girder and the maximum likelihood estimates ($\rho = 0.0, 0.8, 1.0$)

	Coefficient of Correlation		
	0.0	0.8	1.0
Distribution	Lognormal	Lognormal	Lognormal
Parameter 1	21.15172	21.15074	21.15048
Parameter 2	0.07778600	0.08137556	0.08230746
Coefficient of variation	0.0777	0.0813	0.0822
K-S statistics	0.0055	0.0089	0.0101
P value	0.9243	0.4096	0.2612

Table 4 Comparison of the incremental method, *fminbnd*, and *fmincon* details for the VLCC Energy Concentration

Method	Number of Increments or Iterations	Number of Function Evaluations	Ultimate Sagging Moment (N · mm)	Computation Time (sec)
		Sagging Condition		
Incremental method	180	180	1.69186×10^{13}	20.58
Fminbnd	7	8	1.691691×10^{13}	2.91
Fmincon	2	9	1.690656×10^{13}	3.28
		Hogging Condition		
Incremental method	183	183	1.79254×10^{13}	22.59
Fminbnd	5	6	1.792356×10^{13}	3.16
Fmincon	2	6	1.779753×10^{13}	4.35

Consider again the box girder shown in Fig. 1. Latin hypercube sampling simulation is conducted with 10,000 samples. Figure 4 shows a plot of the probability distributions obtained from fitting the outcome sample of simulating the maximum sagging bending moment of this box girder. It is visually clear that the Weibull and type I extreme value distributions are not good fit for this case. It is still necessary to systematically determine the best fit among these distributions. Goodness-of-fit tests are used for this purpose.

7. Goodness-of fit tests

The goodness-of-fit test involves visual observation of the probability plot and conducting a statistics hypothesis test. Visually, the data are plotted on a probability plot of the given distribution. If the distribution fits the data, the plotted points will appear roughly linear and will fall close the fitted distribution line (Ang & Tang 2007). Figure 5 shows the probability plot for the outcome sample

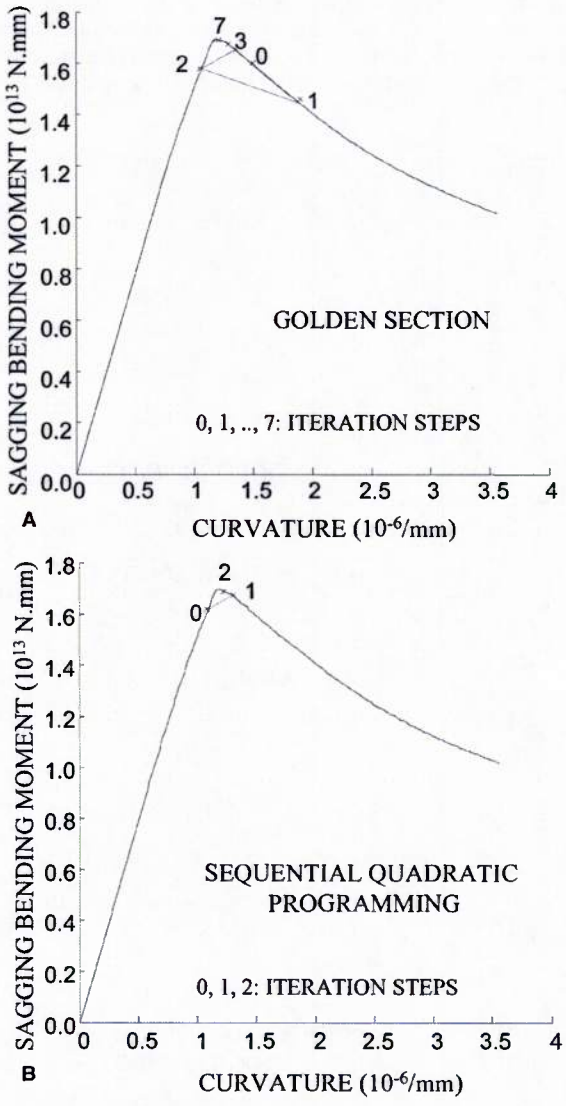

Fig. 6 Results of the optimization method for the VLCC Energy Concentration maximum sagging moment using (A) golden section and (B) sequential quadratic programming

of simulating the maximum sagging bending moment of the box girder example shown in Fig. 1. It is clear that the Weibull and type I extreme value distributions are not good fit for this case. It is also clear that the lognormal distribution shows better fit for the data sample.

Hypothesis testing is a common method of drawing inferences about a population based on statistical evidence from a sample (MathWorks 2008b). To conduct a hypothesis test, a test statistic relevant to the distribution is computed to summarize the sample. The smaller the statistics, the better the fit and the distribution with the smallest statistics is the best fit. It is also possible to determine if the distribution is suitable or not for a given data set by calculating the P value. The P value of a test is the probability, under the null hypothesis, of obtaining a value of the test statistic as extreme or more extreme than the value computed from the sample (MathWorks 2008b). A null hypothesis is an assertion about the data set. It is "null" in the sense that it often represents a status quo belief, such as the absence of a characteristic or the lack of an effect. A significance level needs to be decided. The significance level of a test is a threshold of probability α of rejecting the null hypothesis when it is actually true. A typical value of α is 0.05. If the P value of a test is less than α, the test rejects the null hypothesis. If the P value is greater than α, there is insufficient evidence to reject the null hypothesis. Note that lack of evidence for rejecting the null hypothesis is not evidence for accepting the null hypothesis (MathWorks 2008b). Many hypothesis tests are available. MATLAB (MathWorks 2008b) provides a wide range of these tests, and the one-sample Kolmogorov-Smirnov test is used for this study.

Table 2 shows results of conducting the one-sample Kolmogorov-Smirnov test for the maximum sagging moment of the box girder shown in Fig. 1 against the considered four distributions and the maximum likelihood estimates of the parameters of these distributions. The typical significance level of 0.05 is used. The meaning of the parameters depends on the distribution. For example, the first and second parameters of the normal distribution are its mean and standard deviation, respectively. It turns out that the lognormal distribution is the only distribution that is not rejected with this significance level. The normal distribution is rejected at this signif-

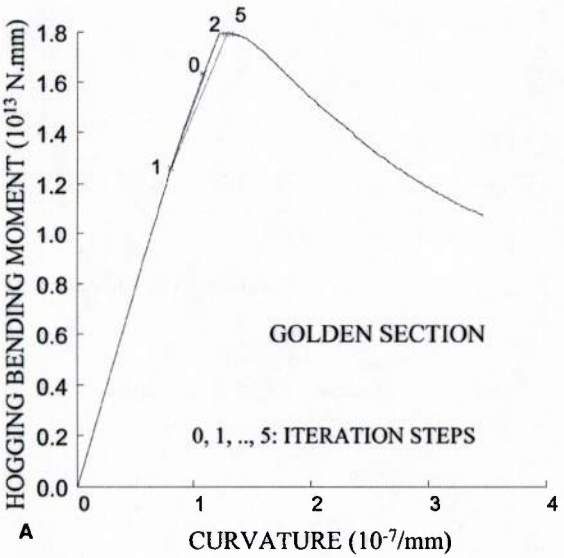

Fig. 7 Results of the optimization method for the VLCC Energy Concentration maximum hogging moment using (A) golden section and (B) sequential quadratic programming

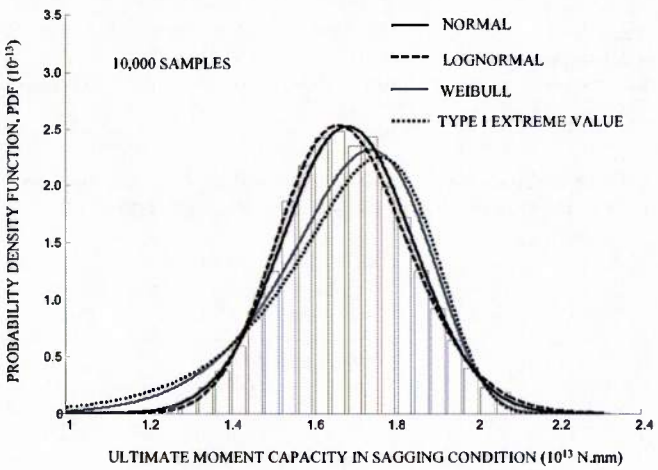

Fig. 8 Probability density function of the VLCC Energy Concentration maximum sagging moment

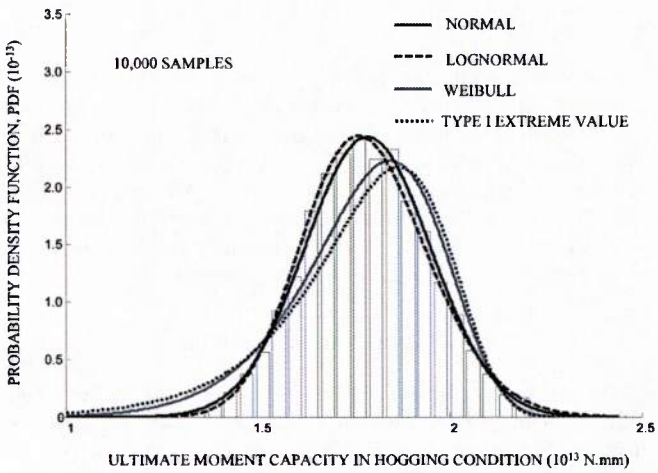

Fig. 9 Probability density function of the VLCC Energy Concentration maximum hogging moment

icance level despite its good visual fit using the probability paper. Reducing the significance level only to 0.028 though will prevent the normal distribution from being rejected. However, the lognormal distribution provides the lowest Kolmogorov-Smirnov test statistics, and thus it should be used for this sample anyway.

Now, the impact of the assumed coefficient of correlation is studied. Two simulations with 10,000 Latin hypercube samples each are conducted where a coefficient of correlation of 0.0 is used in one simulation and 1.0 in the other. The Kolmogorov-Smirnov test is conducted for the results of both samples, and it was concluded that the lognormal distribution is the best fit for both cases. The results are shown in Table 3. It can be seen that the effect of the correlation coefficient in not significant.

8. Application

As previously mentioned, the proposed approach for finding the maximum bending moment of a ship hull shares most of the features of the rigorous incremental curvature method. It departs from the rigorous incremental curvature method at the point where incrementation of the curvature is performed. Instead, an optimization search algorithm is implemented. Therefore, any result obtained for the maximum bending moment lies on the moment curvature curve obtained by the incremental method and not necessarily at the same curvature increments of the incremental method. Hence, it is rational to compare the performance of this method with the performance of the incremental method.

A good example of a large-scale ship hull that has already been investigated by the rigorous incremental method as presented by Gordo et al. (1996) is the VLCC Energy Concentration. The validity of the results was checked with other predictions of the strength of the same ship (Rutherford & Caldwell 1990). The plate strength models used in Gordo et al. (1996) are based on the models reported in Gordo and Guedes Soares (1993). However, these models are obtained in this study based on the IACS (2008) formulations described previously and considering initial imperfections due to initial deflections and initial residual stresses. The initial normalized residual stress ratio assumed is 0.05.

The VLCC Energy Concentration collapsed in Europort on July 22, 1980 (Paik & Mansour 1995). The ship was 10 years old and had been constructed by Kawasaki Heavy Industries, in March 1970, in Japan, according the current design practice at the time for VLCC (Gordo et al. 1996). Calculations performed by Rutherford and Caldwell (1990) concluded that the failure hogging moment should be 17,940 MN · m. A detailed description of this ship can be found in Gordo et al. (1996). This model has 242 reinforced elements and 2 plate elements.

The maximum sagging and hogging bending moments are first obtained deterministically using the incremental and optimization approaches and based on the mean values of the strength random variables. The results are shown in Table 4 and Figs. 6 and 7. The significant reduction in the amount of computations in the optimization approach with respect to the incremental method is evident. The savings in computational time becomes more apparent when a simulation is conducted and the strength evaluation is required to be performed thousands of times. Table 4 also shows that the results obtained by optimization are in good agreement with the results of the incremental method, although the incremental method provided slightly higher maximum bending moments. However, reducing the convergence tolerance on the curvature design variable used was

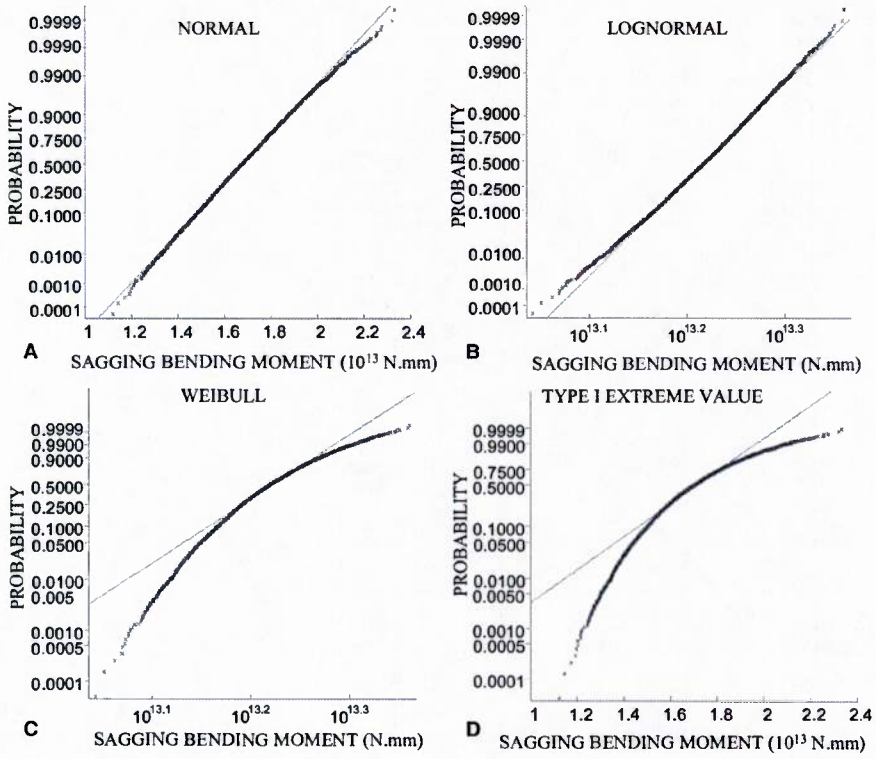

Fig. 10 Probability plots for the VLCC Energy Concentration maximum sagging moment

found to overcome this point, but with an increase in the number of iterations function, evaluations, and computational time.

Next, a Latin hypercube sampling simulation is performed with 10,000 samples. The resulting fitted probability density functions are shown in Figs. 8 and 9 for the maximum sagging and hogging bending moments, respectively. Also, the probability plots for these two bending moments are shown in Figs. 10 and 11, respectively. It is clear in the figures that the normal distribution shows the best fit for the data. This observation is confirmed with the results of the performed Kolmogorov-Smirnov test shown in Table 5. In fact, the normal distribution hypothesis is the only one not rejected by the test. Furthermore, the Kolmogorov-Smirnov test statistics for the normal distribution is the lowest among the four distributions considered. Thus, it can be concluded that the bending resistance of the VLCC Energy Concentration follows a normal distribution with mean and standard deviation shown in Table 5 for both the sagging and hogging conditions and coefficient of variations of 0.0934 and 0.0915 for the sagging and hogging conditions, respectively.

9. Conclusions

In this study, an efficient approach for the determination of the probabilistic strength of the ship hull is presented. Since the probabilistic aspects are captured using simulation, which requires the calculation of the strength a large number of times, a fast and accurate method for analyzing the ship hull is required. In order to obtain this required speed and accuracy, this study presents a novel deterministic method for the calculation of the strength of the ship hull. In this method, the ship hull cross section is discretized into elements, each composed of a longitudinal stiffener and its attached plate. Stresses in these elements are determined using their respective constitutive models. These models take into account the various possible failure modes and initial imperfections. The ultimate strength is found by an optimization search algorithm. For a given curvature, the bending moment in the section is determined in a way similar to that of the rigorous incremental method. However, instead of finding the ultimate strength by incrementing the curvature, the ultimate strength is found by an optimization search algorithm. The curvature is treated as a design variable, and the objective is to find the curvature that maximizes the bending moment.

It is shown that the optimization requires a fraction of the number of function evaluations the incremental method requires. In addition, it is concluded that for a simple convex problem such as finding the peak of a moment curvature function, a nonderivative-based algorithm such as the golden section method with parabolic interpolation is sufficient.

The method is then applied with a Latin-hypercube sampling algorithm. This sampling technique allows the reduction of the number of necessary samples to reach a certain level of confidence. The output sample is tested against several potential distributions. The parameters of these distributions are found by the maximum likelihood estimate method. Goodness-of-fit tests such as the one-sample Kolmogorov-Smirnov test are performed to determine the best-fit distribution. Eventually, the ultimate strength is provided in terms of its best-fit probability distribution and the parameters of this distribution.

In conclusion, the computational framework presented in this study provides efficient means for finding the probabilistic ultimate strength of ship hulls considering fabrication and material uncertainties.

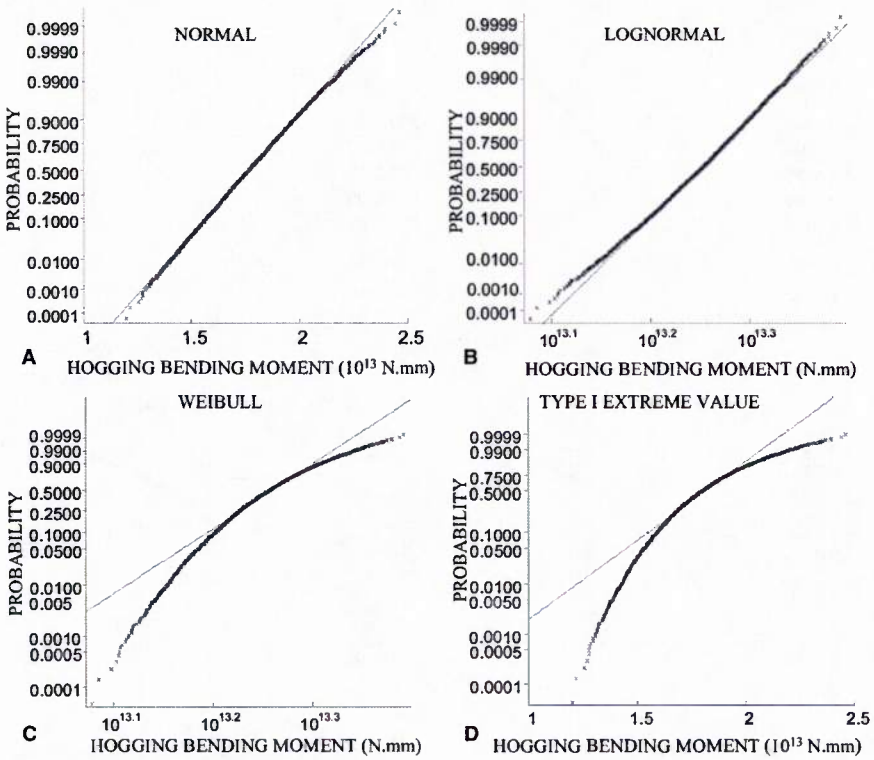

Fig. 11 Probability plots for the VLCC Energy Concentration maximum hogging moment

Table 5 Results of the one-sample Kolmogorov-Smirnov (K-S) test for the maximum sagging and hogging moments of the VLCC Energy Concentration and the maximum likelihood estimates

	Normal	Lognormal	Weibull	Type 1 Extreme Value
		Sagging Condition		
Parameter 1	1.688411×10^{13}	30.45301	1.760682×10^{13}	1.768078×10^{13}
Parameter 2	1.576827×10^{12}	0.09388781	11.02848	1.634328×10^{12}
K-S statistics	0.0109	0.0147	0.0517	0.0725
P value	0.1854	0.0267	1.0654×10^{-23}	3.5636×10^{-46}
Hypothesis rejected?	No	Yes	Yes	Yes
		Hogging Condition		
Parameter 1	1.787968×10^{13}	30.51047	1.863090×10^{13}	1.870597×10^{13}
Parameter 2	1.636424×10^{12}	0.09201282	11.26021	1.692360×10^{12}
K-S statistics	0.0106	0.0142	0.0510	0.0726
P value	0.2071	0.0350	4.4494×10^{-23}	2.4717×10^{-46}
Hypothesis rejected?	No	Yes	Yes	Yes

Acknowledgment

The support from the Office of Naval Research under award N-00014-08-0188 is gratefully acknowledged. The opinions and conclusions presented in this paper are those of the authors and do not necessarily reflect the views of the sponsoring organization.

References

Ang, A. H.-S., and Tang, W. H. 2007 *Probability Concepts in Engineering: Emphasis on Applications to Civil and Environmental Engineering*, vol. II, Wiley and Sons, New York, 406 pages.

Arora, J. 2004 *Introduction to Optimum Design*, 2nd ed., Elsevier Academic Press, New York, 728 pages.

Assakkaf, I. A. 1998 *Reliability-Based Design of Panels and Fatigue Details of Ship Structures*, dissertation submitted to the Faculty of the Graduate School of the University of Maryland, College Park, MD, in partial fulfillment of the requirements for the degree of Doctor of Philosophy.

Assakkaf, I. A., Ayyub, B. M., and Mattei, N. J. 2000 Reliability-based load and resistance factor design (LRFD) of hull structural components of surface ships. *Proceedings*, 37th Annual Technical Symposium, Association of Scientists and Engineers.

Atua, K. I. 1998 *Reliability-Based Structural Design of Ship Hull Girders and Stiffened Panels*, dissertation submitted to the Faculty of the Graduate School of the University of Maryland, College Park, MD in partial fulfillment of the requirements for the degree of Doctor of Philosophy.

Atua, K. I., Assakkaf, I. A., and Ayyub, B. M. 1996 Statistical characteristics of strength and load random variables of ship structures. *Proceedings*, 1996 ASCE Specialty Conference on Probabilistic Mechanics and Structure Reliability, Frangopol, D. M., and Grigoriu, M. D., editors, August 7–9, 106–109.

Caldwell, J. B. 1965 Ultimate longitudinal strength, *Transactions of RINA*, **107,** 411–430.

Chen, Y.-K., Kutt, L. M., Piaszczyk, C. M., and Bieniek, M. P. 1983 Ultimate strength of ship structures, *SNAME Transactions*, **91,** 149–168.

Dowling, P. J., Chatterjee, S., Frieze, P. A., and Moolani, F. M. 1973 Experimental and predicted collapse behavior of rectangular steel box girders. *Proceedings*, International Conference on Steel Box Girder Bridges, Institute of Civil Engineers, London, 77–94.

Faulkner, D. 1975 A review of effective plating for use in the analysis of stiffened plating in bending and compression. Journal of Ship Research, **19,** 1, 1–17.

Gordo, J. M., and Guedes Soares, C. 1993 Approximate load shortening curves for stiffened plates under uniaxial compression. *Proceedings*, Fifth International Conference on the Integrity of Offshore Structures, Faulkner, D., Cowling, M. J., Incecik, A., and Das, P. K., editors, EMAS, Glasgow, U.K., June 17–18, 189–211.

Gordo, J. M., and Guedes Soares, C. 1996 Approximate method to evaluate the hull girder collapse strength, *Marine Structures*, **9,** 3–4, 449–471.

Gordo, J. M., Guedes Soares, C., and Faulkner, D. 1996 Approximate assessment of the ultimate longitudinal strength of the hull girder. Journal of Ship Research, **40,** 1, 60–69.

Guedes Soares, C. 1988 Design equation for the compressive strength of unstiffened plate elements with initial imperfections, *Journal of Constructional Steel Research*, **9,** 287–310.

Guedes Soares, C., Dogliani, M., Ostergaard, C., Parmentier, G., and Pedersen, P. T. 1996 Reliability based ship structural design, *Transactions of the Society of Naval Architects and Marine Engineers*, **104,** 357–389.

Guedes Soares, C., and Teixeira, A. P. 2000 Structural reliability of two bulk carrier designs, *Marine Structures*, **13,** 2, 107–128.

Hess, P. E., and Lua, J. 2003 Hybrid reliability predictions of single and advanced double-hull ship structures. Journal of Ship Research, **47,** 2, 155–176.

Hughes, O. F. 1983 *Ship Structural Design: A Rationally-Based, Computer-Aided, Optimization Approach*, Wiley and Sons, New York, 582 pages.

IACS 2008 Common structural rules for double hull oil tankers, International Association of Classification Societies. Available at: http://www.iacs.org.uk.

Iman, R. L., and Conover, W. J. 1982 A distribution-free approach to inducing rank correlation among input variables. *Communications in Statistics Part B, Simulation and Computation*, **11,** 3, 311–334.

Kutt, L. M., Piaszczyk, C. M., Chen, Y. K., and Lin, D. 1985 Evaluation of the longitudinal ultimate strength of various ship hull configurations, *SNAME Transactions*, **93,** 33–53.

Kyriakidis, P. C. 2005 Sequential spatial simulation using Latin hypercube sampling (In: Leuangthong, O., and Deutsch, C. V., editors, *Proceedings*, Geostatistics Banff 2004, Seventh International Geostatistics Congress) *Quantitative Geology and Geostatistics*, **14,** 1, 65–74.

Mansour, A. E. 1997 *Assessment of Reliability of Ship Structures*, Ship Structure Committee, Washington, D. C., SSC-398.

Mansour, A. E., and Hovem, L. 1994 Probability based ship structural analysis, Journal of Ship Research, **38,** 4, 329–339.

MathWorks 2008a *Optimization Toolbox 4 User's Guide*, The MathWorks, Inc., 575 pages.

MathWorks 2008b *Statistics Toolbox 7 User's Guide*, The MathWorks, Inc., 1749 pages.

McKay, M. D., Conover, W. J., and Beckman, R. J. 1979 A comparison of three methods for selecting values of output variables in the analysis of output from a computer code, *Technometrics*, **21,** 2, 239–245.

Morgan, M. G., and Henrion, M. 1990 Uncertainty: A guide to dealing with uncertainty in quantitative risk and policy analysis, *Cambridge University Press*.

Neves, L. C., Frangopol, D. M., and Cruz, P. J. 2006 Probabilistic lifetime-oriented multiobjective optimization of bridge maintenance: single maintenance type, *Journal of Structural Engineering*, **132,** 6, 991–1005.

Olsson, A., Sandberg, G., and Dahlblom, O. 2003 On Latin hypercube sampling for structural reliability analysis, *Structural Safety*, **25,** 1, 47–68.

Owen, A. B. 1994 Controlling correlations in Latin hypercube samples, *Journal of the American Statistical Association*, **89,** 428, 1517–1522.

Özgüç, Ö., Das, P. K., and Barltrop, N. 2006 The new simple equations for the ultimate compressive strength of imperfect stiffened plates, *Ocean Engineering*, **34,** 7, 970–986.

PAIK, J. K., AND FRIEZE, P. A. 2001 Ship structural safety and reliability, *Progress in Structural Engineering and Materials,* **3,** 2, 198–210.

PAIK, J. K., AND MANSOUR, A. E. 1995 A simple formulation for predicting the ultimate strength of ships, *Journal of Marine Science and Technology,* **1,** 1, 52–62.

RUTHERFORD, S. E., AND CALDWELL, J. B. 1990 Ultimate longitudinal strength of ships: a case study, *SNAME Transactions,* **98,** 441–471.

SMITH, C. 1977 Influence of local compressive failure on ultimate longitudinal strength of a ship's hull, *Proceedings,* PRADS: International Symposium on Practical Design in Shipbuilding, Tokyo, 18–20.

SMITH, M. J., AND PEGG, N. G. 2003 Automated assessment of ultimate hull girder strength. *Journal of Offshore Mechanics and Arctic Engineering,* **125,** 3, 211–218.

STEIN, M. 1987 Large sample properties of simulations using Latin hypercube sampling, *Technometrics,* **29,** 2, 143–151.

Appendix II

Alberto Decò, Dan M. Frangopol and Nader M. Okasha, (2011). Time-variant redundancy of ship structures. *Journal of Ship Research*, 55(3):208-219, 2011.

Journal of Ship Research, Vol. 55, No. 3, September 2011, pp. 208–219

Time-Variant Redundancy of Ship Structures

Alberto Decò,* **Dan M. Frangopol,†** and **Nader M. Okasha***

**Graduate Research Assistant, Department of Civil & Environmental Engineering, Center for Advanced Technology for Large Structural Systems (ATLSS) Lehigh University, Bethlehem, Pennsylvania, USA*

†*Professor and Fazlur R. Khan Endowed Chair of Structural Engineering and Architecture, Department of Civil & Environmental Engineering, Center for Advanced Technology for Large Structural Systems (ATLSS) Lehigh University, Bethlehem, Pennsylvania, USA*

An efficient procedure for the computation of the redundancy of ship structures is presented. The changes in the redundancy due to corrosion section loss over time are also studied. Moreover, uncertainties associated with structural geometry, material properties, and loading, are accounted for. In order to calculate the redundancy index, the probability of failure of the first component and the probability of ultimate failure of the whole hull girder must be evaluated. The probability of failure is computed using a hybrid Latin Hypercube - second-order reliability method (SORM) technique. The deterministic analyses during the simulations are conducted using an optimization approach for computing the ultimate bending strength of the whole hull girder and the progressive collapse method for computing the first bending failure.

Keywords: design (vessels); redundancy

1. Introduction

A SHIP STRUCTURE can be represented and analyzed as a stiffened box girder. The longitudinal strength of the hull girder at midship is of critical interest because the structure is primarily subjected to vertical bending moments that induce axial stresses on the box girder panels (Luís et al. 2009). Accordingly, failure of a ship structure is most likely to occur at midship as a result of the vertical moments induced by still water and waves.

Complete collapse of the ship hull is achieved by reaching its ultimate bending strength. However, in redundant ship structures, this limit state is preceded by a series of failures in the stiffeners and/or panels. The occurrence of the failure of the first component (i.e., stiffened plate) of a ship, denoted herein as the first failure, should be a clear warning that collapse of this ship may be imminent. The range between first failure moment and ultimate failure moment can be used to quantify system redundancy (Hendawi & Frangopol 1994). Measures of redundancy have been intensely investigated and proposed (Frangopol 1987, Frangopol & Curley 1987, Fu 1987, Frangopol et al. 1992). It was generally concluded that the associated probability can be effectively used to represent the occurrence of each of these events (i.e., first and ultimate failures) under uncertainty and hence used to quantify the redundancy of the system.

The variation of redundancy over time is an issue that should be part of any decision-making process. Okasha and Frangopol (2010a) have shown that redundancy of certain structural systems may decrease to critical levels over time. In addition, Frangopol and Okasha (2008) investigated and proposed several measures of time-variant redundancy.

Because of the presence of uncertainties, structural performance evaluation, in general, involves a great deal of variability, and the considered variables are usually described by their associated probability distributions (Ang & Tang 2007). For instance, dimensions, material properties, applied loads, and model-related uncertainties all contribute to the uncertainty in the analysis results. Uncertainties are always present; some of them can be reduced by improving the knowledge or the quality of the prediction model (epistemic uncertainties), and others cannot be reduced because of the intrinsic nature of the randomness (aleatory uncertainties) (Ang & de Leon 2005). The probability of failure of a structure, computed by well-established reliability methods, is an efficient measure for quantifying its safety under uncertainty.

Ship reliability-based studies were conducted, not only to account for optimum and safe design, but also to obtain a life-cycle performance assessment including costs associated with maintenance actions (Ayyub et al. 1989, Ayyub & White 1990,

Manuscript received at SNAME headquarters November 18, 2009; revised manuscript received March 15, 2011.

Nikolaidis et al. 1993). The literature is rich with studies of the reliability of ship structures with respect to their ultimate flexural failure (Mansour & Hovem 1994, Mansour 1997, a special issue of the *Naval Engineers Journal* 2002, Ayyub et al. 2002, Hussein & Guedes Soares 2009). Even studies targeting the estimation of the service life of ship structures were conducted based on the ultimate flexural failure (Ayyub et al. 2000). In addition, numerous studies of time-variant reliability with respect to the ultimate flexural failure of ship structures have been conducted (Guedes Soares & Garbatov 1998, 1999, Paik et al. 1998, Paik & Frieze 2001, Akpan et al. 2002). Only recently, Lua and Hess (2006) analyzed the reliability of ship structures with respect to the first failure. In their study, a hybrid Monte Carlo simulation—FORM method, proposed in Lua and Hess (2003) was used.

The objective of this paper is to investigate the time-variant redundancy of ship structures. The resistance with respect to the ultimate and first failure vertical bending moments is calculated by a MATLAB program (MathWorks 2008a, 2008b) developed by the authors, where the ultimate failure moment is computed using an optimization-based method (Okasha & Frangopol 2010b), and the first failure moment is computed using the progressive collapse method (Hughes 1983). The reliability computations are performed using the program CALREL (Liu et al. 1989), which is linked to the developed MATLAB program. The resistance degrades with time because of corrosion. The developed MATLAB program provides probability of failure, reliability, and redundancy over time using a hybrid Latin Hypercube sampling (Olsson et al. 2003) - second-order reliability method (SORM) technique (Fiessler et al. 1979). Moreover, the components associated with the probability of occurrence of the first failure are identified in this paper. The concepts presented are applied to two ship structures.

2. Resistance modeling

The ultimate and first failure moment analyses are performed assuming that the structure is subdivided into two types of elements as suggested by the IACS guidelines (IACS 2008):

- Hard corners such as plating areas adjacent to intersecting plates
- Stiffened plates (components) such as the structural system composed of the stiffener and its portion of plating.

Initial imperfections in the stiffened panels can be taken into account by introducing reduction factors applied to the effective width b_E of the plating (Özgüc et al. 2006). The reduced effective width b'_E is expressed as:

$$b'_E = b_E R_d R_r R_y R_\tau R_q \tag{1}$$

in which R_d is a reduction factor due to nonstraightness of stiffened panel, R_r is a reduction factor due to residual stresses induced by welding, R_y is a reduction factor due to yielding, R_τ is a reduction factor due to shear stress, and R_q is a reduction factor due to lateral pressure load. In this study, only nonstraightness of stiffened panel and residual stress induced by welding are considered. The reduction factors R_d and R_r are (Özgüc et al. 2006):

$$R_d = 1.0 - 0.2323\, f(\lambda) g(\beta_s) \tag{2}$$

$$f(\lambda) = \begin{cases} 0.015 & \text{for } 0 < \lambda \le 0.35 \\ -1.03 + 2.341\lambda - 1.344\lambda^2 + 0.212\lambda^3 & \text{for } \lambda > 0.35 \end{cases} \tag{3}$$

$$g(\beta_s) = \begin{cases} 10.818 + 0.204\beta_s - 5.177\beta_s^2 & \text{for } 1 < \beta_s \le 1.5 \\ 4.594 - 0.805\beta_s + 0.255\beta_s^2 & \text{for } 1.5 < \beta_s \le 2.0 \\ 6.404 - 1.847\beta_s + 0.371\beta_s^2 & \text{for } 2.0 < \beta_s \le 2.5 \\ 5.435 - 1.213\beta_s + 0.202\beta_s^2 & \text{for } 2.5 < \beta_s \le 4.0 \end{cases} \tag{4}$$

$$R_r = 1.0 - \left[\frac{\mu}{8.1(\beta_s - 1.901)^2 + 1}\right] \tag{5}$$

where $\mu = \sigma_r/\sigma_{Yp}$ is the normalized welding residual stress, σ_r is the welding-induced residual stress, σ_{Yp} is the plating yielding stress, λ is the beam-column slenderness ratio, and β_s is the slenderness ratio. Accordingly, the aforementioned introduced reduced effective width is used while evaluating the ultimate strength and the strength associated with the occurrence of first yielding. Moreover, as already mentioned, geometry uncertainties are taken into consideration.

2.1. First failure evaluation

The first failure in the ship is determined herein using the method presented in Hughes (1983). This approach is based on solving the mathematical closed-form equations governing the stability problem of axially loaded stiffened plates. In essence, the method provides the ultimate strength of the ship hull. In this approach, the assumption made is that a stiffened panel is removed from the system once it fails (i.e., its postultimate behavior is neglected). However, in this paper, this method is only used for the computation of the failure of the first component. Hence, the mentioned assumption used for continuing the computations up to the ultimate strength is not needed and has no bearing on the computation of the first bending failure. While considering the imperfection given by the approach provided by Özgüc et al. (2006), the ones included in Hughes's method are neglected (residual stresses and nonstraightness of stiffened panel), and the associated equations are accordingly modified in order to avoid double-counting such imperfections. The following two collapse modes are considered (Hughes 1983).

2.1.1. Mode collapse I: compression failure of the stiffener. The first failure mode is characterized by the combination of in-plane compression and negative bending moment as shown in Fig. 1(a). The collapse occurs because of compression failure of the stiffener flange when the total stress throughout the thickness of the flange has reached the failure value, which is the minimum between the stiffener yielding stress and the tripping stress.

In this failure mode the stiffener flange is compressed; therefore, the stiffener is subjected to local buckling effects by twisting about its line of attachment to the plating (tripping). The tripping stress can be calculated as (Hughes 1983):

$$\sigma_{a,T} = \min_{m=1,2,\ldots} \left\{ \frac{1}{I_{sp} + (2C_r b^3 t/\pi^4)} \left[GJ + \frac{m^2\pi^2}{a^2} EI_{sz} d^2 + \frac{4dC_r}{\pi^2 b}\left(\frac{a^2}{m^2} + b^2\right)\right]\right\} \tag{6}$$

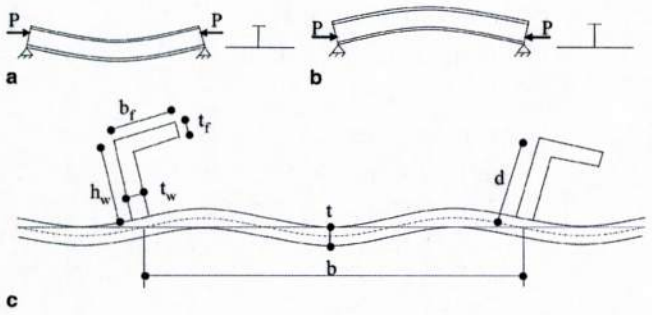

Fig. 1 Modes I (a) and II (b) of collapse and (c) tripping of an in-plane compressed stiffened panel (adapted from Hughes 1983)

where I_{sz} is the moment of inertia of the stiffener (only) about an axis through the centroid of the stiffener and parallel to the web, I_{sp} is the polar moment of inertia of the stiffener (only) about the center of rotation, d is the distance from the shear center to the point of attachment, t is the plating thickness, a is the panel length, G is the shear modulus, J is the torsion constant, E is the elastic modulus, m is the failure mode, and C_r is a correction factor defined as:

$$C_r = \frac{1}{1 + 0.4(t/t_w)^3(d/b)} \tag{7}$$

in which t_w is the stiffener web thickness.

The failure modes considered for the tripping stress determination are the first five (i.e., $m = 1, 2, 3, 4, 5$). Higher modes are unnecessary because they would provide higher stress values. For example, Fig. 1(c) shows the second failure mode ($m = 2$). The tripping stress is the minimum stress associated with each failure mode.

Once the effect of buckling has been taken into account, the failure stress $\sigma_{F,I}$ will be the minimum stress between the tripping $\sigma_{a,T}$ and the yielding stress σ_Y:

$$\sigma_{F,I} = \min(\sigma_{a,T}, \sigma_Y) \tag{8}$$

According to Hughes (1983), once the strength ratio R_I (associated with Mode I of collapse) is obtained, the maximum stress (failure value) that can be reached by the cross section at the farthest point from the centroid is:

$$\sigma_{a,u,I} = \sigma_{F,I} R_I \tag{9}$$

2.1.2. Mode collapse II: compression failure of the plating. In the second mode, the collapse occurs as a result of the compression failure of the plating. In this case, the combination of in-plane compression and positive bending moment induces compression on the plating as shown in Fig. 1(b).

Because of the compression of the welded plating, which has a complex inelastic failure behavior, the relation between the applied stress and the average strain becomes highly nonlinear. The procedure introduced involves the consideration of the secant elastic modulus E_s, which is the slope of the line joining the origin and the point of plate failure in the stress-strain diagram, so that $E_s = TE$ (E is the original value of the elastic modulus) in which (Hughes 1983):

$$T = 0.25\left(2 + \xi - \sqrt{\xi^2 - \frac{10.4}{\beta_p^2}}\right) \tag{10}$$

$$\xi = 1 + \frac{2.75}{\beta_p^2} \tag{11}$$

where β_p is the plate slenderness:

$$\beta_p = \frac{b'_E}{t}\sqrt{\frac{\sigma_{Yp}}{E_p}} \tag{12}$$

in which b'_E is the reduced effective width, σ_{Yp} is the plating yielding stress, and E_p is the plating elastic modulus.

In order to include such nonlinear behavior, parameter T transforms the reduced plate width $b'_{E,tr}$:

$$b'_{E,tr} = Tb'_E \tag{13}$$

Analogously, the plate failure stress $\sigma_{F,II}$ becomes a portion of the plate yielding stress σ_{Yp}:

$$\sigma_{F,II} = \frac{T - 0.1}{T}\sigma_{Yp} \tag{14}$$

Moreover, when the load eccentricity is considered, an additional nondimensional parameter must be introduced as (Hughes 1983):

$$\eta_{p,II} = \frac{\Delta_p y_{p,tr}}{\rho_{tr}^2} \tag{15}$$

$$\Delta_p = hA_s\left[\frac{1}{A_{tr}} - \frac{1}{A}\right] \tag{16}$$

where Δ_p is the load eccentricity acting on the section of plating-stiffener system, h is the distance from the midplane of the plating to the centroid of the stiffener, A_s is the sectional area of the stiffener, $A_{tr} = A_s + b'_{E,tr}t$ is the total transformed area, $A = A_s + b'_E t$ is the total nontransformed area, $y_{p,tr}$ is the distance between the neutral axis of the transformed section and the plating, and ρ_{tr} is the transformed radius of gyration defined as:

$$\rho_{tr} = \sqrt{\frac{I_{tr}}{A_{tr}}} \tag{17}$$

where I_{tr} is the moment of inertia of the stiffened plate about an axis through the centroid and parallel to the plate.

The effect of this eccentricity combined with the section slenderness is taken into consideration by the strength ratio R_{II} (associated with Mode II of collapse). Thus, the maximum stress that can be reached by the section is given by:

$$\sigma_{a,u,II} = \sigma_{F,II} R_{II}\left(\frac{A_{tr}}{A}\right) \tag{18}$$

Hence, once the failure stress is evaluated for each stiffener-plating system, the relation between strain and curvature can be easily obtained using the stress-strain relationship (Hughes 1983):

$$\varepsilon_{a,u} = \begin{cases} \dfrac{\sigma_{a,u,I}}{E} & \text{for Mode I} \\ \dfrac{A}{A_{tr}}\dfrac{\sigma_{a,u,II}}{E} & \text{for Mode II} \end{cases} \tag{19}$$

$$\Phi_0 = \min_{i=1}^{N_p}\left(\left|\frac{(\varepsilon_{a,u})_i}{y_i}\right|\right) \tag{20}$$

where $\varepsilon_{a,u}$ is the stiffened plate ultimate strain, Φ_0 is the curvature of the whole hull girder corresponding to the first stiffened plate

failure (component failure), N_p is the number of stiffened plates, y is the distance between the centroid of the stiffened plate and the neutral axis of the whole hull, and i refers to the ith stiffened plate under consideration. However, it is also necessary to check for a possible failure occurring by tensile yielding of the stiffened plate; thus the curvature equation becomes:

$$\Phi_0 = \min_{i=1}^{N_p} \left(\left| \frac{(\varepsilon_{a,u})_i}{y_i} \right|, \left| \frac{\varepsilon_Y}{y_i} \right| \right) \tag{21}$$

where ε_Y is the yielding strain of the stiffened plates. Finally, the first failure moment of the whole structural system, represented by the hull girder, is:

$$M_{1F} = EI_0\Phi_0 \tag{22}$$

in which I_0 is the inertia of the whole box girder having all the panels intact and having the transformed plating area ($A_{p,tr} = b'_{E,tr}\, t$) being used if the panel fails according to Mode II of collapse.

2.2. Ultimate failure evaluation

The ultimate failure moment of the hull girder is calculated by using the optimization-based method proposed by Okasha and Frangopol (2010b). In this method, the ultimate moment is obtained by adopting an optimization-based procedure instead of a classic incremental curvature method.

Briefly, the moment-curvature relationship can be treated as an implicit function. For a given curvature value κ, a corresponding value of bending moment $M(\kappa)$ can be computed by following the procedure proposed by the IACS (2008) guidelines. Therefore, by using an optimization search algorithm, it is possible to find the curvature value that maximizes the associated bending moment $M(\kappa)$. The result obtained is the ultimate failure moment of the whole structure.

The main steps of the optimized iterative method are summarized as (Okasha & Frangopol 2010b):

Step 1. Divide the hull girder midship transverse section into structural elements, stiffened plates (system components), and hard corners.
Step 2. Derive the stress-strain curves for all structural elements.
Step 3. Provide the first trial of the curvature.
Step 4. Optimize the function $M(\kappa)$ by using an optimization algorithm.

The optimization process is subjected to constraints; the curvature is bounded by lower and upper limits. A realistic lower bound is the yielding curvature, while a reasonable upper bound can be set as three times the yielding curvature, as specified by the IACS guidelines (IACS 2008). Therefore, the considered constraints are set up as:

$$\kappa \leq 3\kappa_y \text{ and } \kappa > \kappa_y \text{ for sagging} \tag{23}$$

$$\kappa \geq -3\kappa_y \text{ and } \kappa < -\kappa_y \text{ for hogging} \tag{24}$$

The first trial curvature value (step 3) can be set as the yielding curvature value (lower bound). In step 4 optimization of the objective $M(\kappa)$ is performed where each time the $M(\kappa)$ objective is calculated by performing the following steps:

1. For each jth element calculate the strain $\varepsilon_{ij} = \kappa_i(z_j - NA_i)$ corresponding to κ_i, then calculate the corresponding stress σ_{ij}, and hence the force in the element $\sigma_{ij}A_j$, where z_j and A_j are the centroid and the cross-sectional area of the jth element, respectively, and NA_i and κ_i are the neutral axis position and the curvature at the ith iteration, respectively.
2. Determine the new neutral axis position NA_i by checking the longitudinal force equilibrium over the whole transverse section. Hence, adjust NA_i until the force is $F_i = \Sigma\sigma_{ij}A_j = 0$.
3. Calculate the corresponding moment by summing the force contributions of all the element as $M_i = \sum_j \sigma_{ij} A_j(z_j - NA_i)$.

This novel optimization method is able to find the ultimate moment in a limited number of steps, lower than the classic incremental method. In fact, by applying this method, the convergence to the ultimate moment value is much faster, so that much computational time and resources can be saved. This procedure is included in the developed MATLAB program.

2.3. Corrosion model

As previously stated, the main purpose of this study is the evaluation of the time-variant redundancy index of ship structures. A time horizon of 30 years is used as the target period.

Over time, the resistance of the hull section changes due to corrosion attack that reduces the thickness of plates and stiffeners; consequently, the global section modulus decreases. The assumed corrosion model is defined as follows (Akpan et al. 2002):

$$r(t) = C_1(t - t_0)^{C_2} \tag{25}$$

in which $r(t)$ is the thickness loss (mm), t_0 is the corrosion initiation time depending on coating life (years), C_1 is the annual corrosion rate (mm/years), C_2 is a constant usually set to unity, and t is the time expressed in years. The annual corrosion rate and the initiation corrosion time are treated as random variables. Table 1 summarizes type of distribution, mean, and coefficient of variation (COV) of the assumed annual corrosion rate with respect to the location of the stiffened plates (Akpan et al. 2002). Corrosion initiation time is described by a log-normal distribution with mean of 5 years and coefficient of variation of 0.4.

3. Load effects

The hull is mainly subjected to two types of bending moments, due to still water and wave-induced. Sagging bending moment is induced when the deck of the ship is in compression due to waves located at the extreme points of the hull; contrarily hogging bending moment is caused by the compression of the keel (the bottom part of the ship) due to waves positioned under the midship.

Table 1 Statistical parameters of the corrosion model based on Akpan et al. (2002)

	Corrosion Level	Mean (mm/years)	COV	Distribution
1	Bottom shell plating	0.17	0.5	Log normal
	Bottom stiffener web	0.065	0.5	Log normal
2	Deck plating	0.065	0.5	Log normal
	Deck stiffener web	0.065	0.5	Log normal
3	Side shell plating	0.03	0.1	Log normal
	Side stiffener web	0.03	0.1	Log normal

The load components applied on the structure are defined by IACS guidelines (IACS 2008):

$$M_{\text{sw-min-sea-mid}} = 0.05185 C_{\text{wv}} L^2 B (C_{\text{b}} + 0.7) \text{ for sagging} \quad (26)$$

$$M_{\text{sw-min-sea-mid}} = 0.01 C_{\text{wv}} L^2 B (11.97 + 1.9 C_{\text{b}}) \text{ for hogging} \quad (27)$$

$$M_{\text{wv-sag}} = f_{\text{prob}} 0.11 C_{\text{wv}} f_{\text{wv-v}} L^2 B (C_{\text{b}} + 0.7) \text{ for sagging} \quad (28)$$

$$M_{\text{wv-hog}} = f_{\text{prob}} 0.19 C_{\text{wv}} f_{\text{wv-v}} L^2 B C_{\text{b}} \text{ for hogging} \quad (29)$$

in which $M_{\text{sw-min-sea-mid}}$ are the vertical still water bending moments (sagging and hogging), $M_{\text{wv-sag}}$ and $M_{\text{wv-hog}}$ are the vertical wave-induced sagging and hogging moments, respectively, f_{prob} is a coefficient to be taken as 1.0, $f_{\text{wv-v}}$ is the distribution factor for vertical wave-induced bending moments along the vessel length equal to 1.0 at midship, C_{b} is the block coefficient of the ship, L is the ship length, B is the ship breadth, and C_{wv} is a coefficient calculated as follows (IACS 2008):

$$C_{wv} = \begin{cases} 10.75 - \left(\dfrac{300 - L}{100}\right)^{\frac{3}{2}} & \text{for } 150 \le L \le 300 \\ 10.75 & \text{for } 300 < L \le 350 \\ 10.75 - \left(\dfrac{L - 350}{150}\right)^{\frac{3}{2}} & \text{for } 350 < L \le 500 \end{cases} \quad (30)$$

4. Reliability analysis

As previously mentioned, because of the uncertainties related to structural system analysis, some geometric parameters, and material properties used for the model, such as plating thickness t, elastic modulus E, plating yielding stress σ_{Yp}, and stiffener yielding stress σ_{Ys}, are treated as random variables (Hess et al. 2002). Moreover, corrosion initiation time and annual corrosion rate are considered random variables.

As suggested by McKay et al. (1979), generation of random numbers by using Latin Hypercube method can be a valid alternative to Monte Carlo simulation because it provides a sample space that better represents the given probability distribution with a limited number of samples. In fact, it is well known that the application of Latin Hypercube technique allows a considerable reduction of the sample space as discussed by Olsson et al. (2003). Therefore, the number of operations to be performed is reduced and a good amount of time and computer resources can be saved (Neves et al. 2006, Okasha & Frangopol 2010b). Briefly, this method is based on stratified sampling method in which the sample space of each random variable is subdivided into intervals (stratification). Then, one sample is generated for each interval in order to cover the entire sample space.

In this paper, the instantaneous reliability of the structure is investigated. The reliability indices associated with first failure and ultimate failure varies over time because of the degradation of the steel structure due to corrosion; thus the reliability is time variant. The limit state function is defined as (Paik & Frieze 2001):

$$g(t) = x_{\text{R}} M(t) - x_{\text{sw}} M_{\text{sw}} - x_{\text{w}} M_{\text{w}} = 0 \quad (31)$$

where $g(t)$ is the time-variant performance function, $M(t)$ is the time-variant resisting bending moment, M_{sw} is the still water bending moment, M_{w} is the wave-induced bending moment, x_{R} is the model uncertainty associated with the resistance determination, x_{sw} is the model uncertainty related to the still water bending moment prediction, and x_{w} is the model uncertainty associated with the wave-induced bending moment prediction. In case of high-speed vessels, dynamic effects must be included. The effect of dynamic load on the flexural reliability can be accommodated as indicated in Okasha et al. (2010).

Statistical parameters, concerning the model uncertainty coefficients (x_{R}, x_{sw}, and x_{w}), are normal distributed with mean values of 1.0, 1.0, and 0.9, and coefficients of variation equal to 0.10, 0.05, and 0.15, respectively (Paik & Frieze 2001). In addition, the variability of the applied bending moments is taken into account by considering the still water moment and wave-induced moment as normal and Type I largest, respectively, with coefficient of variation of 0.15 (Ayyub et al. 2000).

Log-normal distribution is used to fit the outcoming simulation results for the cross-section resisting moments $M(t)$ at midship (sagging and hogging). Mean and standard deviation are found directly from the generated Latin Hypercube sample space by evaluating the deterministic values of the resisting moment associated with each sample. The instantaneous reliability index and the corresponding probability of failure are provided by the program CALREL (Liu et al. 1989), which is able to perform different reliability methods. In this paper the SORM is used (Der Kiureghian et al. 1987).

5. System redundancy

Redundancy is a useful performance indicator that provides collapse warning. A redundant system has enough resources to survive even though one component within itself fails; the structural system will collapse only if the failure pattern propagates throughout multiple components. A high level of redundancy can contribute to the mitigation of unexpected actions generated by potential hazard-induced events. In fact, if an extreme event hits the ship, producing critical damage, a high level of redundancy will be crucial in limiting the potential of further unexpected consequences.

Several definitions were investigated by Frangopol and Curley (1987) in order to relate redundancy to the meaning of "warning provider," including:

Reserve capacity factor:

$$R_1 = \frac{L_{\text{intact}}}{L_{\text{design}}} \quad (32)$$

in which L_{intact} is the load-carrying capacity of the intact structure and L_{design} is the design load.

Residual capacity factor:

$$R_2 = \frac{L_{\text{damaged}}}{L_{\text{intact}}} \quad (33)$$

where L_{damaged} is the load-carrying capacity of the damaged structure.

Normalized capacity factor:

$$R_3 = \frac{L_{\text{intact}}}{L_{\text{intact}} - L_{\text{damaged}}} \quad (34)$$

If a probabilistic approach is pursued, the system must be analyzed based on probability distributions associated with the random variables introduced. Once reliability index is obtained, time-variant redundancy index definitions can be calculated using the reliability indices (Frangopol & Okasha 2008):

$$R_4(t) = \beta_{f(sys)}(t) - \beta_{y(sys)}(t) \tag{35}$$

$$R_5(t) = \frac{\beta_{f(sys)}(t) - \beta_{y(sys)}(t)}{\beta_{f(sys)}(t)} \tag{36}$$

where $\beta_{f(sys)}(t)$ and $\beta_{y(sys)}(t)$ are the reliability indices with respect to the occurrence of first yielding and system failure at time t, respectively.

Analogously, the time-variant redundancy indices can be calculated using the probabilities of failure (Frangopol & Okasha 2008, Okasha & Frangopol 2010a):

$$R_6(t) = P_{y(sys)}(t) - P_{f(sys)}(t) \tag{37}$$

$$R_7(t) = \frac{P_{y(sys)}(t) - P_{f(sys)}(t)}{P_{f(sys)}(t)} \tag{38}$$

in which $P_{y(sys)}(t)$ and $P_{f(sys)}(t)$ are the probabilities of first yielding and system failure at time t, respectively.

The aforementioned redundancy measures have been developed for applications to civil infrastructure systems. In the case of marine infrastructure such as ship structures, these formulations can be easily modified to accommodate the difference in system configuration. For instance, the probability of system failure represents the probability of ultimate failure moment of the whole hull $P_{f,UFM}(t)$, and the probability of occurrence of damage in the system corresponds to the probability of first failure moment in the hull $P_{f,FFM}(t)$. Thus, the time-variant normalized probability-based redundancy index can be expressed for ship structures as:

$$RI_1(t) = \frac{P_{f,FFM}(t) - P_{f,UFM}(t)}{P_{f,UFM}(t)} \tag{39}$$

and the time-variant reliability-based redundancy index is given by:

$$RI_2(t) = \beta_{UFM}(t) - \beta_{FFM}(t) \tag{40}$$

where $\beta_{UFM}(t)$ and $\beta_{FFM}(t)$ are the reliability indices associated with ultimate failure moment of the whole hull and first failure moment in the hull, respectively. The correlation among the basic random variables is automatically accounted for while performing reliability analysis with respect the occurrence of ultimate and first failures (UFM and FFM). Redundancy calculations are based on the results obtained by the reliability analysis. The proposed definitions of redundancy are based on the evaluation of the reliability associated with the occurrence of failure in one component. This concept is accepted in the scientific literature, and such definition is adopted in order to avoid excessive plastification of some components associated with potential unexpected large deformations. Furthermore, for the ship structure to be safe, the hull girder must satisfy reliability (associated with the ultimate capacity) and minimum redundancy requirements.

6. Applications

6.1. First example

Based on a tanker analyzed by Dinovitzer (2003), a modified example having the following properties, is herein investigated: length $L=255$ m, breadth $B=57$ m, height $H=31.1$ m, block coefficient $C_b=0.842$, mean value of the elastic modulus $E=207{,}000$ MPa, mean value of the plating yielding stress $\sigma_{Yp}=353$ MPa, and mean value of the stiffener yielding stress $\sigma_{Ys}=353$ MPa. The section geometry of the structure at midship is shown in Fig. 2, while Table 2 shows the dimensions of the stiffened plates associated with each component. The headings in Table 2 are denoted as: "Component ID" is the component identification number (from 1 to 47 located as illustrated in Fig. 2), "Location" indicates the position of the component (i.e., the distance (cm) between the centroid of the component and the keel of the ship), b is the plating breadth concerning a single stiffener (cm), t is the mean value of the plating thickness (cm), h_w is the stiffener web height (cm), t_w is the stiffener web thickness (cm), b_f is the stiffener flange breadth (cm), t_f is the stiffener flange thickness (cm), "No." is the number of component with the same properties, and "Corrosion level" indicates the corrosion rate associated with the component depending on its position (see Table 1). The coefficients of variation of the random variables t, E, σ_{Yp}, and σ_{Ys} are assumed to be equal to 0.05, 0.03, 0.1, and 0.1, respectively (Paik & Frieze 2001). The residual stress value has been assumed to be equal to 5% of the plating yielding stress for both applications.

Figures 3(a), (b), (c), and (d) show the first and ultimate failure mean moment profiles (sagging and hogging) over 30 years (2 year interval), profiles of the mean plus and minus one

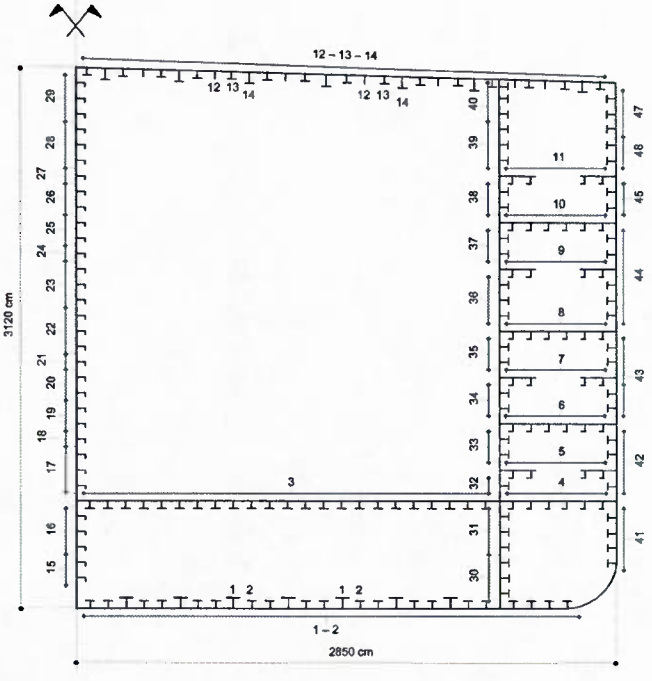

Fig. 2 First example: cross-section geometry of a symmetric half hull at midship. Numbers in figure refer to component types (adapted from Dinovitzer (2003), see Table 2)

Table 2 Geometric properties of the components in Fig. 2 and their locations

Component ID	Location (cm)	b (cm)	t (cm)	h_w (cm)	t_w (cm)	b_f (cm)	t_f (cm)	No.	Corrosion level
1	0	91.9	2.7	70	1.5	15	2	14	1
2	0	91.9	2.7	55	1.5	5	1	40	1
3	622.2	91.9	2.7	60	1.2	15	2	46	0
4	622.2	91.9	1.2	21.5	1	4.4	2.5	12	0
5	801	91.9	1.2	21.5	1	4.4	2.5	8	0
6	1,068.3	91.9	1.2	21.5	1	4.4	2.5	12	0
7	1,335.5	91.9	1.2	21.5	1	4.4	2.5	8	0
8	1,602.3	91.9	1.2	21.5	1	4.4	2.5	12	0
9	1959	91.9	1.2	21.5	1	4.4	2.5	8	0
10	2,226.2	91.9	1.2	21.5	1	4.4	2.5	12	0
11	2,493.4	91.9	1.2	21.5	1	4.4	2.5	8	0
12	3,117.5	91.9	2	35	2.5	0	0	14	2
13	3,117.5	91.9	2	55	1.2	10	2	30	2
14	3,117.5	91.9	2	95	2.5	10	2	14	2
15	222.7	89.1	2.1	5.5	1.2	15	2	4	0
16	489.9	89.1	2.2	5.5	1.2	15	2	6	0
17	846.2	89.1	2.1	60	1.2	15	2	6	0
18	1,024.3	89.1	2	60	1.2	15	2	2	0
19	1,131.4	89.1	2	55	1.2	15	2	4	0
20	1,291.5	89.1	1.95	55	1.2	15	2	4	0
21	1,469.7	89.1	1.95	50	1.2	15	2	2	0
22	1,647.8	89.1	1.85	50	1.2	15	2	6	0
23	1,915	89.1	1.75	45	1.2	15	2	6	0
24	2,093.2	89.1	1.7	45	1.2	15	2	2	0
25	2,182.2	89.1	1.7	40	1.2	15	2	4	0
26	2,360.4	89.1	1.45	40	1.2	15	2	4	0
27	2,538.5	89.1	1.45	30	1.2	15	2	2	0
28	2,716.7	89.1	1.7	30	1.2	15	2	6	0
29	2,983.9	89.1	1.6	35	2.5	0	0	6	0
30	222.7	89.1	2.3	65	1.2	15	2.5	6	0
31	489.9	89.1	2.2	65	1.2	15	2.5	6	0
32	757.1	89.1	2.1	60	1.2	15	2	2	0
33	935.2	89.1	2	55	1.2	15	1.2	4	0
34	1,202.5	89.1	1.9	55	1.2	15	1.2	4	0
35	1,469.7	89.1	1.8	50	1.2	15	1.5	4	0
36	1,826	89.1	1.7	50	1.2	15	1.5	6	0
37	2,093.2	89.1	1.7	50	1.2	15	1.5	4	0
38	2,360.4	89.1	1.4	40	1.2	15	1.2	4	0
39	2,716.7	89.1	1.7	40	1.2	15	1.2	6	0
40	2,983.9	89.1	1.8	35	2.5	0	0	3	0
41	400.8	89.1	2.5	65	1.2	15	2	8	3
42	846.2	89.1	2.5	60	1.2	15	2	6	3
43	1,380.6	89.1	2.2	65	1.2	15	2	8	3
44	1,915	89.1	2	55	1.2	15	2	10	3
45	2,360.4	89.1	2	50	1.2	15	1.5	4	3
46	2,627.6	89.1	2	30	1	15	1.5	4	3
47	2,894.8	89.1	2	35	2.5	0	0	6	3

standard deviation, and PDFs of the moments at 0, 10, and 20 years. Figures 4(a) and (b) show the probability of failure profiles (sagging and hogging), computed by using the program CALREL (Liu et al. 1989) and Figs. 5(a) and (b) show the reliability index profiles (sagging and hogging). Figures 6(a) and (b) show the redundancy index profiles for sagging and hogging moments according to equations (39) and (40), respectively.

Table 3 shows how the probability of occurrence of first failure (POC_f) evolves with time. Accordingly, the components involved in the first failure do not change over time. For sagging moment, first failure occurs only in component 14. Meanwhile, for hogging moment, 1 and 2 are the only components involved in first failure. In both cases, the components under compression fail first. In fact, when sagging moment is applied, component 14 is subjected to compression; contrarily, components 1 and 2 are under compression when hogging moment is acting on the hull. It is also shown in Table 3 that for hogging moment, the POC_f of component 2 increases over time because its rate of corrosion is higher than the other components closer to the neutral axis; hence component 2 is becoming more vulnerable and fails first. Furthermore, Table 4 shows the probability of occurrence of first failure modes

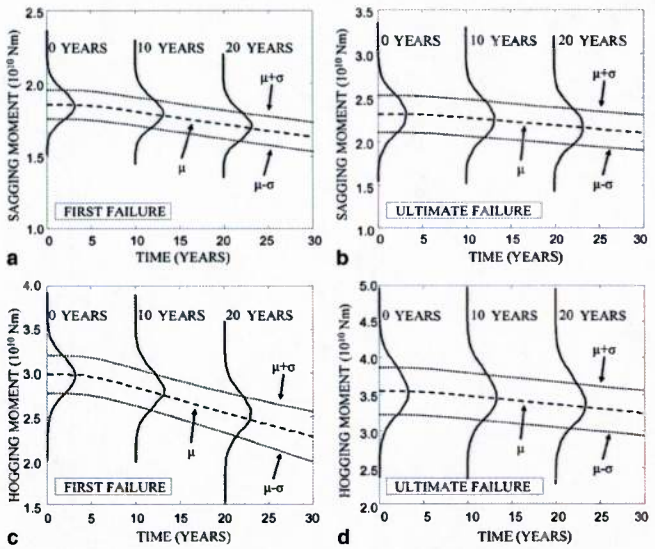

Fig. 3 First example: profiles of first and ultimate failure moments for sagging (a) and (b), hogging (c) and (d), mean profiles, mean ±1 standard deviation profiles, and PDFs of the moments at 0, 10, and 20 years

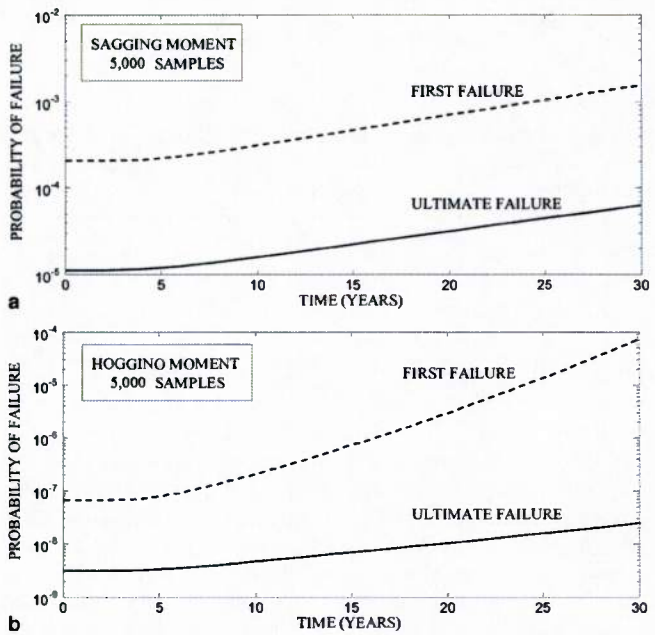

Fig. 4 First example: probability of failure profiles for (a) sagging and (b) hogging moments (first and ultimate failures)

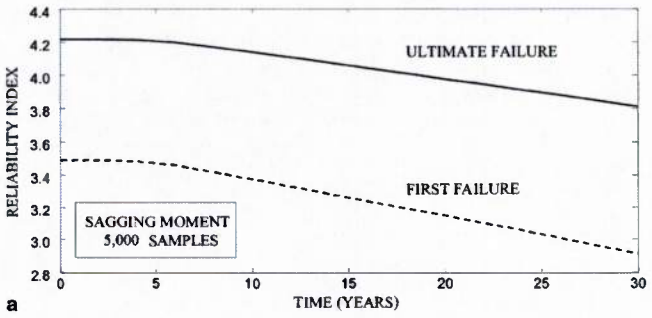

Fig. 5 First example: reliability index profiles for (a) sagging and (b) hogging moments (first and ultimate failures)

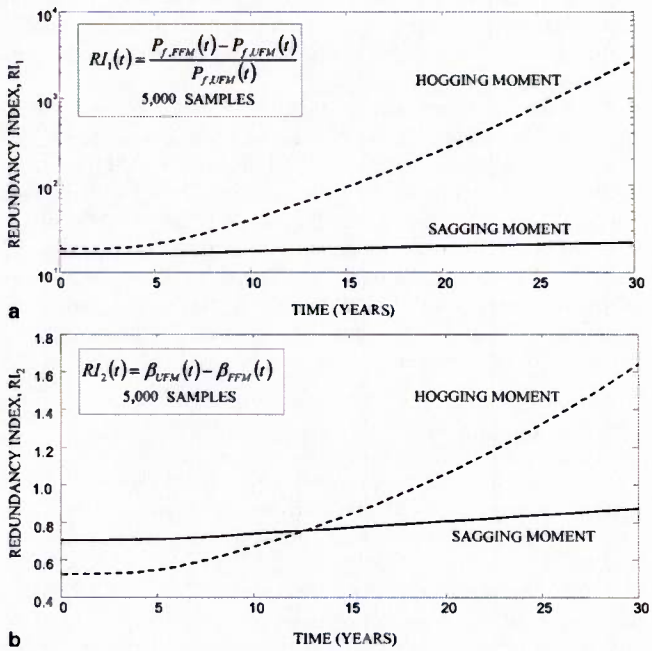

Fig. 6 First example: redundancy profiles for sagging and hogging moments, considering (a) normalized probability-based redundancy index and (b) reliability-based redundancy index

(POC_m) associated with the failure of the weakest components. It can be seen that for the hogging moment, the probability of having first failure due to instability of the stiffener plates (tripping) increases with time.

In this example, the redundancy of the ship in sagging slightly increases with time (Fig. 6). However, the redundancy of the ship in hogging significantly improves with respect to time (Fig. 6). In fact, for hogging moment, the POC_f of component 2 increases over time (Table 3); thus the difference between the probability of first failure and the probability of ultimate failure becomes higher. This has also been seen in Fig. 5(b) where the reliability index associated with the first failure deteriorates at a higher rate than

Table 3 Probability of occurrence of first failure (POC_f) at the component locations (sagging and hogging)

Moment type	First failure (component)	POC_f at year 0	POC_f at year 10	POC_f at year 20	POC_f at year 30
Sagging	14	1.0000	1.0000	1.0000	1.0000
Hogging	2	0.9464	0.9732	0.9912	0.9948
	1	0.0536	0.0268	0.0088	0.0052

Table 4 Probability of occurrence of first failure modes, POC_m (sagging and hogging)

Moment type	Type of first failure	POC_m at year 0	POC_m at year 10	POC_m at year 20	POC_m at year 30
Sagging	Mode I—tripping	0.9996	0.9998	1.0000	1.0000
	Mode II	0.0004	0.0002	0.0000	0.0000
Hogging	Mode I—tripping	0.8368	0.9186	0.9776	0.9918
	Mode II	0.1630	0.0812	0.0224	0.0082
	Yielding	0.0002	0.0002	0.0000	0.0000

that of the reliability index associated with the ultimate failure in the hogging moment case. The redundancy index of the ship in hogging is strongly influenced by the increasing in failure (plastification) of component 2. Moreover, the double-hull configuration (Fig. 2) can improve the redundancy index associated with the hogging moment.

The aforementioned observations on redundancy and occurrence of first yielding can help to locate critical components that need to be reinforced if a higher level of safety would need to be provided to the ship structure. Furthermore, based on corrosion attack and on the sea state, speeding, and heading incurred by the ship during its lifetime, the location of critical components (the first to fail) can change over time. Thus, in order to maintain adequate reliability and redundancy levels, the effort to implement maintenance actions will require the time-variant localization of the most critical components.

6.2. Second example

The second example investigated is a modified version of a ship structure based on an example analyzed by Akpan et al. (2002). This vessel has the following properties: length $L=220$ m, breadth $B=38.1$ m, height $H=17.4$ m, block coefficient $C_b=0.75$, mean value of the elastic modulus $E=208{,}500$ MPa, mean value of the deck and keel yielding stress $\sigma_{Yp}=315$ MPa, and mean value of the side panels yielding stress $\sigma_{Ys}=281$ MPa. The midship section geometry is shown in Fig. 7 and Table 5 summarizes the stiffener dimensions. As for the first example, the coefficients of variation of the random variables t, E, σ_{Yp}, and σ_{Ys} are assumed to be equal to 0.05, 0.03, 0.1, and 0.1, respectively (Paik & Frieze 2001).

Analogous to what has been shown for the first example, Figs. 8(a), (b), (c), and (d) show the first and ultimate mean failure moment profiles (sagging and hogging) over 30 years, profiles of the mean ±1 standard deviation, and the PDFs of the moments

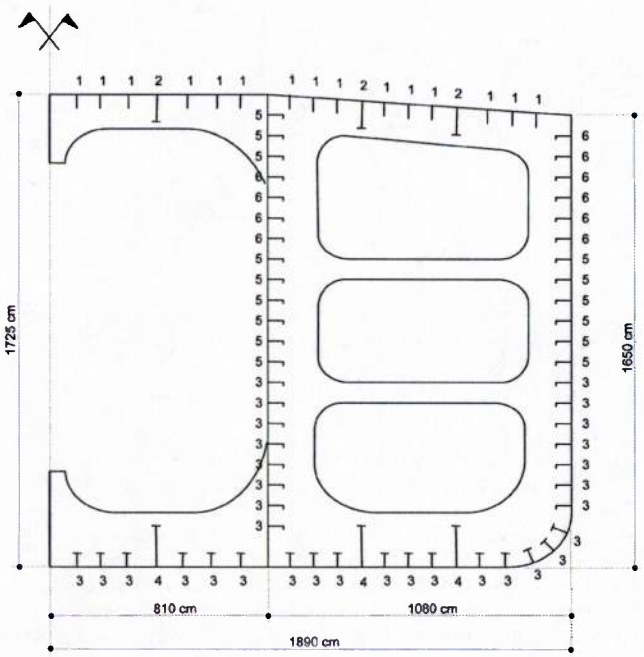

Fig. 7 Second example: cross-section geometry of a symmetric half hull at midship. Numbers in figure refer to component types (adapted from Akpan et al. (2002), see Table 5)

Table 5 Stiffeners types and dimensions (Akpan et al. 2002)

Stiffener	Web (mm)	Flange (mm)
1	450 × 36	None
2	1000 × 16	400 × 16
3	465 × 18	190.5 × 25.5
4	1220 × 16	350 × 25.5
5	370 × 16	100 × 16
6	297 × 11.5	100 × 16

at 0, 10, and 20 years. Figures 9(a) and (b) and Figs. 10(a) and (b) show the probability of failure and the reliability index over time for sagging and hogging, respectively. Figures 11(a) and (b) show the redundancy indices for sagging and hogging moments as defined by equations (39) and (40), respectively.

In this example, according to Table 6, the components involved in the first failure event vary over time. For sagging moment, the most critical components are 5 and 1. Component 5, which belongs to the vertical panel, is initially the most critical component. Over time, component 1 becomes more critical because of the different rates of section loss due to corrosion. Meanwhile, for hogging moment, only the components 3 and 4 are involved in first failure. Furthermore, most of the time, first failure in the components occurs following Mode II (high value of POC_m) as reported in Table 7.

The results for this ship structure are different from those obtained in the first example. The redundancy index of the ship in sagging decreases over time, while the redundancy index of the ship in hogging does not change significantly. Over time, the

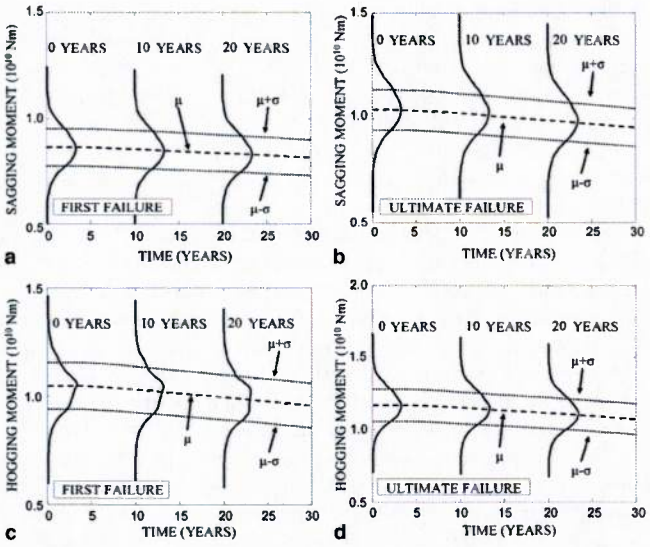

Fig. 8 Second example: profiles of first and ultimate failure moments for sagging (a) and (b), hogging (c) and (d), mean profiles, mean ±1 standard deviation profiles, and PDFs of the moments at 0, 10, and 20 years

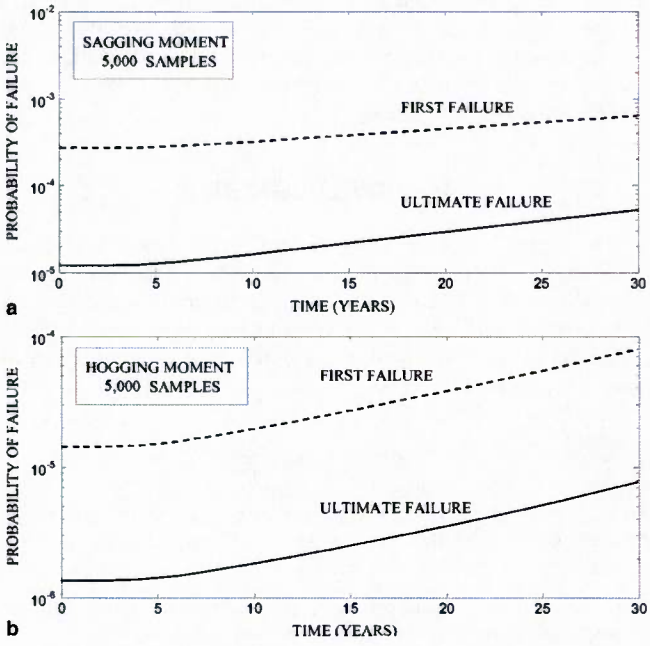

Fig. 9 Second example: probability of failure profiles for (a) sagging and (b) hogging moments (first and ultimate failures)

POC_f of component 5 decreases and then additional components become critical as a result of corrosion. For this reason, the difference between the reliability indices associated with the ultimate and first failure decreases in the sagging case; thus the redundancy index decreases.

Differently from the previous case (first example), the most critical component (No. 5) is located on the side of the structure.

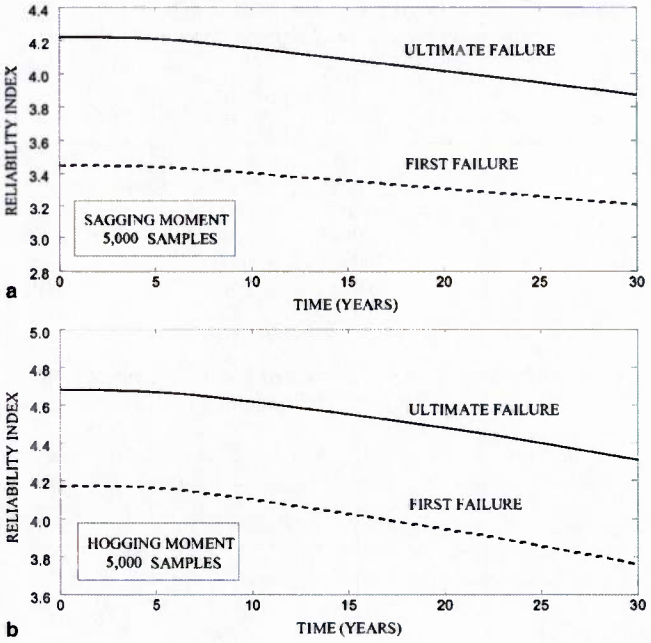

Fig. 10 Second example: reliability index profiles for (a) sagging and (b) hogging moments (first and ultimate failures)

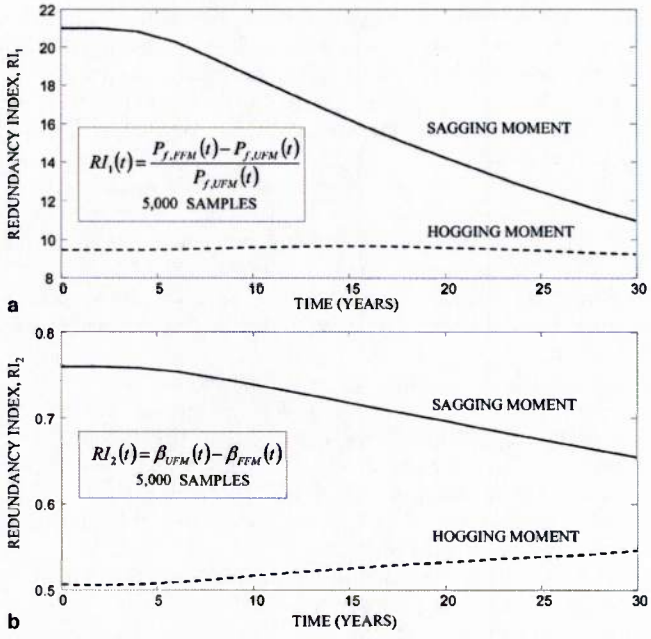

Fig. 11 Second example: redundancy profiles for sagging and hogging moments, considering (a) normalized probability-based redundancy index and (b) reliability-based redundancy index

Accordingly, this implies that the side panel formed by such components is weaker than the other panels, and thus it fails first. This is different from the common assumption in which yielding propagates starting from the farthest point from the neutral axis.

Table 6 Probability of occurrence of first failure (POC_f) at the component locations (sagging and hogging)

Moment type	First failure (component)	POC_f at year 0	POC_f at year 10	POC_f at year 20	POC_f at year 30
Sagging	5	0.9734	0.9626	0.9186	0.8340
	1	0.0264	0.0372	0.0810	0.1640
	2	0.0000	0.0000	0.0002	0.0018
	6	0.0002	0.0002	0.0002	0.0002
Hogging	3	1.0000	1.0000	0.9996	0.9964
	4	0.0000	0.0000	0.0004	0.0036

Table 7 Probability of occurrence of first failure modes, POC_m (sagging and hogging)

Moment type	Type of first failure	POC_m at year 0	POC_m at year 10	POC_m at year 20	POC_m at year 30
Sagging	Mode II	0.9958	0.9962	0.9964	0.9972
	Yielding	0.0042	0.0038	0.0036	0.0028
Hogging	Mode II	0.9976	0.9976	0.9984	0.9986
	Yielding	0.0024	0.0024	0.0016	0.0014

7. Conclusions

Ensuring adequate levels of redundancy of ship structures and the upkeep of their redundancy above target levels provides additional warning before failure for the users of these structures. Indeed, reacting to the signs of warning provided by the failure of the first component in the ship structural system may prevent the complete collapse of this system. Redundancy and reliability are excellent performance indicators to be incorporated in decision-making platforms.

Evaluation of the time-variant reliability and redundancy is a process fraught with uncertainties. Treatment of uncertainty in modeling the ship performance over time requires special considerations. The power of computers and the capabilities of today's software can provide efficient means for achieving more accurate assessment of the time-variant reliability and redundancy of ship structures.

In this paper, the time-variant redundancy of ship structures is investigated. Redundancy is defined based on the probability of ultimate failure and the probability of first failure of ship structures. A redundancy index analogous to that used in civil infrastructure systems is considered. The computations of the probabilities of failure are performed using a hybrid Latin Hypercube sampling - SORM approach.

The accurate computation of the probabilities of failure relies heavily on the accurate computations of the deterministic strength with respect to both ultimate and first failures. There exists a trade-off between accuracy and computational cost when it comes to the computing of the strength of ships. Even though the rigorous incremental curvature method can be used to provide both values of strength (i.e., first and ultimate), the computational cost associated with this method when implemented in a repetitive simulation analysis becomes significantly high. Alternatively, in this paper, the ultimate and first failure strength values are obtained separately using two different methods. The ultimate strength is computed using an optimization-based approach in which the curvature at which the bending moment is maximum is found by a fast-search algorithm. On the other hand, the first failure strength is computed based on closed-form solutions used in the progressive collapse method. Both resistances degrade during time as a result of the effects of corrosion, which impacts the reliability and redundancy of ship structures.

The computations in this paper are conducted using a MATLAB program developed by the authors. The strength simulation in which the deterministic computations are embedded, the load computations, and the corrosion effects are conducted in the program at each considered time increment in order to determine the parameters of the random variables required for the reliability computations. The developed MATLAB program is linked with the reliability program CALREL to compute the probability of ultimate failure and the probability of first failure at each time increment using the determined random variable parameters.

The time-variant reliability and redundancy of two ship structures are investigated. It was found from the results of the examples that the reliability continuously decreases with time as a result of the effects of corrosion. However, redundancy may degrade, remain the same, or even increase over time. Based on the results of the first example, it can be stated that the double hull configuration (Fig. 2) can improve the redundancy index associated with the hogging moment. Situations where the redundancy of the ship structure may be significantly compromised are possible. It is therefore believed necessary to assess the time-variant redundancy to ensure that it remains above adequate levels. In addition, considering the redundancy during the design stages of civil and marine structures is also beneficial (Frangopol 2011).

ACKNOWLEDGMENTS

The support from the US Office of Naval Research (contract number N-00014-08-0188, Structural Reliability Program, Director Dr. Paul E. Hess III, ONR, Code 331) is gratefully acknowledged. The opinions and conclusions presented in this paper are those of the authors and do not necessarily reflect the views of the sponsoring organization.

REFERENCES

Akpan, U. O., Koko, T. S., Ayyub, B., and Dunbar, T. E. 2002 Risk assessment of aging ship hull structures in the presence of corrosion and fatigue, *Marine Structures*, **15**, 3, 211–231.

Ang, A. H.-S., and de Leon, D. 2005 Modeling and analysis of uncertainties for risk-informed decisions in infrastructures engineering, *Structure and Infrastructure Engineering*, Taylor & Francis, **1**, 1, 19–31.

Ang, A. H.-S., and Tang, W. H. 2007 *Probability Concepts in Engineering: Emphasis on Applications to Civil and Environmental Engineering*, 2nd ed., Wiley and Sons, New York.

Ayyub, B. M., Assakkaf, I. A., and Atua, K. I. 2000 Reliability-based load and resistance factor design (LRFD) of hull girders for surface ships, *Naval Engineers Journal*, **112**, 4, 279–296.

Ayyub, B. M., Assakkaf, I. A., Sikora, J. P., Adamchak, J. C., Atua, K., Melton, W., and Hess, P. E. 2002 Reliability-based load and resistance factor design (LRFD) guidelines for hull girder bending, *Naval Engineers Journal*, **114**, 2, 43–68.

Ayyub, B. M., and White, G. J. 1990 Life expectancy assessment of marine structures, *Marine Structures*, **3**, 4, 301–317.

Ayyub, B. M., White, G. J., and Purcell, E. S. 1989 Estimation of structural service life of ships, *Naval Engineers Journal*, **101**, 3, 156–166.

Der Kiureghian, A., Lin, H. Z., and Hwang, S.-Z. 1987 Second-order reliability approximations, *Journal of Engineering Mechanics*, **113**, 8, 1208–1225.
Dinovitzer, A. 2003 *Life Expectancy Assessment of Ship Structures*, Ship Structure Committee, Washington, D.C., SSC-427.
Fiessler, B., Neumann, H.-J., and Rackwitz, R. 1979 Quadratic limit states in structural reliability, *Journal of Engineering Mechanics*, **105**, 4, 661–676.
Frangopol, D. M. 2011 Life-cycle performance, management, and optimization of structural systems under uncertainty: accomplishments and challenges, *Structure and Infrastructure Engineering*, Taylor & Francis, 7(6), 389–413.
Frangopol, D. M., editor 1987 *Effects of Damage and Redundancy on Structural Performance*, ASCE, New York.
Frangopol, D. M., and Curley, J. P. 1987 Effects of damage and redundancy on structural reliability, *Journal of Structural Engineering*, **113**, 7, 1533–1549.
Frangopol, D. M., Izuka, M., and Yoshida, K. 1992 Redundancy measure for design and evaluation of structural systems, *Transactions of ASME, Journal of Offshore Mechanics and Arctic Engineering*, **114**, 4, 285–290.
Frangopol, D. M., and Okasha, N. M. 2008 Probabilistic measures for time-variant redundancy, *Proceedings*, Inaugural International Conference of the Engineering Mechanic Institute (EM08), of ASCE, University of Minnesota, Minneapolis, MN, May 18–21, CD-ROM.
Fu, G. 1987 *Modeling of Lifetime Structural System Reliability*, Department of Civil Engineering, University of Case Western Reserve University, Cleveland, OH, Report No. 87-9.
Guedes Soares, C., and Garbatov, Y. 1998 Reliability of maintained ship hulls girders subjected to corrosion and fatigue, *Structural Safety*, **20**, 3, 201–219.
Guedes Soares, C., and Garbatov, Y. 1999 Reliability of maintained ship hulls subjected to corrosion and fatigue under combined loading, *Journal of Constructional Steel Research*, **52**, 1, 93–115.
Hendawi, S., and Frangopol, D. M. 1994 System reliability and redundancy in structural design and evaluation, *Structural Safety*, **16**, 1+2, 47–71.
Hess, P. E., Bruchman, D., Assakkaf, I. A., and Ayyub, B. M. 2002 Uncertainties in material and geometric strength and load variables, *Naval Engineers Journal*, **114**, 2, 139–166.
Hughes, O. F. 1983 *Ship Structural Design: A Rationally-Based, Computer-Aided, Optimization Approoch*, Wiley and Sons, New York.
Hussein, W., and Guedes Soares, C. 2009 Reliability and residual strength of double hull tankers designed according to the new IACS common structural rules, *Ocean Engineering*, **36**, 17–18, 1446–1459.
IACS 2008 *Common Structural Rules for Double Hull Oil Tankers*, International Association of Classification Societies. Available at http://www.iacs.org.uk.
Liu, P. L., Lin, H. Z., and Der Kiureghian, A. 1989 *CALREL User Manual, Department of Civil Engineering*, University of California, Berkeley, CA.
Lua, J., and Hess, P. E. 2003 Hybrid reliability predictions of single and advanced double-hull ship structures, Journal of Ship Research, **47**, 2, 155–176.
Lua, J., and Hess, P. E. 2006 First-failure-based reliability assessment and sensitivity analysis of a naval vessel under hogging, Journal of Ship Research, **50**, 2, 158–170.
Luís, R. M., Teixeira, A. P., and Guedes Soares, C. 2009 Longitudinal strength reliability of a tanker hull accidentally grounded, *Structural Safety*, **31**, 3, 224–233.
Mansour, A. E. 1997 *Assessment of Reliability of Ship Structures*, Ship Structure Committee: SSC-398, Washington, D.C.
Mansour, A. E., and Hovem, L. 1994 Probability based ship structural safety analysis, Journal of Ship Research, **38**, 4, 329–339.
MathWorks 2008a *Optimization Toolbox 4 User's Guide*. The MathWork, Inc., Natick, MA.
MathWorks 2008b *Statistics Toolbox 7 User's Guide*. The MathWork, Inc., Natick, MA.
McKay, M. D., Conover, W. J., and Beckman, R. J. 1979 A comparison of three methods for selecting values of output variables in the analysis of output from a computer code, *Technometrics*, **21**, 2, 239–245.
Naval Engineers Journal 2002 Special Issue on Reliability-Based Load and Resistance Factor Design (LRFD) Guidelines for Surface Ship Structures, http://www3.interscience.wiley.com/journal/121489477/issue, **114**, 2.
Neves, L. C., Frangopol, D. M., and Cruz, P. J. 2006 Probabilistic lifetime-oriented multiobjective optimization of bridge maintenance: single maintenance type, *Journal of Structural Engineering*, **132**, 6, 991–1005.
Nikolaidis, E., Hughes, O., Ayyub, B. M., and White, G. J. 1993 A Methodology for Reliability Assessment of Ship Structures. *Ship Structures Symposium'93*, Sheraton National Hotel, Arlington, Virginia, November 16-17.
Okasha, N. M., and Frangopol, D. M. 2010a Time-Variant Redundancy of Structural Systems. *Structure and Infrastructure Engineering*, Taylor & Francis, **6**, 1-2, 279–301.
Okasha, N. M., and Frangopol, D. M. 2010b Efficient method based on optimization and simulation for the probabilistic strength computation of the ship hull, Journal of Ship Research, **54**, 4, 244–256.
Okasha, N. M., Frangopol, D. M., Saydam, D., and Salvino, L. W. 2010 Reliability analysis and damage detection in high speed naval crafts based on structural health monitoring data, *Structural Health Monitoring*, doi: 10.1177/1475921710379516 (in press).
Olsson, A., Sandberg, G., and Dahlblom, O. 2003 On Latin Hypercube sampling for structural reliability analysis, *Structural Safety*, **25**, 1, 47–68.
Özgüç, Ö., Das, P. K., and Barltrop, N. 2006 The new simple equations for the ultimate compressive strength of imperfected stiffened plates, *Ocean Engineering*, **34**, 7, 970–986.
Paik, J. K., and Frieze, P. A. 2001 Ship structural safety and reliability, *Progress in Structural Engineering and Materials*, **3**, 2, 198–210.
Paik, J. K., Thayamballi, A. K., Kim, S. K., and Yang, S. H. 1998 Ship hull ultimate strength reliability considering corrosion. Journal of Ship Research, **42**, 2, 154–165.

Appendix III

Nader M. Okasha, Dan M. Frangopol, and Alberto Decò. Integration of structural health monitoring in life-cycle performance assessment of ship structures under uncertainty. *Marine Structures*, 23(3):303–321, 2010.

Marine Structures 23 (2010) 303–321

Contents lists available at ScienceDirect

Marine Structures

journal homepage: www.elsevier.com/locate/marstruc

Integration of structural health monitoring in life-cycle performance assessment of ship structures under uncertainty

Nader M. Okasha, Dan M. Frangopol*, Alberto Decò

Department of Civil & Environmental Engineering, Engineering Research Center for Advanced Technology for Large Structural Systems (ATLSS), Lehigh University, Bethlehem, PA 18015-4729, USA

ARTICLE INFO

Article history:
Received 29 December 2009
Received in revised form 20 April 2010
Accepted 26 July 2010

Keywords:
Structural health monitoring
Bayesian updating
Reliability
Redundancy
Life-cycle
Ships

ABSTRACT

In this paper, an approach for integrating the data obtained from structural health monitoring (SHM) in the life-cycle performance assessment of ship structures under uncertainty is presented. Life-cycle performance of the ship structure is quantified in terms of the reliability with respect to first and ultimate failures and the system redundancy. The performance assessment of the structure is enhanced by incorporating prior design code-based knowledge and information obtained by SHM using Bayesian updating concepts. Advanced modeling techniques are used for the hull strength computations needed for the life-cycle performance analysis. SHM data obtained by testing a scaled model of a Joint High-speed Sealift Ship is used to update its life-cycle performance.

1. Introduction

Efficiently ensuring the adequacy of the life-cycle performance of ship structures is fundamental for their safe use and can only be attained by integrating every valuable information gathered about the structural health into the assessment of this performance. Sustainment and life-cycle engineering of ships and ship systems represent major and fast growing challenges for the US Navy [1]. Structural health monitoring (SHM) is emerging as a very powerful technique in ship structures for collecting accurate information about the operational loads the ships are exposed to and detecting damages in the structure once they occur.

* Corresponding author. Tel.: +1 610 758 6103; fax: +1 610 758 4115.
E-mail address: dan.frangopol@lehigh.edu (D.M. Frangopol).

0951-8339/$ – see front matter © 2010 Elsevier Ltd. All rights reserved.
doi:10.1016/j.marstruc.2010.07.004

In principle, among the potential direct applications of SHM, the following is essential in the performance assessment of ship structures. Monitoring the response of a ship structure to its exposure to wave loads provides a volume of valuable information that if used properly can provide a platform for predicting lifetime loads for design and assessment of structural performance. A common monitored response in structures is the strain inflicted by the various load effects experienced by the structure. Using proper calibration, the measured strains may be converted to global ship responses, such as vertical wave-induced bending moments. In the absence of monitoring information, design code formulas [2] are typically used for conservatively estimating the wave-induced load effect in the reliability analysis of ship structures. Even in this case, design codes do not provide formulas for estimating high frequency load effects for cases in which these effects are significant. Either way, incorporating the information obtained from SHM with the prior code derived information can enhance the established life-cycle assessment of ship structures.

The nature of SHM data dictates the fundamental need for accounting for uncertainty in the treatment of this data for integration in the performance assessment methodologies and only recently such research has emerged in the bridge engineering field [3 and references therein]. However, these studies have mainly focused on information related to the load effects that SHM provides, primarily using classical inference concepts in which prior information cannot be easily incorporated and, in fact, is neglected.

Ship reliability-based studies that account for optimum and safe design and life-cycle performance assessment have been conducted. Various studies investigated the reliability of ship structures with respect to their ultimate flexural failure [4–7]. On the other hand, Lua and Hess [8] analyzed the reliability of ship structures with respect to the first failure. Life-cycle redundancy of ship structures has also been recently investigated [9]. These studies provide a wealth of procedures for establishing the life-cycle performance prior to monitoring. Within the outline of these procedures, a methodology for updating the life-cycle performance with obtained SHM data is yet to be developed.

The objective of this paper is to present an approach for integrating the information obtained from SHM in the life-cycle performance assessment of ship structures under uncertainty. The resistances with respect to the ultimate and first failure vertical bending moments are determined such that the ultimate failure moment is computed using an optimization-based method [10] and the first failure moment is computed using the progressive collapse method [11]. The probabilities of failure are computed using a hybrid Latin hypercube sampling – SORM technique. This paper uses Bayesian inference concepts which enable the inclusion of necessary prior information with the SHM data for updating the load effects. The approach is illustrated on the Joint High-speed Sealift Ship (JHSS). SHM data obtained by testing of a scaled model of the JHSS ship is used to update its life-cycle performance.

2. First and ultimate strength

Being the most critical limit state in a ship structure, the longitudinal strength of the midship hull girder is of particular interest because the vertical bending moment is one of the highest load effects that a ship structure has to withstand [12]. Even though the complete failure of the ship hull will not be attained until the ultimate bending strength is reached, reaching the first failure moment (i.e., the moment at which the first plate or panel fails) serves as a crucial sign of warning against collapse.

The first failure moment is determined herein using a simplified progressive collapse method [11]. The method is designed to provide the ultimate strength of the ship hull. However, the sequence of failures preceding the ultimate failure is followed in the process. The first failure moment is found as the first encountered failure mode. In this method, an assumption is made where a stiffened panel is removed from the system once it fails (i.e., its post ultimate behavior is neglected). However, using this method only for the computation of the first failure omits the need for this assumption and it has no bearing on the computation of the first failure moment. Decò et al. [9] integrated this method in a sampling technique to obtain a probabilistic distribution for the first failure moment.

The ultimate failure moment of the hull girder is typically determined using well-documented simplified methods for predicting the load-shortening curves of steel plates and panels considering the effects of initial imperfections that are used in a systematic incremental curvature procedure to determine the ultimate bending moment of the ship hull. However, Okasha and Frangopol [10] made use of optimization search algorithms to speed up the process of finding the ultimate failure moment

rather than generating the full moment-curvature curve for obtaining this value. This facilitated the inclusion of this method in a sampling technique for generating a probabilistic distribution for the ultimate moment time-effectively.

Over time, corrosion causes loss in the cross section of the ship hull that leads to deterioration of both the first and ultimate failure moments. The most commonly used model for predicting corrosion is given as [5]

$$r(t) = C_1(t - t_0)^{C_2} \tag{1}$$

in which $r(t)$ is the thickness loss (mm), t_0 is the corrosion initiation time depending on coating life (years), C_1 is the annual corrosion rate (mm/years), C_2 is a constant usually set to unity, and t is the time (years). The annual corrosion rate and the corrosion initiation time are treated as random variables. Corrosion initiation time is described by a lognormal distribution with mean of 5 years and coefficient of variation (COV) of 0.4.

3. Prior load effects

In the absence of SHM data, the load effects can be predicted using design code formulations. The load effects obtained are lifetime maxima and are conservative. Herein the IACS [2] guidelines are used to determine these load effects. The IACS [2] provide formulas for predicting the still water bending moment and wave-induced (low frequency) bending moments. In monitoring ship structures, the wave-induced and dynamic loads are of particular interest, and mostly no information about the still water bending moment is provided. Therefore, the still water bending moments remain the same after monitoring. However, once SHM data become available, the wave-induced bending moments can be updated. Hence, the wave-induced bending moment determined using the IACS [2] guidelines constitutes the prior knowledge in the performance prediction process.

The still water and wave-induced bending moments can be predicted using the IACS [2] guidelines as

$$M_{sw-min-sea-mid} = 0.05185C_{wv}L^2B(C_b + 0.7) \quad \text{for sagging} \tag{2}$$

$$M_{sw-min-sea-mid} = 0.01C_{wv}L^2B(11.97 + 1.9C_b) \quad \text{for hogging} \tag{3}$$

$$M_{wv-sag} = f_{prob}0.11C_{wv}f_{wv-v}L^2B(C_b + 0.7) \quad \text{for sagging} \tag{4}$$

$$M_{wv-hog} = f_{prob}0.19C_{wv}f_{wv-v}L^2BC_b \quad \text{for hogging} \tag{5}$$

in which $M_{\text{sw-min-sea-mid}}$ is the vertical still water bending moment (sagging and hogging), $M_{\text{wv-sag}}$ and $M_{\text{wv-hog}}$ are the wave-induced sagging and hogging moments, respectively, f_{prob} is a coefficient to be taken as 1.0, $f_{\text{wv-v}}$ is the distribution factor for wave-induced bending moment along the vessel length equal to 1.0 at midship, C_b is the block coefficient of the ship, L is the ship length, B is the ship breadth, and C_{wv} is a coefficient calculated as follows [2]:

$$C_{wv} = \begin{cases} 10.75 - \left(\dfrac{300 - L}{100}\right)^{\frac{3}{2}} & \text{for } 150 \le L \le 300 \\ 10.75 & \text{for } 300 \le L \le 350 \\ 10.75 - \left(\dfrac{L - 350}{150}\right)^{\frac{3}{2}} & \text{for } 350 \le L \le 500 \end{cases} \tag{6}$$

For reliability purposes, the safety of the ship structure is quantified with respect to extreme events produced by the load effect L_n. Appropriate probabilistic tools to model this type of loading are the extreme value distributions. Exact modeling of extreme value distributions is usually a formidable task.

Alternatively, one of three asymptotic extreme value distributions are assigned based on the tail behavior of the original distribution [13]. An appropriate extreme value distribution to be used for modeling sea loads is usually the type I extreme value distribution L_n and is given as [13]

$$f_{L_n}(l) = \alpha_n e^{-\alpha_n(l-u_n)} \exp\left[-e^{-\alpha_n(l-u_n)}\right] \tag{7}$$

where u_n is the characteristic largest value of the initial variate L, and α_n is an inverse measure of the dispersion of L_n. These values are related to the mean μ_{L_n} and standard deviation σ_{L_n} of L_n according to

$$\alpha_n = \frac{\pi}{\sqrt{6}\sigma_{L_n}} \tag{8}$$

$$u_n = \mu_{L_n} - \frac{\gamma}{\alpha_n} \tag{9}$$

where $\gamma = 0.577216$ is the Euler number.

4. Statistical analysis of SHM data

4.1. Preprocessing

Ship structures are subjected to loads with various intensities depending on their operational profiles, described by the sea state, heading and ship speed. For design and assessment purposes, the critical load effects resulting from the worst sea state, heading and ship speed combination are typically considered. Therefore, when incorporating SHM data into the reliability analysis, one option is to identify this combination and use the data from monitoring the ship while it is subjected to this loading scenario. This approach is used herein.

The approach presented in this paper intends to be applicable with in-service monitoring such that the data is used in updating the reliability of the monitored ship. However, an in-service monitoring case was not available to illustrate the concepts and thus monitoring data from a scaled test model is used as an application under the assumption that it was collected from the actual ship. The SHM data utilized in this paper are collected from monitoring a Froude-scaled test model. Therefore, all data are first scaled up to the full-scale ship dimensions using the Froude-scaling factors, such that the bending moment is scaled by $1.025\lambda^4$ and the time is scaled by $\sqrt{\lambda}$, where λ is the scale factor.

As mentioned previously, the SHM data is used for the Bayesian updating in the lifetime reliability assessment. The collected SHM signal constitutes the high frequency waves produced by the slamming effects superimposed over the low frequency waves produced by the regular sea wave-induced bending moments. For the reliability analysis, these two components need to be separated by filtering the signal so that they are statistically analyzed independently. In this paper, the signal is filtered using a Butterworth filter [14].

4.2. Peak extraction

Monitoring the strains caused by the longitudinal bending moments on the ship hull yields a signal that oscillates from negative to positive values as the bending moments go from sagging to hogging. Based on the sign convention of the SHM data used in this paper, negative represents sagging and positive represents hogging. In each wave cycle, the signal provides all the values recorded at the sampling rate, but only the peak sagging and hogging values are of interest in the reliability analysis. Therefore, the peak signals need to be extracted from the complete record for the sagging and hogging moments independently.

In this paper, a peak extraction algorithm is developed and implemented to obtain the datasets of maximum bending moments in hogging and sagging separately from the signal. This algorithm is described as follows.

1- Let $X = [x_1, x_2, \ldots, x_k]$ be the recorded SHM signal. Let also $a = 1$, $b = 1$.
2- Starting from $x_1 = 0$, find first $x_i \neq 0$.
3- Starting from x_{i+1}, search the rest of signal to find x_j which has a different sign from x_i or $j = k$.
4- If sign of x_i is positive, find $P_a = \max(x_i, x_{i+1}, \ldots, x_{j-1})$ and let $a = a + 1$.
5- If sign of x_i is negative, find $N_b = \min(x_i, x_{i+1}, \ldots, x_{j-1})$ and let $b = b + 1$.
6- Make $i = j$ and repeat from Step 3 until $j = k$.

Accordingly, the above algorithm provides two vectors, namely the vector of positive (hogging) peaks P and the vector of negative (sagging) peaks N. In fact, this algorithm is applied with the low frequency waves, giving the two vectors P_L and N_L and with the high frequency waves, giving the two vectors P_H and N_H.

4.3. Low frequency waves

The low frequency waves are those associated with sea wave-induced bending moments. As mentioned previously, prior knowledge is available from the IACS [2] regarding these loads. Therefore, the two vectors P_L and N_L are used to update the prior loads (i.e., $M_{wv\text{-}hog}$ and $M_{wv\text{-}sag}$, respectively) using Bayesian updating. Section 5 of this paper is dedicated to presenting the details of this process.

4.4. High frequency waves

Unlike the case of the low frequency waves, prior knowledge may not be available for the high frequency waves. Hence, being the only source for this load effect, the two vectors P_H and N_H are used with classical estimation techniques to generate the probability distribution for the dynamic bending moments in hogging and sagging, respectively. Several classical estimation techniques are available, but the maximum likelihood method is used herein to obtain the parameters of the considered distributions for the data and goodness-of-fit tests are used to select the best fitting distribution. As shown later, it turns out that the exponential distribution provides a very good fit for the high frequency peak moments, where the probability density function (PDF) of the exponential distribution is given as

$$f(t) = \begin{cases} \lambda e^{-\lambda t} & \text{for } t > 0 \\ 0 & \text{otherwise} \end{cases} \tag{10}$$

where λ is the mean occurrence rate.

The choice of the exponential distribution may be criticized by the fact that it gives zero as the most probable realization. However, the interest in the data is in the upper tail behavior (i.e., the maximum values) far away from zero and the exponential distribution represents that part of the data very well. In fact, for design and assessment, the obtained results need to be extrapolated using extreme value statistics. The largest value of the exponential distribution asymptotically converges to the type I extreme value distribution (see Eq. (7)) with parameters

$$\alpha_n = \frac{1}{\lambda} \tag{11}$$

$$u_n = \lambda \ln n \tag{12}$$

where n is the number of waves encountered in the period of design storm T, where T is taken as 3 h [15]. The value of n is obtained based on the rate of peak waves encountered during an SHM run as

$$n = \frac{\text{number of peaks collected during an SHM run}}{\text{duration of the SHM run}} \times T \tag{13}$$

5. SHM and Bayesian updating

The Bayesian estimation approach treats the parameters of the PDF as random variables, θ_i, and makes it possible to make use of prior knowledge [16]. In the Bayesian approach, the θ_i parameters are described by a PDF called the prior PDF $f'(\theta)$, which constitutes the prior knowledge that is intended for combining with the SHM data. In addition, the prior PDF has parameters of its own called hyper-parameters [17]. The new information obtained from SHM, is in a form of a discrete sample. This data is used to construct the likelihood function $L(\theta)$ as [16]

$$L(\theta) = \prod_{i=1}^{N} f_X(x_i|\theta) \tag{14}$$

where $f_X(x_i|\theta)$ is the PDF of X evaluated at the SHM data value x_i, given that the parameter of the PDF is θ. Combining the prior with the likelihood provides the new updated information about the parameter θ, which is in the form of the posterior PDF $f''(\theta)$ given as [16]

$$f''(\theta) = kL(\theta)f'(\theta) \tag{15}$$

where k is a normalizing constant required to make $f''(\theta)$ a proper PDF and is calculated independently of θ as

$$k = \left[\int_{-\infty}^{\infty} L(\theta)f'(\theta)\mathrm{d}\theta\right]^{-1} \tag{16}$$

The basic random variable X is then updated based on the updated posterior PDF of its parameters. By virtue of the total probability theorem, the updated PDF of X is

$$f'_X(x) = \int_{-\infty}^{\infty} f_X(x|\theta)f''(\theta)\mathrm{d}\theta \tag{17}$$

Closed-form solutions for Eq. (17) are not always possible, and alternatively, an approximate updated distribution can be found by first performing numerical integration to obtain the cumulative distribution function (CDF)

$$F'_X(y_i) = \int_{-\infty}^{y_i}\int_{-\infty}^{\infty} f_X(u|\theta)f''(\theta)\mathrm{d}\theta\mathrm{d}u \quad i = 1,2,\ldots,k \tag{18}$$

where $Y = [y_1, y_2, \ldots, y_k]$ is an array of values large enough to cover the range of probable values of X and with small enough interval, and then, an appropriate CDF is fitted to the obtained values using the method of least squares, where the parameters p of the distribution are determined by solving the following optimization problem [18]

$$\textit{Find: the parameters vector } P = \{p_1, p_2, \ldots, p_n\} \tag{19}$$

$$\textit{To minimize: } s = \sum_{i=1}^{k}[F(y_i) - F^*(y_i,p)]^2 \tag{20}$$

where $F^*(y_i, P)$ is the fitted CDF at y_i with parameters P.

In this paper, it is considered that the extreme value distribution parameter u_n has a greater impact on $f_{L_n}(l)$ than the parameter α_n, and thus α_n is known while u_n is updated with the SHM data using

Bayesian updating. Also, from the prior information an initial estimate of u_n is used, i.e., the prior PDF of u_n, where it is assumed that the u_n is lognormal and given as

$$f'(u_n) = \frac{1}{\zeta u_n \sqrt{2\pi}} e^{\left[-\frac{1}{2}\left(\frac{\ln u_n - \lambda}{\zeta}\right)^2\right]} \tag{21}$$

where ζ and λ are the hyperparameters of the variate u_n and are related to the mean and standard deviation of the variate u_n according to

$$\zeta = \sqrt{\ln\left(1 + \frac{\sigma^2}{\mu^2}\right)} \tag{22}$$

$$\lambda = \ln\mu - \frac{1}{2}\zeta^2 \tag{23}$$

The mean μ is obtained from the prior information and σ is calculated based on an assumed COV of 10%.

The literature linking the themes of Bayesian updating and extreme value modeling is sparse, in part due to computational difficulties that some of which have recently been overcome by techniques such as Markov chain Monte Carlo (McMC) [19]. Okasha and Frangopol [20] have used the slice sampler algorithm [21] for this purpose, and it is also used herein.

6. Lifetime reliability and redundancy

The Latin Hypercube sampling [22] is used herein, as an efficient alternative to Monte Carlo simulation, to propagate the uncertainties associated with the basic random variables into the ultimate and first bending moments. The basic random variables pertinent to the ship resistance are the plating thickness t, elastic modulus E, plating yielding stress σ_{Yp}, stiffener yielding stress σ_{Ys}, corrosion initiation time and annual corrosion rate. In addition, the variability of the applied bending moments is taken into account by considering the statistical parameters shown in Ayyub et al. [7]. The lognormal distribution, concerning the resisting moment, has its mean and standard deviation found directly from the generated Latin Hypercube samples.

In this paper, the instantaneous reliabilities of the ship hull with respect to first and ultimate failures are studied. Without (i.e., before) SHM, the reliability is analyzed without considering the dynamic load effect and hence the instantaneous limit state function is defined as

$$g(t) = x_R M(t) - x_{sw} M_{sw} - x_w k_w M_w = 0 \tag{24}$$

where $g(t)$ is the time-dependent performance function, $M(t)$ is the time-variant resisting bending moment, M_{sw} is the still water bending moment, M_w is the wave-induced bending moment, x_R is the model uncertainty associated to the resistance determination, x_{sw} is the model uncertainty related to the still water bending moment prediction, x_w is the model uncertainty associated to the wave-induced bending moment prediction, and k_w is a correlation factor for wave-induced bending moment and is set to 1.0 [7]. The model uncertainty coefficients x_R, x_{sw}, and x_w, are assumed normally distributed with mean values of 1.0, 1.0, and 0.9, and COV equal to 0.10, 0.05, and 0.15, respectively [4].

With SHM, the dynamic bending moment is present and considered and hence the limit state function (i.e., Eq. (24)) becomes

$$g(t) = x_R M(t) - x_{sw} M_{sw} - x_w (M_w + k_d M_d) = 0 \tag{25}$$

where M_d is the dynamic bending moment and k_d is the correlation factor between wave-induced and dynamic bending moments and is conservatively assumed as 1.0.

The instantaneous reliability index and the corresponding probability of failure are computed by the program CALREL [23] where the second-order reliability method (SORM) is used herein.

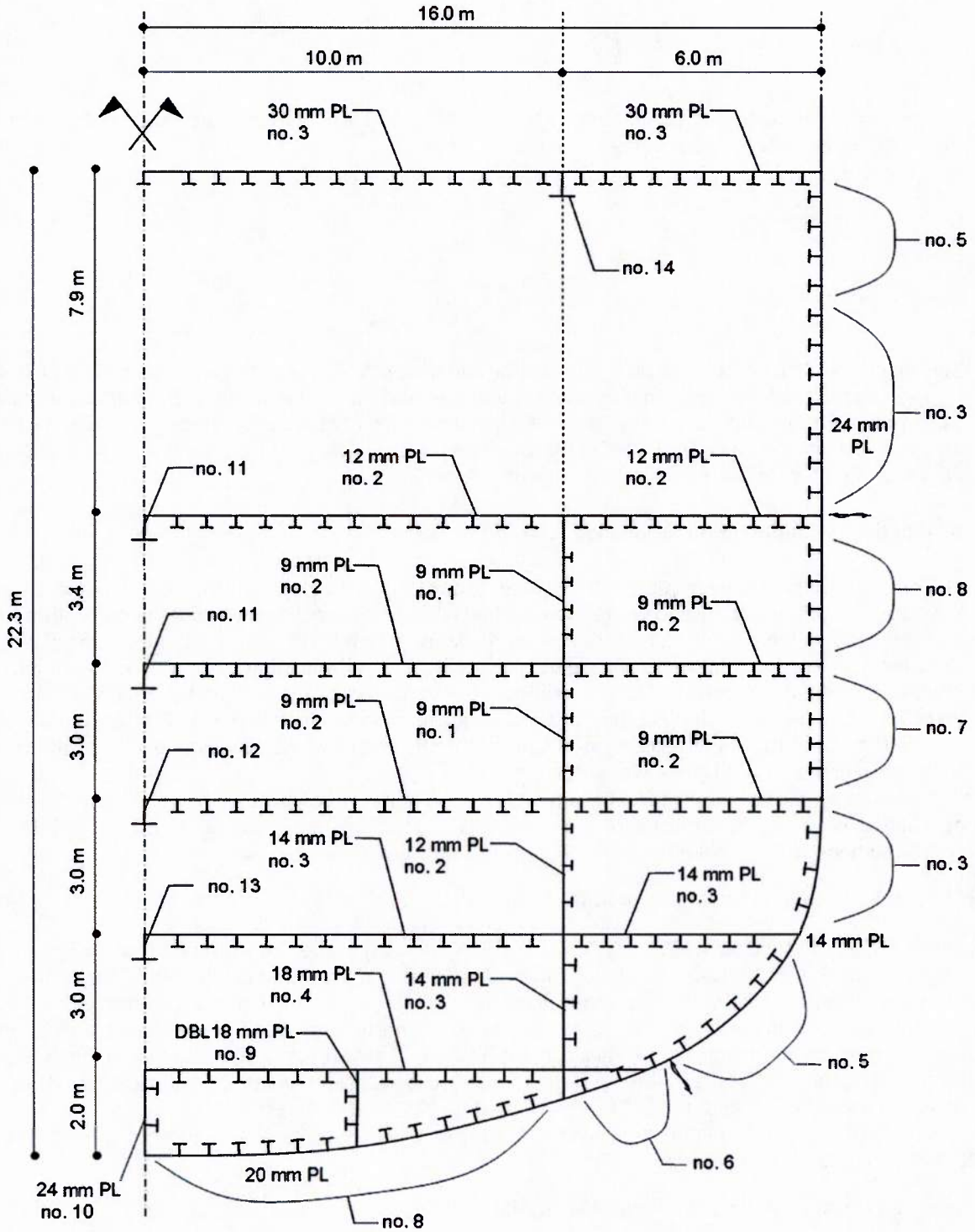

Fig. 1. Cross-section geometry of a symmetric half hull at Station 10 (midship). Numbers in figure refer to component types (see Table 1).

Table 1
Geometric properties of the components in Fig. 1.[24].

Stiffener No.	Designation	d (mm)	t_w (mm)	b (mm)	t_f (mm)
1	5 × 4 × 6	125.5	4.8	100.6	5.3
2	8 × 4 × 10	200.4	4.3	100.1	5.2
3	10 × 4 × 12	250.7	4.8	100.6	5.3
4	8 × 4 × 15	206	6.2	102.1	8
5	12 × 4 × 16	304.5	5.6	101.3	6.7
6	12 × 4 × 19	308.9	6	101.9	8.9
7	10 × 5 3/4 × 22	258.3	6.1	146.1	9.1
8	14 × 5 × 22	349	5.8	127	8.5
9	8 × 6 1/2 × 28	204.7	7.2	166.1	11.8
10	7 × 8 × 21.5	173.5	7.7	203.2	13.5
11	24 × 9 × 94	616.7	13.2	230.1	22.1
12	24 × 12 × 119	616.2	14	325.1	21.6
13	24 × 14 × 146	628.4	16.5	327.7	27.7
14	36 × 16 1/2 × 230	911.4	19.6	418.3	32

d = depth of stiffener, t_w = thickness of web, b = width of web and t_f = thickness of flange.

Redundancy is a useful performance indicator that provides warnings of partial failure. Once the reliability index and probability of failure are obtained, the time-dependent redundancy index can be calculated using the following redundancy index [9]

$$RI(t) = \frac{P_{f,FF}(t) - P_{f,UF}(t)}{P_{f,UF}(t)} \tag{26}$$

where $P_{f,UF}(t)$ is the probability of ultimate failure of the hull, and $P_{f,FF}(t)$ is the probability of first failure in the hull.

7. Application: JHSS

7.1. Description of the ship, its model and testing procedure

The concepts presented in this paper are illustrated on the Joint High-Speed Sealift Ship (JHSS). The hull of this ship is characterized by an unusually-fine hull form and a "gooseneck" bulbous bow for improved high-speed performance. A scaled structural segmented seakeeping model was constructed and successfully tested in the NSWCCD Maneuvering and SeaKeeping (MASK) basin during July and August of 2007 to obtain representative ship motions and structural primary and secondary loading data in support of validation studies for numerical tools for simulation of ship motions and loads, specifically the Large Amplitude Motions Program (LAMP) [24]. Sectional design properties for the full-scale hull and model backspline along with geometric properties of the components are provided in Devine [24]. A schematic diagram of the midship design section (Station 10) is shown in Fig. 1 [24]. Geometric properties of the components in Fig. 1 are shown in Table 1 [24].

Table 2
Statistical descriptors of the corrosion model parameter C_1.

Location	Mean (mm/year)	Standard deviation (mm/year)
Deck plating	0.008125	0.000406
Deck stiffener web	0.008125	0.000406
Side shell plating	0.003750	0.000188
Side stiffener web	0.003750	0.000188
Bottom shell plating	0.021250	0.001063
Bottom stiffener web	0.008125	0.000406

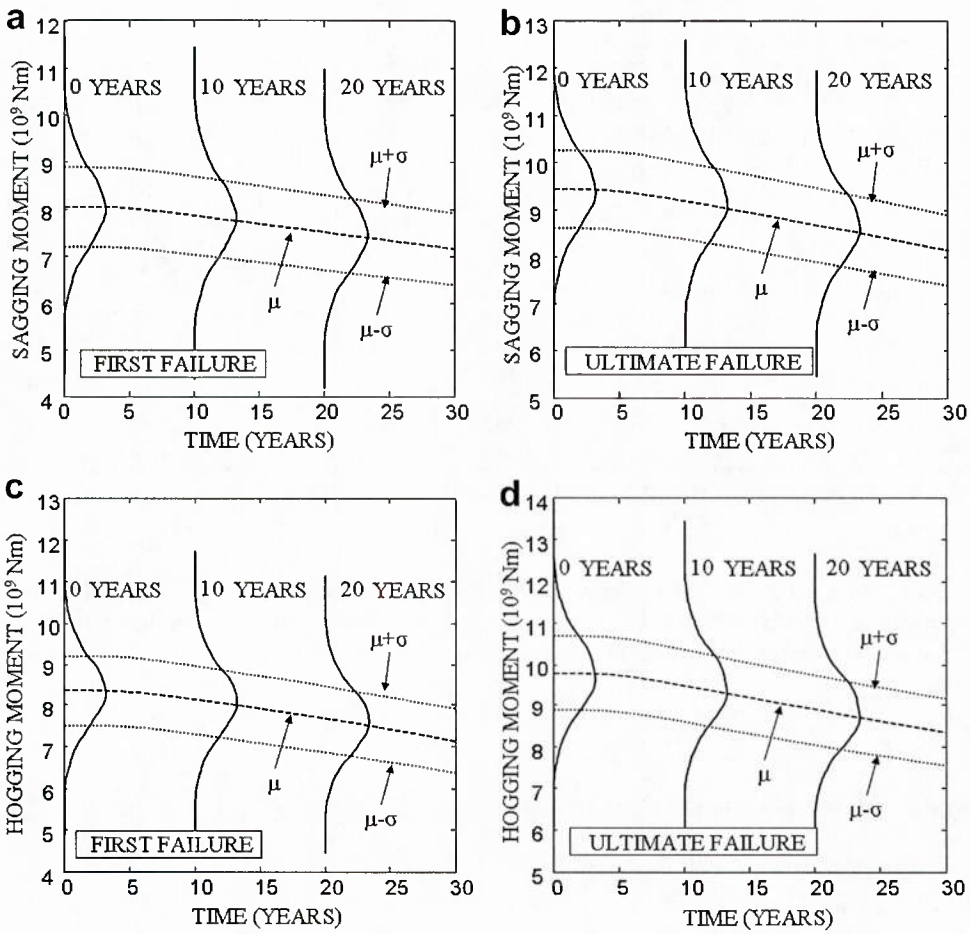

Fig. 2. Profiles of first and ultimate failure moments for sagging ((a) and (b)), hogging ((c) and (d)); mean profiles, mean plus and minus one standard deviation profiles, and PDF of the moments at 0, 10, and 20 years.

The model was Froude-scaled down with the selected scale factor ($\lambda = 47.2533$) to make it small enough to perform the tests within the constraints of the MASK test facility while keeping the model large enough to provide meaningful results [24]. A Froude-scaled continuous aluminum backspline beam connected the shell sections to provide realistic vibrational response due to wave-induced forces including hull primary and secondary loads due to wave and slam-induced hull whipping [24]. Strain-gages, calibrated to known loads prior to the test, were used to measure the primary and secondary structural response during each test run and were mounted at each segment cut to measure the vertical, lateral and torsional bending moments and vertical and lateral shear forces. Static load calibrations were used to generate sensitivities to convert structural response to load so that the output voltage from a strain gage bridge circuit were converted directly to load, bending moment or shear force [24].

Table 3
Statistical descriptors and distributions of the prior applied loads.

Load effect	Mean (Nm)	Coefficient of variation	Distribution type
Sagging still water bending moment	1.823×10^9	0.15	Normal
Sagging wave-induced bending moment	3.867×10^9	0.15	Extreme value type I
Hogging still water bending moment	3.283×10^9	0.15	Normal
Hogging wave-induced bending moment	2.729×10^9	0.15	Extreme value type I

In this paper, the bending moment readings from midship (Station 10) from all 21 runs at speed 35 knot and heading 0° and in sea state 7 are used. The size of the datasets for each run ranges from 3200 to 4000 samples, with a total of 73,800 samples. The sampling rate was 200 Hz and hence the total duration of the test was about 6.15 min. All data were scaled up to the full-scale ship dimensions using the Froude-scaling factors, such that the bending moment is scaled by $1.025\lambda^4$ and the time is scaled by $\sqrt{\lambda}$. Accordingly, the time duration of the test measured in full scale is about 42.28 min.

7.2. Resistance modeling

The first failure and ultimate bending moments are computed probabilistically. The Latin hypercube sampling is used to generate 5000 samples for the random variables considered. These random variables are the plating thickness t, elastic modulus E, plating yielding stress σ_{Yp}, and stiffener yielding stress σ_{Ys} and they have the lognormal distribution with COV 0.05, 0.03, 0.1, and 0.1, respectively [24]. The residual stress value has been assumed to be equal to 5% of the plating yielding stress. For each sample, the first failure and ultimate bending moments are

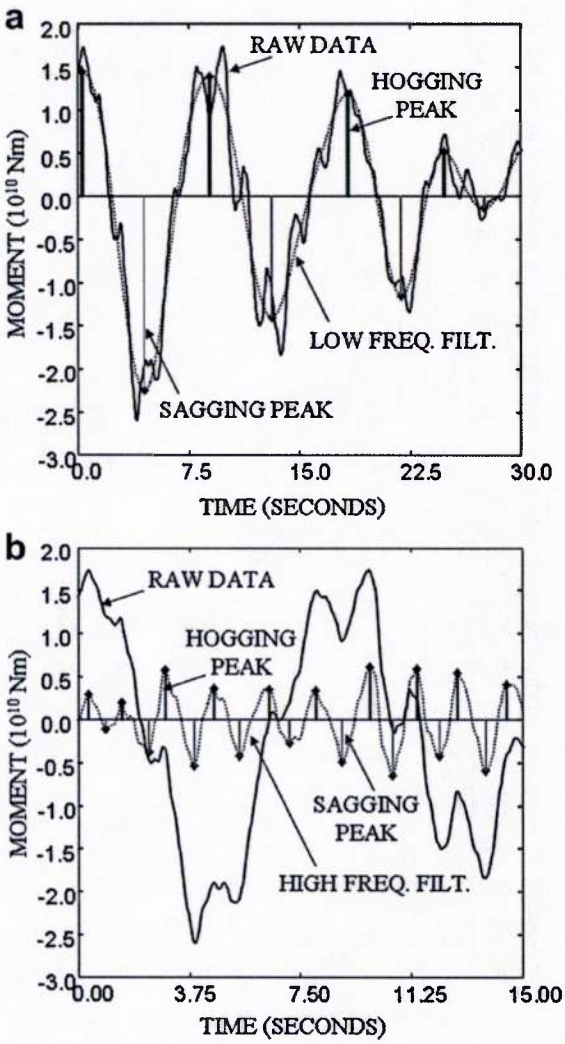

Fig. 3. Peak extraction from SHM signal for: (a) low and (b) high frequency filtered signals.

computed and the resulting set of moments in each case are used to fit its probability distribution. This is repeated for 30 years in two year increments where at each increment the plate and stiffener web thicknesses are reduced to account for the corrosion loss at that time increment.

Table 2 shows the mean and standard deviation of the assumed annual lognormal corrosion rate C_1 with respect to the location of the stiffened plates. Prior to using the values in Table 2, others from the literature have been tried. However, it was found that owing to the high values of corrosion penetration and very high COV provided by these corrosion models, in addition to the small plate thicknesses used in the section of this ship, the corrosion loss obtained after few years become larger than some of the generated plate thicknesses samples. Indeed, these corrosion models are conservative and the light weight design of this ship yielded very thin plates such that more accurate corrosion models are needed for time-dependent reliability. The values in Table 2 are proportional fractions of those in Akpan et al. [5]. The results of the strength analyses are shown in Fig. 2.

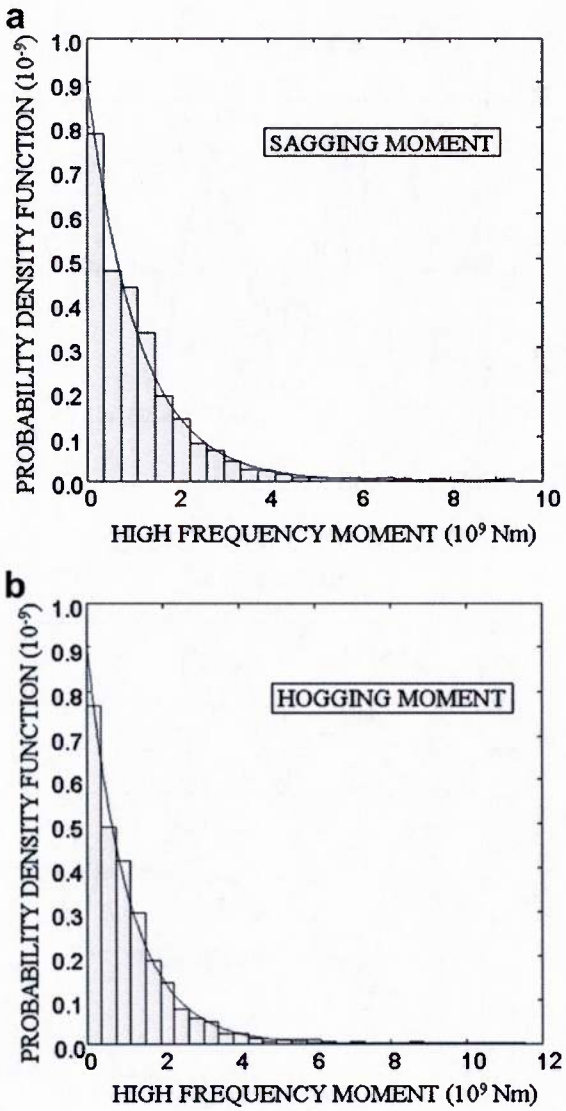

Fig. 4. Histograms and probability density function of the high frequency moments in: (a) sagging and (b) hogging.

Table 4
Statistical descriptors and distributions of the high frequency moment.

Loading condition	Mean (Nm)	Coefficient of variation	Distribution type
Sagging	1.183×10^9	0.134	Extreme value type I
Hogging	1.185×10^9	0.134	Extreme value type I

7.3. Prior loads

The still water and wave-induced bending moments are computed using Eqs. 2 through 5 [2]. The variability of these moments is taken into account by considering the still water moment and wave-induced moment as normal and type I extreme value, respectively, with COV of 0.15 for both [7]. A summary of the results is shown in Table 3.

7.4. Reliability, redundancy, SHM and Bayesian updating

The load and resistance information obtained thus far provide the means to compute the initial prediction of reliability and redundancy over time for the JHSS ship. Next, the SHM data is integrated

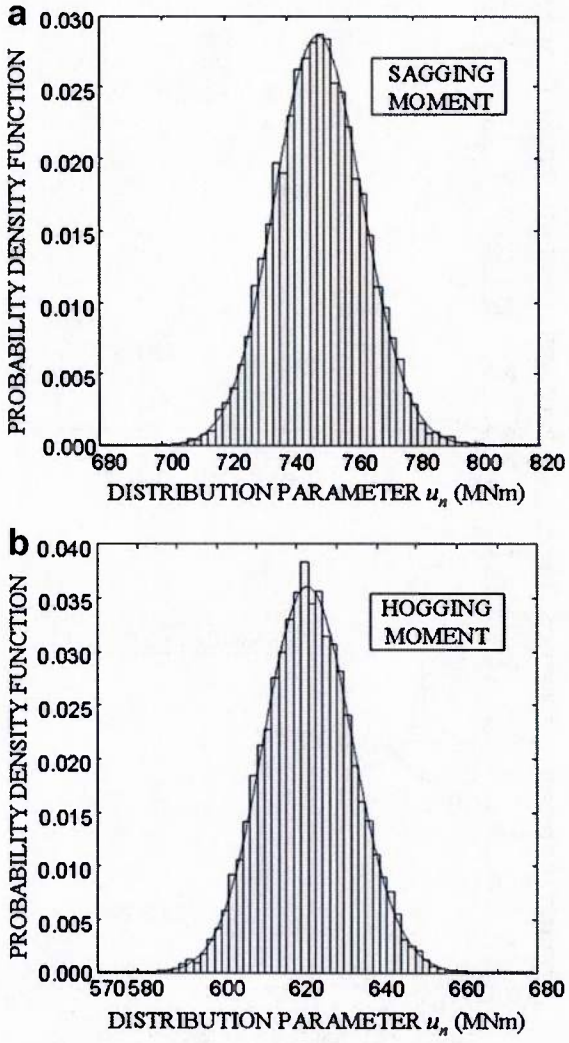

Fig. 5. Histograms and probability density function of the extreme value distribution parameter u_n of the high frequency moment samples generated from the slice sampler in Bayesian updating for: (a) sagging and (b) hogging moments.

into this prediction to provide an updated assessment of the ship performance. First, the SHM data is preprocessed. The bending moment readings from midship (Station 10) from all 21 runs at speed 35 and heading 0° and in sea state 7 are scaled up using the Froude-scaling rules ($1.025\lambda^4$). Then, the signal is filtered using the Butterworth filter in the MATLAB signal processing toolbox [14] to separate the low frequency waves from the high frequency waves. In each case, the developed peak extraction algorithm is used to extract the maximum moment readings from the wave cycles. Fig. 3 shows an example of the results from sampling and peak extraction of run 215 for both the low and the high frequency filtered signals. The process provided 397 peaks of low frequency moment peaks (in each of the sagging and hogging moments) and 1861 peaks of high frequency moment peaks (in each of the sagging and hogging moments).

The histograms of the obtained high frequency moment peaks in sagging and hogging are shown in Fig. 4. It is clear from the figure and the results of the Kolmogorov–Smirnov test [16] that the exponential distribution fits these peaks very well. Using the parameters of the obtained exponential

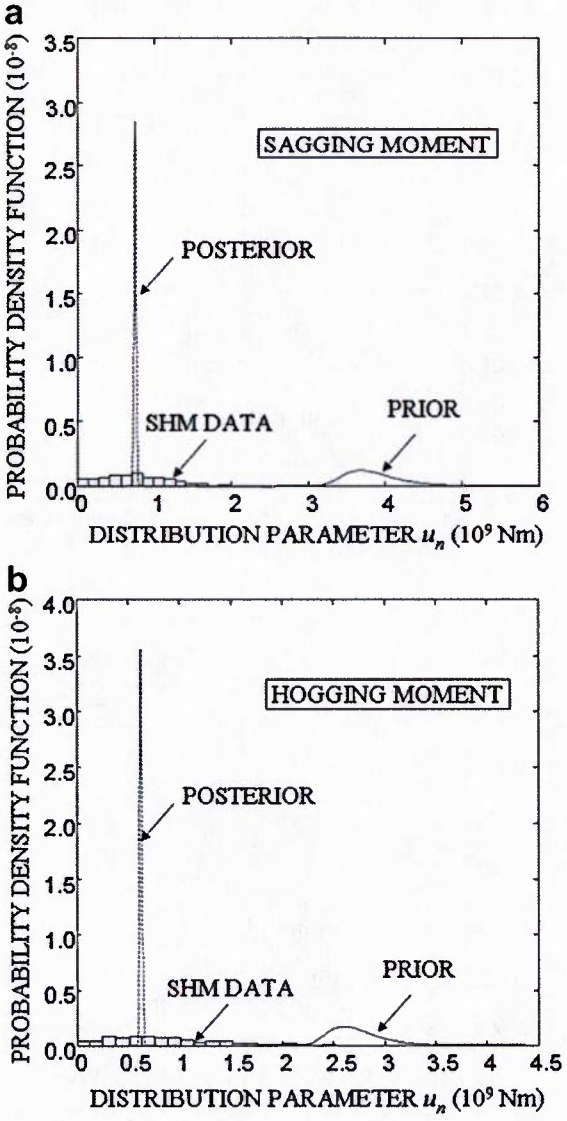

Fig. 6. Bayesian updating results of the extreme value distribution parameter u_n for: (a) sagging and (b) hogging moment.

distributions, extreme value statistics are used to find the parameters of the corresponding extreme value type I distributions. The results are shown in Table 4. The results in the table show that the dynamic load effects can be very large in rough operational conditions. However, the sea state 7, 35 knot speed and head seas example data set provided by the NSWCCD and considered as the worst operational conditions herein represents conditions more severe than the ship would be expected to encounter. Therefore, the results are expected to be exaggerated and conservative. However, the methodology remains applicable with any SHM data collected during any operational conditions.

Next, the low frequency moment peaks are integrated with the prior information using Bayesian updating. The slice sampler is used sequentially with 50 peaks increments to obtain the samples of the posterior distributions. Recall that the parameter to be updated is the extreme value parameter u_n and it is assumed to be lognormally distributed with prior mean calculated using the IACS [2] guidelines and assumed COV of 10%. The obtained posterior samples for the parameter u_n is used to fit a posterior distribution, which was also found to be best modeled by the lognormal distribution.

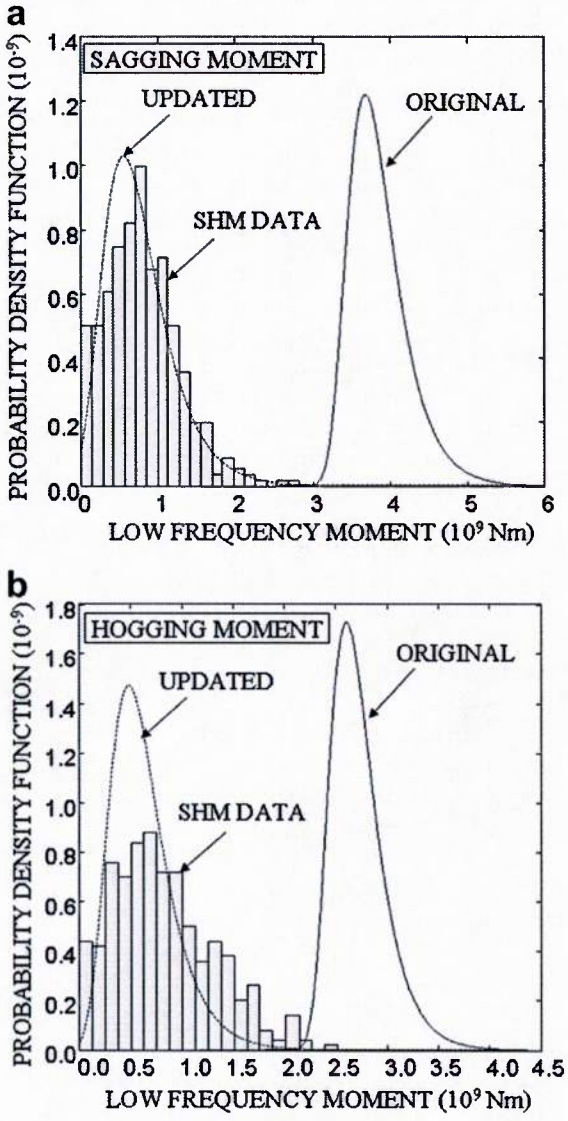

Fig. 7. Original and updated PDF of the low frequency moment in: (a) sagging and (b) hogging.

Fig. 5 shows the histograms and fitted PDFs of the updated parameter u_n for both sagging and hogging moments. The posterior distributions are plot with the prior distributions and showing the histograms of the low frequency peaks found from the SHM data as well in Fig. 6. It is evident that integrating the SHM significantly reduced the uncertainty in this parameter (i.e., the assumed 10% COV in parameter u_n). The posterior distributions are used to update the underlying distribution of the low frequency bending moment and the results are shown in Fig. 7. As shown in the figure, the updated PDF has embraced the low frequency peaks found from the SHM data but with less uncertainty than that exhibited in the data. It is also clear that the prior distribution, which represents design code belief, is conservative with respect to the low frequency peaks obtained from the SHM data and the posterior distribution, even though the operational conditions represented by the SHM data are also conservative. However, when taking into account the high dynamic load effects in addition to the low frequency moments, the total updated effect is more severe. This is shown in Fig. 8 which shows the time-dependent reliability indices associated with first and ultimate failures, in Fig. 9 which shows the time-dependent probabilities of failure associated with first and ultimate failures, and in Fig. 10 which shows the time-dependent redundancy index with and without integrating the SHM data. Clearly, the new total load effect obtained by integrating the SHM data is more severe than the prior load effect (note that the resistance is the same and that the SHM operational conditions are conservative).

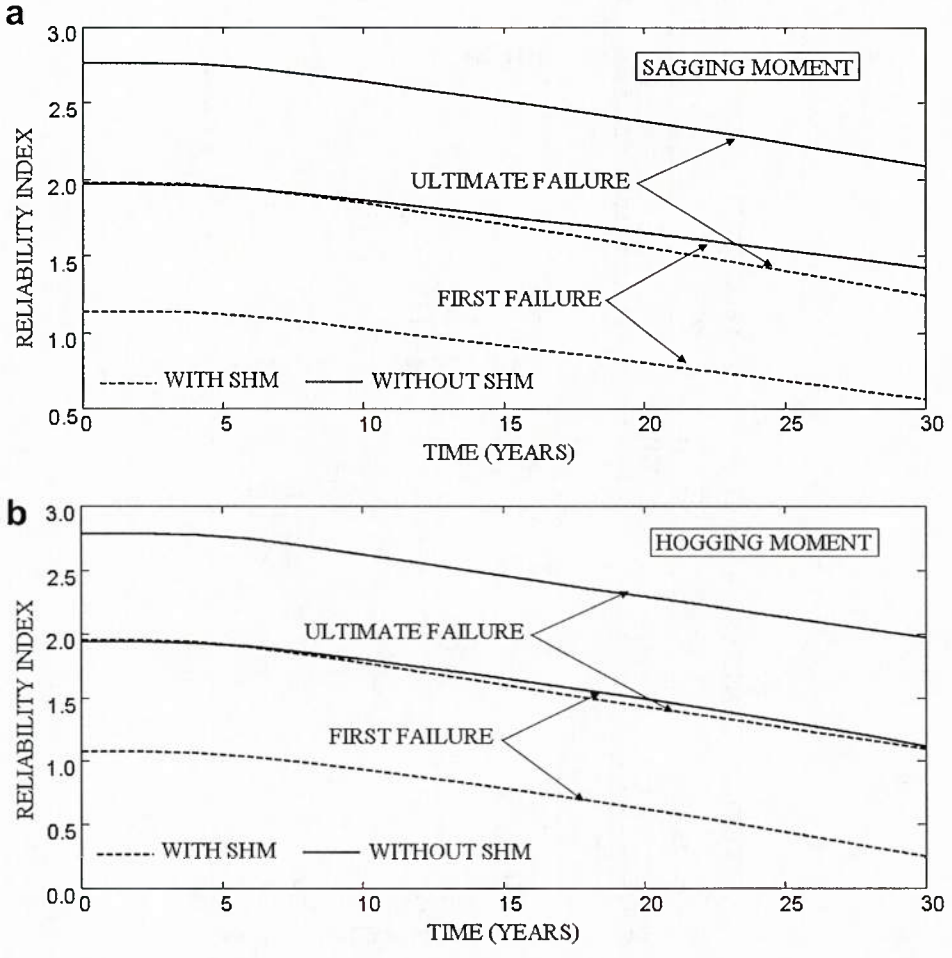

Fig. 8. Reliability index profiles before and after updating for: (a) sagging and (b) hogging moments (first and ultimate failures).

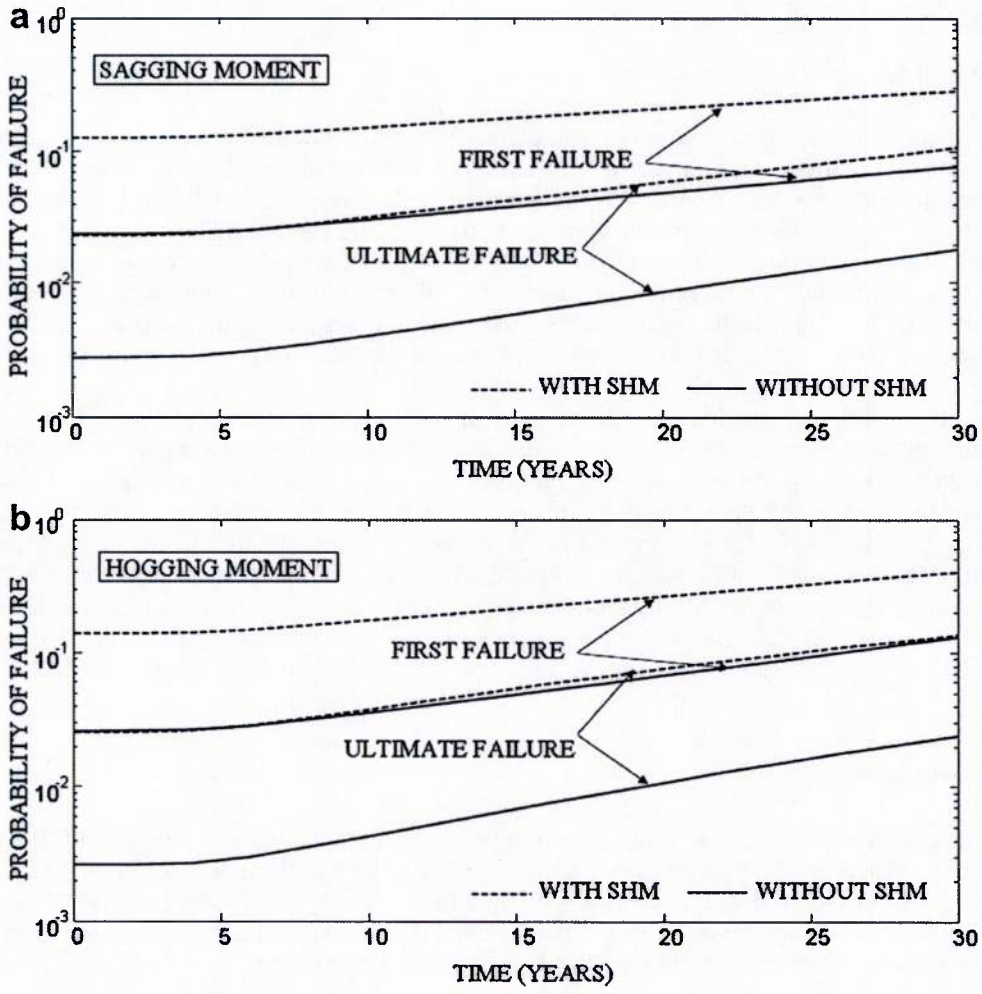

Fig. 9. Probability of failure profiles before and after updating for: (a) sagging and (b) hogging moments (first and ultimate failures).

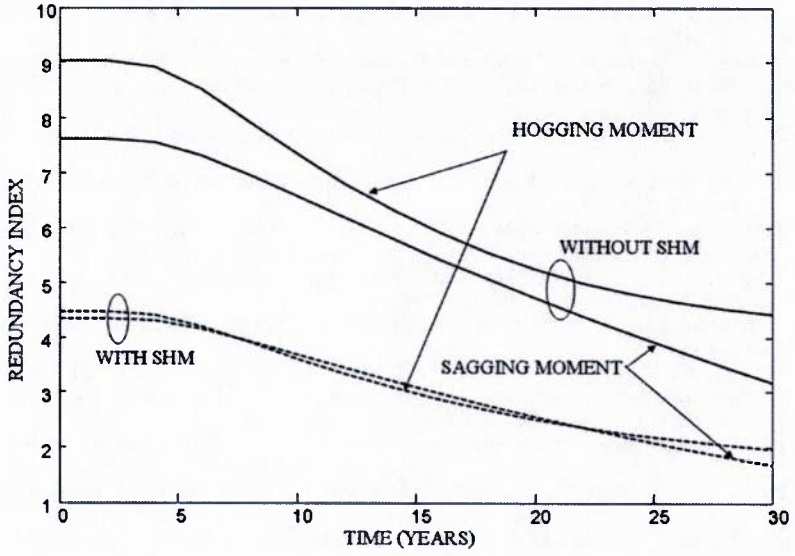

Fig. 10. Redundancy index profiles before and after updating for sagging and hogging moments before and after updating.

8. Conclusions

In this paper, an approach for integrating the information obtained from SHM in the life-cycle performance assessment of ship structures under uncertainty is presented. The resistance with respect to the first and ultimate failure vertical bending moments is determined such that the ultimate failure moment is computed using an optimization-based method and the first failure moment is computed using the progressive collapse method. The reliability indices and probability of failure are computed using a hybrid Latin hypercube sampling – SORM technique. In order to integrate the SHM data with necessary prior information, Bayesian inference concepts are used for updating the load effects. SHM data obtained by testing a scaled model of a Joint High-speed Sealift Ship is used to update its life-cycle reliability and redundancy.

An example data set provided (representing the operational conditions of sea state 7, 35 knot speed and head seas) was considered as the worst operational conditions the ship may encounter. The results are expected to be very conservative. However, the methodology remains applicable with any SHM data collected during any operational conditions. The data set was scaled up to the full-scale ship, filtered and the peaks were extracted using a developed peak extraction algorithm. High frequency moment peaks were used with classical estimation techniques and extreme value statistics to generate the probability distribution of the dynamic bending moment. The results obtained showed that the dynamic load effects can be significant in rough operational conditions. The updated PDF has embraced the low frequency peaks found from the SHM data but with less uncertainty than that exhibited in the data.

Acknowledgments

The support from the Office of Naval Research to Lehigh University under award N-00014-08-0188 is gratefully acknowledged. The authors greatly appreciate the technical discussions with Dr. Edward Devine and Dr. Liming Salvino, Naval Surface Warfare Center, Carderock Division (NSWCCD) and thank them for providing the data used in this paper. The opinions and conclusions presented in this paper are those of the authors and do not necessarily reflect the views of the sponsoring organization.

References

[1] Salvino LW, Brady TF. Hull monitoring system development using a hierarchical framework for data and information management. In: Proceedings of 7th International conference on computer and IT applications in the maritime industries, (COMPIT'08). Liege, Belgium; April (2008).
[2] IACS. Common structural rules for Double hull Oil Tankers. International Association of Classification Societies. Available at, http://www.iacs.org.uk; 2008.
[3] Frangopol DM. Life-cycle performance, management, and optimization of structural systems under uncertainty: Accomplishments and challenges. Structure and Infrastructure Engineering, Taylor & Francis, in press, doi:10.1080/15732471003594427.
[4] Paik JK, Frieze PA. Ship structural safety and reliability. Progress in Structural Engineering and Materials 2001;3:198–210. doi:10.1002/pse.74.
[5] Akpan UO, Koko TS, Ayyub B, Dunbar TE. Risk assessment of aging ship hull structures in the presence of corrosion and fatigue. Marine Structures 2002;15:211–31.
[6] Hussein W, Guedes Soares C. Reliability and residual strength of double hull tankers designed according to the new IACS common structural rules. Ocean Engineering; 2009; doi:10.1016/j.oceaneng.2009.04.006.
[7] Ayyub BM, Assakkaf IA, Atua KI. Reliability-Based load and resistance factor design (LRFD) of hull girders for surface ships. Naval Engineers Journal 2000;112:279–96.
[8] Lua J, Hess PE. First-failure-based reliability assessment and sensitivity analysis of a naval vessel under hogging. Journal of Ship Research 2006;50:158–70.
[9] Decò A, Frangopol DM, Okasha NM. Time-variant redundancy of ship structures, submitted for publication.
[10] Okasha NM, Frangopol DM. Efficient method based on optimization and simulation for the probabilistic strength computation of the ship hull. Journal of Ship Research 2010;54(4):1–13.
[11] Hughes OF. Ship structural design – a rationally-based, computed-aided, optimization approach. New York: Wiley & Sons; 1983.
[12] Luís M, Teixeira AP, Guedes Soares C. Longitudinal strength reliability of a tanker hull accidentally grounded. Structural Safety 2009;31:224–33.
[13] Ang AH-S, Tang WH. Probability concepts in engineering planning and design. In: Decision, risk and reliability, vol. II. New York: Wiley & Sons; 1984.
[14] MathWorks. Signal processing toolbox™ 6-User's Guide. The MathWorks, Inc.; 2009. 1427 pp.

[15] Mansour AE, Hovem L. Probability-based ship structural safety analysis. Journal of Ship Research 1994;38:329–39.
[16] Ang AH-S, Tang WH. Probability concepts in engineering. Emphasis on applications to civil and environmental engineering. 2nd ed. New York: Wiley & Sons; 2007.
[17] Fink D. A compendium of conjugate priors. In Progress Report: Extension and enhancement of methods for setting data quality objectives; 1995, (DOE contract 95-831).
[18] Bucher C. In: Frangopol DM, editor. Computational analysis of randomness in structural mechanics. Structures & infrastructures series, vol. 3. Leiden, The Netherlands: CRC Press - Balkema - Taylor & Francis; 2009. p. 248.
[19] Coles SG, Powell EA. Bayesian methods in extreme value modelling: a review and new developments. International Statistical Review 1996;64:119–36.
[20] Okasha NM, Frangopol DM. Integration of structural health monitoring in a system performance based life-cycle bridge management framework. Structure and Infrastructure Engineering, Taylor & Francis, in press, doi:10.1080/15732479.2010.485726.
[21] Neal RM. Slice sampling, the annals of statistics. Institute of Mathematical Statistics 2003;31:705–41.
[22] Olsson A, Sandberg G, Dahlblom O. On Latin hypercube sampling for structural reliability analysis. Structural Safety 2003;25:47–68.
[23] Liu PL, Lin HZ, Der Kiureghian A. CALREL User Manual. Berkeley, CA: Department of Civil Engineering, University of California; 1983.
[24] Devine EA. An overview of the recently-completed JHSS Monohull and Trimaran structural seaways loads test program. Naval Surface Warfare Center, Carderock Division (NSWCCD) PowerPoint Briefing; 30 October, 2009.

Appendix IV

Nader M. Okasha, Dan M. Frangopol, Duygu Saydam, and Liming W. Salvino. Reliability analysis and damage detection in high-speed naval craft based on structural health monitoring data. *Structural Health Monitoring*, 10(4): 361-379, 2011.

Article

SHM Structural Health Monitoring

Structural Health Monitoring
10(4) 361–379

DOI: 10.1177/1475921710379516
shm.sagepub.com
SAGE

Reliability analysis and damage detection in high-speed naval craft based on structural health monitoring data

Nader M Okasha[1], Dan M Frangopol[1], Duygu Saydam[1] and Liming W Salvino[2]

Abstract

Current and future trends in naval craft design are leaning toward the development of high-speed and high-performance vessels. Lack of information on wave-induced loads for these vessels presents a challenge in ensuring their safety that is best tackled with monitoring operational loads and detecting damage *via* structural health monitoring (SHM) systems. These monitoring systems, however, require efficient statistical and probabilistic procedures that are able to effectively treat the uncertainties inherent in the massive volumes of collected data and provide interpretable information regarding the reliability and condition of the craft structure. In this article, an approach for using SHM data in the reliability analysis and damage detection in high-speed naval craft (HSNC) under uncertainty is presented. This statistical damage detection technique makes use of vector autoregressive modeling for detection and localization of damage in the ship structure. The methodology is illustrated on an HSNC, HSV-2. Data obtained from seakeeping trials of HSV-2 were treated as the SHM data mentioned above.

Keywords

structural health monitoring, damage detection, vector autoregressive modeling, reliability, naval craft

Introduction

Conventional ship structures have received significant research attention over the past several decades which yielded a rich literature. Knowledge on these structures is mature enough that, today, code procedures and even commercial software to compute the ultimate global strength and design loads are well established.[1] The performance of the ship hull can be determined by computing its global strength using the formulation supporting a section analysis and calculating the loads using design expressions. For instance, simplified methods for predicting the load-shortening curves of steel plates and panels considering the effects of initial imperfections are available. These methods facilitates the use of a systematic incremental curvature procedure to determine the ultimate bending moment of a conventional ship hull.

More recently, larger, faster, and more powerful naval craft have been designed. In order to allow higher speeds and increased cargo capacity, high-speed vessels often employ novel and aggressive structural designs using composite or aluminum alloys with innovative arrangements and fabrications to maximize lightship weight reduction.[2] Due to lingering questions related to issues such as the effects of transverse welds and localized heat affected zones resulting from weld attachment, methodologies for predicting the load-shortening of plates and panels, considering initial imperfections and determining the ultimate hull

[1]Department of Civil and Environmental Engineering, Engineering Research Center for Advanced Technology for Large Structural Systems (ATLSS), Lehigh University, Bethlehem, PA 18015-4729, USA.
[2]Structures and Composite (Code 652), Carderock Division, NSWC, 9500 MacArthur Boulevard, West Bethesda, MD 20817-5700, USA.

Corresponding author:
Dan M. Frangopol, Department of Civil and Environmental Engineering, Engineering Research Center for Advanced Technology for Large Structural Systems (ATLSS), Lehigh University, Bethlehem, PA 18015-4729, USA
Email: dan.frangopol@lehigh.edu

strength are not as established or validated for aluminum ship structures as in the case of steel ship structures.[3] Unlike the case of conventional steel ship structures, the performance of high-speed naval craft (HSNC) is specified to be quantified based on comparison of resistance and load effects at the stress (or strain) level and not the global level. According to the American Bureau of Shipping (ABS),[4] direct analyses are required in all naval craft to demonstrate the adequacy of the structural design using the dynamic load approach (DLA).

The DLA is based on using a detailed full-scale three-dimensional finite element model (FEM) of the ship. The most critical loading conditions are determined from seakeeping or testing. The loads associated with these conditions are applied to the FEM and the maximum stresses are checked against acceptable limits.[5]

When performing the DLA, out of the entire record of measured responses from the seakeeping trial, only the worst conditions are selected for application to the FEM. However, the measured responses during the seakeeping trials exhibit significant variability. The odds of encountering this worst condition may not be high enough to justify the design or assess the ship solely upon. Uncertainty is a considerable factor in this process, neglected in the DLA.

To support the conclusions obtained from the DLA, a probabilistic approach in which the variability in the measured load effects are carefully addressed is certainly of high importance. In this article, such an approach is proposed. With this approach, the performance of the HSNC structure is quantified by determining its reliability using the structural health monitoring (SHM) data. In addition, the SHM data are used as an instrument for damage detection in the HSNC structure.

Structural reliability offers a rational framework to quantify uncertainties in strength and demand, and to evaluate the probability of failure. It combines theories of probability, statistics, and random processes with principles of structural mechanics and forms the basis on which modern structural design and assessment codes are developed and calibrated.[6]

The potential economic and life safety implications of early damage detection in aerospace and civil and mechanical engineering systems have motivated a significant amount of research in SHM and vibration-based damage detection.[7] According to a literature survey conducted by Doebling et al.[8] most damage detection methods are global in nature, that is, the dynamic properties (natural frequencies and mode shapes) are obtained for the entire structure from the input–output data using a global structural analysis. However, global damage measures are not sensitive to minor and local damages.[9] Furthermore, such methods involve FEM and system identification methods, which can be computationally expensive.[9] Because all vibration-based damage detection processes rely on monitoring data with inherent uncertainties, statistical analysis procedures are necessary if one is to state in a quantifiable manner that changes in the vibration response of a structure are indicative of damage as opposed to operational and/or environmental variability.[7] It is hence natural and necessary to integrate a statistical damage detection process into the overall assessment of ship structures.

In this article, an approach for using the data obtained from SHM in the reliability analysis and damage detection in HSNC structures under uncertainty is presented. The employed statistical damage detection technique makes use of vector autoregressive (ARV) modeling for detection and localization of damage in the HSNC structure. The methodology is illustrated on an HSNC and uses data obtained from previous seakeeping trials.

Reliability analysis

Analyzing the safety of structures using reliability methods has been recognized as far more rational than deterministically oriented methods. The DLA is a purely deterministic approach relying on a one-time exceedance of the load effect to an acceptable limit, ignoring all other load occurrences, the rate of occurrence, and the associated uncertainties. It is, therefore, deemed essential to conduct a reliability analysis in lieu of the deterministic acceptable limit check stated by the DLA.

To be in line with, and comparable to, the DLA, the reliability analysis approach established herein also aims to quantify the safety of the structure at key locations, predetermined by finite element analysis and engineering judgment. These key locations are instrumented with proper monitoring sensors to gather the data needed for the reliability assessment. The reliability is quantified in terms of the strain induced by global or local load effects. Herein, the strains induced by the global longitudinal bending moments are considered. Since the longitudinal bending moment acts in sagging and hogging, the reliability of the craft structure at the key locations associated with the induced strain is also determined in both sagging and hogging.

In addition to the wave-induced bending moments experienced by HSNC structures due to the speed of these vessels, slamming loads (i.e., dynamic load effects) are significant. Slamming impact creates whipping strains that should also be taken into account in addition to the strains produced by the ordinary wave-induced

bending moments in the reliability analysis. Therefore, the limit state at a given key location is given as:

$$g = x_R \varepsilon_R - x_w(\varepsilon_w + k_d \varepsilon_d) = 0 \quad (1)$$

where g is the performance function, ε_R the resisting strain, ε_w and ε_d the strains produced by the wave-induced bending moment and the dynamic load effects, respectively, x_R the model uncertainty associated with the resisting strain, x_w the model uncertainty associated to the wave-induced load effect prediction, and k_d the correlation factor between wave-induced moment and dynamic load effects, and is conservatively assumed as 1.0. The model uncertainty coefficients x_R and x_w are assumed to be normally distributed with mean values of 1.0 and 0.9, and coefficient of variation (COV) equal to 0.10 and 0.15, respectively.[10]

In reliability analysis, the safety is measured by the reliability index $\beta = \Phi^{-1}(1 - P_f)$ where Φ is the cumulative distribution function (CDF) of the standard normal distribution and P_f is the probability of failure computed as $P_f = P[g < 0]$, where $P[E]$ the probability of occurrence of the event E.

Statistical analysis of SHM data

Filtering

As previously mentioned, the load effects (i.e., strains) considered herein are associated with both wave-induced bending moments and slam impact waves. These loads act on the structure simultaneously such that their effects are combined. Thus, the collected SHM signal constitutes of the high-frequency waves produced by the slamming effects superimposed over the low-frequency waves produced by the ordinary sea wave-induced bending moments.

Figure 1(a) shows a hypothetical time history of the strains induced in an extreme fiber of the hull amidship and Figures 1(b) and (c) show its filtered low- and high-frequency signals, respectively. At a point in time, a slam impact is encountered, which induces whipping strains. These strains are superimposed on the ordinary wave-induced strains, where the whipping strains oscillate at higher frequency than the frequency of the ordinary wave-induced strains. As shown in Figure 1(a), some of the whipping strains are added to the positive ordinary wave-induced strains to increase the combined sagging strains, while others are added to the negative ordinary wave-induced strains to increase the combined hogging strains. The filtered high-frequency waves that contribute to the combined sagging strains are those with positive sign and that of the combined hogging strains are those with negative sign (Figure 1(c)). Therefore, positive and negative high-frequency strains

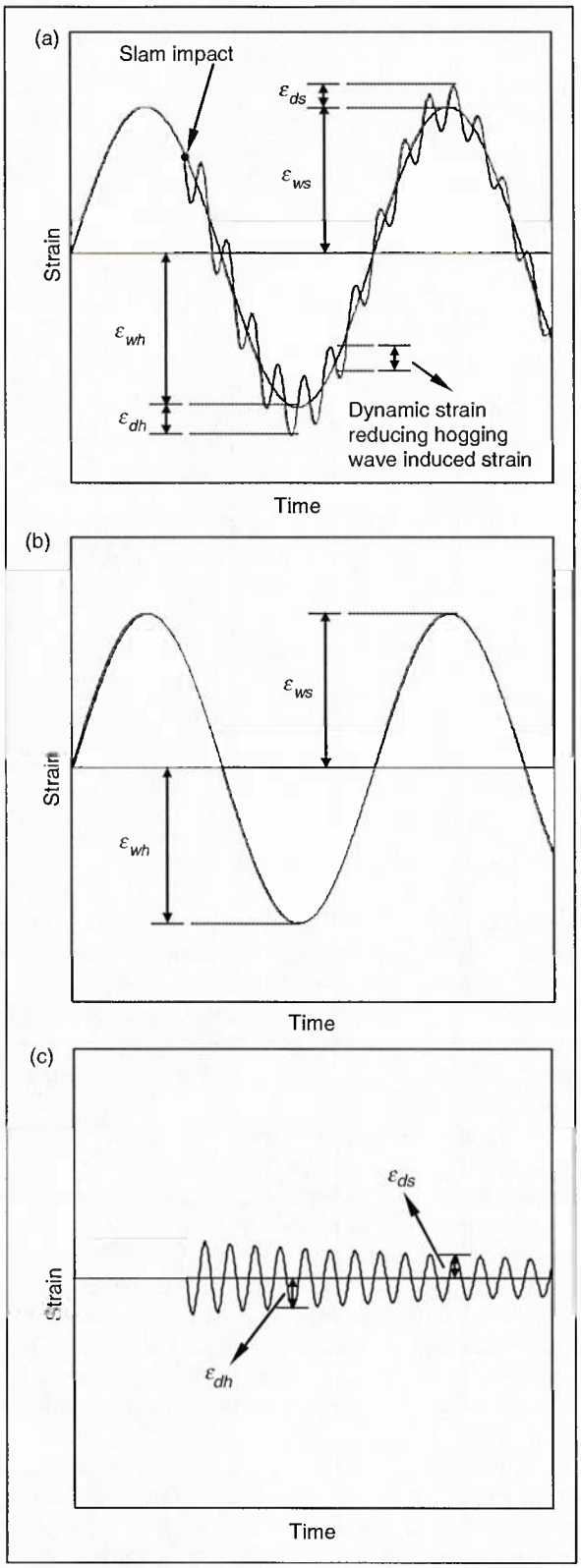

Figure 1. (a) Hypothetical time history of the strains induced in an extreme fiber of the hull amidship, and its filtered (b) low- and (c) high-frequency signals.

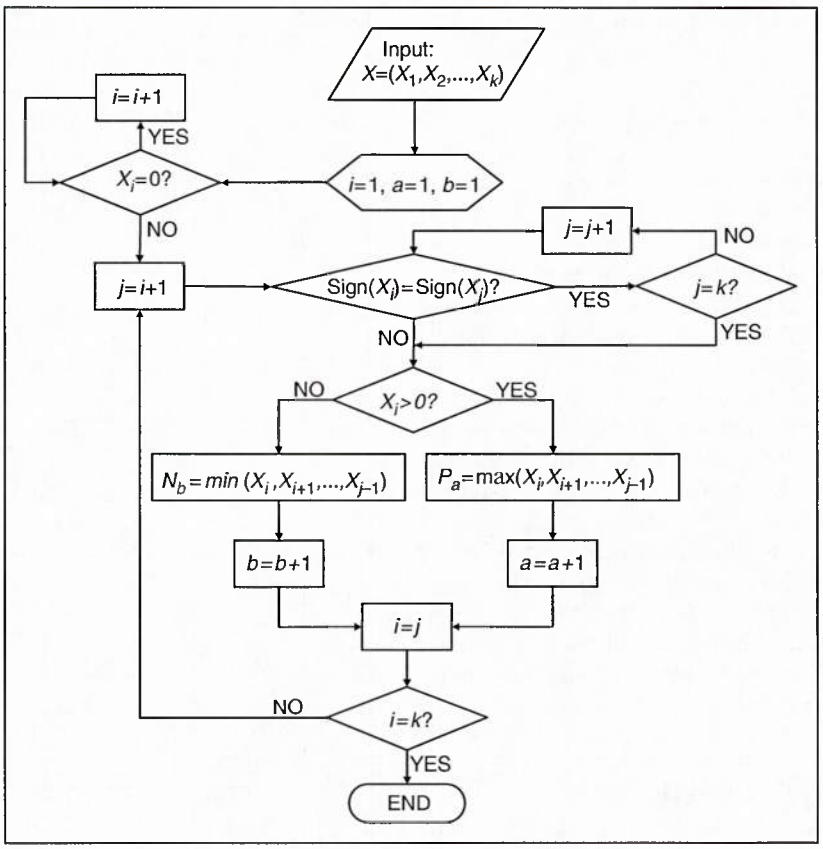

Figure 2. Peak extraction algorithm.

are termed sagging and hogging high-frequeney strains, respectively, to express their association with the eombined hogging and sagging strains. However, it is important to realize that high-frequeney strains, eaused by slam impacts, do not necessarily cause physieal global sagging and hogging bending of the ship hull.

It ean also be seen in Figure 1(a) that some of the high-frequency strains reduee the eombined strains in sagging or hogging. This is a safe scenario that should not eause worry. The randomness in the oeeurrenee of these waves, in high and low frequeney, dietates that all positive high-frequeney strains be treated as realizations of a random variable and be associated with the combined sagging strains. Likewise, all negative high-frequeney strains are treated as realization of a random variable and assoeiated with the combined hogging strains.

In this artiele, the signal is filtered using a Butterworth filter[11] with the eut-off frequency used as 2 Hz (0.04 of the Nyquist frequency). The Butterworth filter is a type of linear analog electronic filters. A digital implementation of Butterworth filter is used to separate low-and high-frequency strains in this study. Butterworth filters are eharacterized by a magnitude response that is maximally flat in the passband and monotonie overall. They have a trade-off between the roll-off steepness and the monotonicity in the passband and stopband. Butterworth filters have a monotonieally changing magnitude funetion with frequency, unlike other filter types that have nonmonotonic ripple in the passband and the stopband. MeClellan–Parks filter design algorithm, which was used in Brady,[12] is an iterative algorithm for finding the optimal Chebyshev finite impulse response filter. Compared with a Chebyshev filter or an elliptie filter, the Butterworth filter has a slower roll-off, and thus will require a higher order to implement a particular stopband speeifieation. However, Butterworth filters have a more linear phase response in the passband than the Chebyshev and elliptie filters.

Peak extraction

In this artiele, positive readings of the strain sensors are associated with sagging-induced strains and negative readings are associated with hogging-indueed strains. In eaeh wave eycle, the signal provides all the values recorded at the sampling rate, but only the peak sagging and hogging strains are of interest in the reliability

analysis. Therefore, the peak strains need to be extracted from the complete record for the sagging and hogging strains independently.

The datasets of peak strains in hogging and sagging are obtained from the monitoring signal using a peak extraction algorithm developed herein. This algorithm is described in the flowchart shown in Figure 2. The algorithm first searches among the readings to determine all those belonging to the current half cycle and determines whether this half cycle is positive or negative. Then, the peak in the current cycle is found as the maximum value if the half cycle is positive or as the minimum value if the half cycle is negative. Positive peaks are amended to the vector of positive peaks $\boldsymbol{P}$ and negative peaks to the vector of negative peaks $\boldsymbol{N}$. This is repeated for the next half cycle and so on, until all readings are considered.

Accordingly, the developed algorithm provides two vectors, namely the vector of positive (hogging) peaks $\boldsymbol{P}$ and the vector of negative (sagging) peaks $\boldsymbol{N}$. In fact, this algorithm is applied with the low-frequency waves, giving the two vectors $\boldsymbol{P_L}$ and $\boldsymbol{N_L}$ and with the high-frequency waves, giving the two vectors $\boldsymbol{P_H}$ and $\boldsymbol{N_H}$. The vectors $\boldsymbol{P_L}$ and $\boldsymbol{N_L}$ represent the data for wave-induced load effects in sagging and hogging, respectively, whereas the vectors $\boldsymbol{P_H}$ and $\boldsymbol{N_H}$ refer to the data for the dynamic load effects in sagging and hogging, respectively.

Distribution fitting

The vectors of peaks, $\boldsymbol{P_L}$, $\boldsymbol{N_L}$, $\boldsymbol{P_H}$, and $\boldsymbol{N_H}$, constitute records of possible values for each of the associated loading effects. The variation of the values in each vector creates uncertainties in estimating these quantities that are best handled by probability distributions. It is, therefore, necessary to establish a probability distribution for representing each of these vectors.

The first step in this process is selecting the distribution function that best represents each dataset. This selection is guided by the results of statistical testings such as the Anderson–Darling and the Kolmogorov–Smirnov tests.[13] Once the proper distribution is selected, the parameters of this distribution need to be determined. Since in this study SHM is the only source of information regarding the load effects, classical estimation techniques are used to determine the parameters of the probability distribution. Several classical estimation techniques are available, but the maximum likelihood method is used herein to obtain the parameters of the considered distributions for the datasets.

As shown later, it turns out that the Rayleigh distribution and the exponential distribution provide a very good fit for the low- and high-frequency peaks, respectively. The probability density functions (PDFs) of the Rayleigh and exponential distributions are given, respectively, as

$$f(x) = \begin{cases} \frac{x}{\sigma^2} e^{-(1/2)(x/\sigma)^2} & \text{for} \quad x \geq 0 \\ 0 & \text{otherwise} \end{cases} \tag{2}$$

$$f(x) = \begin{cases} \lambda e^{-\lambda x} & \text{for} \quad x \geq 0 \\ 0 & \text{otherwise} \end{cases} \tag{3}$$

where σ is the modal value and λ the mean occurrence rate.

It is noted that even though the exponential distribution gives zero as the most probable realization, the interest in the data is in the upper tail behavior (i.e., the maximum values) far away from zero and the exponential distribution represents that part of the data very well. In fact, for consideration of extreme effects, the obtained results need to be extrapolated using extreme value statistics, a process that depends only on the tail behavior of distributions.

Extreme value analysis

For reliability purposes, the safety of the HSNC is quantified with respect to extreme events produced by the load effect L. Appropriate probabilistic tools to model this type of loading are the extreme value distributions. Exact modeling of extreme value distributions is usually a formidable task. Alternatively, one of the three asymptotic extreme value distributions are assigned based on the tail behavior of the original distribution. The largest value of both the Raylcigh and exponential distributions asymptotically converge to the Type I extreme value distribution, which is given as:[14]

$$f_{L_n}(l) = \alpha_n e^{-\alpha_n(l-u_n)} \exp[-e^{-\alpha_n(l-u_n)}] \tag{4}$$

where u_n is the characteristic largest value of the initial variate L and α_n an inverse measure of the dispersion of L_n.

The parameters of the Type I extreme value distribution are found for an initial Rayleigh distribution as:

$$\alpha_n = \frac{\sqrt{2\ln n}}{\sigma} \tag{5}$$

$$u_n = \sigma\sqrt{2\ln n} \tag{6}$$

where n is the number of waves encountered in the period of design storm T; T is taken as 3 h.[15] The value of n is obtained based on the rate of peak waves encountered during an SHM trial as:

$$n = \frac{\text{Number of peaks collected during a SHM trial}}{\text{Duration of the SHM trial}} \times T \tag{7}$$

For an initial exponential distribution, however, the parameters of the Type I extreme value distribution are found as:

$$\alpha_n = \lambda^{-1} \tag{8}$$

$$u_n = \lambda \ln n \tag{9}$$

Statistical damage detection

Motivation

The basic premise of vibration-based damage detection is that changes in the physical properties, such as reductions in stiffness resulting from the onset of cracks or loosening of a connection, will cause changes in the measured dynamic response of the structure.[16] It has been recognized that the vibration-based damage detection problem is fundamentally one of statistical pattern recognition.[17] Such methods rely on the signatures obtained from the recorded vibration, strain or other data to extract features that change with the onset of damage.[9]

Time series methods for damage detection account for the inherent uncertainty (measurement, environmental, etc.) through statistical tools.[18] Over the past decade, time series methods for structural damage diagnosis have been successfully applied to simulated and laboratory experimental data.[19] However, the vast majority of these studies have primarily treated the data from each sensor as an independent measurement to construct scalar autoregressive (AR) models.[7,9,16,19–24]

Mattson and Pandit[25] proposed a method based on ARV models and using the statistical moments of the residuals of these models as damage-sensitive features. Vector models allow a particular series to be described not only in terms of its own past values, but also in terms of the past values in the other sensors, and provides a thorough description of the interaction between response sensors.[25]

ARV modeling

In essence, detecting damage using ARV modeling is conducted by modeling a vibration signal, called the reference signal, obtained from the intact structure, and then fitting this model to the measured structural response data. The parameters of this model, such as the predictive errors, are the damage-sensitive features. This model is assumed to provide an accurate prediction (i.e., a small residual error) for the measured response data. An increase in the residual error, which is an increase in the difference between the measured and the model data, is then interpreted as an indication of structural damage.

Prior to constructing an ARV model, the monitored signals, which are measured data with respect to varying operational and environmental conditions, need to be normalized. All appropriately collected signals are standardized and normalized using the following expression[19]

$$x(t) = \frac{\tilde{x}(t) - \mu_x}{\sigma_x} \tag{10}$$

where $\tilde{x}(t)$ is the signal obtained from a given sensor and μ_x and σ_x the mean and standard deviation of the signal, respectively.

AR models can be constructed by the following expression:

$$x(t) = \sum_{k=1}^{p} \alpha_k x(t-k) + e_x(t) \tag{11}$$

where $x(t)$ is the normalized signal, α_k the k-th AR coefficient, p the AR model order, and $e_x(t)$ the residual term for signal x. At each time point, the AR model provides a scalar value for the unique signal modeled. The coefficients of the model α_k are also scalars. In ARV modeling, the dependence between past values of n signals is taken into account to provide a vector of values with entries representing the predicted signals for the n sensors at time t as:

$$\begin{pmatrix} x_{1,t} \\ x_{2,t} \\ \vdots \\ x_{n,t} \end{pmatrix} = \sum_{k=1}^{p} \begin{bmatrix} \alpha_{1,1,k} & \alpha_{1,2,k} & \cdots & \alpha_{1,n,k} \\ \alpha_{2,1,k} & \alpha_{2,2,k} & \cdots & \alpha_{1,n,k} \\ \vdots & \vdots & \cdots & \vdots \\ \alpha_{n,1,k} & \alpha_{n,2,k} & \cdots & \alpha_{n,n,k} \end{bmatrix} \begin{pmatrix} x_{1,t-k} \\ x_{2t-k} \\ \vdots \\ x_{n,t-k} \end{pmatrix} + \begin{pmatrix} (\varepsilon_x)_{1,t} \\ (\varepsilon_x)_{2,t} \\ \vdots \\ (\varepsilon_x)_{n,t} \end{pmatrix} \tag{12}$$

where $x_{i,t}$ is the signal of the i-th sensor at time t from the signal set x, $\alpha_{i,j,k}$ the ARV coefficient relating the value of the i-th sensor at time t with the value of the j-th sensor at time $t-k$, and $(\varepsilon_x)_{i,t}$ the residual of the i-th sensor at time t from predicting the signal set x. This ARV model with order p is denoted as ARV(p). Using this ARV(p) model, the residuals obtained by predicting new signals from these n sensors can be found as:

$$\begin{pmatrix} (\varepsilon_y)_{1,t} \\ (\varepsilon_y)_{2,t} \\ \vdots \\ (\varepsilon_y)_{n,t} \end{pmatrix} = \begin{pmatrix} y_{1,t} \\ y_{2,t} \\ \vdots \\ y_{n,t} \end{pmatrix} - \sum_{k=1}^{p} \begin{bmatrix} \alpha_{1,1,k} & \alpha_{1,2,k} & \cdots & \alpha_{1,n,k} \\ \alpha_{2,1,k} & \alpha_{2,2,k} & \cdots & \alpha_{1,n,k} \\ \vdots & \vdots & \cdots & \vdots \\ \alpha_{n,1,k} & \alpha_{n,2,k} & \cdots & \alpha_{n,n,k} \end{bmatrix} \begin{pmatrix} y_{1,t-k} \\ y_{2t-k} \\ \vdots \\ y_{n,t-k} \end{pmatrix} \tag{13}$$

where $(\varepsilon_y)_{i,t}$ is the residual of the i-th sensor at time t from predicting the signal set y and $y_{i,t}$ the signal of

the i-th sensor at time t from the signal set y. Herein, compact forms for denoting the series of signals x_i and y_i of the i-th sensor are given as X_i and Y_i, and the residual series for the x_i and y_i signals of the i-th sensor are used as $E_{x,i}$ and $E_{y,i}$, respectively.

A measure of goodness of fit is used to select the order of the ARV(p) model. The fit function is given as:[25]

$$\mathrm{FIT} = \left[1 - \frac{\mathrm{norm}(X - \tilde{X})}{\mathrm{norm}(X - \mathrm{mean}(X))}\right] \times 100 \qquad (14)$$

where X is the measured signal and given as the matrix $[X_1\ X_2, \ldots, X_n]$ and $\tilde{X}$ the predicted signal found using the ARV(p) model with the signal X.

Hypothesis testing for damage detection

As discussed previously, the predictive capability of the model ARV(p), such as the residual series $E_{x,i}$ and $E_{y,i}$ obtained from the vicinity of sensor i, is used as the damage-sensitive feature. Both $E_{x,i}$ and $E_{y,i}$ have zero means and standard deviations $\sigma_{x,i}$ and $\sigma_{y,i}$, respectively, and are typically assumed to follow normal distributions. If the ARV(p) model constructed with the reference signals x_i is not a good representation for the new signals y_i, the standard deviation of the residual error of the new signals $\sigma_{y,i}$ would be higher than that of the reference signals $\sigma_{x,i}$. Statistical decision making is then conducted by formal statistical hypothesis testing procedures on quantity σ_x and its counterpart σ_y.[18] This is accomplished by testing the null hypothesis that the structure is intact (H_0: $\sigma_{x,i} = \sigma_{y,i}$) against the alternative hypothesis that the structure is damaged (H_1: $\sigma_{x,i} < \sigma_{y,i}$).

This hypothesis can be tested by using the two-sample left-tailed F-test, which tests whether the two independent samples ($E_{x,i}$ and $E_{y,i}$) come from normal distributions with the same variance (H_0) against the alternative that they come from normal distributions with the variance of $E_{x,i}$ less than the variance of $E_{y,i}$ (H_1).[26]

Damage localization

Damage detection based on time series modeling is a process that relies on the interpretation of the outcomes of a selected feature that is sensitive to damage. Accordingly, the closer the sensor is to the location of damage, the larger the value of the damage sensitivity feature. In essence, the standard deviation of the residuals of the ARV(p) models is found to provide the best indication for both the presence and location of damage.[25] Using scalar AR–ARX modeling, Sohn and Farrar[23] used the standard deviation ratio of the measured and model signals as the damage sensitivity feature and the increase in this ratio is monitored to detect system anomalies. This ratio is used to identify the location of damage and is defined as:

$$h_i = \frac{\sigma_{y,i}}{\sigma_{x,i}} \qquad (15)$$

Therefore, the larger the ratio h_i is, the closer the sensor i is to the location of damage. To use h_i to detect damage in the vicinity of sensor i, h_i must be larger than some chosen threshold value. The value $h_i = 1.0$ is a reasonable threshold; establishing a more accurate threshold value requires rigorous statistical analyses of test data acquired under different operational conditions in order to obtain the probability distribution for h.[16] In this study, the damage detection is performed using the statistical hypothesis testing explained above. Then, the h_i values of the sensors that were found from the hypothesis testing to detect damage are compared to determine the location of damage. It is then concluded that damage is located closer to the sensors with higher h_i values among the sensors found to pass the H_1 decision from the hypothesis test.

Application: HSV-2

Description of the ship, its model and testing procedure

The methods presented in this article are illustrated on a HSNC, HSV-2. The HSV-2 is a 98-m long, high speed, all aluminum, wave-piercing catamaran designed by Revolution Design, and built by Incat in Tasmania, Australia. HSV-2 is capable of maintaining an average speed of 35 knots or greater. It was delivered to the US Navy in 2003 and underwent rough sea trials in early 2004. The ship was instrumented with various types of sensors, placed throughout the ship, to monitor and evaluate response and performance.[2] The objectives of these sea trials were to determine whether the measured responses were acceptable with code-set safety levels when the ship is operated within the safe operational envelope defined by the ABS.

There were a total of 16 strain gages (T1-1, T1-2, ..., T1-16) instrumented to measure responses due to primary (global) wave loads (i.e., any of the rules-based design loads derived for the purpose of sizing longitudinally or transversely continuous structures). These gages were optimally located based on results of a full-ship finite element analysis.[12] During the sea trials, the ship was operated in such a manner as to collect data at specific speed and heading combinations,

where by traversing an octagon course relative to the predominate wave direction, at certain speeds, strain data were collected at headings of 0°, 45°, 90°, 135°, 180°, 225°, and 270° and speeds of 10, 15, 20, 30, and 35 knots.[2] In addition to the T1 strain gage group, other groups were instrumented to measure stress concentrations T2 and secondary loads T3/T4.[12] T1 and T2 sensors were set to continuously record data from the start until the end of each trial run (about 30 min each) with a sample rate of 100 Hz.[12] Six of the T1 sensors were dedicated for recording strains induced by the longitudinal bending moments (T1-5, T1-6,..., T1-10). These six sensors are presented with their locations in Table 1[12] and their positions relative to the frames on the overall sketch of HSV-2 in Figure 3,[12] and are selected for this study.

Table 1. Locations of sensors T1-5, T1-6,..., T1-10[12]

Sensor	Frame	Side
T1-5	24	Port
T1-6	46	Port
T1-7	61	Port
T1-8	24	Starboard
T1-9	46	Starboard
T1-10	61	Starboard

Reliability analysis

The six T1 bending moment sensors are distributed symmetrically on both sides (i.e., port and starboard) of the HSV-2. The three sensors located on the port (i.e., T1-5, T1-6, and T1-7) are selected to demonstrate the application of the reliability analysis explained above. As shown in Table 1, the sensors T1-5, T1-6,

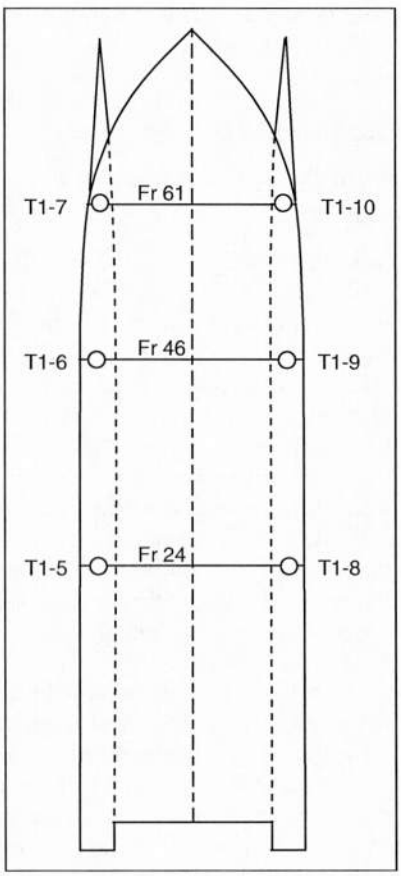

Figure 3. Sketch of the top view of HSV-2 with the positions of the sensors T1-5 to T1-10 relative to the frames.

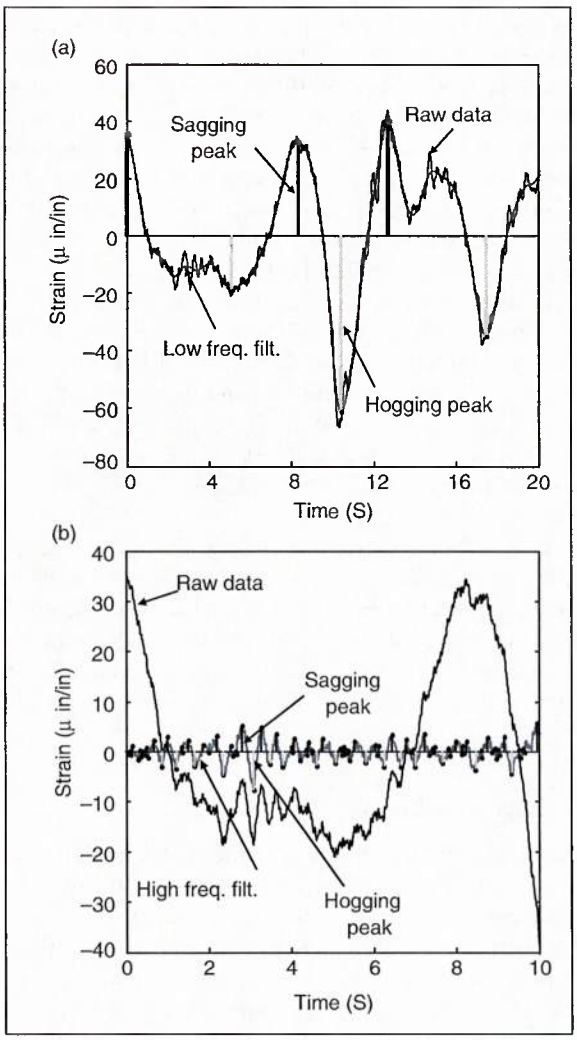

Figure 4. Peak extraction from SHM signal for: (a) low- and (b) high-frequency filtered signals.

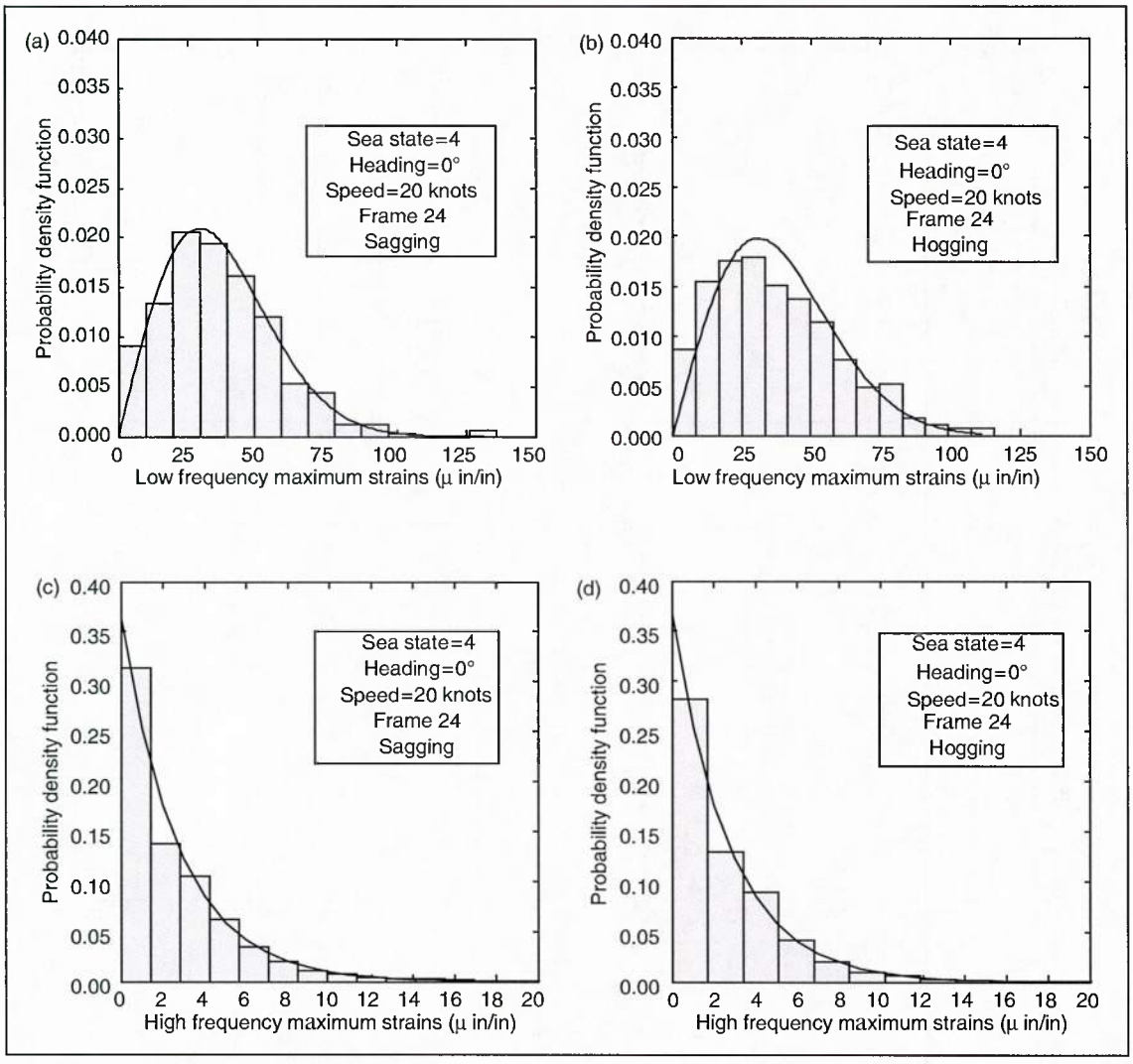

Figure 5. Histograms and PDF of: (a) low-frequency peaks in sagging; (b) low-frequency peaks in hogging; (c) high-frequency peaks in sagging; and (d) high-frequency peaks in hogging.

and T1-7 monitor the strain at frames 24, 46, and 61, respectively, which lie between the aft and forward perpendiculars defined as frames 0 and 77, respectively.

As previously explained, the first step in the process is to filter the signal for the separation of low-frequency waves from the higher ones. For each of these filtered signals, the peak extraction algorithm is used to collect the datasets of the peaks in sagging and hogging. The results of one example signal are shown in Figure 4. In this figure, the signal was collected at sea state 4, heading angle 0°, and speed 20 knots. The signal is filtered and the peaks are extracted for both low- and high-frequency signal components.

The histograms of the obtained low- and high-frequency peaks in sagging and hogging are shown in Figure 5. It is clear from the figure and the results of the Kolmogorov–Smirnov test[13] that the Rayleigh distribution fits the low-frequency peaks very well, while the exponential distribution fits the high-frequency peaks. Using the parameters of the obtained distributions, extreme value statistics are used to find the parameters of the corresponding extreme value Type I distributions.

In the DLA, the maximum values of strain are deterministically checked against the allowable design limits. In the design of ship structures, material properties of the weld metal are used to derive allowable stresses for welded joint details using knockdown factors, which is complicated by the fact that the allowable limit may also be related to a specific load case and the failure mechanism associated with a particular portion of the structure.[12] It is evident that research geared toward establishing the probabilistic resistance of aluminum HSNC structures is crucial for the accurate

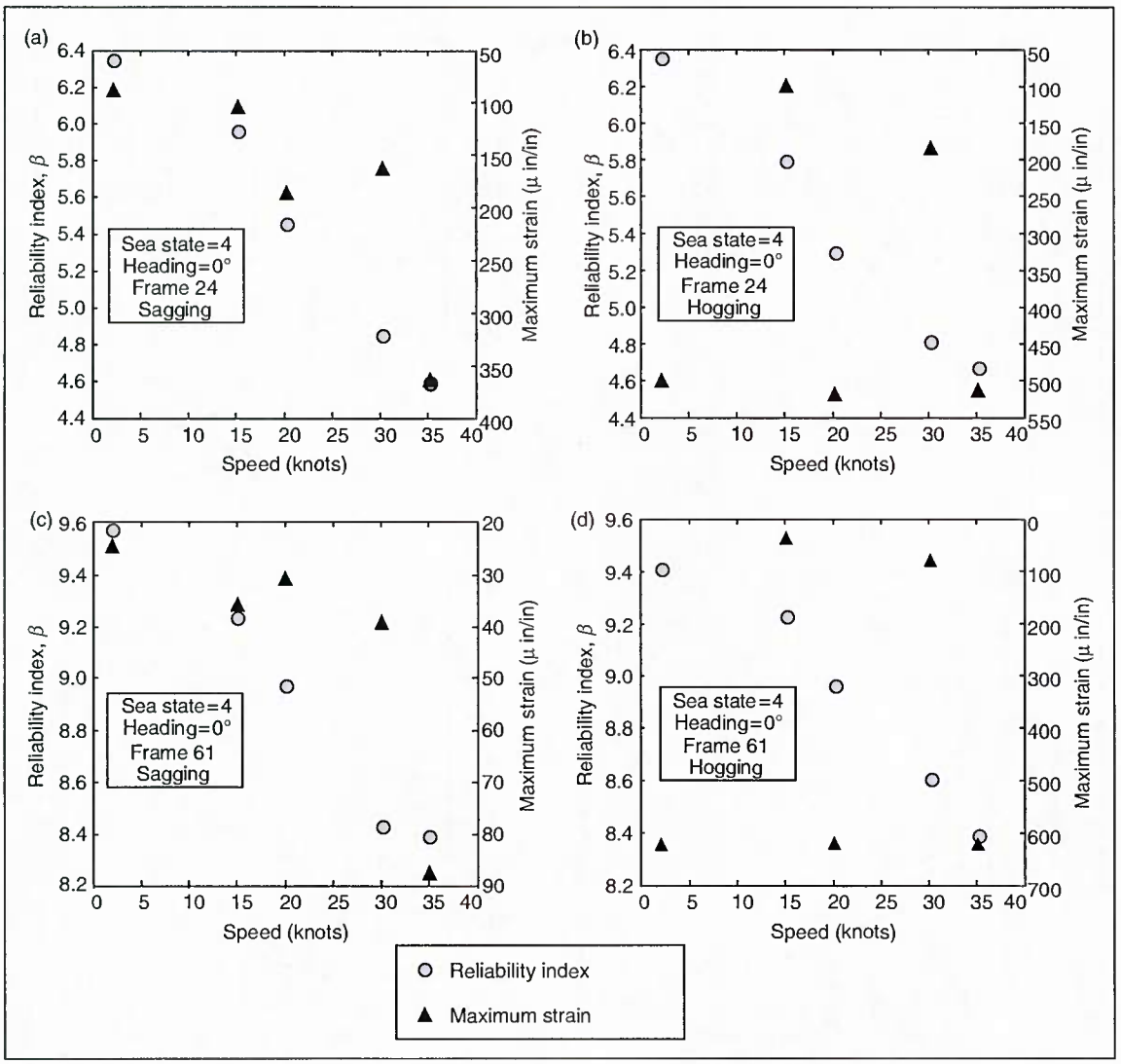

Figure 6. Variation of the reliability index and maximum strain of the HSV-2 with respect to speed for sea state 4, heading angle of 0° at: (a) frame 24 in sagging; (b) frame 24 in hogging; (c) frame 61 in sagging; and (d) frame 61 in hogging.

analysis of their reliability. Such research is well established for conventional steel ship structures,[27–29] but lacking for aluminum HSNC. In Brady,[12] deterministic allowable limits set forth by the ABS and Revolution Design are used for conducting the safety check. The allowable strain limit for sensors T1-5, T1-6, and T1-7 is 870 μin/in. In this article, this limit is used as the mean of the resisting strain ε_R, and the COV is assumed as 10%. Also, the resisting strain is assumed to follow the lognormal distribution. It is emphasized that these assumptions can be discarded, without affecting the validity of the current approach, once a comprehensive probabilistic approach for establishing the resisting strain is available.

Selected samples of a large database, obtained from many seakeeping trials of different operational loading conditions, are used to illustrate the reliability analysis and identify existing patterns. The reliability computations are conducted with the software CALREL[30] using the second order reliability method (SORM).[31]

Figure 6 displays the effect of speed on the reliability index of the HSV-2 at frames 24 (Figure 6(a) and (b)) and 61 (Figure 6(c) and (d)) in sea state 4 and heading 0°. As expected, the reliability index decreases as the speed increases. In fact, the relationship between speed and reliability seems to be almost linear. Also shown in the figure are the absolute maximum strains recorded by these sensors corresponding to each speed. It is immediately evident that these absolute maxima do not follow the expected pattern that the reliability indices do. Clearly, deterministic analyses that are based on one recorded value, ignoring the entire record, can be

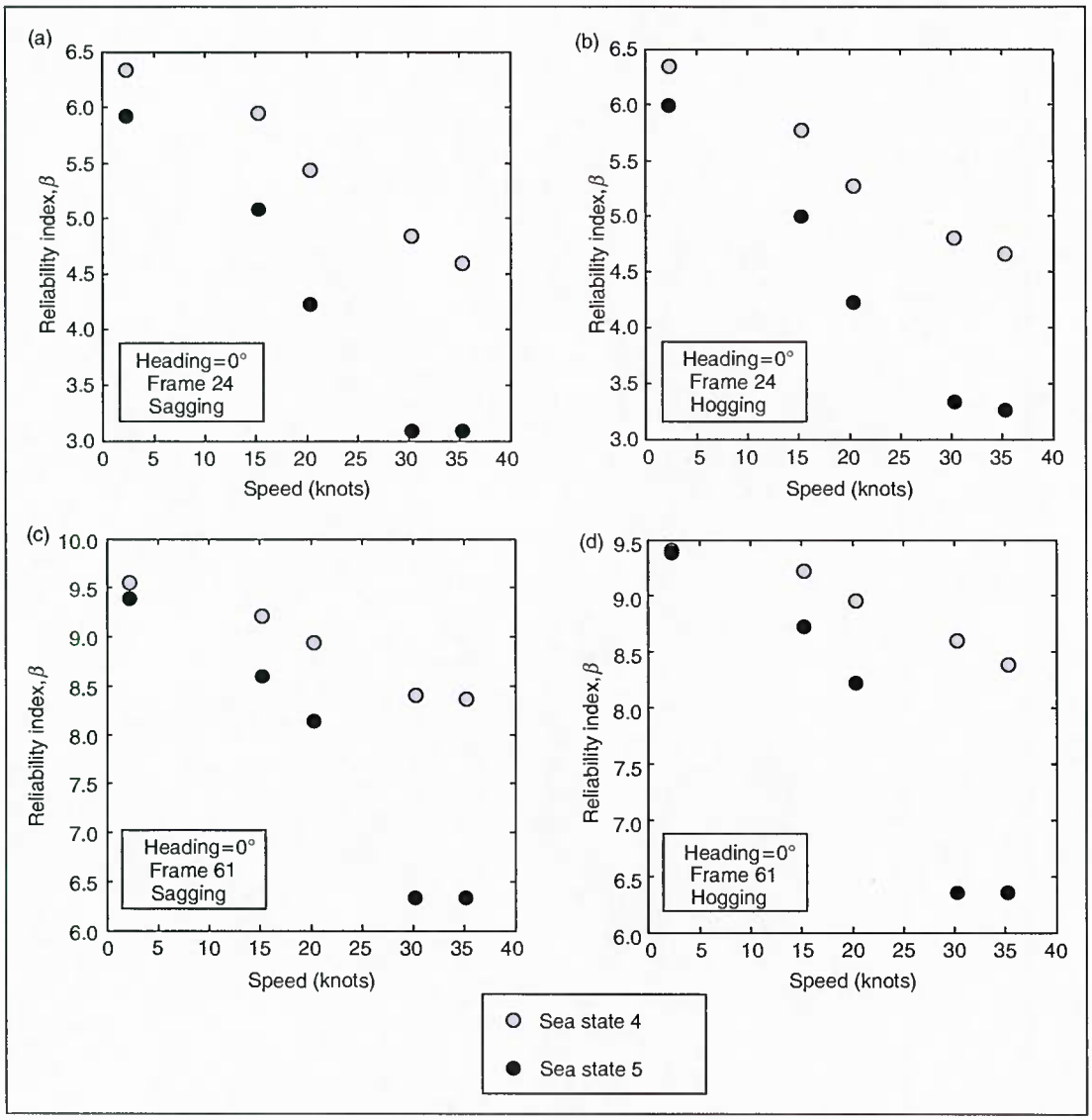

Figure 7. Variation of the reliability index of the HSV-2 with respect to speed and sea state with heading angle of 0° at: (a) frame 24 in sagging; (b) frame 24 in hogging; (c) frame 61 in sagging; and (d) frame 61 in hogging.

misleading and incorrect. On the other hand, taking into account the entire record of monitoring data and properly treating the inherent uncertainty in this record in a reliability analysis is far more superior. It is clear from the figure that the reliability levels computed at frame 24 are lower than those at frame 61. The longitudinal bending moment induced by low-frequency wave loads should be the highest at mid-ship which results in the lowest reliability index values. Frame 24 is located closer to mid-ship than frame 61 and therefore, has a lower reliability index. Furthermore, it is clear that the reliability indices in sagging are close to their respective ones in hogging. Figure 7 shows the effect of speed on the reliability index of the HSV-2 at frames 24 (Figure 7(a) and (b)) and 61 (Figure 7(e) and (d)) in both sea states 4 and 5 and heading 0°. It is observed, as expected, that the reliability indices in sea state 5 are lower than in sea state 4. The difference is also seen to increase as the speed increases.

Figure 8 shows the effect of head angle on the reliability index of the HSV-2 at frames 24 (Figure 8(a) and (b)) and 61 (Figure 8(e) and (d)) in sea state 5 and a speed of 20 knots. It is seen that the reliability index at angle 0° is the lowest in all cases. At frame 61, the reliability index almost linearly increases with the heading angle from 0° to 180°. However, at frame 24, the highest reliability index is at angle 90°. This is expected because the sensors are on the port side of the ship and a 90° angle produces the lowest longitudinal bending moment from the wave load. Also shown in the figure are the absolute maximum

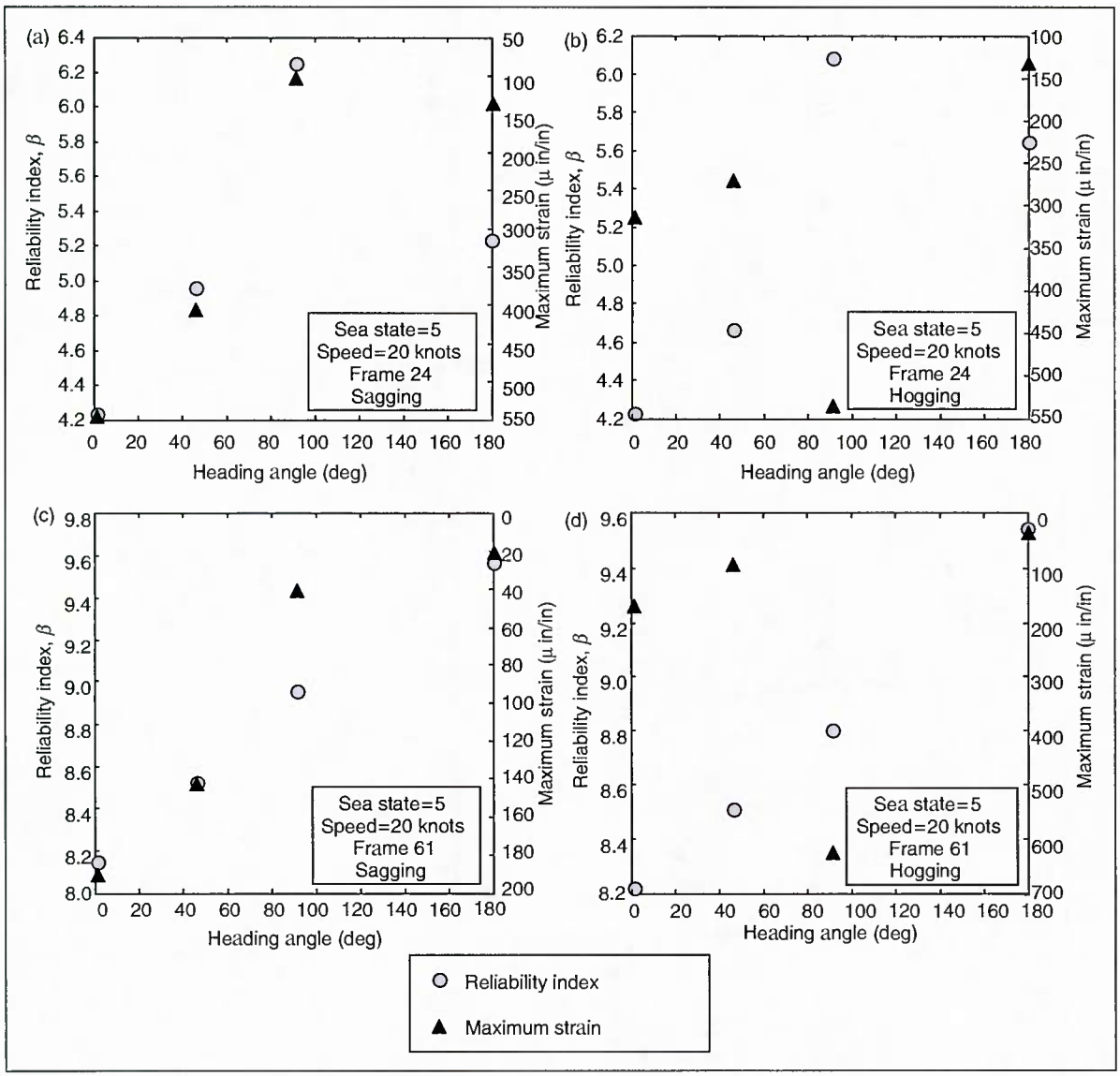

Figure 8. Variation of the reliability index and maximum strain of the HSV-2 with respect to heading angle for sea state 5, speed of 20 knots at: (a) frame 24 in sagging; (b) frame 24 in hogging; (c) frame 61 in sagging; and (d) frame 61 in hogging.

strains corresponding to each heading angle. Clearly, these absolute maxima do not always provide a meaningful conclusion for safety assessment. In Figure 9, the effect of heading angle on the reliability index of the HSV-2 at frames 24 (Figure 9(a) and (b)) and 61 (Figure 9(c) and (d)) in both sea states 4 and 5 and a speed of 20 knots is shown. The reliability indices in sea state 4 follow nearly the same pattern of those in sea state 5 and have been discussed above.

Figure 10 presents the variation of the reliability index over the longitudinal span. It shows the reliability indices at frames 24, 46, and 61 in sea state 5, heading angle 0°, and speeds 2 knots (Figure 10(a) and (b)) and 20 knots (Figure 10(c) and (d)). In addition, the absolute maximum strains at these frames are shown in the figure. It is clear that the reliability indices at frames 24 and 46 are similar, while at frame 61 they are relatively much higher. However, according to the maximum strains, frame 46 exhibits the largest strains. Basing a decision solely on the maximum strains clearly could lead to an unsafe assessment of the craft at frame 24. In Figure 11, the effects of the three operational variables: speed (Figure 11(a) and (b)), heading angle (Figure 11(c) and (d)), and sea state (Figure 11(e) and (f)) on the reliability of HSV-2 at the three frames are displayed. In all cases, the reliability indices at frames 24 and 46 are similar, while at frame 61 they are relatively higher. Since the reliability is a function of speed,

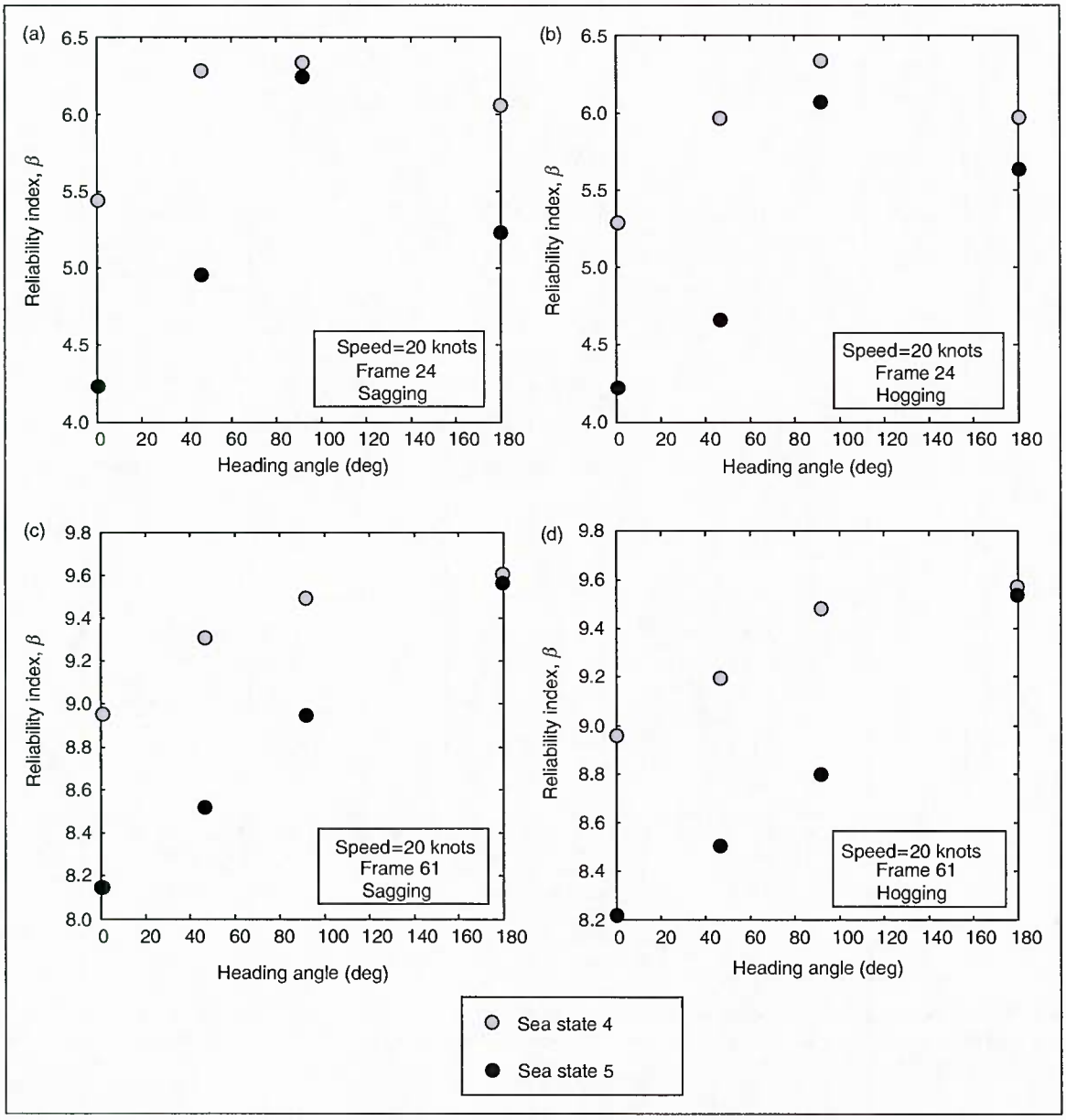

Figure 9. Variation of the reliability index of the HSV-2 with respect to heading angle and sea state with speed of 20 knots at: (a) frame 24 in sagging; (b) frame 24 in hogging; (c) frame 61 in sagging; and (d) frame 61 in hogging.

heading angle, and sea state, it is apparent that holding the other two variables constant, the reliability is consistently lower for higher speeds, smaller heading angles, and higher sea states.

Damage detection

To address the need for structural state awareness and SHM of ships, the ARV method described above is applied to T1 global response sensor data for detecting and localizing damage. The six T1 bending moment sensors are selected for their spatial locations over the ship structure. Run 117 conducted on May 14, 2004, was arbitrarily selected as the reference dataset for training and construction of the ARV(p) model. During this run, the ship was operated at a 2-knot speed and 0° heading in sea state 4.

The MATLAB System Identification Toolbox[32] was used to obtain the coefficients of the ARV(p) model. Using the fitness test in Equation (14), a model with order $p=5$, having 180 ARV coefficients provided a fitness of 98.63%. On the other hand, a model with order $p=10$, having 360 ARV coefficients provided a fitness of 98.71%. Accordingly, the ARV (5) model was

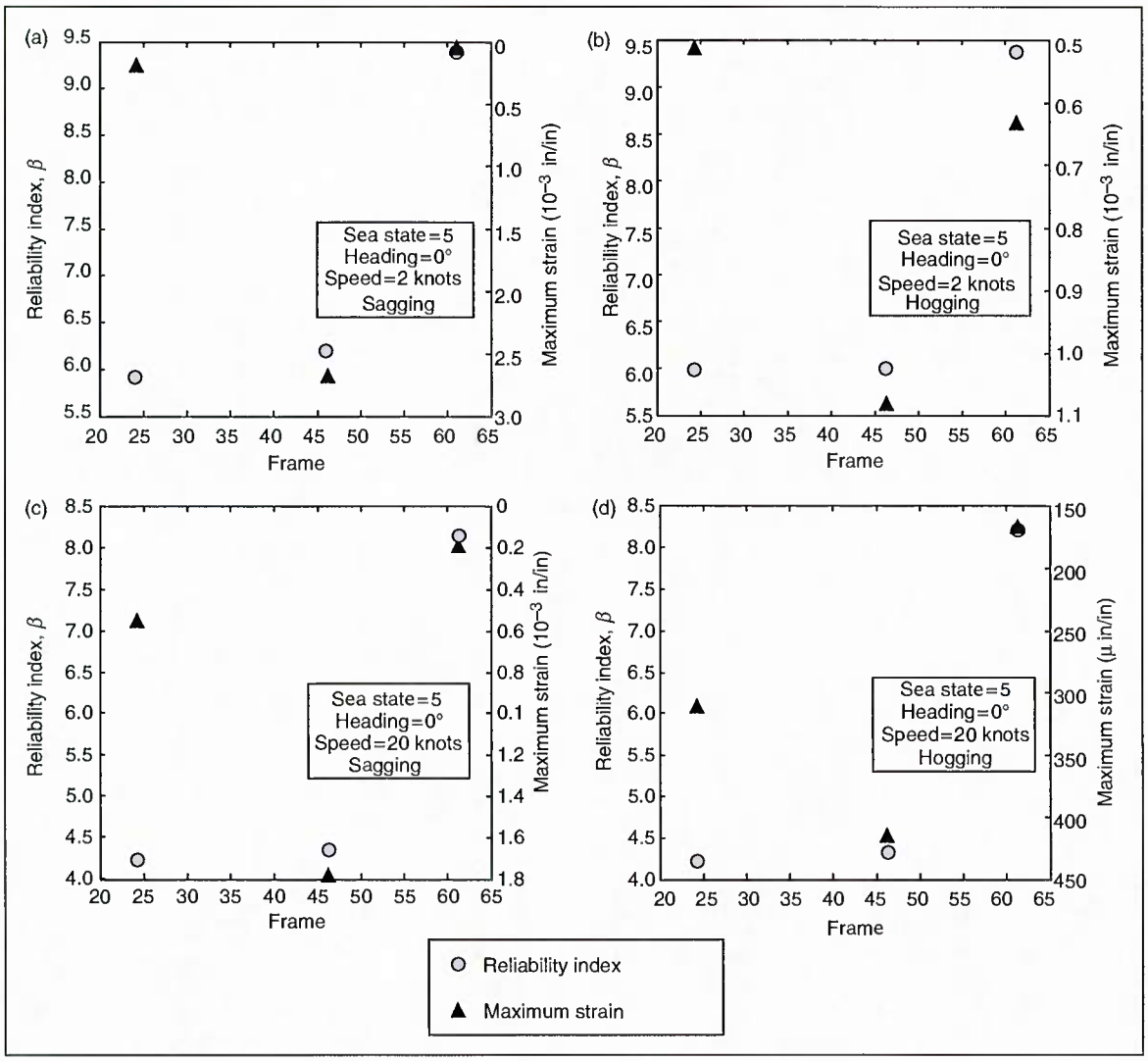

Figure 10. Variation of the reliability index and maximum strain of the HSV-2 with respect to frame position for sea state 5, heading angle of 0° and (a) speed of 2 knots in sagging; (b) speed of 2 knots in hogging; (c) speed of 20 knots in sagging; and (d) speed of 20 knots in hogging.

selected since the insignificant increase in fitness does not justify the added computational cost associated with the ARV(10) model.

The constructed model (with Run 117) was used to predict the signal from Run 150, recorded on May 15, 2004, and Run 211, recorded on May 17, 2004. The ship was operated at 2-knot speed and 0° heading in sea state 4 for both Runs 150 and 211. The prediction of sensor T1-5 in Run 150 using the generated ARV (5) model is shown in Figure 12. Clearly, the model is able to predict the new signal with high accuracy.

Now, the series of residuals obtained from predicting the reference signal (Run 117) forms a baseline for comparing against residuals obtained from predicting signals from the Runs 150 and 211, respectively, to test the hypothesis of damage presence in the structure. The testing was conducted using the MATLAB statistics toolbox[26] and the results are shown in Table 2. As shown in the table, none of the sensors indicated damage in Run 150. Given that this run was conducted soon after the reference Run 117 (the next day), the results of the hypothesis testing reveals that damage has not occurred. However, Run 211 was conducted after a few more dates of rough water, and the ship had experienced severe sea conditions that may have inflicted damage in areas around sensors T1-5, T1-6, and T1-8 as shown in Figure 13. Table 2 shows the sensitivity factors found for both runs, which are also shown in Figure 14. The highest concentration of damage seems to be located near T1-6. It is important

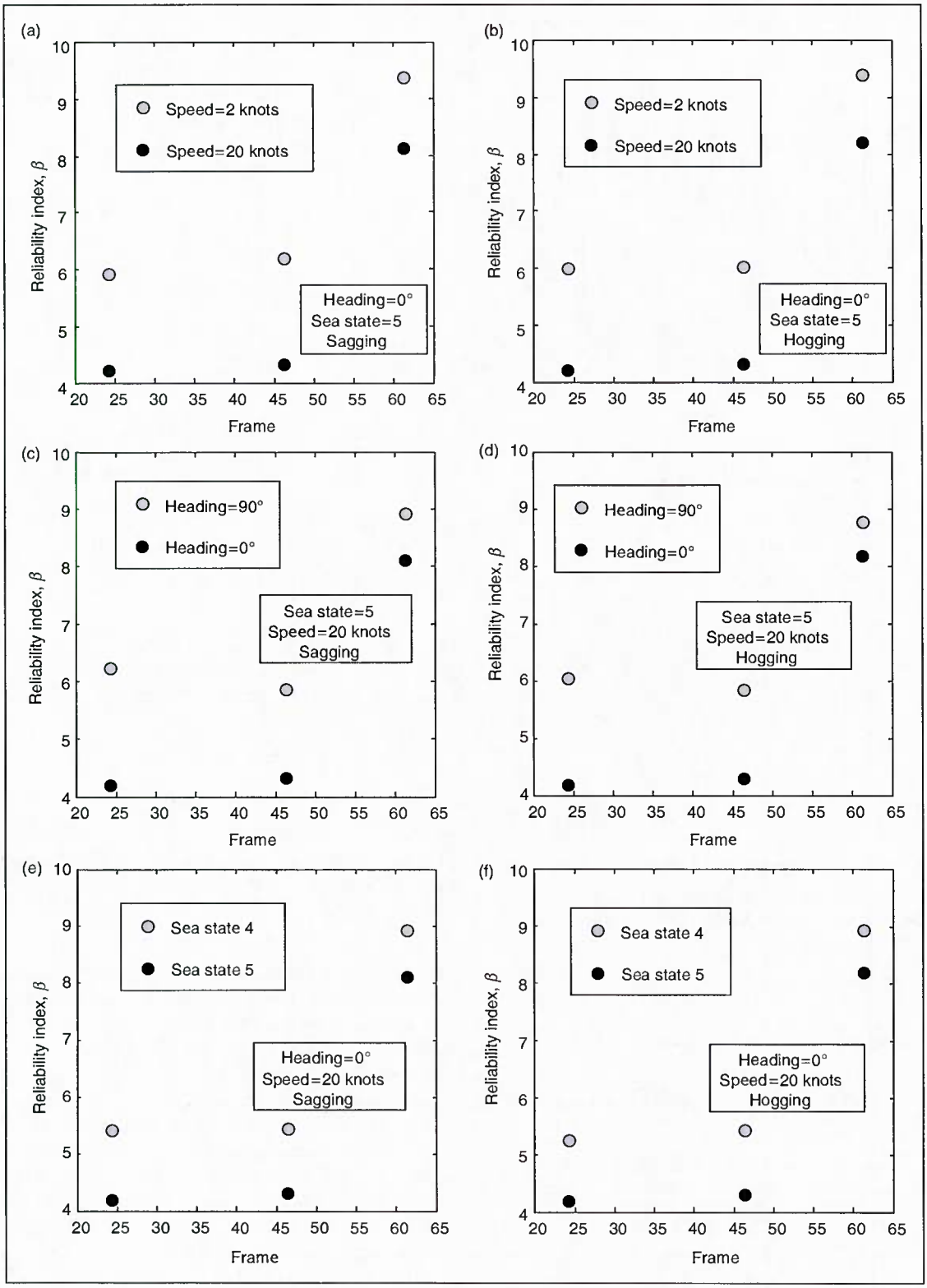

Figure 11. Variation of the reliability index of the HSV-2 with respect to frame position and (a) speed for sea state 5 and heading angle of 0° in sagging; (b) speed for sea state 5 and heading angle of 0° in hogging; (c) heading angle for sea state 5 and speed of 20 knots in sagging; (d) heading angle for sea state 5 and speed of 20 knots in hogging; (e) sea state with heading angle of 0° and speed of 20 knots in sagging; and (f) sea state with heading angle of 0° and speed of 20 knots in hogging.

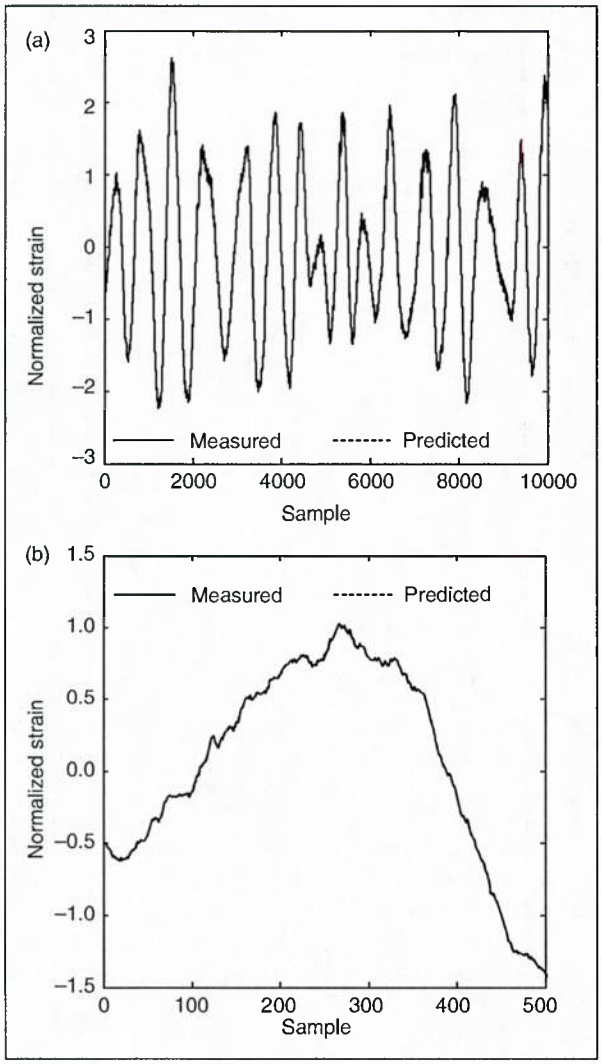

Figure 12. Measured and predicted signal from Sensor T1-5 in Run 150 with: (a) a view of 10000 samples and (b) an expanded view with 500 samples.

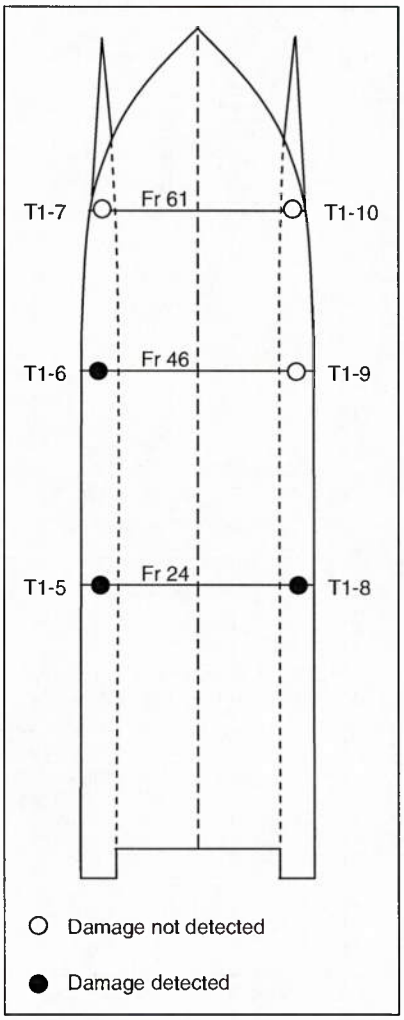

Figure 13. Sketch of the top view of the HSV-2 showing the potentially damaged locations found by damage detection.

Table 2. Damage detection results for sensors T1-5, T1-6, . . . , T1-10

	Run 150 (intact case)		Run 211 (damaged case)	
Sensor	Damage decision	Damage sensitivity factor	Damage decision	Damage sensitivity factor
T1-5	H_0	0.9852	H_1	1.1246
T1-6	H_0	0.7889	H_1	2.9819
T1-7	H_0	0.9399	H_0	0.8801
T1-8	H_0	0.9506	H_1	1.2292
T1-9	H_0	0.9541	H_0	0.9666
T1-10	H_0	0.9728	H_0	0.9497

to emphasize that whether the structure is intact or damaged entails a decision that is entirely based upon hypothesis testing of the data. These types of methods for structural damage diagnosis have been successfully applied for simulated data and well-controlled laboratory experimental data. However, the method has not been applied on data recorded from full-ship sea trials. Many factors, such as data requirement, lack of data from known damage conditions, and sensors that were not designed specifically for SHM, in addition to the validity of this application, are largely unknown.

In light of Figure 14, a follow-up investigation may be undertaken in which the potentially damaged locations are visually inspected for further confirmation of damage presence and condition assessment may be made rigorously. Thus, the damage detection process

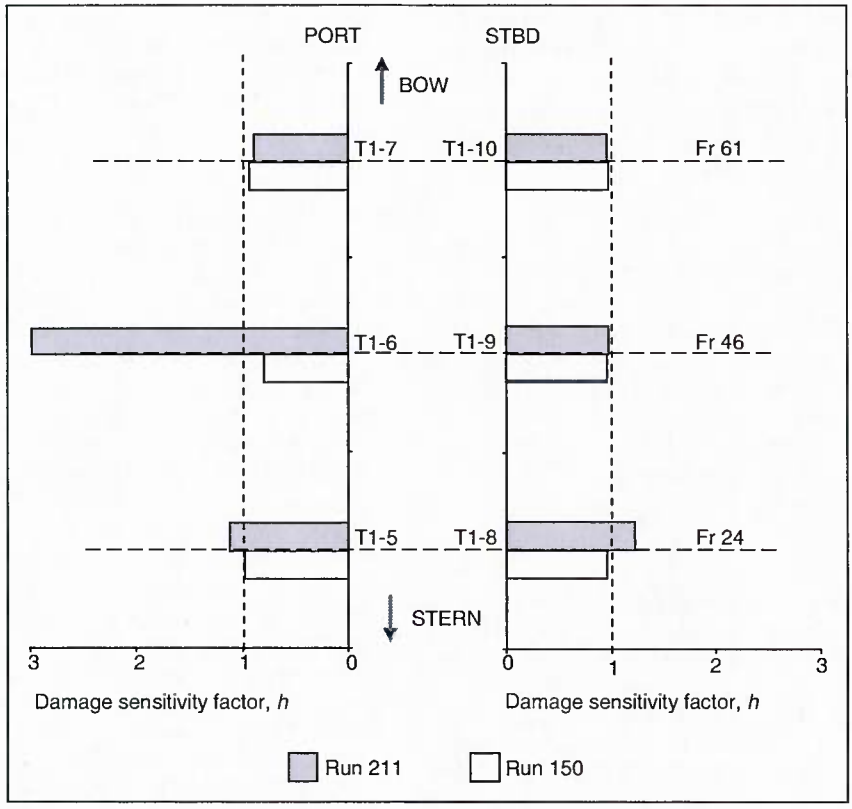

Figure 14. Damage sensitivity factor *h* at frames 24, 46, and 61 for Runs 150 (intact) and 211 (damaged).

provides motivation for initiating a neeessary visual inspection over a limited area of the ship when it might not have been scheduled, and saves the time and effort by not inspecting the areas that have not shown any sign of anomaly. Based on the findings of the visual inspection, it may be suggested to repair eertain components of the ship or perform additional nondestructive testing to further ineur information about the health of the strueture. Clearly, damage deteetion using SHM ean be a powerful and important tool in an integrated framework for assessment and management of ship struetures. In addition, similar to most large and complex eivil and aerospaee struetures, ships ean only be sparsely instrumented relative to their size. Therefore, it is eritieal to develop an optimal strategy and to implement an effeetive data proeessing plan for SHM. On the global level, strain measurement sueh as T1 sensors eombined with reliability methods and statistieal-based damage deteetion algorithms can pinpoint possible problems and identify their approximate loeations in a timely fashion. Then, further evaluations are justified using more loealized techniques as well as ineorporate sensor and inspeetion information into fracture-based fatigue models to evaluate details of known or suspected flaws.

Conclusions

In this artiele, an approach for using the data obtained from SHM in the reliability analysis and damage deteetion in HSNC under uncertainty was presented. A statistical damage deteetion teehnique that makes use of ARV modeling was implemented for deteetion and loealization of damage in HSNC struetures. The methodology was illustrated on a naval HSV-2. Strain data obtained from seakeeping trials of the HSV-2 were used as SHM data to demonstrate the methodology.

The patterns observed in the HSV-2 example fall in line with the expeeted behavior of the craft in the different operational loading eases eonsidered and at the different locations investigated. For example, it was evident that speed is inversely related to the reliability of the eraft structure.

As expeeted, the results of the illustrative example reinforce the preexisting belief that the probabilistie approach for analysis of structural safety is far superior to that of deterministie approaches. This is indeed the case, sinee as shown by the results of the example HSV-2, neglecting uncertainties could lead to ineonsistent and misleading results.

The potential for using SHM data for detecting damage in HSNC structures has been highlighted by the use of a ARV modeling technique. The damage that may be inflicted by high speed and/or combat is a source of concern that can be effectively addressed by exploiting the capabilities of SHM.

Acknowledgments

The support from the Office of Naval Research to Lehigh University under award N-00014-08-0188 is gratefully acknowledged. The authors greatly appreciate the technical guidance and overall support from Mr Thomas Brady, Code 653, Naval Surface Warfare Center, Carderock Division (NSWCCD), for providing the data and other materials. The opinions and conclusions presented in this article are those of the authors and do not necessarily reflect the views of the sponsoring organization.

References

1. IACS. 'Common Structural Rules for Double Hull Oil Tankers', *International Association of Classification Societies*, http://www.iacs.org.uk (consulted 24 November 2008).
2. Salvino LW and Brady TF. Hull monitoring system development using a hierarchical framework for data and information management. In: *Proceedings of 7th International Conference on Computer and IT Applications in the Maritime Industries* (COMPIT'08), Liege, Belgium, April 2008.
3. Sielski RA. Research needs in aluminum structure. *Ships Offshore Struct* 2008; 3(1): 57–65.
4. ABS. *Guide for building and classing, high speed naval craft. Part 1: Conditions of classification*. Houston, TX: American Bureau of Shipping, 2007.
5. ABS. *Guidance on the dynamic load approach and direct analysis for high speed craft*. Houston, TX: American Bureau of Shipping, 2003.
6. Frangopol DM and Okasha NM. Life-cycle performance and redundancy of structures. In: Graubner CA, Schmidt H, and Proske D (eds) *Proceedings of the Sixth International Probabilistic Workshop*, Darmstadt, Germany, 26–27 November, 2008 (Keynote Lecture), pp. 1–14.
7. Fugate ML, Sohn H and Farrar CR. Vibration-based damage detection using statistical process control. *Mech Syst Signal Process* 2001; 15(4): 707–721.
8. Doebling SW, Farrar CR, Prime MB and Shevitz DW. Damage identification and health monitoring of structural and mechanical systems from changes in their vibration characteristics: a literature review. Los Alamos National Laboratory Report LA-13070-MS, Los Alamos National Laboratory, Los Alamos, NM 87545 1996.
9. Nair KK, Kiremidjian AS and Law KH. Time series-based damage detection and localization algorithm with application to the ASCE benchmark structure. *J Sound Vib* 2006; 291: 349–368.
10. Paik JK and Frieze PA. Ship structural safety and reliability. *Prog Struct Eng Mater* 2001; 3(2): 198–210.
11. MathWorks. *Signal processing toolbox™ 6–user's guide*. Natick, MA: MathWorks Inc., 2009, p.1427.
12. Brady TF. *Global structural response measurement of SWIFT (HSV-2) from JLOTS and blue game rough water trials*. West Bethesda, MD: NSWCCD-65-TR-2004/33, Naval Surface Warfare Center, Carderock Division, 2004.
13. Ang AH-S and Tang WH. *Probability concepts in engineering. Emphasis on applications to civil and environmental engineering*, 2nd edn. New York: Wiley & Sons, 2007.
14. Ang AH-S and Tang WH. *Probability concepts in engineering planning and design, Vol. II: decision, risk and reliability*. New York: Wiley & Sons, 1984.
15. Mansour AE and Hovem L. Probability-based ship structural safety analysis. *J Ship Res* 1994; 38(4): 329–339.
16. Sohn H, Farrar CR, Hunter NF and Worden K. Structural health monitoring using statistical pattern recognition techniques. *J Dyn Syst Meas Control, Trans ASME* 2001; 123: 706–711.
17. Farrar CR, Duffey TA, Doebling SW and Nix DA. A statistical pattern recognition paradigm for vibration-based structural health monitoring. In: *Proceedings of the 2nd International Workshop on Structural Health Monitoring*, Stanford, CA, 8–10 September, 1999.
18. Fassois SD and Sakellariou JD. Time-series methods for fault detection and identification in vibrating structures. *Phil Trans R Soc A* 2006; 365: 411–448.
19. Noh H-Y, Nair KK, Kiremidjian AS and Loh C-H. Application of time series based damage detection algorithms to the benchmark experiment at the National Center for Research on Earthquake Engineering (NCREE) in Taipei, Taiwan. *Smart Structures and Systems* 2009; 5(1): 95–117.
20. Da Silva S and Dias Junior M. Statistical damage detection in a stationary rotator systems through time series analysis. *Lat Am Appl Res* 2007; 37: 243–246.
21. Lei Y, Kiremidjian AS, Nair KK, et al. Statistical damage detection using time series analysis on a structural health monitoring benchmark problem. In: *Proceedings of the 9th International Conference on Applications of Statistics and Probability in Civil Engineering*, San Francisco, CA, USA, 6–9 July, 2003.
22. Riveros C, Utsunomiya T, Maeda K and Itoh K. Vibration-based damage detection in flexible risers using time series analysis. *Doboku Gakkai Ronbunshuu A* 2007; 63(3): 423–433.
23. Sohn H and Farrar CR. Damage diagnosis using time series analysis of vibration signals. *Smart Mater Struct* 2001; 10: 446–451.
24. Sohn H, Czarnecki JA and Farrar CR. Structural health monitoring using statistical process control. *J Struct Eng, ASCE* 2000; 126(11): 1354–1363.
25. Mattson SG and Pandit SM. Statistical moments of autoregressive model residuals for damage localization. *Mech Syst Sig Process* 2006; 20(3): 627–645.
26. MathWorks. *Statistics toolbox™ 7 user's guide*. Natick, MA: MathWorks, Inc., 2008, p.1749.
27. Okasha NM and Frangopol DM. Efficient method based on optimization and simulation for the probabilistic

strength computation of the ship hull. *J Ship Res, SNAME* 2010; 54(4): (in press).
28. Lua J and Hess PE. Hybrid reliability predictions of single and advanced double-hull ship structures. *J Ship Res, SNAME* 2003; 47(2): 155–176.
29. Lua J and Hess PE. First-failure-based reliability assessment and sensitivity analysis of a naval vessel under hogging. *J Ship Res, SNAME* 2006; 50(2): 158–170.
30. Liu PL, Lin HZ and Der Kiureghian A. *CALREL User Manual, Department of Civil Engineering*. Berkeley, CA: University of California, 1989.
31. Fiessler B, Neumann H-J and Rackwitz R. Quadratic limit states in structural reliability. *J Eng Mech, ASCE* 1979; 105(4): 661–676.
32. Ljung L. *System Identification Toolbox™ 7, Getting Started Guide*. MathWorks: Natick, MA, 2009.

Appendix V

Kihyon Kwon, Dan M. Frangopol, and Sunyong Kim. Fatigue performance assessment and service life prediction of high-speed ship structures based on probabilistic lifetime sea loads. *Structure and Infrastructure Engineering*, in press and already available online, DOI: 10.1080/15732479.2010.524984.

Structure and Infrastructure Engineering
2010, 1–14, i*First* article

Fatigue performance assessment and service life prediction of high-speed ship structures based on probabilistic lifetime sea loads

Kihyon Kwon, Dan M. Frangopol* and Sunyong Kim

Department of Civil and Environmental Engineering, ATLSS Engineering Research Center, Lehigh University, 117 ATLSS Dr., Bethlehem, PA 18015-4729, USA

(*Received 30 November 2009; final version received 10 May 2010; accepted 31 August 2010*)

This article focuses on estimating probabilistic lifetime sea loads for high-speed ship structures with the aim of assessing fatigue performance and predicting service life from available data. Performance assessment and service life prediction for naval ship structures are extremely important issues. In particular, understanding the effect of sea loading on naval high-speed vessels is still a challenge. Potential lifetime load effects including low frequency wave-induced and high frequency slam-induced whipping loadings are investigated in this article by using a probabilistic approach. Clearly, integration of probabilistic sea loads into structural reliability assessment and service life prediction will provide a more reliable estimation of the long-term structural performance. Accordingly, this article presents an approach for fatigue reliability evaluation of ship structures based on the estimated lifetime sea loads. Loading information associated with sea states, ship speeds and relative wave headings is obtained from a joint high-speed sealift ship monohull structural seakeeping trials, while the *S–N* curves are established based on the British Standards.

Keywords: probabilistic lifetime sea loads; fatigue reliability evaluation; service life; high-speed ship structures

1. Introduction

Ship structures subjected to various sea loads during operations experience strength degradation due to fatigue over their service life. For this reason, service life prediction for fatigue has to be carried out in design and assessment phases. In general, fatigue life can be assessed based on the stress–life (*S–N*) relationship (as a model of fatigue resistance) and the action of sea waves and the sea environment (as a model of fatigue loading), as suggested by Ayyub *et al.* (2002a). If the *S–N* category of the structural detail is correctly classified, the necessary information regarding fatigue resistance can be easily obtained. However, the accurate estimation of fatigue lifetime sea loads may be more challenging in time-dependent fatigue deterioration processes due to various uncertainties. These uncertainties include still water loading, wave-induced loading and transient impact-slamming, among others. Clearly, in fatigue design, experiments or simulations for predicting the potential lifetime sea loads are useful. Similarly, in fatigue assessment, structural health monitoring (SHM) during voyages provides real-time fatigue loadings that can be integrated into a time-dependent structural performance assessment. However, continuous monitoring up to the anticipated service life may not be feasible. This is because there can be many restrictions due to budgetary, environmental and operational constraints. Alternatively, a probabilistic approach for fatigue life evaluation can be used to effectively estimate lifetime sea loads based on given information obtained from model tests, simulations or monitoring.

To date, the use of simulations, model tests and monitoring programs has been widely accepted for the estimation of lifetime sea loads. Kaplan *et al.* (1974) conducted a study with the computer program SCORES in order to estimate wave loads on the SL-7 container ship. The key factors of their study were ship speeds, wave lengths, headings and sea states. Similarly, Sikora *et al.* (1983) used the computer program SPECTRA for predicting primary load fatigue spectra for small waterplane area twin hull (SWATH) ships. Response amplitude operators for desired operating speeds and headings were used as input parameters as well as occurrence probabilities of sea state, heading and speed. As a result of these computer simulations, it was concluded that ship operational and wave conditions are important factors for the estimation of lifetime wave loads.

Ship model tests can be performed to provide various ship structural responses considering wave conditions, ship speeds and relative wave headings.

*Corresponding author. Email: dan.frangopol@lehigh.edu

ISSN 1573-2479 print/ISSN 1744-8980 online

DOI: 10.1080/15732479.2010.524984
http://www.informaworld.com

In general, performance measures obtained from model tests as well as monitoring can be used to provide more reliable structural responses, and to improve the decision-making process for ship maintenance management. The measured data from monitoring or model tests have been successfully used for structural performance assessment (Chiou and Chen 1990, Frangopol *et al.* 2008, Okasha *et al.* 2010a,b). Available sea loading information from model tests may allow not only the assessment of current ship structural performance but also the development of lifetime sea load prediction models using probabilistic methods.

This article focuses on estimating probabilistic lifetime sea loads based on model test and on integrating them into fatigue performance assessment and service life prediction. As illustrations, potential lifetime sea loads including low frequency wave-induced loading and high frequency slam-induced whipping loading are investigated, and a probabilistic approach for fatigue life evaluation is conducted. Occurrence probability associated with potential sea states is used to estimate probabilistic lifetime sea loads. Loading information is provided from the scaled test measurements of joint high-speed sealift ship (JHSS) monohull structural seaways loads test (Devine 2009). Based on all necessary information from the *S–N* approach for resistance and model test data for load effect, a fatigue reliability analysis is conducted by using the reliability software RELSYS (Estes and Frangopol 1998).

2. Fatigue resistance and loads

In many ship structures, the structural deterioration process due to fatigue significantly diminishes their service life. Typically, time-dependent fatigue strength can be assessed based on the *S–N* approach. Simultaneously, information on sea loadings, which is primarily associated with the action of sea waves and the sea environment, can be obtained from simulation programs, sea trial tests, segmented structural seakeeping model tests, and/or real-time SHM.

2.1. *The S–N approach and Miner's rule*

For fatigue life evaluation of steel structures, the *S–N* curve approach has been widely used and adopted by all standards and specifications. Fatigue strength of a structural detail is characterised in the relationship between stress range (nominal applied stresses) and cycles to failure for classified detail categories. The characteristic *S–N* curves are based on fatigue test data and correspond to the mean life of a detail which is shifted horizontally to the left by two standard deviations (Fisher *et al.* 1998). The *S–N* curves are represented as sloping straight lines in logarithmic scale. The basic equation of fatigue strength is

$$S_r = \left(\frac{A}{N}\right)^{1/m} \tag{1}$$

where S_r = nominal fatigue resistance (stress range), A = fatigue detail coefficient which can be treated as a random variable if uncertainty in fatigue strength is considered, N = number of cycles, and m = material constant. A typical set of *S–N* curves, as that shown in Figure 1, can be established based on the BS 5400 (1980).

Typically, fatigue damage is defined to be cumulative and the Palmgren–Miner rule is used to account for this damage accumulation. The linear damage rule proposed by Palmgren in 1924 was further investigated by Miner in 1945 (Fisher *et al.* 1998). It simply assumes that damage fraction at any particular stress range level is a linear function of the corresponding number of cycles. For a structural detail, the total damage can be expressed as the sum of damage occurrences that have taken place at individual stress range levels (i.e. Miner's rule)

$$D = \sum \frac{n_i}{N_i} \tag{2}$$

where n_i = number of cycles at stress range level i and N_i = number of cycles to failure at stress range level i. Theoretically, the fatigue damage ratio, D, is equal to 1.0 at failure, while practically it may be less than 1.0 due to various uncertainties (Fisher *et al.* 1998, Ayyub *et al.* 2002a).

2.2. *Estimation of sea loads based on simulation and monitoring*

In the design phase, accurate estimates of potential sea loadings are important to ensure the desired structural

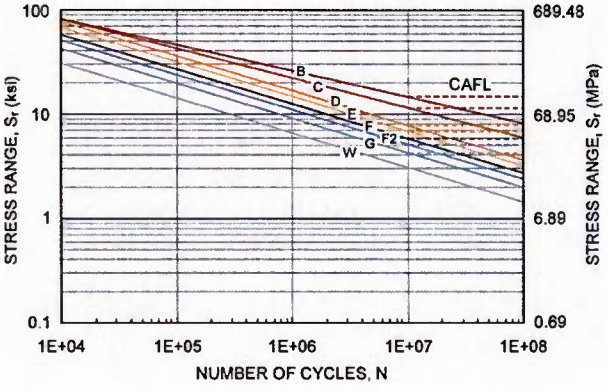

Figure 1. The *S–N* curves based on the BS 5400 (1980).

performance during the entire service life of ship structures, especially for high speed vessels. Primary structural loads on a ship result from its own weight, cargo, buoyancy and operation (Ayyub *et al.* 2002b). In assessing the reliability of ship structures, load effects may be estimated by finite element analysis, simulation and/or monitoring.

According to Paik and Frieze (2001), ship hull girder loads can be classified into three types: still water loads, low and high frequency wave-induced loads, and thermal loads. Still water loads are due to the difference between the weight and buoyancy distributions along the length of the ship. The low frequency wave-induced loads consist of vertical, horizontal and torsional wave loads, whereas the high frequency dynamic loads are due to slamming or whipping and springing (Devine 2009). Wave and dynamic loads are affected by many factors such as ship characteristics, ship speed, relative wave heading and sea states associated with significant wave heights (Ayyub *et al.* 2002b). Significant wave height is usually treated as a random variable that requires statistical analyses of ship response data collected from simulation, experiment or monitoring. For various sea states, efforts to estimate wave-induced load effects more accurately have been made (Glen *et al.* 1999, Wu and Moan 2006, Pedersen and Jensen 2009). For various ship speeds, Aalberts and Nieuwenhuijs (2006) analysed 1-year full scale measurements from a general cargo/container vessel in order to determine the effect of whipping (high frequency) and wave-induced (low frequency) loads on fatigue. Maximum wave-induced and dynamic bending moments that the ship may encounter during its service life should be taken into account in performance assessment and life prediction.

In recent years, the development of effective SHM systems for naval ships, especially for lightweight high speed ships, has been an important issue (Hess 2007, Salvino and Brady 2008). The SHM systems can be used to obtain prompt responses in terms of structural diagnosis and prognosis, and to offer possibilities for supporting operational and maintenance decisions. The use of available information from SHM is the most effective tool for the decision-making process. However, there are many restrictions to the adoption of this kind of SHM systems to high speed and high performance ships. In fact, these systems are still in an early stage of their development (Salvino and Brady 2008). Alternatively, ship model tests (e.g. segmented scaled model) or simulation analyses by using SPECTRA (Sikora *et al.* 1983) or LAMP (Lin and Yue 1990) can be employed to estimate lifetime sea loads considering various wave conditions. The simulation program SPECTRA developed by Sikora *et al.* (1983), is useful for computing vertical, lateral and torsional moments applied to the hull girder of a monohull ship, and for creating a stress range bin histogram to evaluate fatigue life considering ship characteristics and wave conditions associated with specific sea routes (Michaelson 2000). In addition, ship model tests are useful for estimating various ship responses (e.g. stress, strain) in given sea states (e.g. moderate, high, hurricane), ship speeds and relative wave headings. Sea loads obtained from these model tests may be integrated into probabilistic lifetime sea loads prediction models. Consequently, probabilistic lifetime sea loads estimated from model tests can be used effectively for fatigue reliability evaluation.

2.3. Stress range bin histogram and probability density functions (PDFs)

As described previously, in terms of fatigue resistance, the S–N approach may be useful for estimating the total fatigue life including both crack initiation and crack propagation. On the other hand, in terms of fatigue load effects, variable amplitude loadings (i.e. stress range) must be appropriately taken into account for fatigue life evaluation. Cycle counting methods can be used to establish a stress range bin histogram (i.e. stress range vs. number of cycles). The ASTM Standard E 1049-85 (1997) addresses the following cycle counting techniques: level-crossing counting, peak counting, rain-flow counting, among others. In this article, the bending stress range bin histogram of a typical ship structure is computed by means of the peak counting technique. To consider the whole stress cycle (positive and negative), the values of the absolute peak stresses are doubled for the purpose of the histogram computation. This results in a conservative overestimation of the loads.

The procedure for creating a stress range bin histogram using peak counting is summarised as follows:

(1) determine the mean value of all time records
(2) filter all peak values (i.e. stresses) above the determined mean value
(3) set the stress range at two times the peak stress
(4) set the bin size (e.g. 0.5 ksi, 1.0 ksi) and count the assigned stress ranges
(5) establish a histogram of stress range occurrences.

Based on the established stress range bin histogram, effective stress range and number of cycles can be computed. Most importantly, an appropriate PDF for the prediction of sea loads should be determined. The probabilistic approach can be used to predict both resistance, R, and stress range, S, during fatigue life

and eventually to perform fatigue reliability evaluation. The applieable PDFs associated with R and S are usually assumed to be lognormal and Weibull, respectively, for evaluating ship fatigue life. The PDFs of these distributions are

(1) Lognormal distribution

$$f_R(r) = \frac{1}{r \cdot \zeta \cdot \sqrt{2 \cdot \pi}} \cdot \exp\left[-\frac{1}{2} \cdot \left(\frac{\ln(r) - \lambda}{\zeta}\right)^2\right] \quad \text{for } r > 0 \tag{3}$$

where λ = mean of ln r (location parameter), and ζ = standard deviation of ln r (seale parameter).

(2) Weibull distribution

$$f_S(s) = \frac{\beta}{\alpha} \cdot \left(\frac{s}{\alpha}\right)^{\beta-1} \cdot \exp\left[-\left(\frac{s}{\alpha}\right)^{\beta}\right] \text{for } s > 0 \tag{4}$$

where α = scale parameter, β = shape parameter and $\alpha > 0$, $\beta > 0$.

The parameters of the lognormal distribution can be easily obtained from fatigue resistance data, while those of the Weibull distribution are derived from the stress range bin histogram data. The effeetive stress range, S_{re}, eould be derived as the qth moment of the Weibull PDF as follows:

$$S_{\text{re}} = \left[\int_0^{\infty} s^q \cdot f_S(s) \cdot ds\right]^{\frac{1}{q}} = [E(S^q)]^{\frac{1}{q}}. \tag{5}$$

This can be also computed directly from the stress range bin histogram and Miner's rule (Miner 1945, Fisher *et al.* 1998):

$$S_{\text{re}} = \left[\sum \frac{n_i}{n_{\text{total}}} \cdot S_{\text{ri}}^m\right]^{\frac{1}{m}} \tag{6}$$

where n_i = number of observations in the predefined stress range bin, S_{ri}, n_{total} = total number of observations during the monitoring period and m = slope of the S–N eurve (material eonstant).

2.4. *Probabilistic lifetime loads prediction for fatigue*

A probabilistie approaeh to potential sea loads prediction for fatigue is herein addressed. This approach eonsiders both effective stress range at a specifiecl sea wave condition (e.g. sea state 7, ship speed of 35 knots, and heading of 0° for following seas) and number of cycles in its observed time period. As deseribed previously, sea loads are function of ship eharaeteristics, ship speed, relative wave heading and sea states associated with signifieant wave heights (wave eondition). If ship model test data for certain wave conditions are provided, probabilistie lifetime sea loads ean be estimated by eonsidering both effective stress range and average daily number of eyeles.

Based on given information (e.g. stress vs. time), wave-induced and whipping responses ean be separately obtained by filtering. Wave-indueed loadings are produeed by the low-pass filtering, whereas wave impaets eausing global hull girder whipping are eolleeted using high-pass filtering (Brady 2004, Hildstrom 2007). Based on the filtering proeesses of raw data, individual stress range bin histograms for the given wave eonditions are established using the peak eounting method. Then, the effeetive stress range, S_{re}, and average daily number of eyeles, N_{avg}, for an observed time period are ealeulated from the stress range histogram data. To estimate fatigue lifetime sea loads considering all possible wave conditions, the predieted effeetive stress range, S_{re}^*, ean be derived under eonsideration of probabilistie ship operational profiles at a specific seaway. As an approximation, in this study it will be assumed that sea state, ship speed and relative wave heading are independent variables. The various probabilities of occurrence are considered to be the continuous representations of the relative frequeneies n_i/n_{total} in Equation (6). Therefore, the resulting equation is:

$$S_{re}^* = \left[\sum_{i=1}^{ss} \sum_{j=1}^{sp} \sum_{k=1}^{wh} P_{SS,i} \cdot P_{SP,j} \cdot P_{WH,k} \cdot S_{\text{re},ijk}^m\right]^{\frac{1}{m}} \tag{7}$$

where S_{re} = effective stress range; m = material eonstant; $P_{SS,i}$ = probability of oeeurrence of the ith sea state ($i = 1, 2, \ldots, ss$), $P_{SP,j}$ = probability of oeeurrenee of the jth ship speed ($j = 1, 2, \ldots, sp$) and $P_{WH,k}$ = probability of occurrence of the kth relative wave heading ($k = 1, 2, \ldots, wh$) for the applieable sea events. The eorresponding schematic for estimating S_{re}^* is shown in Figure 2. As indieated, a new effeetive stress range bin histogram can be established by the individual effeetive stress ranges from eaeh histogram and the oeeurrence probability associated with wave eonditions.

Similarly, the predicted average daily number of eyeles, N_{avg}^*, may be derived using the three oeeurrence probabilities whieh are assoeiated with all potential sea wave eonditions

$$N_{\text{avg}}^* = \sum_{i=1}^{ss} \sum_{j=1}^{sp} \sum_{k=1}^{wh} P_{SS,i} \cdot P_{SP,j} \cdot P_{WH,k} \cdot N_{\text{avg},ijk}. \tag{8}$$

The eomputed N_{avg}^* is used to estimate the aeeumulated number of stress cycles for futurc years, $N(y)$,

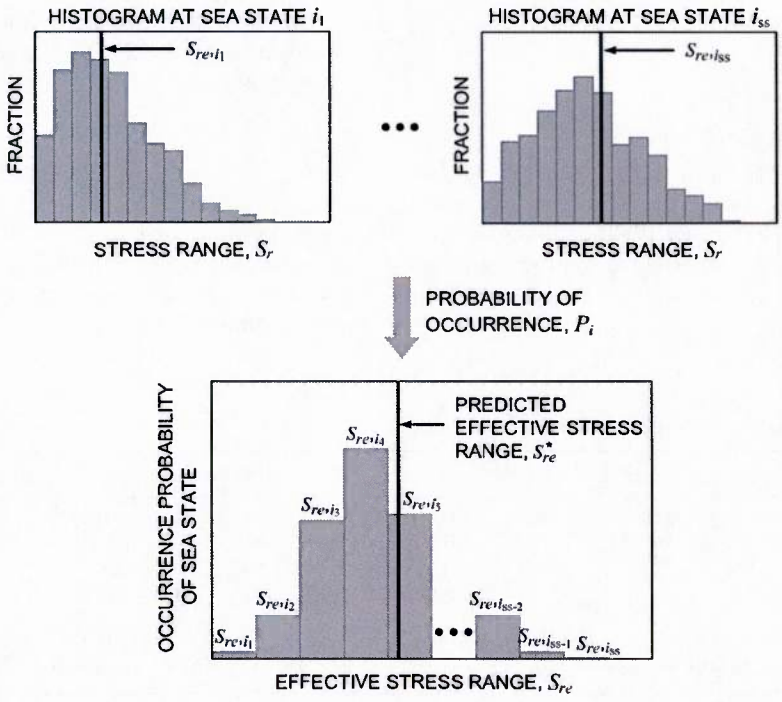

Figure 2. Schematic for estimation of the predicted effective stress range, S_{re}^*.

considering annual ship operation rate, α, in anticipated seaways. Therefore, $N(y)$ is estimated from the linear relationship to ship service life as

$$N(y) = 365 \cdot \alpha \cdot N_{avg}^* \cdot y. \tag{9}$$

where y = number of years, and α = ship operation rate per year (e.g, $\alpha = 50\%$ for six months of operation, 75% or 90%).

3. Fatigue reliability analysis

Performance assessment and service life prediction for fatigue are herein addressed. As mentioned previously, ship fatigue life can be assessed more reliably based on both the *S–N* curve for ship capacity and the test data for load effects under uncertainties. It is noted that the predicted effective stress range, S_{re}^*, derived from Equation (7) is used for the prediction of lifetime load effect for fatigue.

3.1. Fatigue limit state

Under the repeated or fluctuating application of stresses, ship performance assessment and service life prediction for fatigue can be performed by fatigue reliability analysis with a well-defined fatigue limit-state function consisting of fatigue resistance, R, and load effect, S. This is important because maintenance-management actions including inspection, monitoring and repair can be better planned if based on the well-quantified ship reliability. For the fatigue reliability evaluation, the limit-state functions of structural details are established, and PDFs for resistance and stress range are assumed. Typically, the safety of any structure would be preserved when its resistance, R, is larger than the predicted effective stress range, S_{re}^*.

The limit-state function used in fatigue reliability analysis is defined based on the *S–N* approach and Miner's rule (1945) as follows:

$$g(\mathrm{X}) = \Delta - D = 0 \text{ for } D = \sum n_i/N_i = (N/A) \cdot (eS_{re}^*)^m \tag{10}$$

where Δ is Miner's critical damage accumulation index in terms of resistance and is assumed as lognormal with mean value of 1.0 and coefficient of variation (COV) of 0.3 for metallic materials (Wirsching 1984); D is Miner's damage accumulation index, e is a typical measurement error factor and m is a constant defined in the BS 5400 (1980). The number of cycles, N, which is obtained from Equation (9), is treated as random with COV of 0.2 and A is also considered random.

Complete details for all random variables are presented in Table 1.

3.2. *Fatigue reliability evaluation*

Based on the function $g(\boldsymbol{X})$, the fatigue reliability analysis is performed by using the reliability software RELSYS (Estes and Frangopol 1998). S^*_{re} is treated as Weibull PDF with COV of 0.2, while other random variables (i.e. Δ, A, N and e) are Lognormal (see Table 1).

The flowchart for the fatigue reliability evaluation is shown in Figure 3, and the corresponding steps are summarised as follows:

3.2.1. *Step 1. Details of structural members based on the S–N approach*

The S–N approach in terms of fatigue resistance, R, provides relevant information including the S–N category, material constant, m, constant amplitude fatigue limit (CAFL), and fatigue detail coefficient, A.

Table 1. Random variables for fatigue reliability evaluation.

Random variables	Notation	Distribution	Source
Critical damage accumulation index	Δ	Lognormal, E(Δ) = 1.0, COV(Δ) = 0.3	Wirsching (1984)
Fatigue detail coefficient	A	Lognormal, E(A)[a] = 6.29E + 11 MPa^3, (1.92E + 09 ksi^3), COV(A)[a] = 0.54	BS 5400 (1980)
Measurement error factor	e	Lognormal, E(e) = 1.0, COV(e) = 0.1	Ayyub *et al.* (2002) and Frangopol *et al.* (2008)
Predicted effective stress range	S^*_{re}	Weibull (see Table 2), COV(S^*_{re}) = 0.2	Based on model test data
Predicted average daily number of cycles	N^*_{avg}	Lognormal (see Table 2), COV(N^*_{avg}) = 0.2	Based on model test data

Note: [a]The values E(A) and COV(A) assigned by the S–N category F.

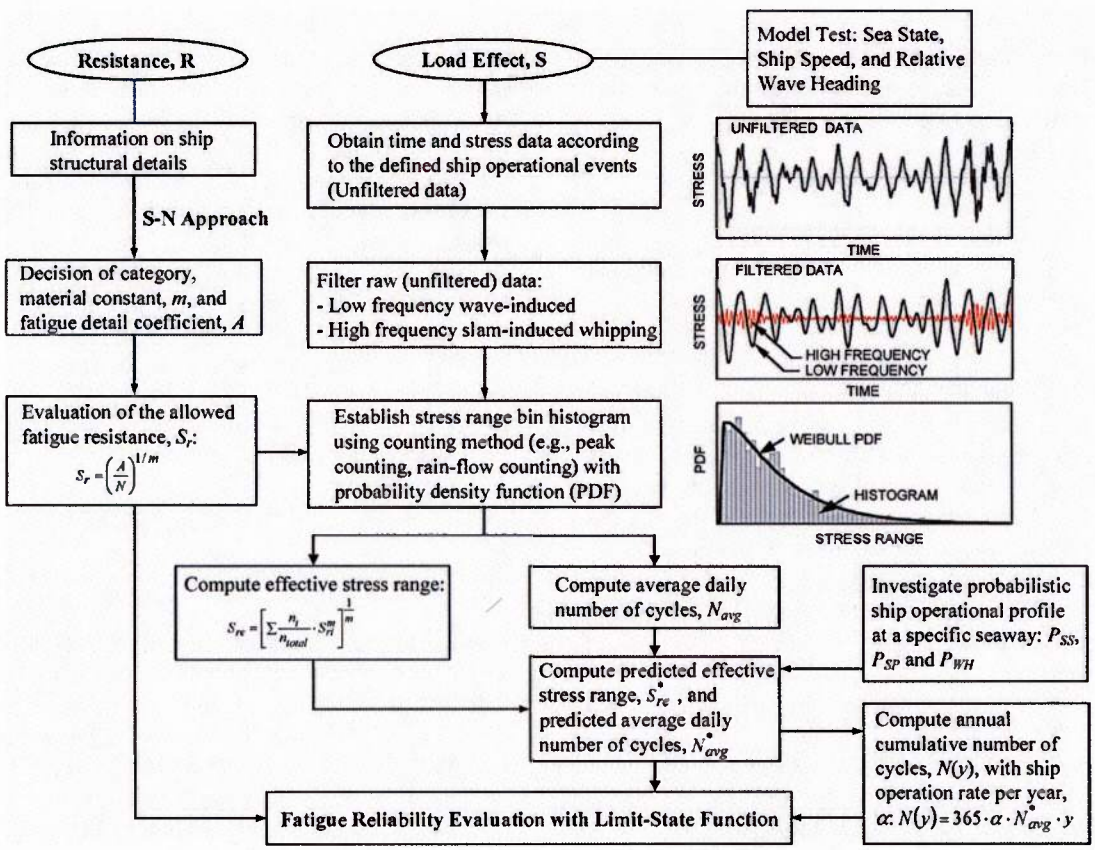

Figure 3. Flowchart for the fatigue reliability evaluation.

3.2.2. Step 2. Low-pass and high-pass filtering based on the collected unfiltered data

From the unfiltered (raw) data, wave-induced and slamming-induced whipping responses are obtained by filtering at low and high frequency levels, respectively, in order to provide separately useful responses for ship fatigue life evaluation.

3.2.3. Step 3. Stress range bin histogram and PDFs

The stress range bin histograms are established by using peak counting method from the unfiltered or filtered data at the selected locations (stations) of structural members. Based on the stress range bin histogram, effective stress range, S_{re}, (see Equations (5) and (6)) and the average daily number of cycles, N_{avg}, from a monitoring time period, T_{mon}, can be computed. Mean modal wave period, T_w, which is different at each sea state, is used to estimate N_{avg} by multiplying the ratio (i.e. T_{mon}/T_w) by the counted number of occurrences during T_{mon}. An appropriate PDF for predicting sea loads is used considering uncertainty during fatigue lifetime. In ship fatigue reliability evaluation, lognormal and Weibull PDFs can be used for resistance and load effects, respectively.

3.2.4. Step 4. Probabilistic lifetime sea loads prediction

The probabilistic approach to potential sea loads prediction for fatigue evaluation is developed considering ship speeds, relative wave headings, and sea states associated with wave heights. The calculated S_{re} and N_{avg} according to the sea states (e.g. $0 \sim 9$) or applicable sea events are used to estimate both the predicted effective stress range, S^*_{re}, and the predicted average daily number of cycles, N^*_{avg}. All possible ship operational conditions through anticipated seaways are taken into account.

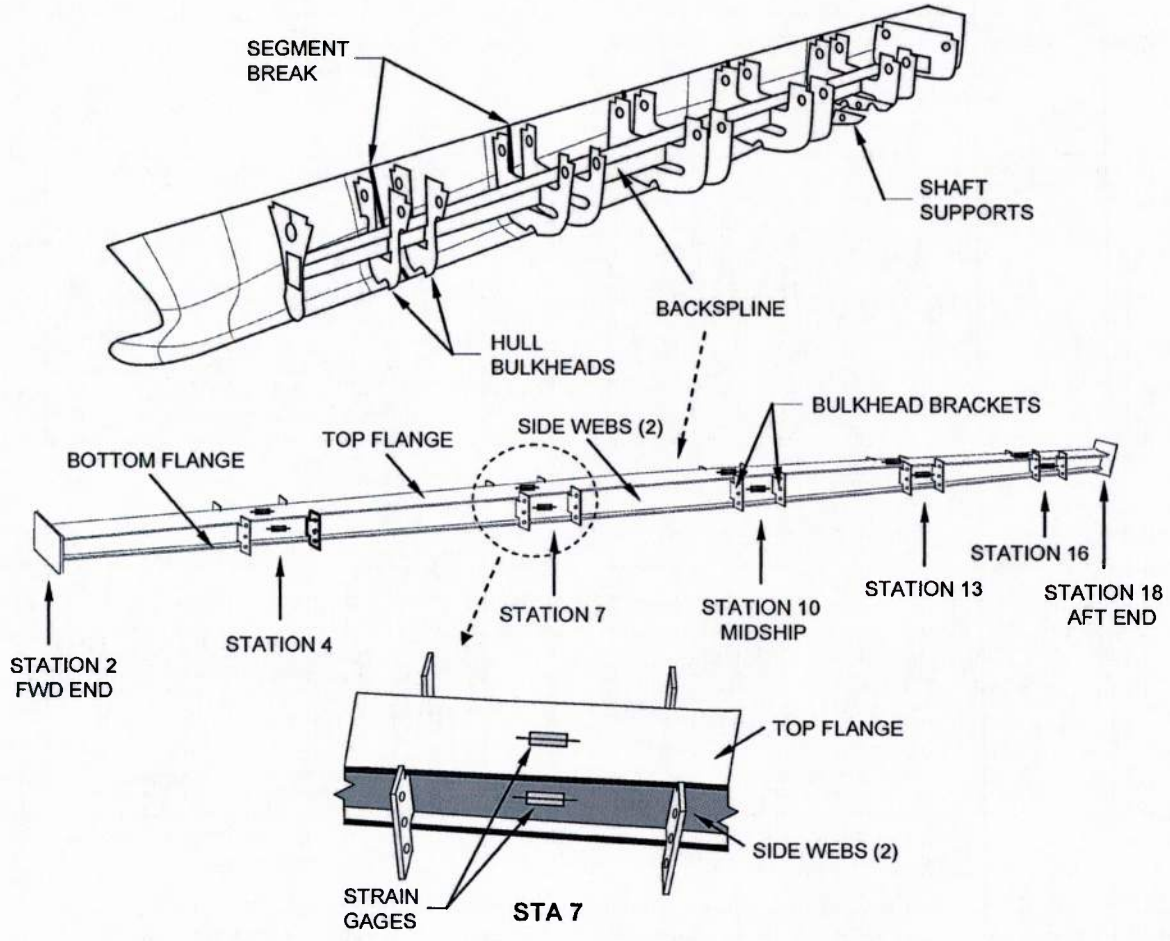

Figure 4. JHSS model (adapted from Devine 2009).

3.2.5. *Step 5. Cumulative number of cycles, N(y)*

By using Equation (9), $N(y)$ is estimated for time-dependent fatigue reliability evaluation. In this study, $N(y)$ does not reflect instantaneous but progressive time effect for fatigue life of ship, meaning that the number of cycles up to a specific year has been accumulated since the first ship operation year.

3.2.6. *Step 6. Fatigue reliability analysis*

For a given service year, the fatigue reliability analysis is performed with all necessary information from steps 1–5. For the assumed PDFs (lognormal and Weibull), the reliability software RELSYS (Estes and Frangopol 1998) is used to compute the fatigue reliability index. This program uses the first-order reliability method (FORM) to compute the reliability index.

4. Application

As an illustration, probabilistic lifetime sea loads of the JHSS for fatigue are estimated based on model test data and integrated into the fatigue performance assessment and service life prediction. Potential lifetime load effects, which are associated with low frequency wave-induced and high frequency slam-induced whipping loadings due to vertical bending moment, are investigated. For fatigue reliability analysis, the collected sea loadings from the scaled test measurements of a JHSS monohull structural seaways loads test (Devine 2009) are used together with the S–N curve provided by the BS 5400 (1980).

4.1. *Segmented model*

A full-scaled JHSS monohull length was scaled down to reach the value of 6.1 m (20 ft) in the segmented model (Devine 2009). It is noted that appropriate scale factors for the involved quantities (e.g. length, time, moment of inertia, bending moment) were obtained based on Froude scaling laws.

The segmented model approach was used to measure detailed hull response using a simple internal backspline (see Figure 4). The vertical, lateral and torsional stiffness and vibrational characteristics of the hull were modelled by using the internal backspline (Devine 2009). During each test run, realistic vibrational response, including hull primary and secondary

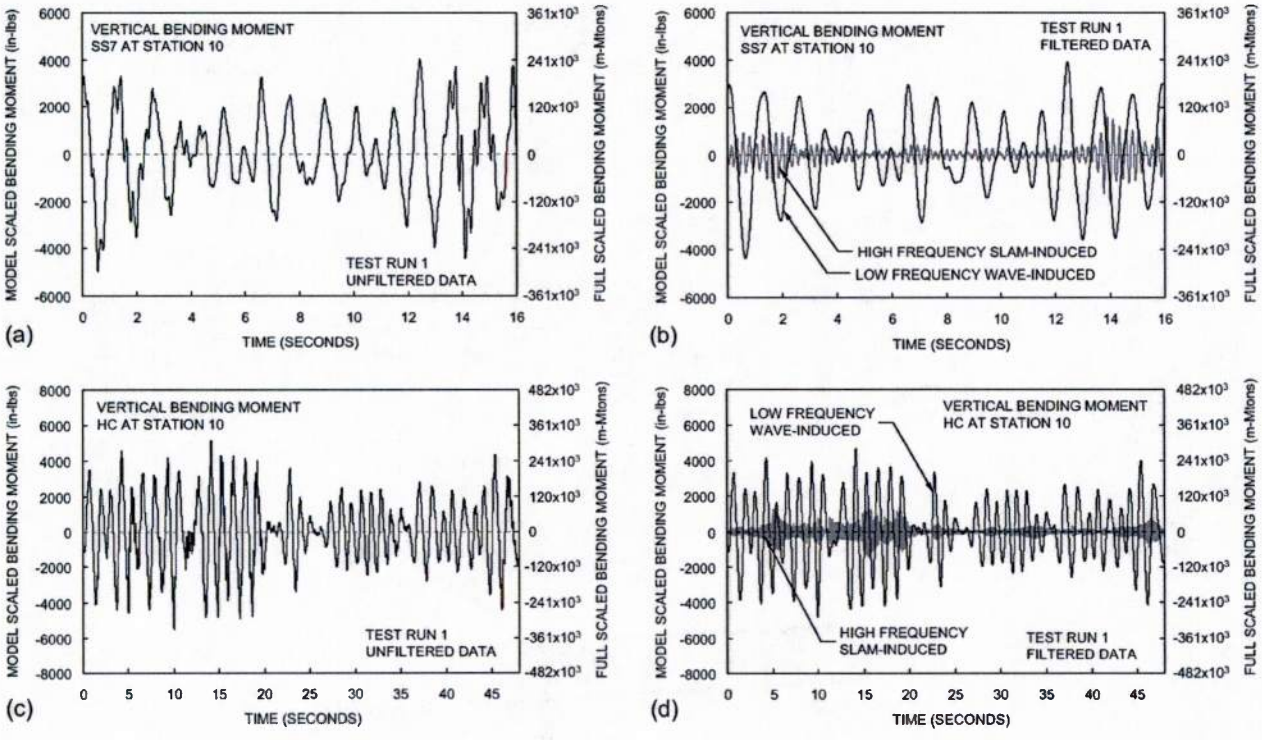

Figure 5. JHSS primary vertical bending moment. (a) unfiltered data at Station 10, 35 knots, SS 7 and heading of 0°. (b) low and high frequency filtered data at Station 10, 35 knots, SS 7 and heading of 0°. (c) unfiltered data at Station 10, 15 knots, HC and heading of 0°. (d) low and high frequency filtered data at Station 10, 15 knots, HC and heading of 0°.

loads, was collected from the installed strain gages on the Froude-scaled structural component at Stations 4, 7, 10, 13 and 16 (see Figure 4). As shown in Figure 4, the shell sections were connected with a continuous backspline beam and strain gages were installed at each segment cut to measure the vertical, lateral and torsional bending moments and vertical/lateral shear forces. It is noted that section modulus at the identified stations on the backspline varies along the beam length. Description of the JHSS segmented model tests and further details can be found in Devine (2009).

4.2. *Fatigue resistance and load effects*

Details of fatigue resistance and the scaled test data, which are associated with the strain gages installed on the top flanges of the backspline at five stations (i.e. Stations 4, 7, 10, 13 and 16 in Figure 4), are used to illustrate the fatigue reliability assessment and service life prediction based on the estimated probabilistic lifetime sea loads. For fatigue resistance, the *S–N* curves based on the BS 5400 (1980) are used and the corresponding *S–N* parameters (i.e. category, CAFL and fatigue detail coefficient, *A*) are investigated at the respective structural details. Typically, the rational procedure to find the *S–N* parameters is to identify the worst weld detail in the design and assessment phases. In this study, for illustrative purposes, the *S–N* category F, which may be the worst case, is assumed for all the details, for illustrative purposes. The material constant, *m*, is 3.0, while the mean value of *A* is 6.29E+11 MPa^3 (1.92E+09 ksi^3) with coefficient of variation COV(*A*) = 0.54. The corresponding constant amplitude fatigue limit is CAFL = 39.78 MPa (5.77 ksi).

In this study, two sets of test data provided by Devine (2009) are used: (i) sea state 7 (SS7); 35 knots and heading of 0°; (ii) Hurricane Camille (HC), 15 knots and heading of 0°. Based on the given model test data, primary vertical hull-girder bending moments are investigated at the gage stations. At midship (i.e. Station 10), vertical bending moments due to SS7 and HC are presented in Figure 5. Hogging moment is positive and sagging is negative. Ship speeds in SS7

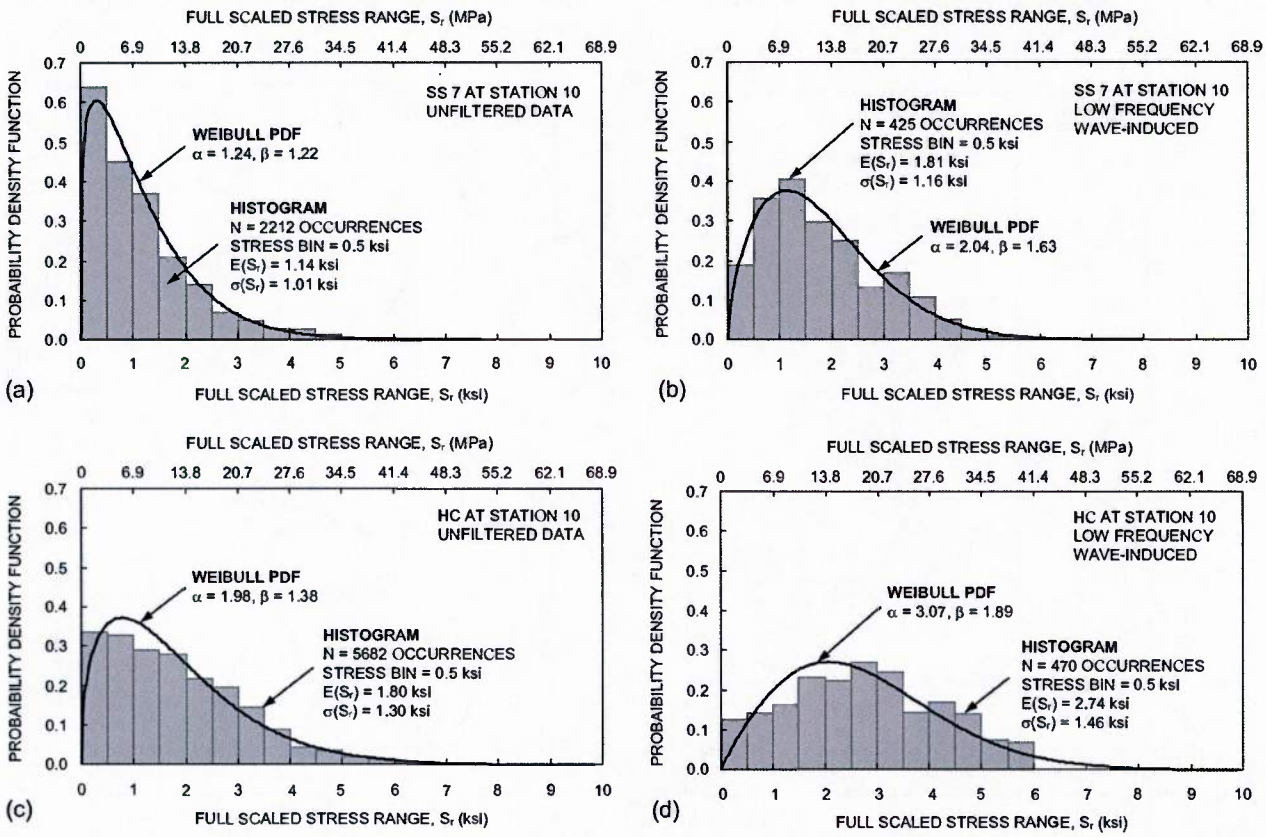

Figure 6. Stress range bin histogram and Weibull PDF. (a) unfiltered data at Station 10, 35 knots, SS 7 and heading of 0°. (b) low frequency wave-induced data at Station 10, 35 knots, SS 7 and heading of 0°. (c) unfiltered data at Station 10, 15 knots, HC and heading of 0°. (d) low frequency wave-induced data at Station 10, 15 knots, HC and heading of 0°.

and HC were 35 knots and 15 knots, respeetively, in the same heading of 0° (i.e. following seas). It is noted that the Froude seale faetor with respeet to the bending moment is $1.025\lambda_F{}^4$ where $\lambda_F = 47.5255$ (Devine 2009). In both wave eonditions, the filtering procedure has been applied to data, using low-pass and high-pass filtering to extraet separately wave-indueed moment and slamming-indueed whipping moment (see Figure 5b and d).

For the wave conditions SS7 and HC, stress range bin histograms using peak eounting are established based on unfiltered (wave-induced and slam-indueed) and filtered (wave-indueed) data. To eonvert bending moment, M, to stress, σ (i.e. $\sigma = M/S_m$), the Froude scale faetor $0.346\lambda_F{}^4$ for seetion modulus, S_m, was used (Devine 2009). Weibull PDF, whieh is widely aeeepted for lifetime sea loads prediction, is used for the probabilistie approaeh. As shown in Figure 6a–d, Weibull PDFs of full sealed stress range are fitted on the established stress range bin histograms, for illustrative purposes. The parameters α and β indieate seale and shape of the Weibull PDF, respectively, while $E(S_r)$ and $\sigma(S_r)$ denote the mean value and standard deviation of the stress range, respectively. It is found that the $E(S_r)$ from the filtered data (i.e. neglecting high frequency load effect) is larger than that from the unfiltered data (i.e. ineluding high frequency) at both loading conditions (see Figure 6). This is because the contribution of lower stress ranges to fatigue damage is diminished in the filtered data, as shown in Figure 5b and d. However, sinee the number of eyeles for high frequeney ean be large, the eumulative effeet of these numbers ean be important.

For eaeh test run of SS7 and HC at Stations 10 and 13, effeetive stress range, S_{re}, and average daily number of eyeles, N_{avg}, in the observed time period are eomputed and presented in Figure 7a–d. With the sampling rate for this primary hull response data of 200 Hz, full sealed observed time periods for the total coneatenated runs of SS7 and HC are about 42.4 min. and 66.6 min., respeetively. As shown in Figure 7, S_{re} and N_{avg} are fluetuating through eaeh test run. For lifetime fatigue assessment and predietion, these two parameters are herein treated as random variables considering loading uneertainty assoeiated with the limited test runs.

4.3. *Fatigue reliability analysis by using probabilistic lifetime sea loads*

As described previously, under uncertainty assoeiated with wave loading, a probabilistie approaeh for

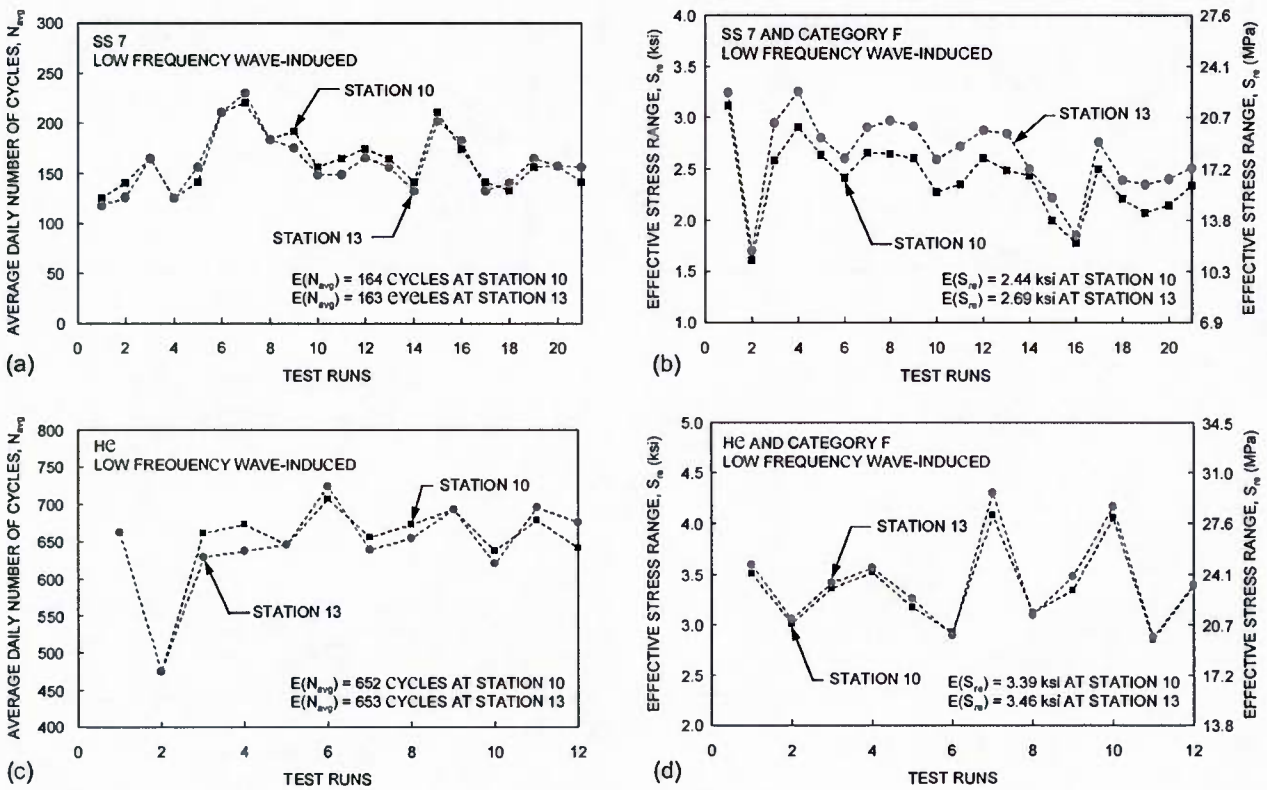

Figure 7. Effective stress range, S_{re}, and average daily number of cycles, N_{avg}, at Stations 10 and 13 for each test run based on low frequency wave-induced moment: (a) N_{avg} of SS 7, (b) S_{re} of SS7, (c) N_{avg} of HC, and (d) S_{re} of HC.

Table 2. Lifetime prediction of sea loads for fatigue at each station.

Station	Sea state 7			Hurricane Camille			Predicted value		
	S_{re}, MPa (ksi)		N_{avg}	S_{re}, MPa (ksi)		N_{avg}	S^*_{re}, MPa (ksi)		N^*_{avg}
	Weibull	Miner	(cycles)	Weibull	Miner	(cycles)	Weibull	Miner	(cycles)
Station 4	5.83 (0.85)	5.93 (0.86)	187	10.99 (1.59)	10.70 (1.55)	703	5.43 (0.79)	5.48 (0.79)	143
Station 7	12.43 (1.80)	12.34 (1.79)	175	19.88 (2.88)	19.41 (2.81)	656	11.40 (1.65)	11.29 (1.64)	134
Station 10	16.93 (2.45)	16.82 (2.44)	164	23.81 (3.45)	23.39 (3.39)	652	15.40 (2.23)	15.27 (2.21)	126
Station 13	18.77 (2.72)	18.55 (2.69)	163	24.17 (3.50)	23.85 (3.46)	653	17.01 (2.47)	16.83 (2.44)	125
Station 16	13.19 (1.91)	13.10 (1.90)	162	15.43 (2.23)	15.29 (2.22)	668	11.91 (1.73)	11.86 (1.72)	125

Note: Equations (5) and (6) are used in the calculation of S_{re} by Weibull PDF and Miner's rule, respectively.

potential sea loads prediction is necessary to be developed based on given information (e.g. model tests, simulations, monitoring). In particular, if model test data for each sea state is available, lifetime sea loads for fatigue life evaluation can be reliably estimated, using occurrence probability of sea states in a seaway, and the computed S_{re} and N_{avg} from applicable operational conditions. As a result, probabilistic lifetime sea loads of JHSS monohull from model test data can be computed by using the proposed approach.

The established stress range bin histograms from low frequency wave-induced data of SS7 and HC, which are filtered from total concatenated runs, are used to estimate S_{re} and N_{avg} at the five stations. In the calculation of S_{re}, Equations (5) and (6) are employed considering Weibull PDF and Miner's rule, respectively. The calculated S_{re} and N_{avg} at the five stations are presented in Table 2. The maximum value of effective stress range was observed at Station 13, not at midship (i.e. Station 10) for both SS7 and HC, whereas the maximum bending moment was recorded at Station 10 (see Figure 8). This is because the section modulus on the backspline varies along the length of JHSS monohull. By using Equations (7) and (8), the predicted effective stress range, S^*_{re}, and predicted average daily number of cycles, N^*_{avg}, considering potential sea states at the worst area (i.e. North Atlantic Ocean) as presented in Table 3 (Brady *et al.* 2004), are estimated to perform the fatigue reliability assessment. Due to the lack of information, occurrence probability of sea state is only considered in order to estimate probabilistic lifetime sea loads. Occurrence probabilities of ship speed and relative wave heading are ignored in this application.

All necessary information for the probabilistic fatigue reliability analysis is obtained from steps 1 to 5 (see also Figure 3), and fatigue reliability analyses are conducted using reliability software RELSYS (Estes and Frangopol 1998). The established S–N curve based on the BS 5400 (1980) is herein used. Predicted lifetime

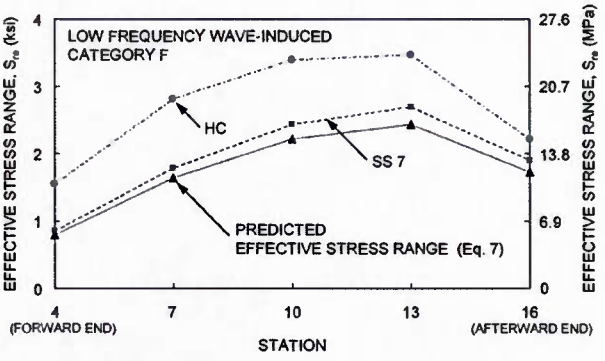

Figure 8. Predicted effective stress range, S^*_{re}, at the five stations of the JHSS.

Table 3. Modal wave period and probability of occurrence according to sea states of North Atlantic Ocean (Brady *et al.* 2004).

Sea state	Mean value of significant wave height (ft)	Mean value of significant wave height (m)	Mean modal wave period (s)	Probability of occurrence[a] (%)
0 – 1	0.16	0.05	–	1.0
2	0.98	0.30	6.9	6.6
3	2.87	0.87	7.5	19.6
4	6.15	1.87	8.8	29.7
5	10.66	3.25	9.7	20.8
6	16.40	5.00	12.4	14.1
7	24.61	7.50	15.0	6.8
8	37.73	11.50	16.4	1.3
>8	>45.90	>13.99	20.0	0.1

Note: [a]Probabilities reported for the North Atlantic annual.

loads are estimated based on the low frequency wave-induced data filtered. Fatigue reliability evaluation at the identified critical location is performed considering (i) annual ship operation rate, α, of 50, 75 and 90% and (ii) low frequency wave-induced moment and complete history including high frequency slam-induced

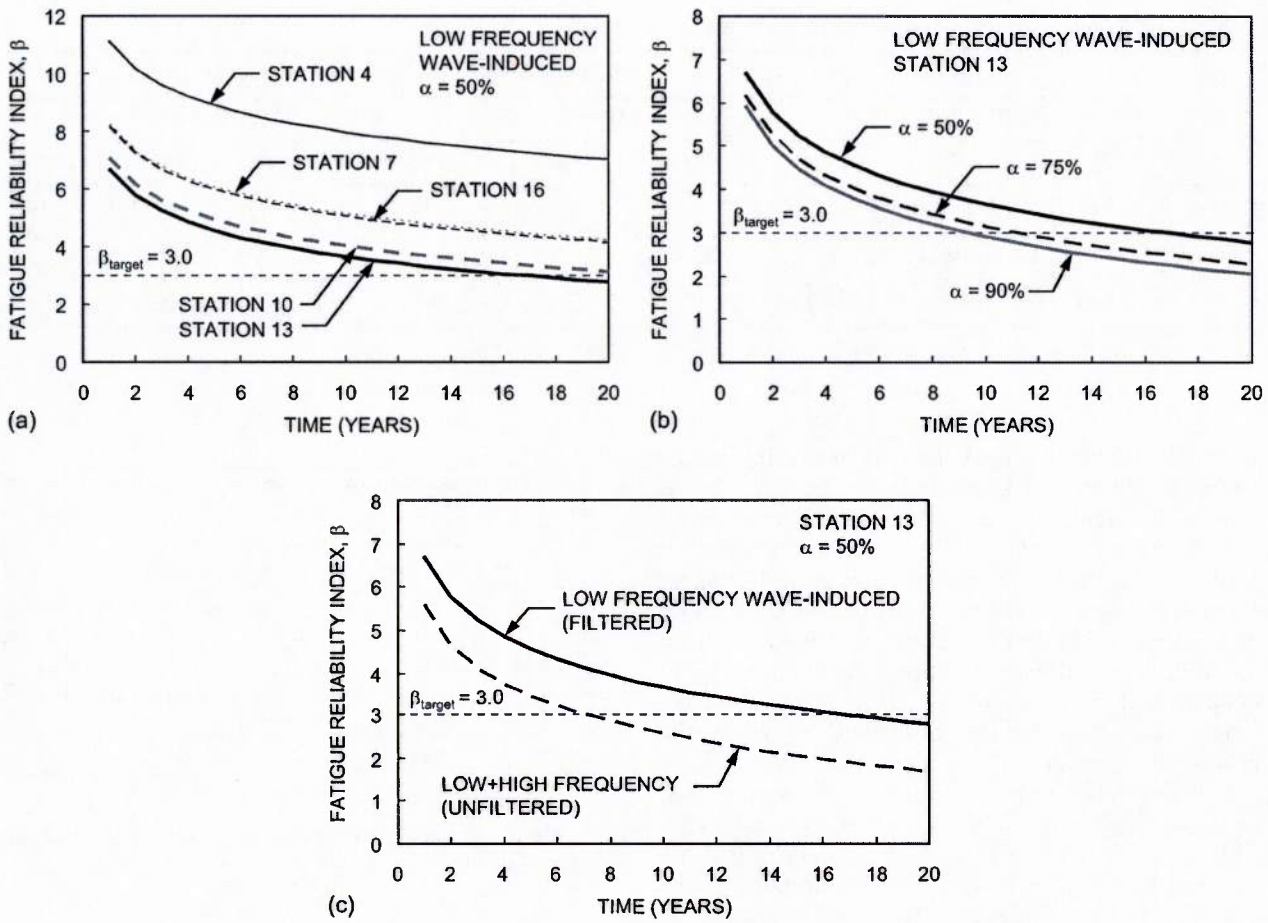

Figure 9. Fatigue performance assessment and service life prediction of the JHSS based on the predicted lifetime sea loads. (a) at the five stations with ship annual operation rate, $\alpha = 50\%$. (b) at Station 13 according to $\alpha = 50\%$, 75% and 90%. (c) using low frequency wave-induced filtered data and unfiltered data at Station 13.

whipping momcnt. Target reliability, β_{target}, is assumed to be 3.0. This target is in the rangc of target reliability indices for fatigue (i.e. $2.0 \leq \beta_{\text{target}} \leq 4.0$) recommended in Mansour *et al.* (1996).

The critical location of JHSS monohull is first identified. As shown in Figure 9a, at Station 13 fatigue reliability attains its lower bound, whereas the upper bound is at Station 4. Fatigue reliability analyses at the critical Station 13 are performed for both cases (i) and (ii). The result for case (i) is shown in Figure 9b. As expected, fatigue life of JHSS decrcases significantly when the ship operation rate increases. For the predefined β_{target} of 3.0, the predicted fatigue life was only about 9 years in the case of α of 90%, whereas it was 16 years in the case of $\alpha = 50\%$. The result of the fatigue reliability analysis for case (ii) is presented in Figure 9c. It is found that the effect of high frequency slam-induced whipping moment on fatigue life could not be neglected when considering operations in the worst areas.

5. Conclusions

This article presents an approach for fatigue reliability assessment and service life prediction of high-speed ship structures based on thc probabilistic lifetime sea loads estimated from model test data. The *S–N* approach applied to the identified structural details was used to estimate structural capacity in the fatigue reliability evaluation, whereas model test data were used to estimate probabilistic lifetime sea loads in terms of load effects. Under uncertainties associated with fatigue resistance and loading history, two PDFs (i.e. Lognormal, Weibull) were used. The unfiltered (raw) data collected on a scaled JHSS monohull was used to establish stress range bin histogram using peak counting method and to illustrate the proposed approach.

The following conclusions are drawn:

(1) The model test data can be used for cstimating probabilistic lifetime sea loads associated with effective stress rangc and number of cycles.

(2) Using filtering process, low frequency wave-induced and high frequency slam-induced whipping moments can be extracted from unfiltered test data in order to identify structural responses separately.
(3) Based on the established stress range bin histogram, individual effective stress ranges for given wave conditions (which are related to ship characteristics, ship speeds, relative wave headings and sea states) can be computed and used to estimate the predicted effective stress range, S_{re}^{*}, considering all possible ship operational conditions.
(4) Based on the estimated probabilistic lifetime sea loads and the *S–N* approach, fatigue performance assessment and service life prediction of ship structures can be performed. Therefore, the remaining fatigue life can be rationally estimated by using the proposed probabilistic approach.

Acknowledgements

The support from the Office of Naval Research to Lehigh University under award N-00014-08-0188 is gratefully acknowledged. The authors greatly appreciate the technical discussions with Dr. Edward Devine and Dr. Liming Salvino, Naval Surface Warfare Center, Carderock Division (NSWCCD) and thank them for providing the data used in this article. The opinions and conclusions presented in this article are those of the authors and do not necessarily reflect the views of the sponsoring organisation.

References

Aalberts, P.J. and Nieuwenhuijs, M., 2006. Full scale wave and whipping induced hull girder loads. *Proceedings of the Fourth International Conference on Hydroelasticity in Marine Technology*, 10–14 September Wuxi, China. Beijing, China: National Defence Industry Press, 65–78.

ASTM Standard E 1049-85, 1997 (reapproved). Standard practices for cycle counting in fatigue analysis. *In: Annual Book of ASTM Standards,* Vol. 03.01, 710-718, Philadelphia.

Ayyub, B.M., *et al.*, 2002a. Reliability-based design guidelines for fatigue of ship structures. *Naval Engineers Journal (ASNE)*, 114 (2), 113–138.

Ayyub, B.M., *et al.*, 2002b. Reliability-based load and resistance factor design (LRFD) guidelines for hull girder bending. *Naval Engineers Journal (ASNE)*, 114 (2), 43–68.

Brady, T.F., 2004. *Global structural response measurement of Swift (HSV-2) from JLOTS and Blue Game rough water trials.* West Bethesda, MD: Naval Surface Warfare Center, Carderock Division, NSWCCD-65-TR-2004/33.

Brady, T.F., *et al.*, 2004. *HSV-2 swift instrumentation and technical trials plan.* West Bethesda, MD: Naval Surface Warfare Center, Carderock Division, NSWCCD-65-TR-2004/18.

BS 5400, Part 10, 1980. *Steel, concrete, and composite bridges: code of practice for fatigue.* London, England: British Standards Institute.

Chiou, J.W. and Chen, Y.K., 1990. *Fatigue prediction analysis validation from SL-7 hatch corner strain data.* Washington, DC, Ship Structure Committee, Report No. SSC-338.

Devine, E.A., 2009. *An overview of the recently-completed JHSS Monohull and Trimaran structural seaways loads test program.* West Bethesda, MD: Naval Surface Warfare Center, Carderock Division (NSWCCD) PowerPoint Briefing.

Estes, A.C. and Frangopol, D.M., 1998. RELSYS: a computer program for structural system reliability analysis. *Structural Engineering and Mechanics*, 6 (8), 901–919.

Fisher, J.W., Kulak, G.L., and Smith, I.F., 1998. *A fatigue primer for structural engineers.* Chicago, IL: National Steel Bridge Alliance.

Frangopol, D.M., Strauss, A., and Kim, S., 2008. Bridge reliability assessment based on monitoring. *Journal of Bridge Engineering (ASCE)*, 13 (3), 258–270.

Glen, I.F., Paterson, R.B., and Luznik, L., 1999. *Sea operational profiles for structural reliability assessment.* Washington, DC, Ship Structure Committee, Report No. SSC-406.

Hess, P.E. III, 2007. Structural health monitoring for high-speed naval ships. *Proceedings of the 6th International Workshop on Structural Health Monitoring,* Inc., Lancaster, PA: DEStech Publications (keynote paper).

Hildstrom, G.A., 2007. *JHSV analysis engine.* West Bethesda, MD: NSWCCD-65-TR-2006/15, Naval Surface Warfare Center, Carderock Division.

Kaplan, P., Sargent, T.P., and Cilmi, J., 1974. *Theoretical estimates of wave loads on the SL-7 container ship in regular and irregular seas.* Washington, DC, Ship Structure Committee, Report No. SSC-246.

Lin, W.M. and Yue, D.K.P., 1990. Numerical solutions for large-amplitude ship motions in the time-domain. *Proceedings of the 18th Symposium Naval Hydrodynamics*, 20–22 August, University of Michigan, Ann Arbor, MI. Washington, DC: National Academy Press, 41–66.

Mansour, A.E., *et al.*, 1996. *Probability-based ship design: implementation of design guidelines.* Washington, DC, Ship Structure Committee, Report No. SSC-392.

Michaelson, R.W., 2000. *User's guide for SPECTRA: Version 8.3.* West Bethesda, MD: Naval Surface Warfare Center, Carderock Division, NSWCCD-65-TR-2000/07.

Miner, M.A., 1945. Cumulative damage in fatigue. *Journal of Applied Mechanics*, 12 (3), 159–164.

Okasha, N.M., Frangopol, D.M., and Decò, A., 2010a. Integration of structural health monitoring in life-cycle performance assessment of ship structures under uncertainty. *Marine Structures*, 23 (3), 303–321.

Okasha, N.M., *et al.*, 2010b. Reliability analysis and damage detection in high-speed naval craft based on structural health monitoring data. *Structural Health Monitoring.* doi: 10.1177/1475921710379516.

Paik, J.K. and Frieze, P.A., 2001. Ship structural safety and reliability. *Progress in Structural Engineering and Materials*, 3 (2), 198–210.

Palmgren, A., 1924. The service life of ball bearings. *Zeitschrift des Vereines Deutscher Ingenieure*, 68 (14), 339–341.

Pedersen, P.T. and Jensen, J.J., 2009. Estimation of hull girder vertical bending moments including non-linear and flexibility effects using closed form expressions. *Proccedings of IMechE*, 223 (3), 377–390.

Salvino, L.W. and Brady, T.F., 2008. Hull monitoring system development using a hierarchical framework for data and information management. *In*: *Proceedings of the 7th International Conference on Computer and IT Applications in the Maritime Industries (COMPIT'08)*, 21–23 April, Liège, Belgium, 589–602.

Sikora, J.P., Dinsenbacher, A., and Beach, J.E., 1983. A method for estimating lifetime loads and fatigue lives for swath and conventional monohull ships. *Naval Engineers Journal*, 95 (3), 63–85.

Wirsching, P.H., 1984. Fatigue reliability for offshore structures. *Journal of Structural Engineering (ASCE)*, 110 (10), 2340–2356.

Wu, M.K. and Moan, T., 2006. Numerical prediction of wave-induced long-term extreme load effects in a flexible high-speed pentamaran. *Journal of Marine Science and Technology*, 11 (1), 39–51.

Appendix VI

Sunyong Kim and Dan M. Frangopol. Optimum inspection planning for minimizing fatigue damage detection delay of ship hull structures. *International Journal of Fatigue*, 33(3):448–459, 2011.

International Journal of Fatigue 33 (2011) 448–459

Contents lists available at ScienceDirect

International Journal of Fatigue

journal homepage: www.elsevier.com/locate/ijfatigue

Optimum inspection planning for minimizing fatigue damage detection delay of ship hull structures

Sunyong Kim, Dan M. Frangopol *

Dept. of Civil and Environmental Engineering, ATLSS Engineering Research Center, Lehigh Univ., 117 ATLSS Dr., Bethlehem, PA 18015-4729, USA

ARTICLE INFO

Article history:
Received 27 January 2010
Received in revised form 21 September 2010
Accepted 30 September 2010
Available online 25 October 2010

Keywords:
Fatigue damage
Ship structure
Probabilistic optimization
Inspection planning
Damage detection

ABSTRACT

Fatigue is one of the main factors which can produce cracks, and lead to failure of ships. For these structures, damage occurrence and propagation due to fatigue are affected by the action of sea water waves and the sea environment as well as operation, fabrication, and modeling of ship structures under uncertainties. In order to efficiently maintain the safety of ship structures, an optimum inspection plan should be made by considering these uncertainties using a probabilistic approach. In this paper, such an approach is presented and applied to ship hull structures subjected to fatigue. The resulting inspection plan is the solution of an optimization problem based on the minimization of expected fatigue damage detection delay. Damage detection delay will produce the maintenance delay which, in turn, is likely to endanger the serviceability and even the survival of the structure. The formulation of the expected damage detection delay includes uncertainties associated with damage occurrence, propagation, and detection. The effects of the quality and number of inspections on the optimum inspection planning are investigated. A well-balanced inspection planning is considered as a solution of an optimization problem with two conflicting criteria. This well-balanced inspection planning provides optimum inspection types and times. Furthermore, the cost-effective inspection plans are designed to provide the optimum strategy either by considering a single type or multiple types of inspections.

1. Introduction

The deterioration of a ship structure over its service life can be the result of fatigue induced by various loadings. The fatigue can develop into crack, and lead to unexpected failure or out-of-service of the ship structure. This problem is one of the major threats to the structural integrity of deteriorating ship structures [1]. Due to both aleatory and epistemic uncertainties associated with the action of sea water waves and the sea environment as well as operation, fabrication, and modeling of ship structures, a probabilistic approach has to be applied to assess and predict their fatigue performance [18,19,27,28,3]. Such an approach can provide cost-effective inspection maintenance strategies for structure managers to maintain or extend the service life of ship structures. Approaches for reliability-based optimum inspection and maintenance planning of ship structures were proposed by Madsen and Sørensen [18], Madsen et al. [19], and Garbatov and Soares [12], among others.

Maintenance actions generally depend on the inspection quality [23,10,11,21]. Ship inspections can lead to effective and timely maintenance actions. If the inspection reveals that cracking due to fatigue is present, an appropriate repair should be applied [9]. However, if damage is not detected, repair will not be applied on time. Damage detection delay will produce maintenance delay which, in turn, is likely to endanger the serviceability and even the survival of the structure. The damage detection delay is caused by the uncertainties related to an inspection method and time of damage occurrence. Therefore, a probabilistic approach considering these uncertainties in a rational way should be used to establish a cost-effective inspection planning associated with minimum damage detection delay. Probabilistic inspection and monitoring planning for reinforced concrete structures based on corrosion damage detection delay was studied in Kim and Frangopol [16].

In this study, a probabilistic approach to establish the cost-effective inspection planning is presented and applied to ship hull structures subjected to fatigue. The optimum inspection plan is based on the minimization of expected fatigue damage detection delay. The formulation of the expected fatigue damage detection delay includes uncertainties associated with damage occurrence time and probability of damage detection. The probability of detection is expressed by the damage intensity in terms of time-dependent crack size under uncertainty. The effects of probability of detection and number of inspections on expected damage

* Corresponding author.
E-mail addresses: suk206@lehigh.edu (S. Kim), dan.frangopol@lehigh.edu (D.M. Frangopol).

0142-1123/$ - see front matter © 2010 Elsevier Ltd. All rights reserved.
doi:10.1016/j.ijfatigue.2010.09.018

detection delay are investigated. Increasing the number of inspections and/or probability of detection require additional cost, while the expected damage detection delay is reduced. A well-balanced inspection planning is considered as a solution of a bi-objective optimization problem with two conflicting criteria associated with the minimization of both expected damage detection delay and total inspection cost. The inspection cost is estimated considering quality of an inspection method. This well-balanced inspection planning provides optimum inspection types and times. Furthermore, the cost-effective inspection plans are provided considering same type or different types of inspections.

2. Prediction of crack length

Fatigue is the process of initiation and growth of cracks under repetitive loads; the crack may be pre-existing from fabrication, and be initiated by fatigue and/or corrosion [9]. The crack growth can be affected by the location and length of initial crack, stress range near the initial crack, number of cycles associated with the stress range, material and geometric properties of a structure with crack damage [9]. All these factors have complex relation to each other. Due to this complexity of the fatigue fracture process, it is difficult to predict crack length accurately. So far several empirical and phenomenological-based crack propagation models have been proposed to predict fatigue life [8,26,22]. In order to predict crack length, Paris' equation based on linear elastic fracture mechanics has been generally used. The ratio of the crack length increment to stress cycle increment is described by the following equation [25]

$$\frac{da}{dN} = C(\Delta K)^m \quad \text{for } \Delta K > \Delta K_{thr} \tag{1}$$

where a is the crack length; N is the number of cycles; ΔK is the stress intensity factor; and ΔK_{thr} is the threshold of stress intensity factor. C and m are material parameters. The stress intensity factor ΔK is [15]

$$\Delta K = S \cdot Y(a)\sqrt{\pi a} \tag{2}$$

where S is the stress range, and $Y(a)$ is the geometry function. If the geometry function is constant (i.e., $Y(a) = Y$) and the stress intensity factor ΔK is larger than ΔK_{thr}, the crack length after N cycles $a(N)$ can be obtained by integrating Eq. (1) [17]

$$a(N) = \left[a_o^{(2-m)/2} + \left(\frac{2-m}{2}\right) \cdot C \cdot S^m \cdot Y^m \cdot \pi^{m/2} \cdot N\right]^{\left(\frac{2}{2-m}\right)} \quad \text{for } m \neq 2 \tag{3a}$$

$$a(N) = a_o \cdot \exp[C \cdot S^m \cdot Y^m \cdot \pi \cdot N] \quad \text{for } m = 2 \tag{3b}$$

where a_0 is the initial crack length when $N = 0$. When the annual number of cycles N_{an} is constant over time t (years), the total number of cycles N after t years is $t \times N_{an}$. The time t to crack propagation from the initial crack length a_0 to the crack length a_t can be obtained as [27,28]

$$t = \frac{a_t^{(2-m)/2} - a_o^{(2-m)/2}}{\left(\frac{2-m}{2}\right) \cdot C \cdot S^m \cdot Y^m \cdot \pi^{m/2} \cdot N_{an}} \quad \text{for } m \neq 2 \tag{4a}$$

$$t = \frac{ln(a_t) - ln(a_o)}{C \cdot S^m \cdot Y^m \cdot \pi \cdot N_{an}} \quad \text{for } m = 2 \tag{4b}$$

3. Probability of damage detection

Inspection methods to detect and measure cracks in steel member include ultrasonic inspection, magnetic particle inspection, penetrant inspection, radiographic inspection, acoustic emission inspection, and visual inspection [9,5]. Results from these inspection methods include significant uncertainties [23,10] related to damage occurrence and the imperfection of an inspection method, among others. In order to detect damage on time, the uncertainties associated with both prediction of damage occurrence/propagation and quality of inspection should be treated in a rational way.

The inspection quality is related to the probability that a given degree of damage is detected [19]. The probability of damage detection depends on the degree of damage intensity (i.e., crack length or defect size) and quality of inspection. Packman et al. [24], Berens and Hovey [4], Madsen et al. [19], Mori and Ellingwood [23], and Chung et al. [5] investigated the relation between probability of detection and crack length or defect size. The representative forms of this relation include a shifted exponential form, logistic curve form, and normal cumulative distribution function (CDF) form. In this study, the normal CDF form based on damage intensity is used. The value of damage intensity ranges from zero (i.e., no damage) to one (i.e., full damage) [10]. The damage intensity function $\delta(t)$ at time t in terms of crack length a_t can be expressed as

$$\delta(t) = 0 \quad \text{for } a_t < a_{\min} \tag{5a}$$

$$\delta(t) = \frac{a_t - a_{\min}}{a_{\max} - a_{\min}} \quad \text{for } a_{\min} \leqslant a_t < a_{\max} \tag{5b}$$

$$\delta(t) = 1 \quad \text{for } a_{\max} \leqslant a_t \tag{5c}$$

where a_t is the crack length at time t. $a_{\min}$ and $a_{\max}$ are the minimum and maximum crack length for damage intensity $\delta(t)$, respectively. When the crack length a_t is less than $a_{\min}$, the damage intensity $\delta(t)$ is zero. Conversely, if the crack length a_t is equal to or larger than $a_{\max}$, the damage intensity is one; in this case the cracked component will lose its structural capacity.

The probability of detection P_d for given damage intensity $\delta(t)$ is estimated as [10]

$$P_d = \Phi\left(\frac{\delta(t) - \delta_{0.5}}{\sigma_\delta}\right) \tag{6}$$

where $\Phi(\cdot)$ is the standard normal CDF; $\delta_{0.5}$ is the damage intensity at which the inspection method has a probability of detection of 0.5; and σ_δ is the standard deviation of the damage intensity. In this study, σ_δ is assumed $0.1\delta_{0.5}$. In Eq. (6), the quality of inspection is characterized by $\delta_{0.5}$. An inspection method with a larger value of $\delta_{0.5}$ has a lower

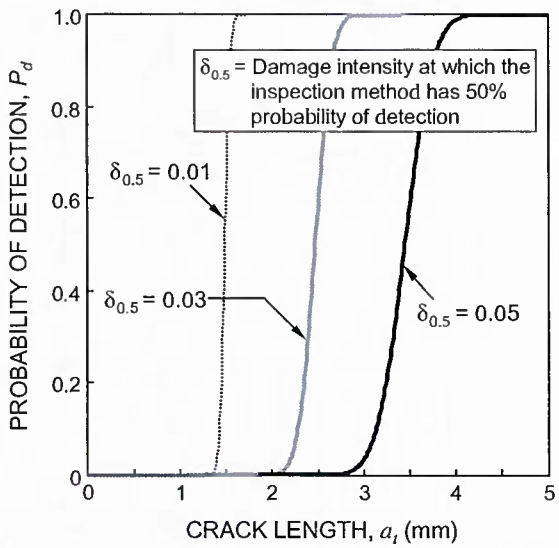

Fig. 1. Relation between probability of detection and crack length for $\delta_{0.5} = 0.01$, $\delta_{0.5} = 0.03$, and $\delta_{0.5} = 0.05$.

probability of detection (i.e., lower quality of inspection). For example, in case the minimum and maximum crack lengths for damage intensity are 1 mm and 50 mm, respectively (i.e., $a_{min} = 1$ mm, and $a_{max} = 50$ mm), the relations between the crack length a_t and probability of detection P_d for three inspections with $\delta_{0.5} = 0.01$, 0.03, and 0.05 are shown in Fig. 1. For the inspection method with $\delta_{0.5} = 0.05$, the probability of detection is 0.5 when the damage intensity $\delta(t)$ is 0.05, and the associated crack length can be obtained as 3.45 mm, using Eq. (5); the crack length associated with probability of detection 0.999 is 4.21 mm as shown in Fig. 1. If the inspection method with $\delta_{0.5} = 0.01$ is used to detect the damage, the probability of damage detection will be 0.999, when the crack length is 1.64 mm.

4. Damage detection delay

Damage detection delay can be defined as the time-lapse from the damage occurrence to the time for the damage to be detected by inspection [14]. If the damage has occurred at time t, and is detected at time t_d, then the damage detection delay t_{del} is expressed by

$$t_{del} = t_d - t \quad \text{for } t_d > t \tag{7}$$

t_d depends on the probability of damage detection and number of inspections. In order to formulate the damage detection delay considering probability of damage detection and number of inspections, an event tree model can be used. This model represents all the possible events having a particular consequence. There is a chance node associated with detection and no detection at every inspection. For instance, assuming that damage occurs in the time interval t_s–t_e and three inspections to detect damage are used, formulation of damage detection delay is based on the four cases according to damage occurrence time t as follows (see Fig. 2a): (a) case 1: $t_s \leqslant t < t_{d,1}$; (b) case 2: $t_{d,1} \leqslant t < t_{d,2}$; (c) case 3: $t_{d,2} \leqslant t < t_{d,3}$; and (d) case 4: $t_{d,3} \leqslant t \leqslant t_e$, where t_s and t_e are the times representing the lower and upper bounds of damage occurrence, respectively, and $t_{d,i}$ is ith inspection time. Fig. 2b and c illustrate event tree and damage detection delay associated with case 2. The gray rectangular node in Fig. 2b indicates a chance node at every inspection where there are two events (i.e., detection and no detection). For case 2 (see Fig. 2b), there are three branches. Branch 1 represents the event of damage detection at the second inspection. The associated probability and damage detection delay are $P_{d,2}$ and $t_{d,2} - t$, respectively, as shown in Fig. 2b and c. If the damage is not detected until the third inspection, and is detected at time $t_{d,e}$, the associated

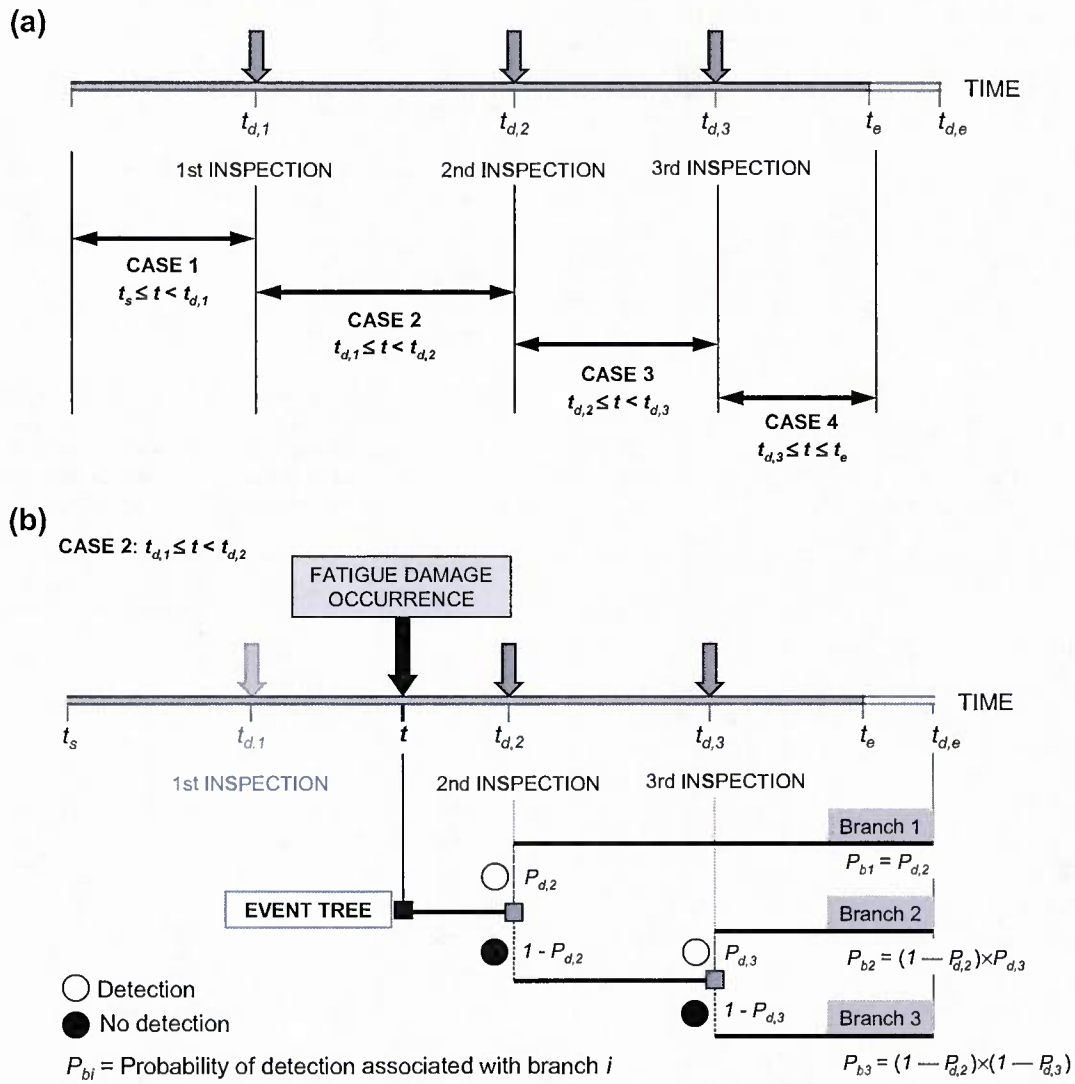

Fig. 2. (a) Four possible cases for number of inspections $n = 3$; (b) event tree model for case 2: $t_{d,1} \leqslant t < t_{d,2}$; (c) damage detection delay of each branch in (b); and (d) PDF of fatigue damage occurrence.

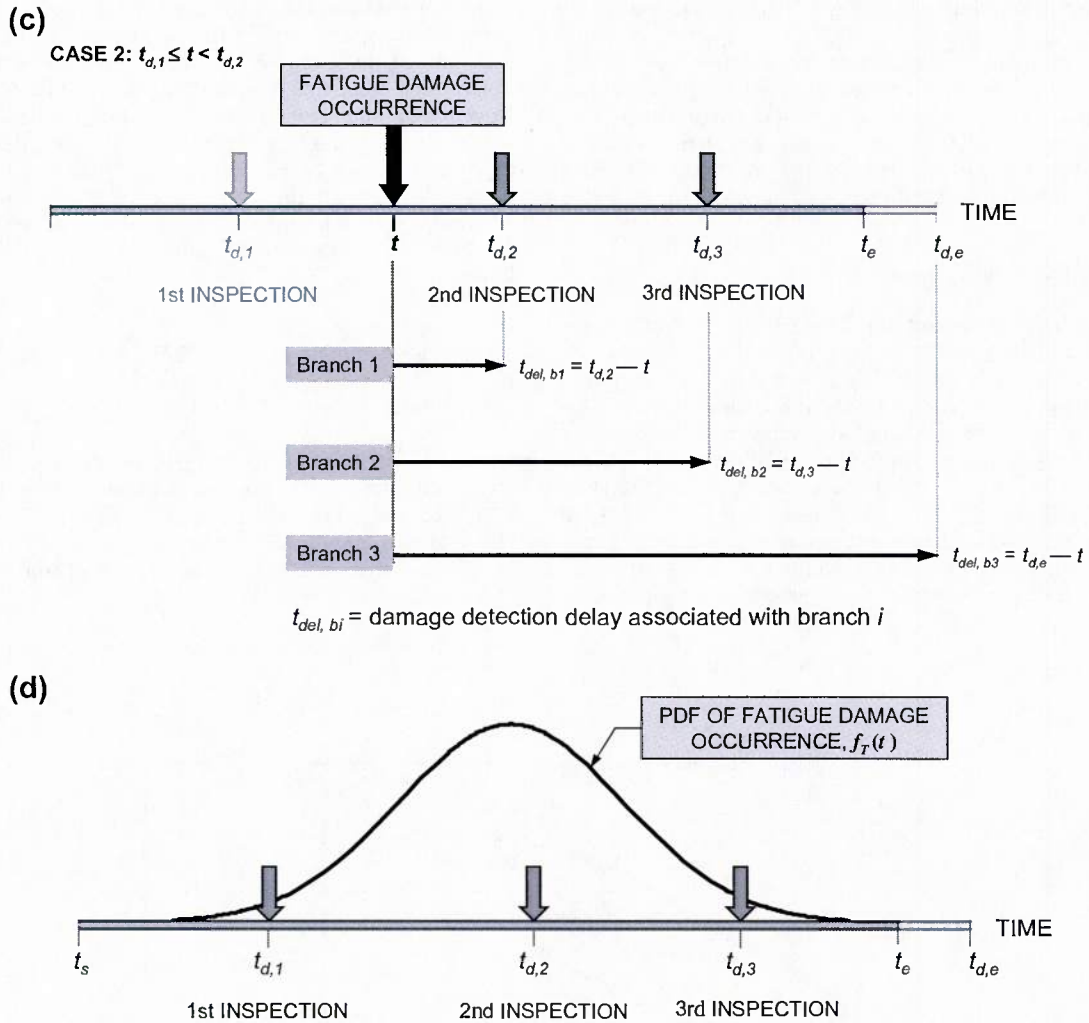

Fig. 2 (*continued*)

probability and damage detection delay will be $(1-P_{d,2})\times(1-P_{d,3})$ and $t_{d,e}-t$, respectively (see branch 3 in Fig. 2b and c). Therefore, considering the damage detection delays and their probabilities associated with all possible branches, the expected damage detection delays for cases 1, 2, 3, and 4 are

$$E(t_{del})_{case,1} = (t_{d,1}-t)\cdot P_{d,1} + (t_{d,2}-t)[(1-P_{d,1})\cdot P_{d,2}] + (t_{d,3}-t)[(1-P_{d,1})(1-P_{d,2})\cdot P_{d,3}] + (t_{d,e}-t)[(1-P_{d,1})(1-P_{d,2})(1-P_{d,3})] \quad \text{for } t_s \leqslant t < t_{d,1} \tag{8a}$$

$$E(t_{del})_{case,2} = (t_{d,2}-t)\cdot P_{d,2} + (t_{d,3}-t)[(1-P_{d,2})\cdot P_{d,3}] + (t_{d,e}-t)[(1-P_{d,2})(1-P_{d,3})] \quad \text{for } t_{d,1} \leqslant t < t_{d,2} \tag{8b}$$

$$E(t_{del})_{case,3} = (t_{d,3}-t)\cdot P_{d,3} + (t_{d,e}-t)(1-P_{d,3}) \quad \text{for } t_{d,2} \leqslant t < t_{d,3} \tag{8c}$$

$$E(t_{del})_{case,4} = (t_{d,e}-t) \quad \text{for } t_{d,3} \leqslant t \leqslant t_e \tag{8d}$$

In Eq. (8), the expected damage detection delay for case i is denoted as $E(t_{del})_{case,i}$.

When the time t for damage to occur is a continuous random variable described by the probability density function (PDF) $f_T(t)$ as shown in Fig. 2d, the expected damage detection delay $E(t_{del})$ of Eq. (8) for n inspections is

$$E(t_{del}) = \sum_{i=1}^{n+1}\left\{\int_{t_{d,i-1}}^{t_{d,i}} [E(t_{del})_{case,i}\cdot f_T(t)]dt\right\} \tag{9}$$

where $E(t_{del})_{case,i}$ is the expected damage detection delay when $t_{d,i-1} \leqslant t < t_{d,i}$. The time $t_{d,0}$ for $i=1$ and $t_{d,n+1}$ for $i=n+1$ in Eq. (9) are t_s and t_e respectively. Based on the PDF of damage occurrence time $f_T(t)$, t_s and t_e, are defined as [16]

$$t_s = F_T^{-1}(\Phi(-u)) \tag{10a}$$

$$t_e = F_T^{-1}(\Phi(u)) \tag{10b}$$

where $F_T^{-1}(\cdot)$ is the inverse CDF of the damage occurrence time t, and $u>0$. If, for example, the time t for damage to occur is assumed log-normally distributed with the mean of 10 years and the standard deviation of 2 years, and u is assumed to be 3.0, t_s and t_e are 5.41 and 17.76 years, respectively, using Eq. (10). The probability that the damage will occur before 5.41 and 17.76 years is 0.0013 and 0.9987, respectively. The value of u is fixed at 3.0 herein.

5. Application to ship hull structures subjected to fatigue

The proposed approach is applied to ship hull as shown in Fig. 3. In this study, the joint between bottom plate and longitudinal plate is considered as a critical location subjected to fatigue. Under longitudinal loading and unloading, the crack in the plate can initiate on the edge connected to the stiffener and propagate away from the stiffener in the transverse direction as shown in Fig. 3.

5.1. Time-dependent crack growth

Crack length over time and time to reach a given crack length are calculated using Eqs. (3) and (4), respectively. Initial crack length a_0, annual stress cycles N_{an}, and material crack growth parameter C are assumed lognormally distributed random variables. The stress range S is treated as a random variable with a Weibull PDF [19]. The mean value of material parameter C is assumed to be 3.54×10^{-11}, and m is assumed 2.54 for high yield steel (HY80) [7]. Descriptors of variables in Eqs. (3) and (4) are given in Table 1. In this study, the geometry function Y is assumed to be one [1,19]. Monte Carlo simulation with sample size of 100,000 is used to predict the crack length over time. Fig. 4a shows the mean and standard deviation of time t associated with crack length a_t, and PDFs of time for $a_t = 10$, 20, 30, and 40 mm. From this figure, it can be seen that the crack length increases at a very high rate after reaching 1.0 mm. In this study, the crack length of 1.0 mm serves as the crack damage criterion. Therefore, a_{min} in Eq. (5) is 1.0 mm. The maximum crack length a_{max} in Eq. (5) is assumed to be 50 mm. Fig. 4b shows the PDF of fatigue damage occurrence time (i.e., time for crack length to reach 1.0 mm) obtained from Monte Carlo simulation and the best fitted PDF (i.e., Generalized Extreme Value (GEV) PDF). The GEV PDF is

$$f_T(t) = \frac{1}{\beta}\left(1+\alpha\frac{(x-\zeta)}{\beta}\right)^{-1/\alpha-1} \cdot \exp\left[-\left(1+\alpha\frac{(x-\zeta)}{\beta}\right)^{-1/\alpha}\right] \quad 1+\alpha(x-\zeta)/\beta > 0 \tag{11}$$

where α is the shape parameter; β is the scale parameter; and ζ is the location parameter. The values of parameters α, β and ζ are 0.15, 1.65 and 3.21, respectively, as shown in Fig. 4b. This GEV PDF is used to formulate the expected damage detection delay in Eq. (9). Based on this PDF, t_s and t_e are obtained as 0.51 and 21.95 years, respectively (see Eq. (10)).

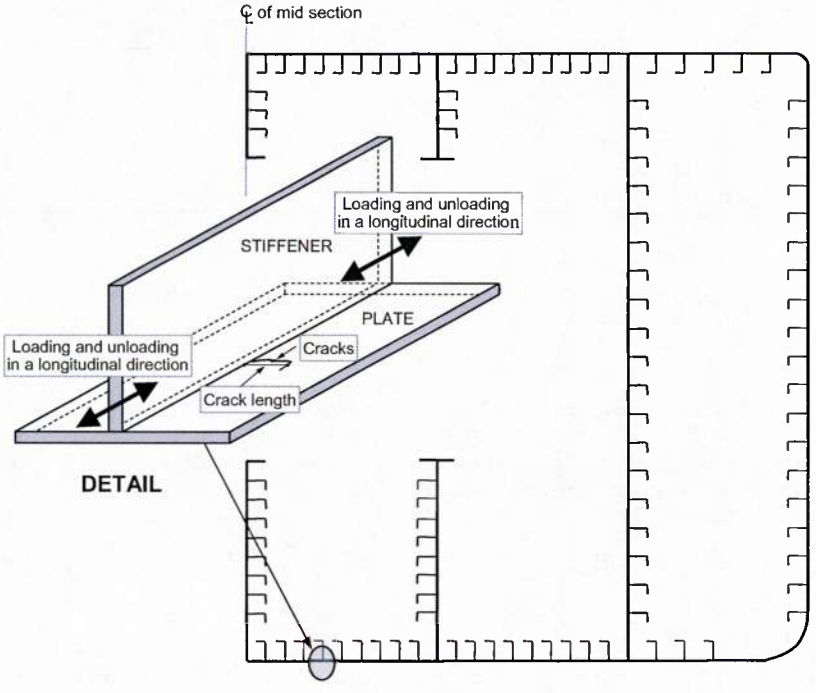

Fig. 3. Schematic representation of the mid-ship section of a ship and the assumed location of cracks.

Table 1
Variables for crack growth model.

Random variables	Notation	Units	Mean	[a]COV	Type of distribution
Initial crack size	o_o	mm (in)	0.5 (0.02)	0.2	Lognormal
Annual number of cycles	N_{an}	Cycles/year	0.8×10^6	0.2	Lognormal
Stress range	S	MPa (ksi)	40 (5.81)	0.1	Weibull
Material crack growth parameter	C		3.54×10^{-11} (1.77×10^{-9})[b]	0.3	Lognormal

[a] COV: coefficient of variation.
[b] 1.77×10^{-9}: material parameter for do/dN and ΔK in units of *in/cycles* and *ksi* $\sqrt{in}$, respectively (see Eqs. (1) and (2)).

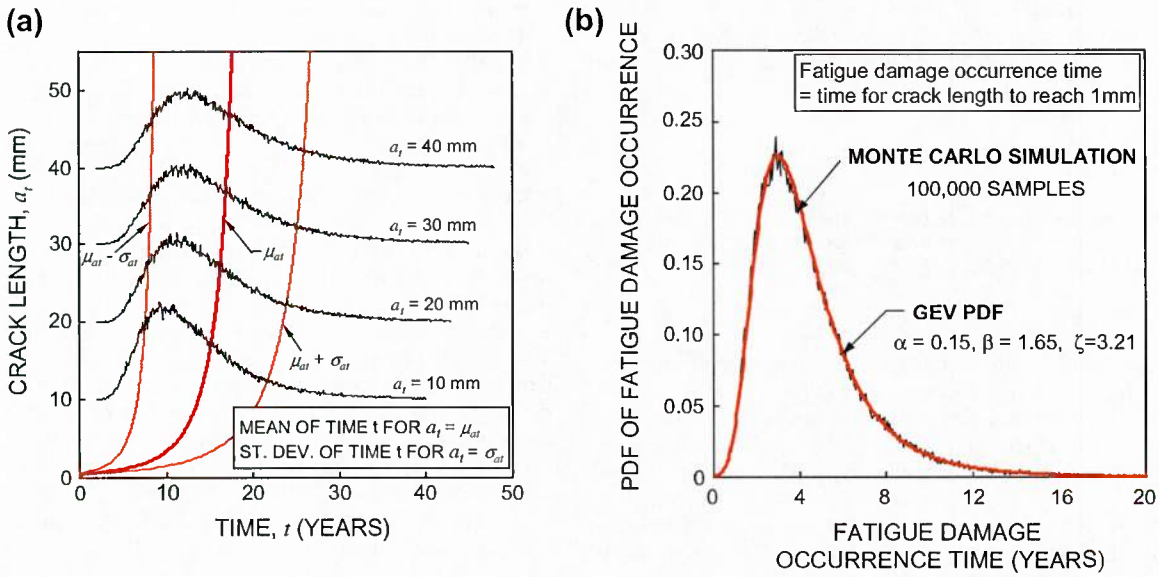

Fig. 4. (a) Time-dependent crack length with PDFs of times when a_t = 10 mm, 20 mm, 30 mm, and 40 mm; (b) GEV PDF of fatigue damage occurrence time.

5.2. Optimum inspection plans to minimize the expected damage detection delay

The type of maintenance/repair generally depends on the outcome of inspection [23,10,11,21]. The type of fatigue repair can be determined according to the results of inspection such as degree of crack damage and estimated cause of crack [9]. Therefore, in order to apply a timely and appropriate maintenance/repair action to a deteriorating structure, the damage should be detected with minimum delay [16].

After fatigue damage has occurred, the crack length grows so that the probability of detection will increase. Therefore, as the damage detection delay increases, the probability of detection increases. Since the variables associated with the crack growth model are not deterministic, the probability of detection in terms of crack length a_t at time t is random. In order to formulate the expected damage detection delay $E(t_{del})$ in Eq. (9), the expected probability of detection using Eq. (6) is applied herein. Fig. 5 shows the expected probability of detection over time after crack damage occurrence (i.e., time for crack length a_t to reach a_{min}) for three inspections with $\delta_{0.5}$ = 0.01, 0.03, and 0.05. As indicated in Eq. (8) and Fig. 2, $t_{d,e}$ is associated with the time when the damage can be detected with perfect detectability. In this study, $t_{d,e}$ is defined as

$$t_{d,e} = t_e + t_p \tag{12}$$

where t_e is the upper-bound of damage occurrence time as indicated in Eq. 10(b), and t_p is the time interval during which the expected probability of damage detection is at least 0.999. When the inspection method with $\delta_{0.5}$ = 0.01 is used, t_p will be 9.74 years when the damage is detected with the expected probability of detection of 0.999 as shown in Fig. 5. Therefore, $t_{d,e}$ for $\delta_{0.5}$ = 0.01 is 31.69 years, since the upper-bound of damage occurrence time t_e is 21.95 years as mentioned previously.

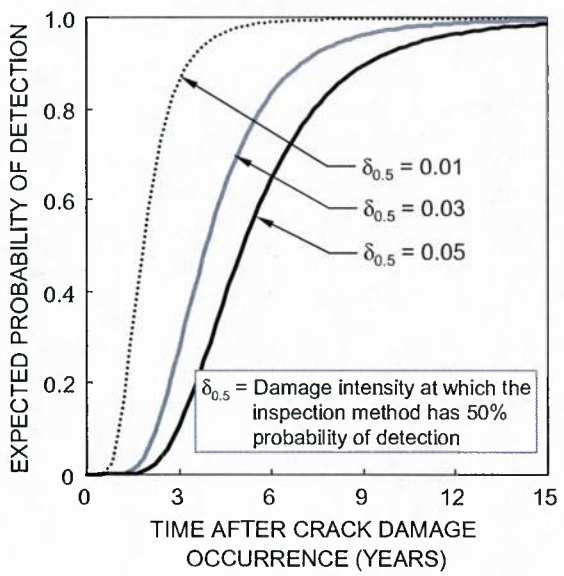

Fig. 5. Expected probability of detection versus time after crack damage occurrence for $\delta_{0.5}$ = 0.01, $\delta_{0.5}$ = 0.03, and $\delta_{0.5}$ = 0.05.

In this study, inspection planning is formulated as an optimization problem by minimizing the expected damage detection delay $E(t_{del})$ in Eq. (9) with given number n of inspections as follows:

$$\text{Find} \quad \mathbf{t_d} = \{t_{d,1}, t_{d,2}, \ldots, t_{d,i}, \ldots, t_{d,n}\} \tag{13}$$

$$\text{to minimize} \quad E(t_{del}) \tag{14}$$

$$\text{such that} \quad t_{d,i} - t_{d,i-1} \geqslant 1 \text{ year} \tag{15}$$

$$\text{given} \quad n, \delta_{0.5}, f_T(t) \tag{16}$$

where $\mathbf{t_d}$ is the vector consisting of n design variables of inspection times $t_{d,1}, \ldots, t_{d,n}$; $t_{d,i}$ is the ith inspection time (years); and $\delta_{0.5}$ is the damage intensity at which the given inspection method has 50% probability of detection. The objective is to minimize the expected time delay $E(t_{del})$ from the crack damage initiation to time for the crack to be detected by inspections. The time interval between inspections is assumed to be at least one year (see Eq. (15)). The times $t_{d,0}$ (for i = 1) and $t_{d,n+1}$ (for i = n + 1) are t_s and t_e respectively, as indicated in Eq. (9). The number of inspections, $\delta_{0.5}$ representing the quality of inspection, and PDF of the damage occurrence time $f_T(t)$ in Fig. 4b are given (see Eq. (16)). The optimization toolbox (i.e., constrained nonlinear minimization) provided in MATLAB® version R2009a [20] was used to solve this problem.

Fig. 6 shows the effects of (a) number of inspections and (b) total inspection costs on minimum expected damage detection delay $E(t_{del})$ for $\delta_{0.5} = 0.01$, $\delta_{0.5} = 0.03$, and $\delta_{0.5} = 0.05$. The total inspection cost C_{Tinsp} is computed as

$$C_{Tinsp} = \sum_{i=1}^{n} \frac{C_{insp}}{(1+r)^{t_{d,i}}} \tag{17}$$

where r is the discount rate of money, and C_{insp} is the cost of an inspection. Considering quality of an inspection method, the cost of an inspection is estimated as [23]

$$C_{insp} = \alpha_{insp}(1 - 0.7\delta_{0.5})^{20} \tag{18}$$

where α_{insp} is 5. It should be noted that the inspection associated with time $t_{d,e}$, when the damage can be detected with perfect detectability, is not accounted in the number of inspections.

The optimal inspection plans associated with the number of inspections $n = 1$, 3, and 5 are shown in Fig. 7. If a single inspection with $\delta_{0.5} = 0.03$ is used to detect fatigue crack damage, the inspection has to be performed at 11.90 years as shown in Fig. 7a. The associated $E(t_{del})$ and C_{Tinsp} are 9.74 years and 3.27, respectively (see Fig. 6). If the number of inspection increases three times (i.e., the number of inspection $n = 3$), the inspections should be applied at 7.66, 10.62, and 16.67 years (see Fig. 7b), and $E(t_{del})$ will be 5.66 years (see Fig. 6a). Furthermore, if three inspections with $\delta_{0.5} = 0.01$ instead of $\delta_{0.5} = 0.03$ are used, $E(t_{del})$ will be reduced by 36% (i.e., from 5.66 to 3.62 years), but the total inspection cost C_{Tinsp} will increase by 33% (i.e., from 9.81 to 13.03), as shown in Fig. 6. The associated optimum inspection times will be 5.64, 8.35, and 13.51 years (see Fig. 7b). From these results, it can be seen that reduction of the minimum $E(t_{del})$ results from increase in the number and/or the quality of inspections. Through comparison among the optimum inspection times associated with $\delta_{0.5} = 0.01$, 0.03 and 0.05, it can also be seen that the inspection with higher quality (i.e., smaller value of $\delta_{0.5}$) has to be applied earlier than the inspection with lower quality (i.e., larger value of $\delta_{0.5}$), in order to minimize $E(t_{del})$.

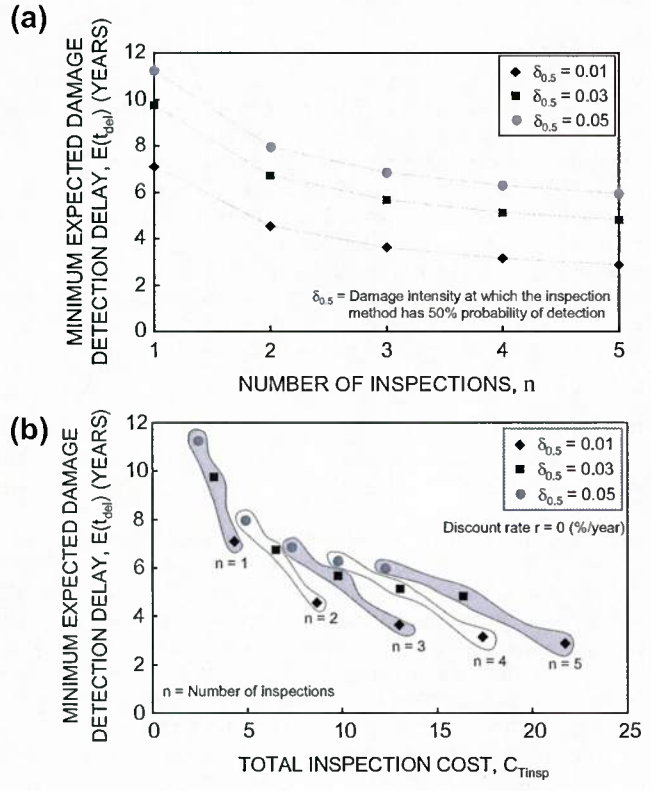

Fig. 6. Effects of (a) number of inspections and (b) total inspection costs on minimum expected damage detection delay for $\delta_{0.5} = 0.01$, $\delta_{0.5} = 0.03$, and $\delta_{0.5} = 0.05$.

5.3. Optimum balance of cost and expected damage detection delay

In order to reduce the expected damage detection delay, it is necessary to increase the number of inspections and/or quality of inspection method. This leads to additional financial resources. Therefore, well-balanced inspection planning should be considered as a solution of a two conflicting criteria optimization problem by simultaneously minimizing both the expected damage detection delay and the total inspection cost. In this paper, optimum balanced inspection planning is obtained, when (a) same type and (b) different types of inspections are used. Non-Dominated Sorting in Genetic Algorithms (NSGA-II) program developed by Deb et al. [6] is used, in order to find the Pareto optimal solution set of this bi-objective optimization problem.

5.3.1. Optimum balance when same type of inspection is applied

When same type of inspection (i.e., constant $\delta_{0.5}$) is applied n-times, the bi-objective optimization problem for inspection planning is formulated as

$$\text{Find} \quad \mathbf{t_d} = \{t_{d,1}, t_{d,2}, \ldots, t_{d,i}, \ldots, t_{d,n}\}, \text{ and } \delta_{0.5} \tag{19}$$

$$\text{to minimize both} \quad E(t_{del}) \text{ and } C_{Tinsp} \tag{20}$$

$$\text{such that} \quad t_{d,i} - t_{d,i-1} \geqslant 1 \text{ year} \tag{21a}$$

$$t_{d,1} \leqslant 20 \text{ years} \tag{21b}$$

$$0.01 \leqslant \delta_{0.5} \leqslant 0.1 \tag{21c}$$

$$\text{given} \quad n, f_T(t) \tag{22}$$

In this bi-objective optimization problem, the objectives are minimization of both the expected damage detection delay $E(t_{del})$ (see Eq. (9)) and the total inspection cost C_{Tinsp} (see Eq. (17)). The design variables are the vector of inspection times $\mathbf{t_d}$, and $\delta_{0.5}$ representing the quality of inspection in Eq. (6). As indicated in Eq. (21), time interval between inspections should be at least one year, and application of the first inspection is required within 20 years. The value of $\delta_{0.5}$ has to be in the interval 0.01–0.1. $f_T(t)$ in Fig. 4b and number of inspections n are given as indicated in Eq. (22).

Through the genetic algorithm (GA) process with 200 generations, a Pareto set of 100 solutions for $n = 1$ is obtained as shown in Fig. 8a. The relations between design variables (i.e., first inspection time $t_{d,1}$ and $\delta_{0.5}$) for solutions A_1–A_5 are also illustrated in Fig. 8a. The expected damage detection delay $E(t_{del})$ of solutions A_1–A_5 decreases from 13.21 to 7.09 years with decrease of both $\delta_{0.5}$ (from 0.1 to 0.01) and $t_{d,1}$ (from 15.27 to 9.35), respectively. Accordingly, the associated total inspection cost C_{Tinsp} increases from 1.17 to 4.35. Fig. 8b shows Pareto optimum solution sets for $n = 1$–5.

In order to find the final Pareto front considering the number of inspections n as a design variable, ε-constraint approach, based on the Pareto solution sets for $n = 1$–5 in Fig. 8b, can be used. In this approach, multi-criteria optimization problem is transformed into a single objective optimization problem by selecting one of the objectives to be minimized and treating other objective functions as constraints [13]. The general formulation of ε-constraint approach is [2]

$$\text{Minimize} \quad f_i \tag{23}$$

$$\text{subject to} \quad f_j \leqslant \varepsilon_j \text{ for all } j = 1, 2, \ldots, k; j \neq i \tag{24}$$

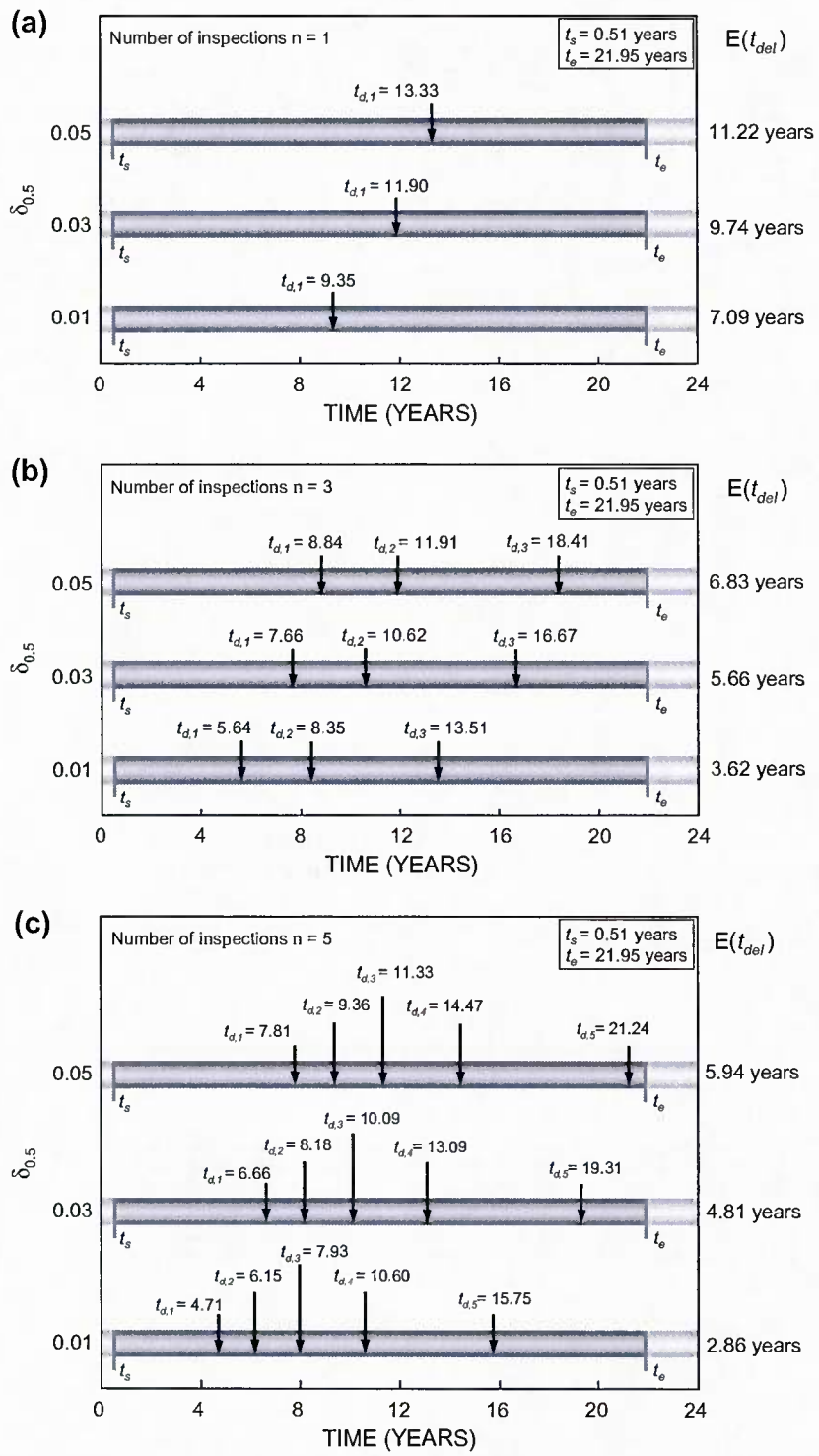

Fig. 7. Optimum inspection plans for number of inspections (a) n = 1; (b) n = 3; (c) n = 5.

where i ∈ {1, 2, ..., k}. The number of objective functions k is equal to 2; $f_i = f_1$ is the expected damage detection delay $E(t_{del})$; and $f_j = f_2$ is the total inspection cost C_{Tinsp}. By changing the value of ε_j from the minimum value of f_2 (i.e., 1.17) to the maximum value of f_2 (i.e., 21.72), the final Pareto front of the Pareto solution sets for n = 1–5 in Fig. 8b is obtained as shown in Fig. 8c. The optimum inspection times for solution B_1, B_2, B_4, and B_6 in Fig. 8c are provided in Table 2 and Fig. 8d. For Pareto point B_4 in Fig. 8c, the associated $E(t_{del})$ and C_{Tinsp} are 4.55 years and 8.69, respectively (see Table 2). The inspection plan for solution B_4 requires two inspections with $\delta_{0.5}$ = 0.01 as shown in Fig. 8d. If Pareto solution B_6 instead of solution B_4 is selected as an inspection plan, the number of inspections has to increase twice (i.e., from 2 to 4), C_{Tinsp} should also increase twice, but $E(t_{del})$ will be reduced from 4.55 to 3.15 years (see

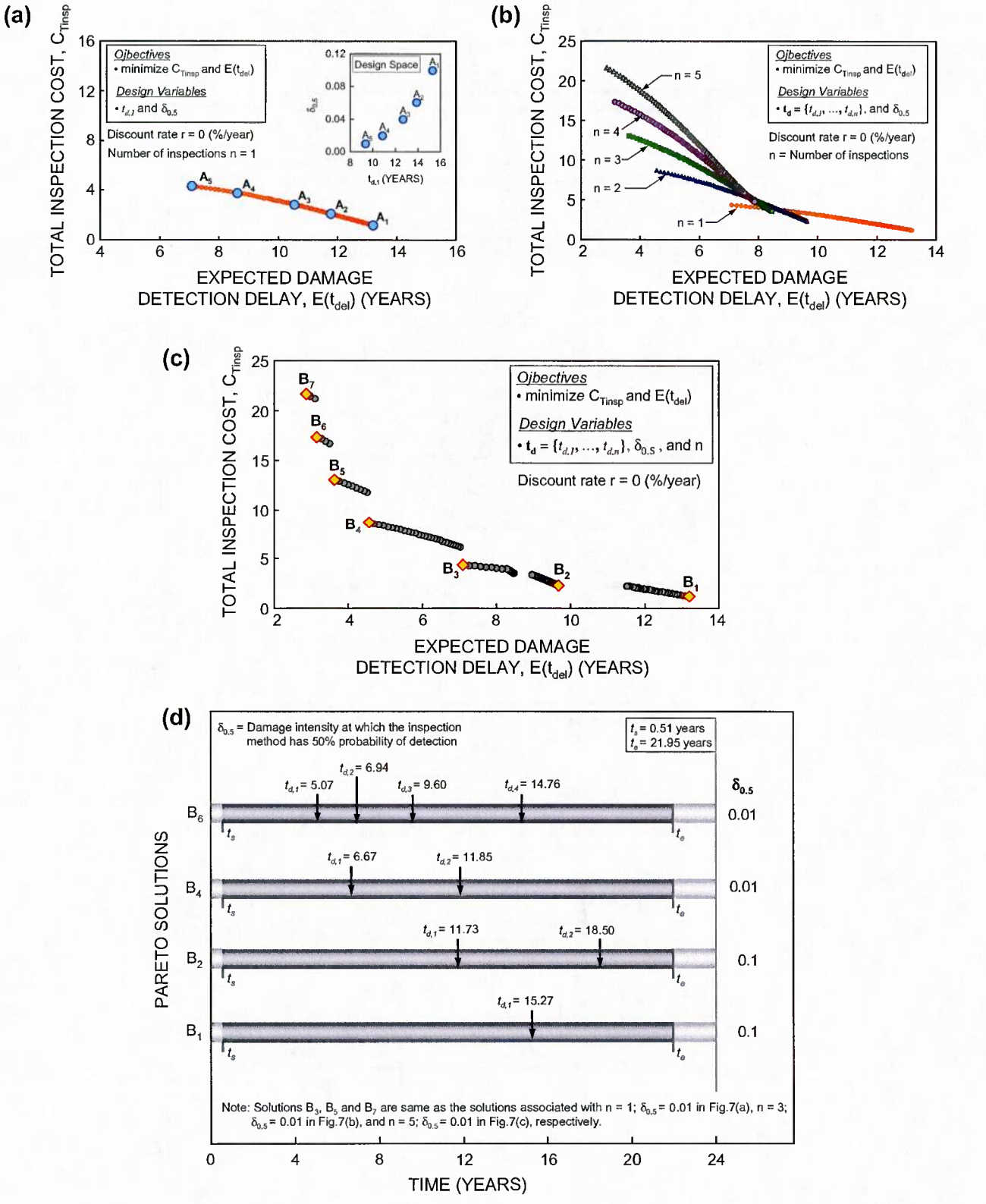

Fig. 8. (a) Pareto solution set and design space of $t_{d,1}$ and $\delta_{0.5}$, for given $n = 1$; (b) Pareto solution sets for design variables t_d and $\delta_{0.5}$, and given $n = 1$–5; (c) final Pareto solution set; and (d) optimum inspection plans for solutions B_1, B_2, B_4, and B_6 in (c).

Table 2). It should be noted that solutions B_3, B_5 and B_7 in Fig. 8c are the same as the solutions associated with $n = 1$; $\delta_{0.5} = 0.01$ in Fig. 7a, $n = 3$; $\delta_{0.5} = 0.01$ in Fig. 7b, and $n = 5$; $\delta_{0.5} = 0.01$ in Fig. 7c, respectively.

Table 2
Design variable and objective function values associated with Pareto optimum solutions in Fig. 8c.

Pareto optimum solution	Objective function values		Design variables						
	Expected damage detection delay, $E(t_{del})$ (years)	Total inspection cost, C_{Tinsp}	Number of inspections, n	Optimum inspection times (years)					$\delta_{0.5}$
				$t_{d,1}$	$t_{d,2}$	$t_{d,3}$	$t_{d,4}$	$t_{d,5}$	
B_1	13.21	1.17	1	15.27	–	–	–	–	0.10
B_2	9.66	2.34	2	11.73	18.50	–	–	–	0.10
B_3	7.09	4.35	1	9.35	–	–	–	–	0.01
B_4	4.55	8.69	2	6.67	11.85	–	–	–	0.01
B_5	3.62	13.03	3	5.64	8.35	13.51	–	–	0.01
B_6	3.15	17.38	4	5.07	6.94	9.60	14.76	–	0.01
B_7	2.86	21.72	5	4.71	6.15	7.93	10.60	15.75	0.01

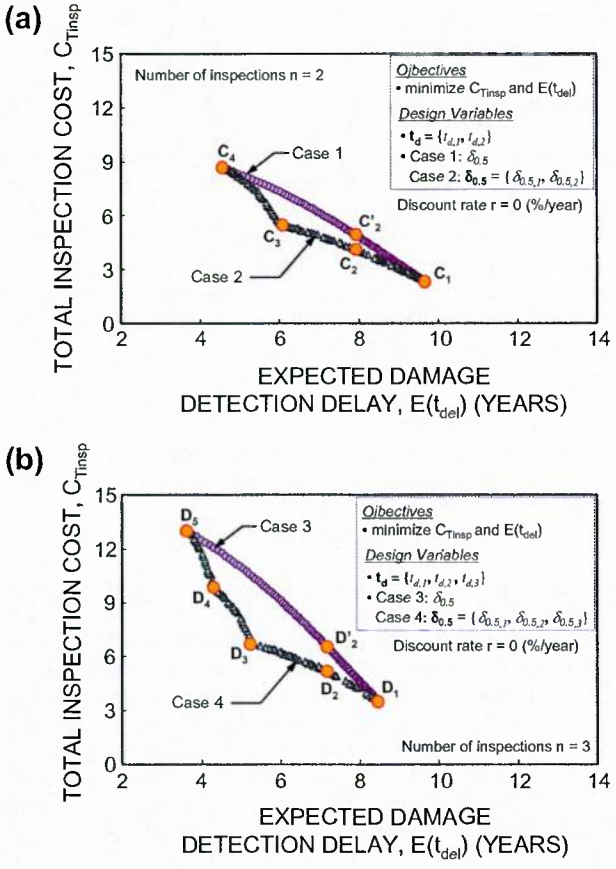

Fig. 9. Comparison between Pareto solution sets based on same type and different types of inspections for number of inspections (a) n = 2; (b) n = 3.

5.3.2. Optimum balance when different inspection types are applied

When different inspection types are applied (*i.e.*, $\delta_{0.5}$ is not the same), the formulation of the bi-objective optimization problem is

$$\text{Find} \quad \mathbf{t_d} = \{t_{d,1}, t_{d,2}, \ldots, t_{d,i}, \ldots, t_{d,n}\}, \text{ and } \boldsymbol{\delta_{0.5}} = \{\delta_{0.5,1}, \delta_{0.5,2}, \ldots, \delta_{0.5,i}, \ldots, \delta_{0.5,n}\} \tag{25}$$

$$\text{to minimize both} \quad E(t_{del}) \text{ and } C_{Tinsp} \tag{26}$$

As indicated, the constraints and given condition of this problem are identical with those in Eqs. (21) and (22). A Pareto set of 100 solutions is obtained after 500 generations. The discount rate of money r in Eq. (17) is assumed to be zero. Fig. 9 shows Pareto solution sets based on both same type (*i.e.*, case 1 in Fig. 9a and case 3 in Fig. 9b) and different types (*i.e.*, case 2 in Fig. 9a and case 4 in Fig. 9b) of inspections. Optimum values of design variables and the associated $E(t_{del})$ and C_{Tinsp} for Pareto solutions in Fig. 9 are provided in Table 3. Solutions C_1, C_4, and D_5 in Fig. 9 are the same as B_2, B_4, and B_5 in Fig. 8c, respectively. As shown in Table 3 and Fig. 9a associated with number of inspections $n = 2$, solutions C_2' of case 1 and C_2 of case 2 have the same $E(t_{del})$ (*i.e.*, 7.92 years), but if solution C_2 instead of C_2' is selected as an inspection plan, the total inspection cost can be reduced by 16% (*i.e.*, from 4.93 to 4.13). Similarly, in Fig. 9b associated with $n = 3$, solutions D_2 (of case 4) and D_2' (of case 3) have the same $E(t_{del})$, but D_2 requires less cost than D_2'. From these comparisons between Pareto solution sets of cases 1 and 2 (or cases 3 and 4), it can be seen that the inspection plan based on different inspection types will require less cost than the inspection plan based on the same type of inspection for given expected damage detection delay. As indicated in Table 3, Pareto solutions C_1 and C_3 have $\delta_{0.5,1} = 0.10$ and 0.01, respectively, while having the same $\delta_{0.5,2} = 0.10$. The values of $\delta_{0.5,1}$ for solutions C_3 and C_4 are the same (i.e., 0.01), but $\delta_{0.5,2}$ for C_3 and C_4 are 0.10 and 0.01, respectively.

Furthermore, the Pareto solution sets of the bi-objective optimization problem for $n = 1$, 4, 5 are obtained. The ε-constraint approach (see Eqs. (23) and (24)) based on Pareto solution sets for

Table 3
Design variable and objective function values associated with Pareto optimum solutions in Fig. 9a and b.

Pareto optimum solution	Objective function values		Design variables						
	Expected damage detection delay, $E(t_{del})$ (years)	Total inspection cost, C_{Tinsp}	Number of inspections, n	Optimum inspection times (years)			$\delta_{0.5}$		
				$t_{d,1}$	$t_{d,2}$	$t_{d,3}$	$\delta_{0.5,1}$	$\delta_{0.5,2}$	$\delta_{0.5,3}$
C_1	9.66	2.34	2	11.73	18.50	–	0.10	0.10	–
C_2	7.92	4.13		9.78	18.80	–	0.37	0.10	–
C_2'	7.92	4.93		10.00	16.34	–	0.05	0.05	–
C_3	6.07	5.49		8.42	19.74	–	0.01	0.10	–
C_4	4.55	8.69		6.67	11.85	–	0.01	0.01	–
D_1	8.46	3.51	3	10.44	13.68	20.70	0.10	0.10	0.10
D_2	7.17	5.17		9.13	14.21	22.32	0.04	0.10	0.10
D_2'	7.17	6.58		9.18	12.28	18.91	0.06	0.06	0.06
D_3	5.24	6.68		8.15	15.40	18.75	0.01	0.10	0.10
D_4	4.32	9.87		6.59	11.13	21.47	0.01	0.01	0.10
D_5	3.62	13.03		5.64	8.35	13.51	0.01	0.01	0.01

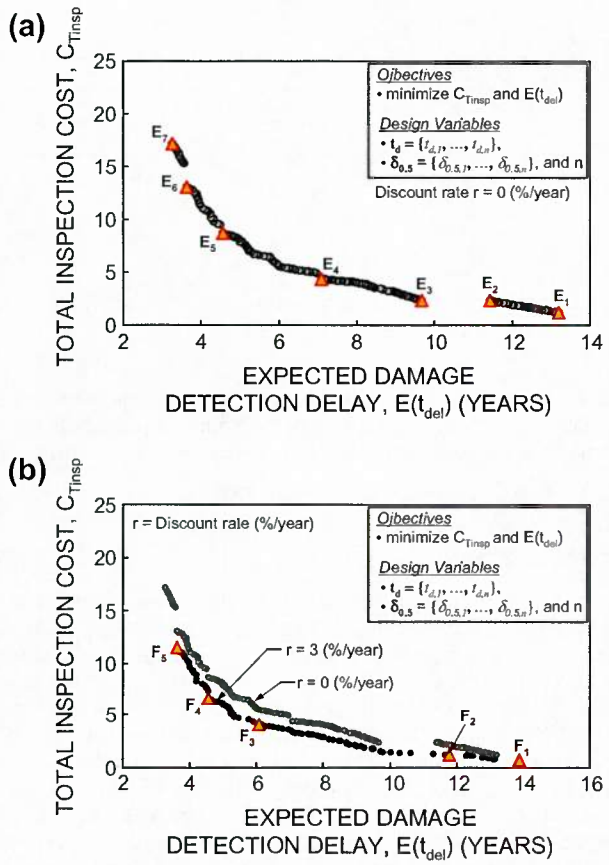

Fig. 10. Pareto solution set of bi-objective optimization problem with design variables t_d, $\delta_{0.5}$, and n (a) without discount rate of money; (b) with discount rate of money $r = 3\%$/year.

$n = 1$–5 provides the final Pareto front as shown Fig. 10a. Values of objective functions and design variables for solutions E_1–E_7 are provided in Table 4. As indicated in this Table, values of objective functions and design variables for solutions E_1, E_3 and E_5 in Fig. 10a are identical to those of solutions B_1, B_2 and B_4 in Fig. 8c, respectively. In the final Pareto front, solution E_1 needs the lowest total inspection cost C_{Tinsp} of 1.17, but leads to the largest expected damage detection delay $E(t_{del})$ of 13.21 years. In contrast, solution E_7 requires the highest inspection cost C_{Tinsp} of 17.38, while results in the least expected damage detection delay $E(t_{del})$ of 3.15 years. It should be noted that there is no solution associated with $n = 5$. When the discount rate of money $r = 3\%$/year for the total inspection cost in Eq. (17) is applied, the final Pareto front is presented in Fig. 10b. Table 4 provides values of objective functions and design variables for solutions F_1–F_5. Solution F_4 in Fig. 10b has the same expected damage detection delay (i.e., $E(t_{del}) = 4.55$ years) as that of solution E_5 in Fig. 10a. However, the total inspection cost C_{Tinsp} associated with solution F_4 is less than that of solution E_5 as indicated in Table 4 and Fig. 10. It can be seen that for given expected damage detection delay, the inspection plan considering discount rate of money requires less cost than that without considering it. Among the final Pareto solution set with $r = 3\%$/year, solution F_5 requires the highest inspection cost C_{Tinsp} of 11.53, leading to the least expected damage detection delay $E(t_{del})$ of 3.63 years.

6. Conclusions

This paper presented an approach for optimum inspection planning of ship hull structures subjected to fatigue. The optimization problem was based on the minimization of expected fatigue damage detection delay. In order to formulate this delay, uncertainties related to inspection method and damage occurrence/propagation were considered. The relation between the inspection cost and the expected damage detection delay was investigated. A well-balanced inspection plan was considered as the solution of a bi-objective optimization problem by simultaneously minimizing both the expected damage detection delay and the total inspection cost. A comparison of the cost-effective inspection plans based on same type and different types of inspections was carried out. The effect of the discount rate of money on the inspection plans was also studied.

The following conclusions can be drawn:

1. Increase in the number of inspections and/or inspection quality can lead to reduction of the expected damage detection delay. However, this increase requires additional financial resources. Therefore, in order to establish cost-effective inspection planning, an optimization problem based on minimization of both expected damage detection delay and inspection cost has to be solved. The result of this optimization provides the Pareto solution set. Based on this set, structure managers can select the appropriate inspection planning considering also the importance of the structural component or system inspected.

Table 4
Design variable and objective function values associated with Pareto optimum solutions in Fig. 10.

Pareto optimum solution	Objective function values		Design variables							
	Expected damage detection delay, $E(t_{del})$ (years)	Total inspection cost, C_{Tinsp}	Number of inspections, n	Optimum inspection times (years)				$\delta_{0.5}$			
				$t_{d,1}$	$t_{d,2}$	$t_{d,3}$	$t_{d,4}$	$\delta_{0.5,1}$	$\delta_{0.5,2}$	$\delta_{0.5,3}$	$\delta_{0.5,4}$
E_1	13.21	1.17	1	15.27	–	–	–	0.10	–	–	–
E_2	11.22	2.34	1	13.33	–	–	–	0.05	–	–	–
E_3	9.66	2.34	2	11.73	18.50	–	–	0.10	0.10	–	–
E_4	7.09	4.35	1	9.35	–	–	–	0.01	–	–	–
E_5	4.55	8.69	2	6.67	11.85	–	–	0.01	0.01	–	–
E_6	3.62	13.03	3	5.64	8.35	13.51	–	0.01	0.01	0.01	–
E_7	3.15	17.38	4	5.07	6.94	9.60	14.76	0.01	0.01	0.01	0.01
F_1	13.88	0.70	1	17.28	–	–	–	0.10	–	–	–
F_2	11.77	1.18	2	14.96	34.78	–	–	0.10	0.10	–	–
F_3	6.08	4.05	2	8.05	20.27	–	–	0.01	0.10	–	–
F_4	4.55	6.63	2	6.67	11.85	–	–	0.01	0.01	–	–
F_5	3.63	11.53	4	5.64	7.24	8.36	13.51	0.01	0.07	0.01	0.01

2. For a predefined expected damage detection delay, an optimum inspection plan based on different inspection types is more economical than that based on the same type of inspection.
3. The probabilistic approach presented in this study was applied to a ship hull structure subjected to fatigue. If the relation between the damage intensity and probability of damage detection of an inspection method can be appropriately quantified, this approach could be extended to include a wide range of structures under different deteriorating processes such as corrosion and cracking in steel and concrete structures.
4. The optimum inspection planning presented in this paper is affected by the accuracy of assumed variables and the models related to the probability of damage detection and time-dependent crack growth. For instance, the geometry function to predict the crack propagation (see Eq. (2)) is assumed 1.0; this limits the application of the method. Also, for ship structures, the load spectrum could be highly variable and, consequently, load sequencing effects have to be considered in crack growth. Therefore, further studies considering the variability of load spectrum in fatigue damage detection delay of ship structure are necessary.
5. Inspection results can be used to update the existing inspection schedule. The updating process after each inspection will lead to a more reliable inspection schedule. Therefore, further studies are necessary to establish the inspection planning considering updating.
6. Finally, it is emphasized that the proposed approach should be extended to cost-effective lifetime management strategies by considering the effects of maintenance and repair [29].

Acknowledgements

The support from the US Office of Naval Research Contract Number N00014-08-1-0188 is gratefully acknowledged. The opinions and conclusions presented in this paper are those of the authors and do not necessarily reflect the views of the sponsoring organization.

References

[1] Akpan UO, Koko TS, Ayyub B, Dunbar TE. Risk assessment of aging ship hull structures in the presence of corrosion and fatigue. Marine Struct 2002;15(3):211–31 (Elsevier).
[2] Arora JS. Introduction to optimum design. London, UK: Elsevier; 2004.
[3] Ayyub BM, Assakkaf IA, Kihl DP, Siev MW. Reliability-based design guidelines for fatigue of ship structures. Naval Eng J ASNE 2002;114(2):113–38.
[4] Berens AP, Hovey PW. Evaluation of NDE reliability characterization. AFWAL-TR-81-4160, vol. 1, Air Force Wright Aeronautical Laboratory, Wright-Patterson Air Force Base, Dayton, Ohio; 1981.
[5] Chung H-Y, Manuel L, Frank KH. Optimal inspection scheduling of steel bridges using nondestructive testing techniques. J Bridge Eng ASCE 2006;11(3):305–19.
[6] Deb K, Pratap A, Agarwal S, Meyarivan T. A fast and elitist multiobjective genetic algorithm: NSGA-II. IEEE Trans Evolution Comput 2002;6(2):182–97.
[7] Dobson WG, Brodrick RF, Wheaton JW, Giannotti J, Stambaugh KA. Fatigue considerations in view of measured load spectra. SSC-315, Ship Structure Committee; 1983.
[8] Fatemi A, Yang L. Cumulative fatigue damage and life prediction theories: a survey of the state of the art for homogeneous materials. Int J Fatigue 1998;20(1):9–34 (Elsevier).
[9] Fisher JW, Kulak GL, Smith IF. A fatigue primer for structural engineers. National Steel Bridge Alliance; 1998.
[10] Frangopol DM, Lin KY, Estes AC. Life-cycle cost design of deteriorating structures. J Struct Eng ASCE 1997;123(10):1390–401.
[11] Frangopol DM, Estes AC. Optimum lifetime planning of bridge inspection/repair programs. Struct Eng Int J IABSE 1999;9(3):219–23.
[12] Garbatov Y, Soares CG. Cost and reliability based strategies for fatigue maintenance planning of floating structures. Reliab Eng Syst Safety 2001;73(3):293–301 (Elsevier).
[13] Haimes YY, Lasdon LS, Wismer DA. On a bicriterion formulation of the problems of integrated system identification and system optimization. IEEE Trans Syst Man Cybernet 1971;1(3):296–7.
[14] Huang B-S, Chiu H-N. The quality management of the imperfect production process under two monitoring policies. Int J Qual Reliab Manage 1995;12(3):19–31. Emerald.
[15] Irwin GR. The crack-extension-force for a crack at a free surface boundary. NRL report 5120; 1958.
[16] Kim S, Frangopol DM. Inspection and monitoring planning for RC structures based on minimization of expected damage detection. Prob Eng Mech, Elsevier; in press. doi:10.1016/j.probengmech.2010.08.009.
[17] Madsen HO, Krenk S, Lind NC. Methods of structural safety. Englewood Cliffs, NJ: Prentice-Hall; 1985.
[18] Madsen HO, Sørensen JD. Probability-based optimization of fatigue design, inspection and maintenance. In: Proceedings of the fourth international symposium on integrity of offshore structures, London, Elsevier; 1990. p. 421–32.
[19] Madsen HO, Torhaug R, Cramer EH. Probability-based cost benefit analysis of fatigue design, inspection and maintenance. In: Proceedings of the marine structural inspection, maintenance and monitoring symposium, SSC/SNAME, Arlington, VA., II.E.1-12; 1991.
[20] MathWorks Inc. Optimization Toolbox™ 4 User's Guide. The MathWorks, Inc., USA; 2009.
[21] Moan T. Reliability-based management of inspection, maintenance and repair of offshore structures. Struct Infrastruct Eng 2005;1(1):33–62. Taylor & Francis.
[22] Mohanty JR, Verma BB, Ray PK. Prediction of fatigue crack growth and residual life using an exponential model: part I (constant amplitude loading). Int J Fatigue 2009;31(3):418–24 (Elsevier).
[23] Mori Y, Ellingwood BR. Maintaining reliability of concrete structures. I: role of inspection/repair. J Struct Eng ASCE 1994;120(3):824–45.
[24] Packman PF, Pearson HS, Owens JS, Young G. Definition of fatigue cracks through nondestructive testing. J Mater 1969;4(3):666–700.
[25] Paris PC, Erdogan FA. Critical analysis of crack propagation laws. J Basic Eng TRANS ASME 1963;85(Series D):528–34.
[26] Schijve J. Fatigue of structures and materials in the 20th century and the state of the art. Int J Fatigue 2003;25(8):679–702 (Elsevier).
[27] Soares CG, Garbatov Y. Fatigue reliability of the ship hull girder accounting for inspection and repair. Reliab Eng Syst Safety 1996;51(3):341–51 (Elsevier).
[28] Soares CG, Garbatov Y. Fatigue reliability of the ship hull girder. Mar Struct 1996;9(3-4):495–516 (Elsevier).
[29] Frangopol DM. Life-cycle performance, management, and optimisation of structural systems under uncertainty: accomplishments and challenges. Struct Infrastruc Eng, Talyor & Francis; in press. doi:10.1080/15732471003594427.

Appendix VII

Sunyong Kim and Dan M. Frangopol. Probabilistic bicriterion optimum inspection/monitoring planning: Application to naval ships and bridges under fatigue. *Structure and Infrastructure Engineering*, 8(10): 912-927, 2012.

Structure and Infrastructure Engineering
Vol. 8, No. 10, October 2012, 912–927

Taylor & Francis
Taylor & Francis Group

Probabilistic bicriterion optimum inspection/monitoring planning: applications to naval ships and bridges under fatigue

Sunyong Kim and Dan M. Frangopol*

Department of Civil and Environmental Engineering, ATLSS Engineering Research Center, Lehigh University, 117 ATLSS Dr., Bethlehem, PA 18015-4729, USA

(*Received 16 April 2010; final version received 27 August 2010; accepted 20 March 2011; published online 16 May 2011*)

Initiation and propagation of fatigue cracks in steel structures induced by repetitive actions are highly random due to both aleatory and epistemic uncertainties related to material properties, loads, damage, modelling and other factors. For this reason, a probabilistic approach is necessary to predict the fatigue crack growth damage. This study presents a probabilistic approach for combined inspection/monitoring planning for fatigue-sensitive structures considering uncertainties associated with fatigue crack initiation, propagation and damage detection. This combined inspection/monitoring planning is the solution of an optimisation formulation, where the objective is minimising the expected damage detection delay. Furthermore, this formulation is extended to a bicriterion optimisation considering the conflicting relation between expected damage detection delay and cost. A set of Pareto solutions is obtained by solving this bicriterion optimisation problem. From this set, a solution can be selected balancing in an optimum manner inspection and monitoring times, quality of inspections, monitoring duration, and number of inspections and monitorings. The proposed approach is applied to a naval ship and a bridge subjected to fatigue.

Keywords: fatigue; damage; uncertainty; inspection; monitoring; damage detection delay; cost; optimisation; naval ships; bridges

Introduction

One of main deterioration processes of steel structures is fatigue, defined as the process of initiation and growth of cracks under repetitive loads. In general, the fatigue evolution is affected by uncertainties associated with the location and size of initial crack, stress range near the initial crack, number of cycles, and material and geometric properties (Fisher *et al.* 1998). For this reason, a probabilistic approach is necessary to predict the fatigue crack growth damage for inspection and monitoring planning. During the last decades, several probabilistic approaches have been developed and applied to steel structures including ships and bridges subjected to fatigue (Madsen and Sørensen 1990, Madsen *et al.* 1991, Ayyub *et al.* 2002, Moan 2005, Kwon and Frangopol 2010). These studies were extended into cost-effective inspection and maintenance planning considering probability of fatigue damage detection (Garbatov and Soares 2001, Chung *et al.* 2006, Moan 2011).

The probability of fatigue damage detection has been generally formulated by including the uncertainties in crack size and inspection quality. In order to increase the probability of fatigue damage detection, advanced damage detection techniques, including structural health monitoring (SHM), have been developed and applied. The objectives of these developments include effective and timely repair actions. The probability of crack detection was defined as the conditional probability that the crack is detected when it has a specific size (Chung *et al.* 2006). Ideally, the probability of damage detection has to be 1.0. However, even in this case, there will be still time lapse from the damage occurrence to the time when the damage is detected (Kim and Frangopol 2011a). Therefore, in order to reduce this time lapse and repair delay, inspection planning should consider, in a rational way, the uncertainties associated with both inspection quality and prediction of damage occurrence. Kim and Frangopol (2011b) proposed a probabilistic approach to establish the optimum inspection planning of ship structures based on minimisation of the expected damage detection delay. However, the effect of SHM on the expected damage detection delay was not investigated.

In this study, a probabilistic approach to establish optimum combined inspection/monitoring planning for fatigue-sensitive structures is presented. In order to compute the expected damage detection delay, the

*Corresponding author. Email: dan.frangopol@lehigh.edu

ISSN 1573-2479 print/ISSN 1744-8980 online

http://dx.doi.org/10.1080/15732479.2011.574811
http://www.tandfonline.com

probabilistic approach considers uncertainties associated with fatigue crack initiation, propagation and damage detection. The combined inspection/monitoring planning is the solution of an optimisation formulation, where the objective is minimising the expected damage detection delay. Furthermore, this formulation is extended to a bicriterion optimisation consisting of minimisation of both (a) expected damage detection delay and (b) expected total inspection and monitoring costs. The cost estimation includes costs associated with the type of inspection (i.e. inspection quality), monitoring duration, number of inspections and monitorings, and discount rate of money. For a given number of inspections and monitorings, all the possible combinations of inspection and monitoring are considered, and the associated bicriterion optimisation problems are formulated and solved. Each bicriterion problem has its own Parcto solution set. Based on these Parcto sets, the final Pareto set is obtained. This procedure is extended to determine the optimum-balanced number of inspections and monitorings. The proposed approach is applied to a naval ship and a bridge subjected to fatigue.

Prediction of crack growth

Various types of steel structures including bridges, offshore structures and naval structures are sensitive to fatigue cracking induced by repetitive loads (Fisher *et al.* 1998). It may not be possible to avoid initial fatigue cracks because the cracks may be pre-existing from fabrication. These initial cracks may be propagated into macro-cracks resulting in structural failure. The rate of crack growth depends on the size of initial crack, stress range near the initial crack, number of cycles associated with the stress range, and material and geometry properties of the steel detail (Fisher 1984). Paris' equation (Paris and Erdogan 1963), among other empirical- and phenomenological-based crack propagation models, has been generally used (Fatemi and Yang 1998, Schijve 2003, Mohanty *et al.* 2009). The ratio of the crack size increment to cycle increment is (Paris and Erdogan 1963)

$$\frac{da}{dN} = C(\Delta K)^m \tag{1}$$

where a = crack size, N = number of cycles and ΔK = stress intensity factor. C and m are material crack growth parameters. The stress intensity factor ΔK is expressed in terms of crack size a and stress range S_{re} as (Irwin 1958)

$$\Delta K = S_{re} \cdot G(a) \cdot \sqrt{\pi a} \tag{2}$$

where $G(a)$ = geometry function. Based on Equations (1) and (2), the cumulative number of cycles N associated with crack size a_N can be predicted as (Fisher 1984)

$$N = \frac{1}{C \cdot S_{re}^m} \cdot \int_{a_o}^{a_N} \frac{1}{(G(a)\sqrt{\pi \cdot a})^m} da \tag{3}$$

where a_o = initial crack size. Furthermore, the time t (years) associated with the occurrence of the crack size a_N is predicted by considering the annual number of cycles N_{an} and the annual increase rate of number of cycles r_c as (Madsen *et al.* 1987)

$$t = \frac{\ln\left[1 + \frac{1}{N_{an} \cdot C \cdot S_{re}^m} \cdot \ln(1+r_c) \cdot \int_{a_o}^{a_N} \frac{1}{(G(a)\sqrt{\pi \cdot a})^m} da\right]}{\ln(1+r_c)} \quad \text{for } r_c > 0 \tag{4a}$$

$$t = \frac{1}{N_{an} \cdot C \cdot S_{re}^m} \cdot \int_{a_o}^{a_N} \frac{1}{(G(a)\sqrt{\pi \cdot a})^m} da \quad \text{for } r_c = 0 \tag{4b}$$

Probability of fatigue damage detection

Probability of fatigue damage detection is defined as the conditional probability that the crack is detected by an inspection method, when the crack exists with a specific size (Chung *et al.* 2006). Probability of damage detection associated with an inspection method has been quantified in terms of crack size (or defect size) and inspection quality (Packman *et al.* 1969, Berens and Hovey 1981, Madsen *et al.* 1991, Mori and Ellingwood 1994a, Frangopol *et al.* 1997, Chung *et al.* 2006). The representative relations between probability of detection P_{ins} and crack size a (or defect size) are:

(a) Shifted exponential form (Packman *et al.* 1969):

$$P_{ins} = 1 - \exp\left(-\frac{a - a_{min}}{\lambda}\right) \quad \text{for } a > a_{min} \tag{5}$$

where a_{min} = smallest detectable crack size and λ = characteristic parameter for inspection quality. The value of this parameter ranges from 0 to ∞, and λ decreases with increasing the quality of inspection.

(b) Log-logistic form (Berens and Hovey 1981):

$$P_{ins} = \frac{\exp[\chi + \kappa \ln(a)]}{1 + \exp[\chi + \kappa \ln(a)]} \tag{6}$$

where χ and κ are statistical parameters. These parameters can be estimated using the maximum

likelihood method for a specific inspection method (Chung *et al.* 2006).

(c) Normal cumulative distribution function (CDF) form (Frangopol *et al.* 1997):

$$P_{\text{ins}} = \Phi\left(\frac{\delta - \delta_{0.5}}{\sigma_\delta}\right) \tag{7}$$

where $\Phi(\cdot)$ = standard normal CDF; δ = damage intensity; $\delta_{0.5}$ = damage intensity at which the inspection method has a probability of detection of 0.5 and σ_δ = standard deviation of $\delta_{0.5}$. The value of $\delta_{0.5}$ represents the quality of inspection. A higher quality of inspection is associated with a smaller value of $\delta_{0.5}$. In this article, the normal CDF form in Equation (7) is used, and the coefficient of variation of $\delta_{0.5}$ is assumed as 0.1 (i.e. $\sigma_\delta = 0.1 \cdot \delta_{0.5}$). The damage intensity δ is defined as (Kim and Frangopol 2011b)

$$\delta = 0 \quad \text{for } a < a_{\min} \tag{8a}$$

$$\delta = \frac{a - a_{\min}}{a_{\max} - a_{\min}} \quad \text{for } a_{\min} \le a < a_{\max} \tag{8b}$$

$$\delta = 1 \quad \text{for } a \ge a_{\max} \tag{8c}$$

where $a_{\min}$ and $a_{\max}$ are the minimum and maximum detectable crack sizes when the result of the detection is uncertain (i.e. if $a < a_{\min}$ and $a \ge a_{\max}$ the probability of detection is 0 and 1, respectively).

Expected damage detection delay

Expected damage detection delay when inspection is used

The time lapse from the damage occurrence to the time for the damage to be detected by an inspection method is referred as damage detection delay (Huang and Chiu 1995). When the damage occurs at time t and is detected at time t_{ins} by an inspection after time t, the damage detection delay t_{del} is $t_{\text{ins}} - t$. The formulation of t_{del} considering probability of detection and number of inspections is based on an event tree model (Kim and Frangopol 2011a, 2011b). For example, if inspections are used at time $t_{\text{ins},1}$ and $t_{\text{ins},2}$, and the damage occurs in the time interval t_s to t_e, there will be three possible cases according to damage occurrence time as follows: (a) case 1: $t_s \le t < t_{\text{ins},1}$; (b) case 2: $t_{\text{ins},1} \le t < t_{\text{ins},2}$; and (c) case 3: $t_{\text{ins},2} \le t < t_e$. For case 1 (i.e. $t_s \le t < t_{\text{ins},1}$), there are three branches as shown in Figure 1. The gray circle node in Figure 1 is a chance node at every inspection where there are two mutually exclusive events (i.e. detection and no detection). The probabilities associated with these two events are P_{ins} (i.e. detection) and $1 - P_{\text{ins}}$ (i.e. no detection), respectively. Branch 1 in Figure 1 represents the event of damage detection at the first inspection. The

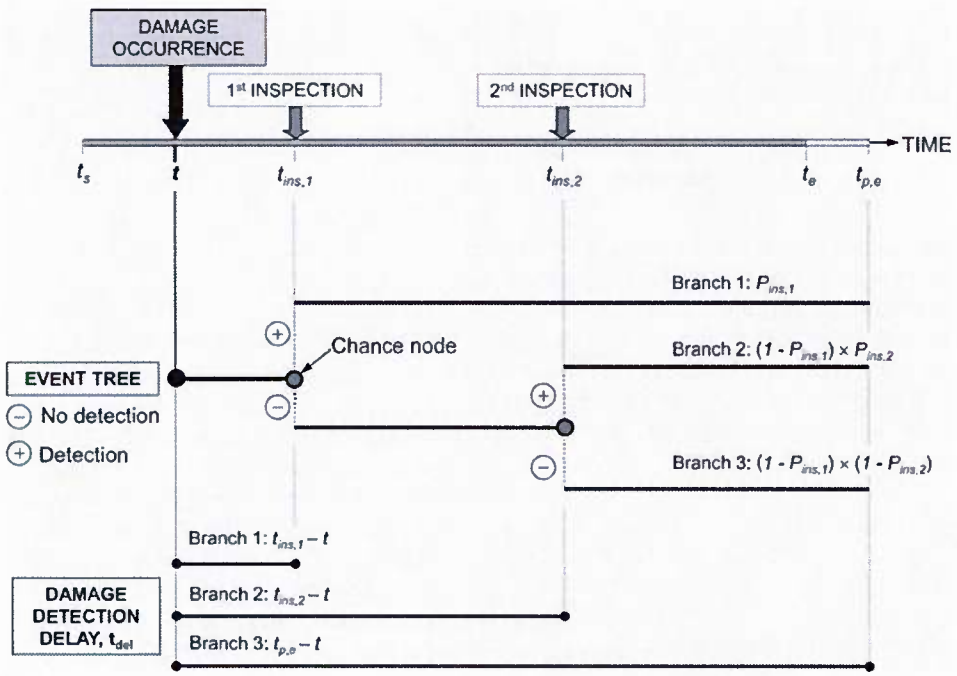

Figure 1. Damage detection delay when damage occurs in the time interval between t_s and $t_{\text{ins},1}$ (i.e. $t_s \le t < t_{\text{ins},1}$).

corresponding expected damage detection delay is $P_{\text{ins},1} \times (t_{\text{ins},1} - t)$. The expected t_{del} for branch 2 is $(1 - P_{\text{ins},1}) \times P_{\text{ins},2} \times (t_{\text{ins},2} - t)$. In this manner, the expected damage detection delay for each case can be formulated. Furthermore, considering the time t for damage to occur as a continuous random variable, the expected damage detection delay $E(t_{\text{del}})$ for N_{i} inspections is formulated as (Kim and Frangopol 2011b)

$$E(t_{\text{del}}) = \sum_{j=1}^{N_{\text{i}}+1} \left\{ \int_{t_{\text{ins},j-1}}^{t_{\text{ins},j}} \left[E(t_{\text{del}})_{\text{case},j} \cdot f_T(t) \right] \text{d}t \right\} \quad (9)$$

where $f_T(t)$ = probability density function (PDF) of damage occurrence time and $E(t_{\text{del}})_{\text{case},j}$ = expected damage detection delay for case j (i.e. $t_{\text{ins},j-1} \leq t < t_{\text{ins},j}$).

$t_{\text{ins},0}$ for $j = 1$ and $t_{\text{ins},N\text{i}+1}$ for $j = N_{\text{i}} + 1$ are t_{s} and t_{e}, respectively. $t_{\text{p,e}}$ in Figure 1 is associated with the time when the damage can be detected with perfect detectability (i.e. probability of damage detection is 1.0). In this study, $t_{\text{p,e}}$ is defined as $t_{\text{p,e}} = t_{\text{e}} + t_{\text{p}}$, where t_{e} = upper bound of the damage occurrence time, and t_{p} = time interval during which the expected probability of damage detection is at least 99.9%. The lower and upper bounds of damage occurrence time (i.e. t_{s} and t_{e}) are defined as (Kim and Frangopol 2011b)

$$t_{\text{s}} = F_T^{-1}[\Phi(-q)] \quad (10a)$$

$$t_{\text{e}} = F_T^{-1}[\Phi(q)] \quad (10b)$$

where $F_T^{-1}(\cdot)$ = the inverse CDF of the damage occurrence time t. The value of q is assumed 3.0 herein.

Expected damage detection delay when monitoring is used

SHM data allow updating the information on the structural performance. The quality of the information is related to the monitoring duration, the location of sensors and the number of sensors installed. If there is no damage detection delay during monitoring duration t_{md}, and monitoring is applied N_{m} times with the same duration t_{md}, the expected damage detection delay $E(t_{\text{del}})$ based on Equation (9) becomes

$$E(t_{\text{del}}) = \sum_{j=1}^{N_{\text{m}}+1} \left[\int_{t_{\text{mon},j-1}+t_{\text{md}}}^{t_{\text{mon},j}} (t_{\text{mon},j} - t) \cdot f_T(t) \text{d}t \right] \quad (11)$$

where $t_{\text{mon},j}$ = jth monitoring starting time. $t_{\text{mon},0} + t_{\text{md}}$ for $j = 1$ and $t_{\text{mon},N\text{m}+1}$ for $j = N_{\text{m}} + 1$ are t_s and t_{e}, respectively.

Expected damage detection delay when combined inspection/monitoring is used

When combined inspection/monitoring is used to detect damage, the expected damage detection delay $E(t_{\text{del}})$ can be formulated using Equations (9) and (11).

For instance, if one inspection and one monitoring are used, and the inspection is applied *before* monitoring (i.e. $t_{\text{mon},1} > t_{\text{ins},1}$) as shown in Figure 2, there will be four possible cases according to damage occurrence time: (a) case 1: $t_{\text{s}} \leq t < t_{\text{ins},1}$; (b) case 2: $t_{\text{ins},1} \leq t < t_{\text{mon},1}$; (c) case 3: $t_{\text{mon},1} \leq t < t_{\text{mon},1} + t_{\text{md}}$; (d) case 4: $t_{\text{mon},1} + t_{\text{md}} \leq t \leq t_{\text{e}}$. The associated expected damage detection delay is formulated as

$$\begin{aligned} E(t_{\text{del}}) = & \int_{t_{\text{s}}}^{t_{\text{ins},1}} \left[P_{\text{ins},1} \cdot (t_{\text{ins},1} - t) + (1 - P_{\text{ins},1}) \right. \\ & \left. \cdot (t_{\text{mon},1} - t) \right] \cdot f_T(t) \text{d}t + \int_{t_{\text{ins},1}}^{t_{\text{mon},1}} (t_{\text{mon},1} - t) \\ & \cdot f_T(t) \text{d}t + \int_{t_{\text{mon},1}+t_{\text{md}}}^{t_{\text{e}}} (t_{\text{p,e}} - t) \cdot f_T(t) \text{d}t \end{aligned} \quad (12)$$

It should be noted that case 3 is not considered in Equation (12) because it is assumed that there is no detection delay during monitoring duration t_{md} (i.e. probability of damage detection is 1.0).

On the contrary, when the inspection is used to detect damage *after* monitoring (i.e. $t_{\text{mon},1} + t_{\text{md}} < t_{\text{ins},1}$), the expected damage detection delay is

$$\begin{aligned} E(t_{\text{del}}) = & \int_{t_{\text{s}}}^{t_{\text{mon},1}} (t_{\text{mon},1} - t) \cdot f_T(t) \text{d}t \\ & + \int_{t_{\text{mon},1}+t_{\text{md}}}^{t_{\text{ins},1}} \left[P_{\text{ins},1} \cdot (t_{\text{ins},1} - t) + (1 - P_{\text{ins},1}) \right. \\ & \left. \cdot (t_{\text{p,e}} - t) \right] \cdot f_T(t) \text{d}t + \int_{t_{\text{ins},1}}^{t_{\text{e}}} (t_{\text{p,e}} - t) \cdot f_T(t) \text{d}t \end{aligned} \quad (13)$$

Inspection and monitoring cost

The inspection cost is related to the quality of an inspection method. In general, inspection methods associated with a higher quality (i.e. higher probability of damage detection) are more expensive (Frangopol *et al.* 1997). In this study, the cost C_{ins} associated with an inspection method is expressed using $\delta_{0.5}$ in Equation (7) (i.e. damage intensity at which the inspection method has a probability of detection of 0.5) as (Mori and Ellingwood 1994b)

$$C_{\text{ins}} = \alpha_{\text{ins}}(1 - 0.7\delta_{0.5})^{20} \quad (14)$$

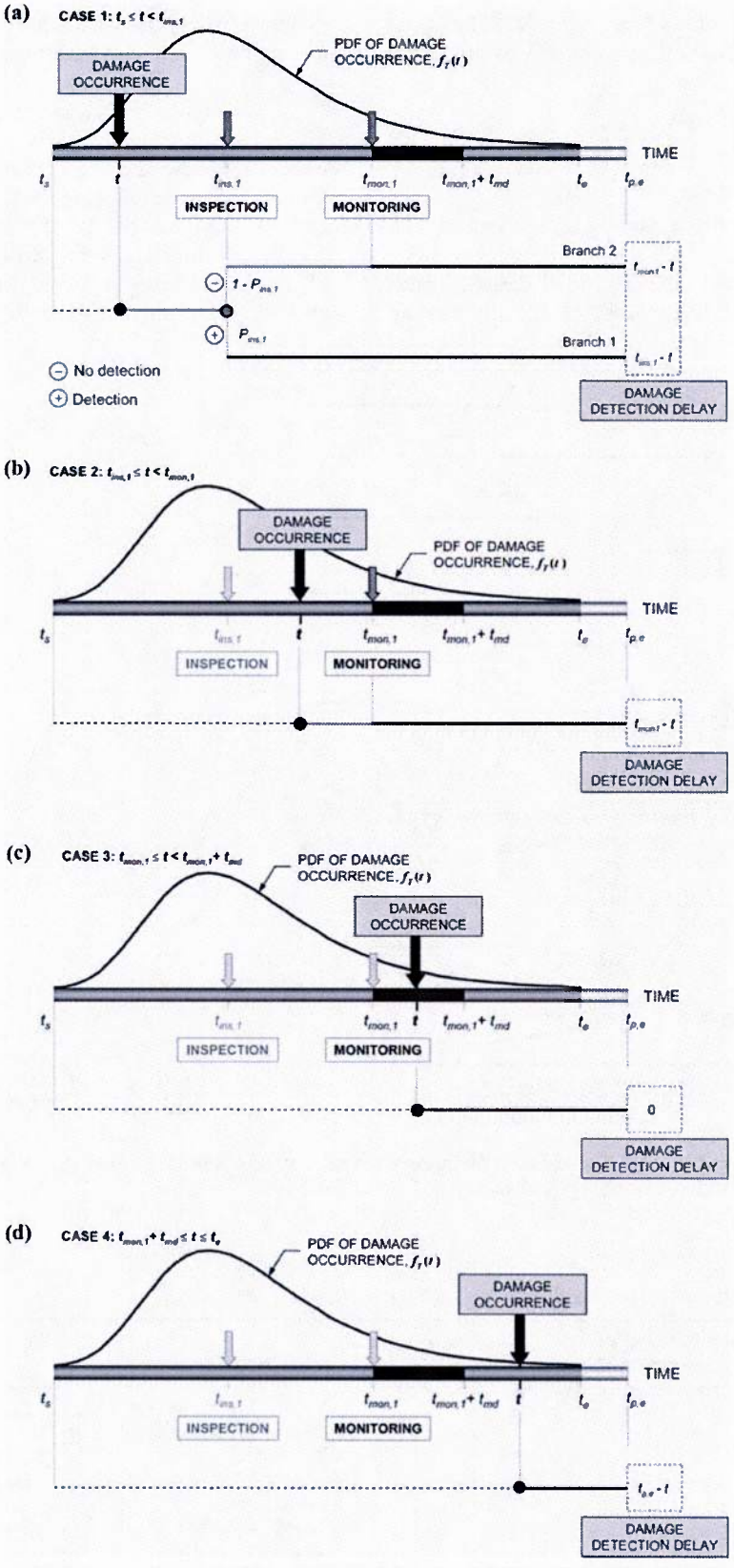

Figure 2. Damage detection delay when inspection and monitoring are used. (a) Case 1: $t_s \le t < t_{\text{ins},1}$; (b) Case 2: $t_{\text{ins},1} \le t < t_{\text{mon},1}$; (c) Case 3: $t_{\text{mon},1} \le t < t_{\text{mon},1} + t_{\text{md}}$ and (d) Case 4: $t_{\text{mon},1} + t_{\text{md}} \le t \le t_e$.

where α_{ins} is a constant (i.e. $\alpha_{ins}=5$). The total inspection cost C_{Tins} for N_i inspections is computed as

$$C_{Tins}=\sum_{j=1}^{N_i}\frac{C_{ins}}{(1+r)^{t_{ins,j}}} \tag{15}$$

where r = discount rate of money, $t_{ins,j}$ = jth inspection time.

The monitoring cost includes initial design, installation, operation and repair cost of the monitoring system (Frangopol and Messervey 2009). The monitoring cost C_{mon} can be estimated as

$$C_{mon}=C_{mon,ini}+t_{md}\times C_{mon,ann} \tag{16}$$

where t_{md} = monitoring duration (years), $C_{mon,ini}$ = initial cost of monitoring system consisting of design and installation cost of the monitoring system and $C_{mon,ann}$ = annual cost related to operation and repair of the monitoring system. In this article, $C_{mon,ini}$ and $C_{mon,ann}$ are assumed 10 and 20, respectively.

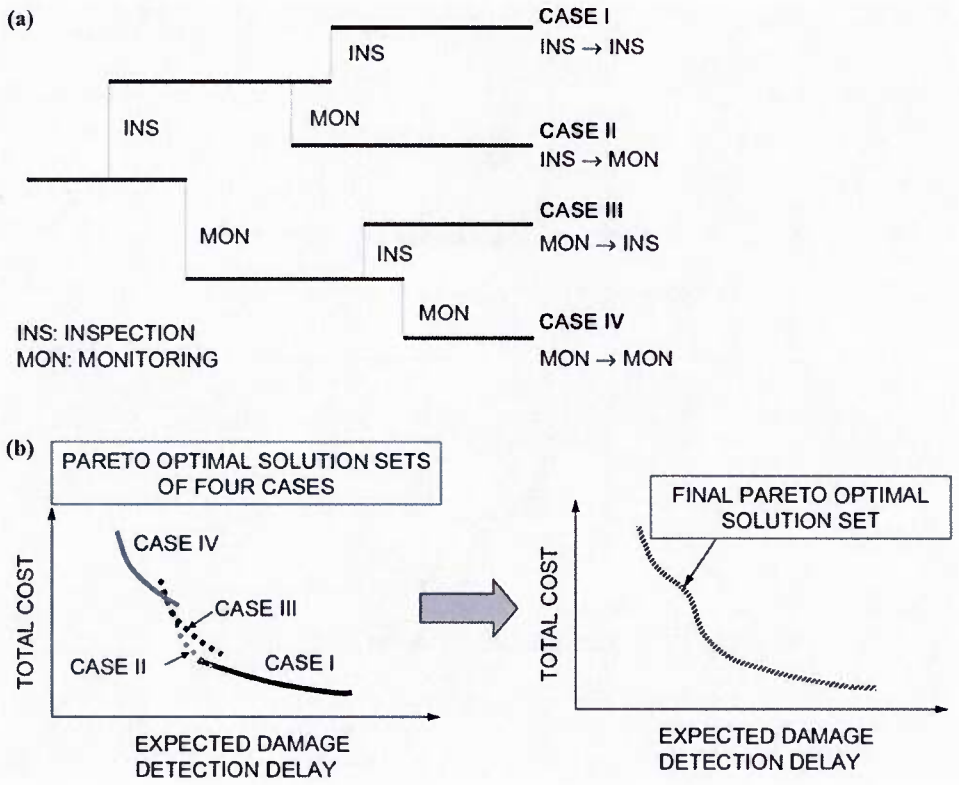

Figure 3. (a) Four possible cases for number of inspections and/or monitorings $N=2$; (b) Pareto optimal solution sets associated with four possible cases, and final Pareto solution set for $N=2$.

Table 1. Design variables associated with each case in Figure 3(a); $N_i + N_m = 2$.

Case		Number of inspections N_i	Number of monitorings N_m	Objective functions	Design variables			
I	INS → INS	2	0	$E(t_{del})$ (see Equation (9)); C_{Tins}	$t_{ins,1}$	$t_{ins,2}$	$\delta_{0.5}$	–
II	INS → MON	1	1	$E(t_{del})$ (see Equation (12)); $C_{Tins}+C_{Tmon}$	$t_{ins,1}$	$t_{mon,1}$	$\delta_{0.5}$	t_{md}
III	MON → INS	1	1	$E(t_{del})$ (see Equation (13)); $C_{Tmon}+C_{Tins}$	$t_{ins,1}$	$t_{mon,1}$	$\delta_{0.5}$	t_{md}
IV	MON → MON	0	2	$E(t_{del})$ (see Equation (11)); C_{Tmon}	$t_{mon,1}$	$t_{mon,2}$	–	t_{md}

Note: INS, inspection; MON, monitoring.

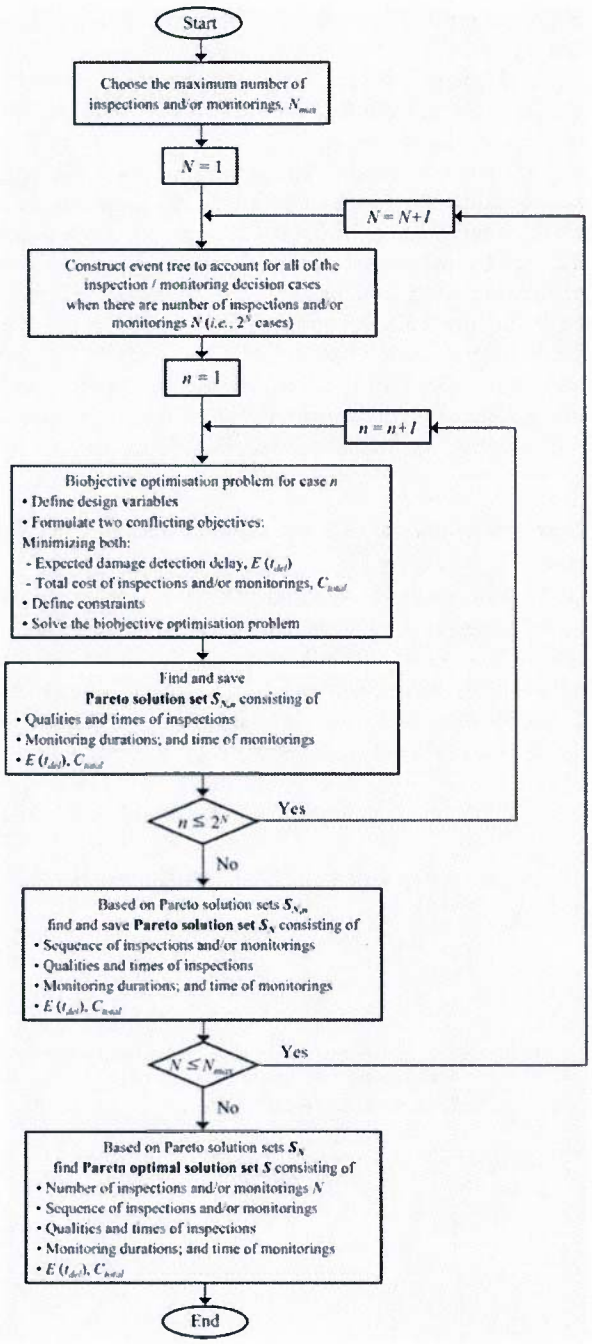

Figure 4. Flow chart to find the final Pareto optimal solution set S.

Furthermore, when a structure is monitored N_m times with the same monitoring duration t_{md}, the total monitoring cost is

$$C_{Tmon} = C_{mon,ini} + \sum_{j=1}^{N_m} \frac{t_{md} \cdot C_{mon,ann}}{(1+r)^{t_{mon,j}}} \quad (17)$$

where $t_{mon,j}$ = jth monitoring starting time.

Bicriterion optimisation

Damage detection with less delay can lead to timely repair actions. In order to reduce damage detection delay, the quality and/or the number of inspections should increase. Furthermore, when monitoring is used to detect damage, damage detection delay depends on monitoring duration and/or number of monitorings. Increasing the monitoring duration and/or number of monitorings can lead to reduction of the damage detection delay (Kim and Frangopol 2011a). However, in general, the limited financial resources constrain the selection of the quality and/or number of inspections and monitorings. Therefore, well-balanced inspection and monitoring planning should be formulated as a bicriterion optimisation with two conflicting objectives by minimising both (a) the expected damage detection delay and (b) the inspection and/or monitoring cost.

If both inspection and monitoring are used to detect damage, and the available number N of inspection N_i and/or monitorings N_m is equal to 2 (i.e. $N = N_i + N_m = 2$), then there will be four possible cases (inspection followed by inspection (case I), inspection followed by monitoring (case II), monitoring followed by inspection (case III) and monitoring followed by monitoring (case IV)) as shown in Figure 3a. The event tree in Figure 3a is used to consider all possible cases (I, II, III and IV). Every case is associated with its own bicriterion optimisation. Each bicriterion optimisation has its own design variables (see Table 1) and produces a Pareto solution set. For example, the design variables of case I in Figure 3a are inspection times (i.e. $t_{ins,1}$ and $t_{ins,2}$) and inspection quality represented by $\delta_{0.5}$ as indicated in Table 1. The objective functions associated with this

Table 2. Random variables used for crack growth model of a joint between bottom plate and longitudinal plate.

	Notation (units)	Mean	COV	Type of distribution
Initial crack size	a_o (mm)	0.5	0.2	Lognormal
Annual number of cycles	N_{an} (cycles/year)	1.0×10^6	0.2	Lognormal
Stress range	S_{re} (MPa)	40	0.1	Weibull
Material crack growth parameter	C	3.54×10^{-11}	0.3	Lognormal

Note: COV, coefficient of variation.

case are the expected damage detection delay $E(t_{del})$ of Equation (9) and the total inspection cost C_{Tins} of Equation (15), when the number of inspections $N_i = 2$. For this case, the total cost C_{total} (i.e. $C_{Tins} + C_{Tmon}$) is equal to C_{Tins}, since there is no monitoring (i.e. $C_{Tmon} = 0$). For case IV in Figure 3a, the bicriterion optimisation problem is formulated by selecting the design variables as monitoring times (i.e. $t_{mon,1}$ and $t_{mon,2}$) and monitoring duration t_{md} (see Table 1). The associated objective functions are indicated in Equations (11) and (17) for $N_m = 2$. Pareto fronts corresponding to the four cases can be obtained after solving bicriterion optimisation problems as shown in Figure 3b. Based on these four Pareto solution sets, the final Pareto solution set can be determined. This Pareto solution set S_N for $N = 2$ will provide the sequence of inspections and monitorings (i.e. inspection followed by inspection, inspection followed by monitoring, monitoring followed by inspection or monitoring followed by monitoring) as well as inspection and/or monitoring times, inspection quality and monitoring durations. This procedure to determine the Pareto solution set S_N for given number of inspections and/or monitorings N can be extended to find the final Pareto solution set S when the available number of inspections and/or monitorings N ranges from 1 to N_{max}. Figure 4 provides a flow chart to find the final Pareto solution set S. The final Pareto solution set S will provide the number of inspections and/or monitorings, the sequence of inspections and monitorings, the inspection and/or monitoring times, inspection quality and monitoring duration.

Application to a naval ship

Description of ship hull structure subjected to fatigue

The proposed approach is applied to a naval ship hull structure. A critical location subjected to fatigue is assumed to be the joint between longitudinal plate and bottom plate. The fatigue crack in the bottom plate can initiate on the edge connected to the stiffener in the transverse direction under repeated loading due to the action of sea water waves. In order to predict the crack length size, Equation (4) is used assuming $m = 2.54$ and using the random variables defined in Table 2. The stress range S_{re} is assumed to be a random variable with a Weibull PDF (Madsen *et al.* 1991). Initial crack length a_o, annual number of cycles N_{an} and material crack growth parameter C are treated as log-normally distributed random variables. The mean value of material crack growth parameter C is assumed as 3.54×10^{-11} for high-yield steel (HY80) (Dobson *et al.* 1983). It should be noted that the geometry function $G(a)$ is assumed to be 1.0 (Madsen *et al.* 1991, Akpan *et al.* 2002), and there is no annual increase rate of the number of cycles r_c (i.e. $r_c = 0$).

In this study, the crack size of 1.0 mm is referred to the fatigue crack damage criterion. In other words, the minimum crack size a_{min} for damage intensity δ in Equation (8) is 1.0 mm. The maximum crack size a_{max} in Equation (8) is assumed to be 50 mm. Figure 5 shows the PDF of fatigue damage occurrence (i.e. $a_{min} = 1.0$ mm) time obtained from Monte Carlo simulation with 100,000 samples and its best fitted PDF (i.e. generalised extreme value (GEV) PDF). The GEV PDF is defined as indicated in a study by Kim and Frangopol (2011b). The lower and upper bounds of damage occurrence time (i.e. t_s and t_e in Equation (10)) are 0.41 and 17.56 years, respectively.

Optimum balance of cost and expected damage detection delay

When the available number of inspections and/or monitorings is $N = 2$, there will be four cases. Each case will have its own bicriterion optimisation formulation as mentioned previously (see Figure 3 and Table 1). The bicriterion optimisation formulations of these four cases are formulated as

$$\text{Find} \quad t_{ins,1}, t_{ins,2} \text{ and } \delta_{0.5} \quad \text{for case I} \tag{18a}$$

$$t_{ins,1}, t_{mon,1}, \delta_{0.5} \text{ and } t_{md} \quad \text{for cases II and III} \tag{18b}$$

$$t_{mon,1}, t_{mon,2} \text{ and } t_{md} \quad \text{for case IV} \tag{18c}$$

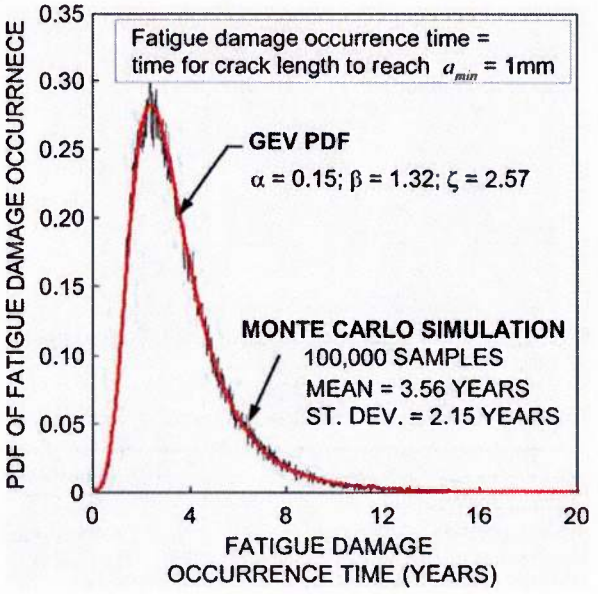

Figure 5. PDF of time for crack length to reach a_{min}.

to minimise both $E(t_{del})$ and C_{total} (19)

such that $t_{ins,2} - t_{ins,1} \geq 1.0$ year, and
$0.01 \leq \delta_{0.5} \leq 0.1$ for case I (20a)

$t_{mon,1} - t_{ins,1} \geq 1.0$ year, $0.01 \leq \delta_{0.5} \leq 0.1$ and
0.3 year $\leq t_{md} \leq 1.0$ year for case II (20b)

$t_{ins,1} - t_{mon,1} \geq 1.0$ year, $0.01 \leq \delta_{0.5} \leq 0.1$ and
0.3 year $\leq t_{md} \leq 1.0$ year for case III (20c)

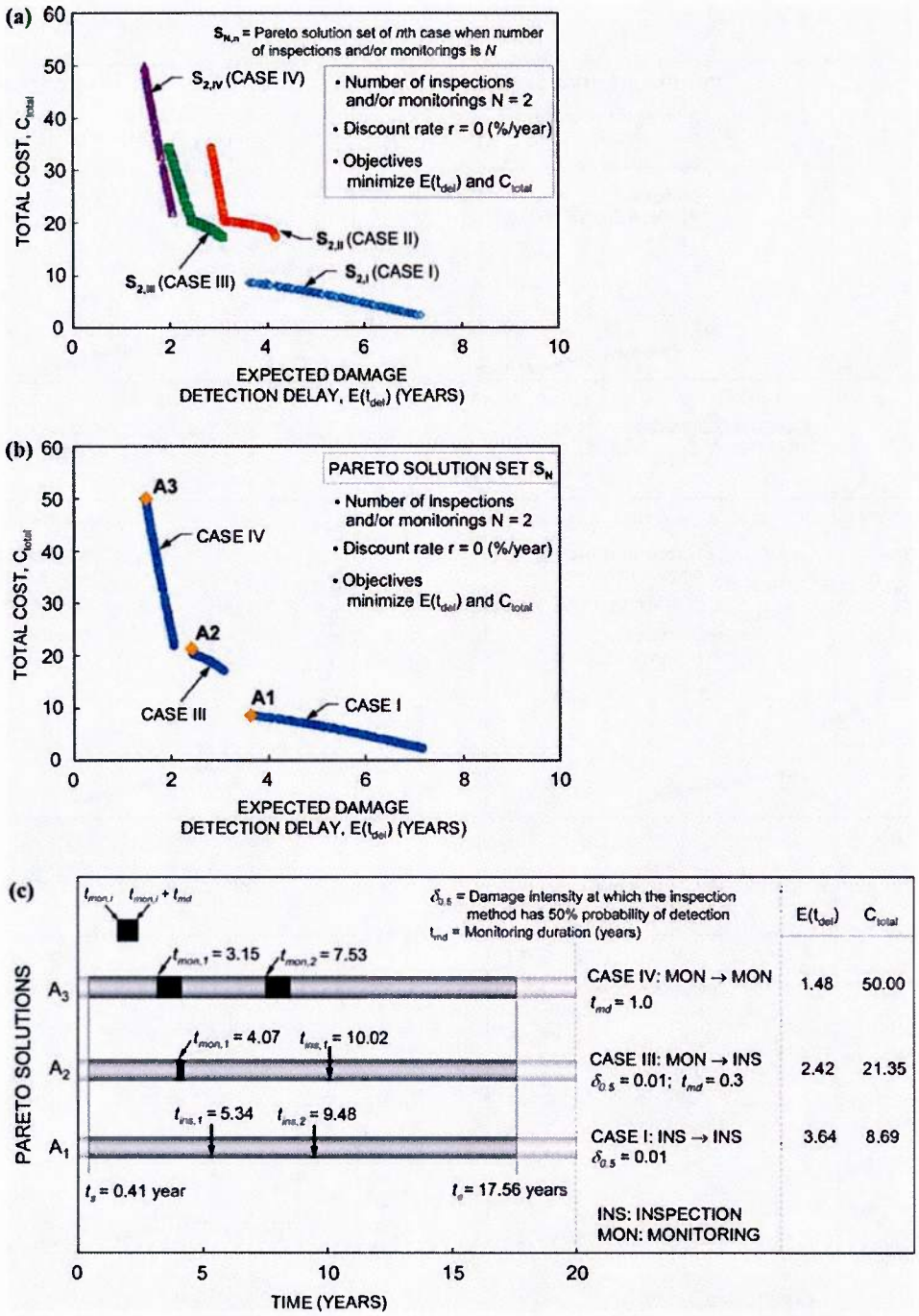

Figure 6. Number of inspections and/or monitorings $N=2$. (a) Pareto solution sets $S_{N,n}$ for cases I, II, III and IV; (b) Pareto solution set S_N; (c) combined inspection/monitoring plans for solutions A_1, A_2 and A_3 in (b).

$t_{mon,2} - t_{mon,1} \geq 1.0$ year and 0.3 year $\leq t_{md} \leq 1.0$ year for case IV (20d)

$$\text{given} \quad N = N_i + N_m = 2, \text{ and } f_T(t) \tag{21}$$

The design variables and constraints of the bicriterion optimisation formulations for cases I, II, III and IV are indicated in Equations (18) and (20), respectively. The objectives are to minimise both expected damage detection delay $E(t_{del})$ and total cost C_{total}. The time interval between inspections and/or monitorings has to be at least 1 year, and $\delta_{0.5}$ representing the quality of inspection should be in the interval 0.01–0.1. Monitoring duration t_{md} has to be in the time interval 0.3–1.0 year. The GEV PDF $f_T(t)$

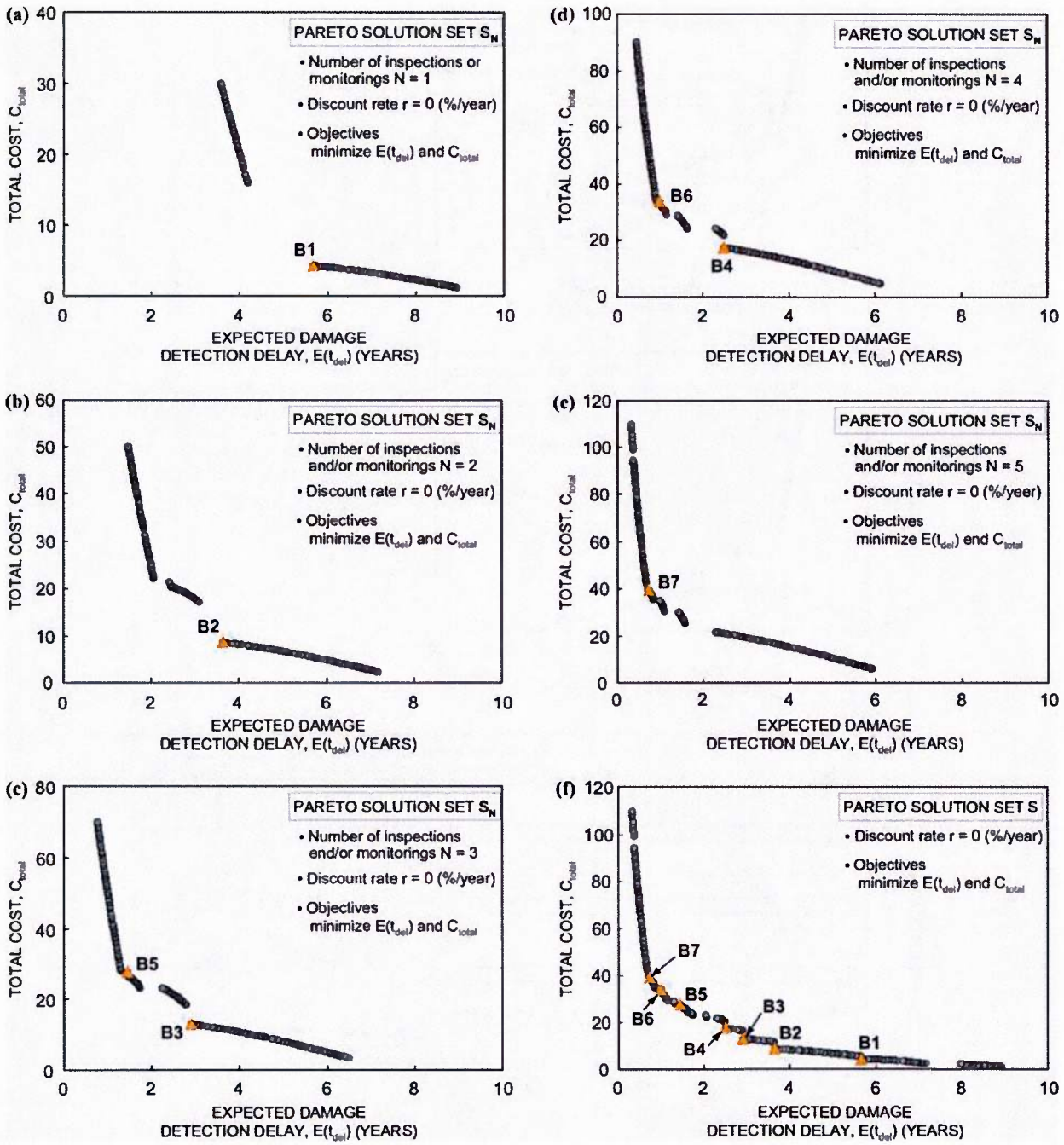

Figure 7. Pareto solution set S_N for (a) $N=1$; (b) $N=2$; (c) $N=3$; (d) $N=4$ and (e) $N=5$, and (f) final Pareto solution set S.

in Figure 5 indicated in Equation (21) is used to formulate $E(t_{del})$. Non-dominated sorting in genetic algorithms (NSGA-II) programme developed by Deb *et al.* (2002) is used to find the Pareto solution set of the bicriterion optimisation formulations in Equations (19)–(21).

The genetic algorithm process with 500 generations provides the Pareto sets for cases I, II, III and IV shown in Figure 6a. $S_{N,n}$ denotes a Pareto set of nth case when available number of inspections and/or monitorings is N. For example, $S_{2,1}$ in Figure 6a is the Pareto solution set of case I (INS → INS case in

Table 3. Pareto optimum solutions in Figure 7: values of objectives and design variables.

Pareto optimum solution	Objectives		Design variables							
	$E(t_{del})$ (years)	C_{total}	N	Optimum inspection or monitoring times (years)					$\delta_{0.5}$	Monitoring duration t_{md} (years)
B_1	5.67	4.35	1	$t_{ins,1}$ 7.47					0.01	–
B_2	3.64	8.69	2	$t_{ins,1}$ 5.34	$t_{ins,2}$ 9.48				0.01	–
B_3	2.90	13.03	3	$t_{ins,1}$ 4.51	$t_{ins,2}$ 6.82	$t_{ins,3}$ 10.82			0.01	–
B_4	2.49	17.38	4	$t_{ins,1}$ 4.11	$t_{ins,2}$ 5.61	$t_{ins,3}$ 7.73	$t_{ins,4}$ 11.81		0.01	–
B_5	1.45	27.69	3	$t_{mon,1}$ 3.03	$t_{mon,2}$ 5.68	$t_{ins,1}$ 11.49			0.01	0.33
B_6	0.99	33.90	4	$t_{mon,1}$ 2.58	$t_{mon,2}$ 4.21	$t_{mon,3}$ 6.68	$t_{ins,1}$ 12.59		0.01	0.33
B_7	0.74	39.44	5	$t_{mon,1}$ 2.19	$t_{mon,2}$ 3.50	$t_{mon,3}$ 5.10	$t_{mon,4}$ 7.79	$t_{ins,1}$ 13.46	0.01	0.31

Note: N, total number of inspections and/or monitorings.

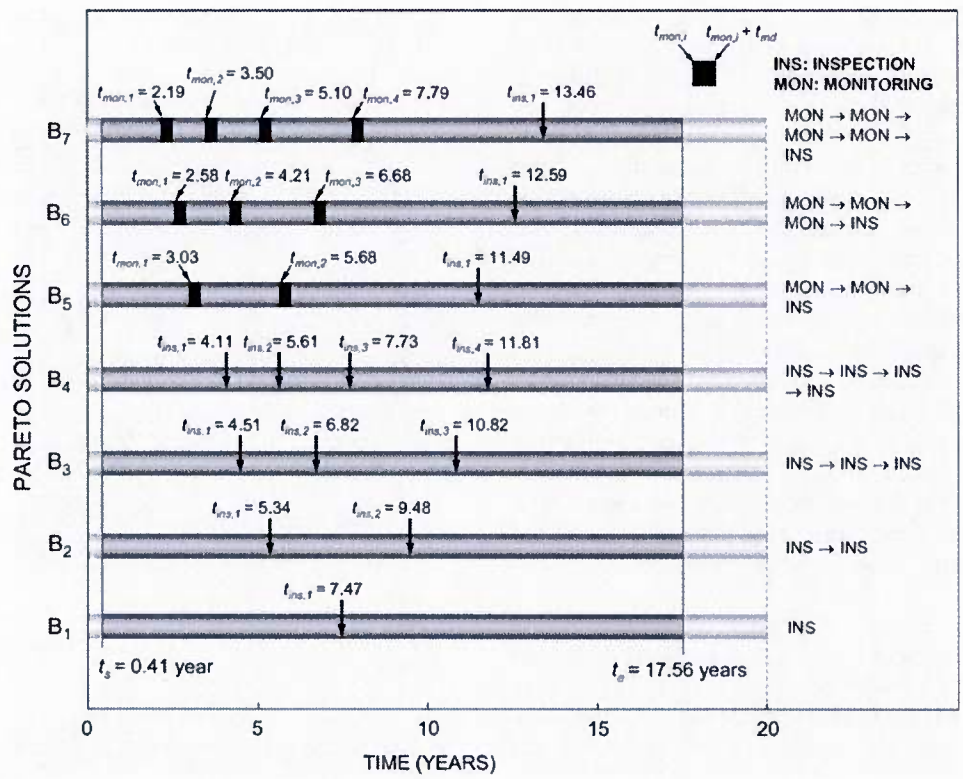

Figure 8. Combined inspection/monitoring plans for solutions B_1–B_7 in Figure 7f.

Table 4. Random variables used for crack growth model of a cover plate.

Random variables	Notation (units)	Mean	COV	Type of distribution
Initial crack size	a_o (mm)	0.5	0.2	Lognormal
Annual number of cycles	N_{an} (cycles/year)	1.62×10^6	0.2	Lognormal
Annual increase rate of number of cycles	r_c (%)	2	0.1	Lognormal
Stress range	S_{re} (Mpa)	13.78	0.1	Weibull
Material crack growth parameter	C	2.024×10^{-13}	0.25	Lognormal
Weld size	Z (mm)	16	0.1	Lognormal

Note: COV, coefficient of variation.

Figure 3 and Table 1). A Pareto set $S_{N,n}$ consists of 100 populations. The final Pareto solution set S_2, based on the Pareto solution sets for $n = $ I–IV in Figure 6a, is obtained using the ε-constraint approach by minimising the selected single objective function, while other objective functions are treated as constraints (Haimes *et al.* 1971) as follows

$$\text{Minimise} \quad f_i \tag{22}$$

$$\text{subject to} \quad f_j \leq \varepsilon_j \text{ for all } j = 1, 2, \ldots, q; j \neq i \tag{23}$$

where $i \in \{1, 2, \ldots, q\}$ and $q =$ number of objective functions. The final Pareto solution set S_2 is shown in Figure 6b. Combined inspection/monitoring plans of the three representative solutions A_1, A_2 and A_3 in Figure 6b are illustrated in Figure 6c. The inspection and monitoring plan for solution A_1 requires two inspections (case I) applied at time $t_{ins,1} = 5.34$ years and $t_{ins,2} = 9.48$ years with $\delta_{0.5} = 0.01$ (see Figure 6c), and the associated $E(t_{del})$ and C_{total} are 3.64 years and 8.69, respectively (see Figure 6b). If Pareto solution A_2 is selected instead of A_1, the expected damage detection delay $E(t_{del})$ will be reduced from 3.64 years to 2.42 years, but an additional cost of 12.66 (i.e. 21.35–8.69) is needed as shown in Figure 6b. The inspection and monitoring plan associated with A_2 (case III) consists of the monitoring starting time $t_{mon,1} = 4.07$ years with monitoring duration $t_{md} = 0.3$ year and the inspection at time $t_{ins,1} = 10.02$ years with $\delta_{0.5} = 0.01$ (see Figure 6c). It should be noted that the discount rate of money was not considered (i.e. $r = 0$); the value of $\delta_{0.5}$ is assumed to be the same for the first and second inspections associated with case I, and the same monitoring duration t_{md} is used for the first and second monitorings associated with case IV.

In a similar way, the Pareto sets S_N for $N = 1$–5 are obtained as shown in Figure 7a–e. The final Pareto set S considering N as a design variable is also found by using the ε-constraint approach based on the Pareto solution sets S_N. The detailed procedure to find the final Pareto set S is provided in Figure 4. Figure 7f shows the Pareto set S. The optimum values of design variables and objective functions of the seven representative solutions B_1–B_7 in Figure 7 are provided in Table 3. Combined inspection/monitoring plans for

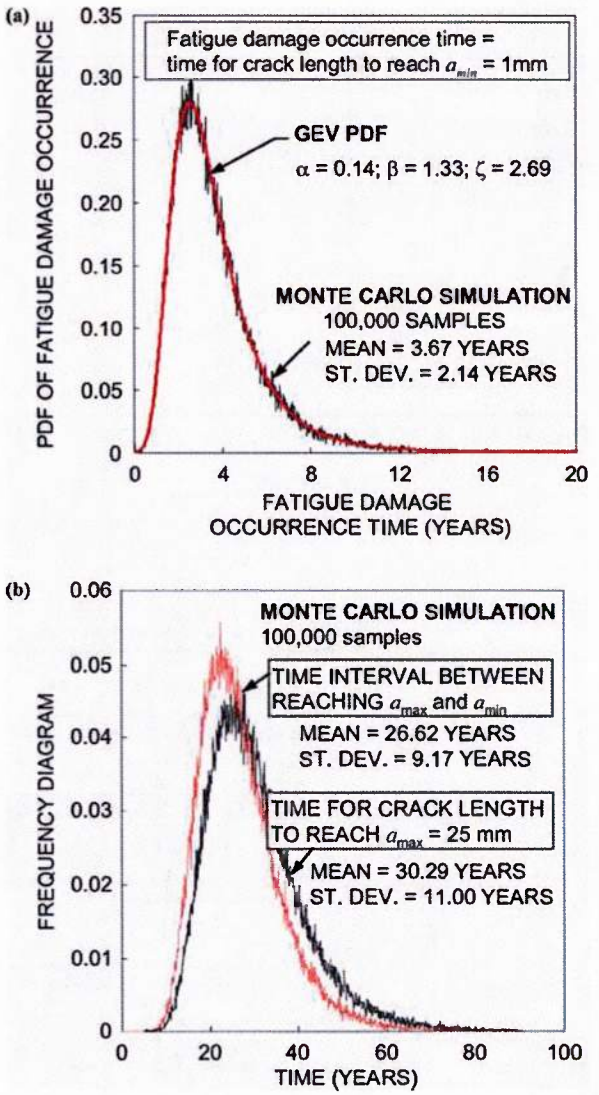

Figure 9. PDF: (a) time for crack length to reach a_{min}; (b) time for crack length to reach a_{max} and time interval between reaching a_{max} and a_{min}.

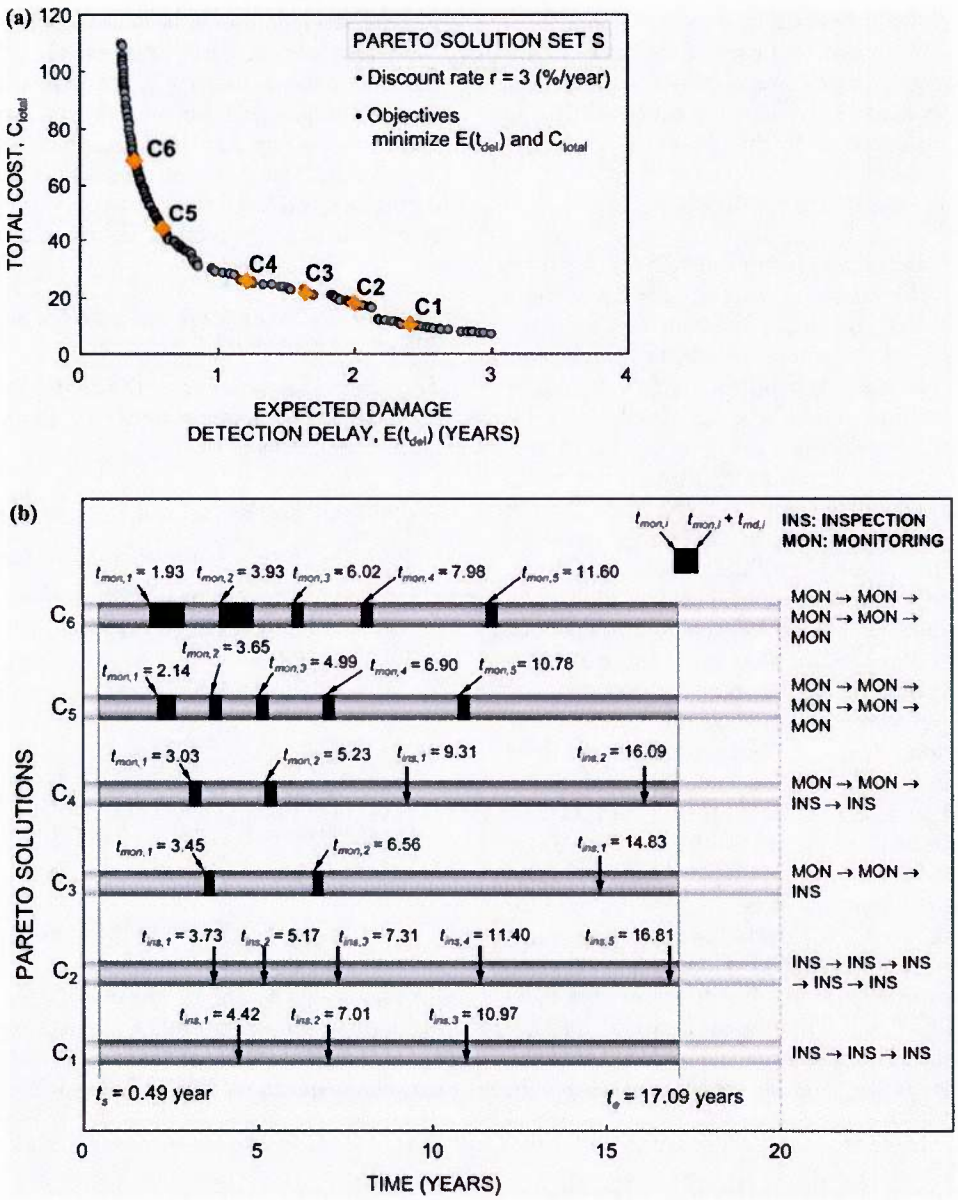

Figure 10. (a) Final Pareto solution set S and (b) combined inspection/monitoring plans for solutions C_1–C_6 in (a).

solutions B_1–B_7 are illustrated in Figure 8. Solutions B_3 and B_5 in Figure 7f are found in the Pareto solution set S_3 in Figure 7c. Solutions B_4 and B_6 in Figure 7f are associated with the Pareto set S_4 in Figure 7d. Solution B_6 requires three monitorings with the same duration $t_{md}=0.33$ year and one inspection with $\delta_{0.5}=0.01$, and the corresponding $E(t_{del})$ and C_{total} are 0.99 year and 33.90, respectively (see Table 3). Monitoring times $t_{mon,1}$, $t_{mon,2}$, $t_{mon,3}$ are 2.58, 4.21, 6.68 years, and inspection time $t_{insp,1}$ is 12.59 years as shown in Figure 8. In order to reduce the total cost C_{total}, solution B_4 consisting of four inspections with $\delta_{0.5}=0.01$ can be selected. As a result, C_{total} can be reduced from 33.90 to 17.38, but $E(t_{del})$ will increase from 0.99 to 2.49 years.

Application to an existing bridge

Description of an existing highway bridge subjected to fatigue

The proposed approach is applied to an existing highway bridge, the Yellow Mill Pond Bridge located in Bridgeport, Connecticut, USA. In this application, critical location is assumed to be the end of the cover

plate weld. Detailed information is available in a study by Fisher (1984). In order to predict the time for the occurrence of a given crack size at this critical location, Equation (4) is used. The geometry function $G(a)$ in Equation (4) is defined as (Fisher 1984)

$$G(a) = G_e(a) \cdot G_s(a) \cdot G_w(a) \cdot G_g(a) \qquad (24)$$

where $G_e(a)$ = crack shape factor = 0.952; $G_s(a)$ = front face factor = $1.211 - 0.186 \cdot \sqrt{a/c}$; $G_w(a)$ = finite width factor = 1.0 and $G_g(a)$ = stress gradient factor = $K_{tm} \cdot [1 + 6.79 \cdot (a/t_f)^{0.435}]^{-1}$, where a = depth crack size; c = width crack size; t_f = flange thickness; K_{tm} = stress concentration factor = $-3.54 \cdot \ln(Z/t_f) + 1.98 \cdot \ln(t_{cp}/t_f) + 5.80$; Z = weld size; t_{cp} = cover plate thickness. The relation between depth crack size a and width crack size c is assumed as $c = 5.462 \times a^{1.133}$. The deterministic parameters used are the flange thickness $t_f = 32.0$ mm, the cover plate thickness $t_{cp} = 31.8$ mm and the material parameter $m = 3.0$ (Shetty and Baker 1990). All random variables necessary to predict crack growth of this critical location are provided in Table 4.

Figure 9a shows the PDF of time for the crack size to reach $a_{min} = 1.0$ mm assumed as the fatigue crack damage criterion. Through comparison with Monte Carlo simulation with 100,000 samples, best fitting PDF (i.e. GEV PDF) with $\alpha = 0.14$, $\beta = 1.33$ and $\zeta = 2.69$ is obtained as shown in Figure 9a. If the maximum crack size a_{max} for damage intensity defined in Equation (8) is assumed to be 25 mm, the time for damage intensity to reach 1.0 will have the mean value of 30.29 years and the standard deviation of 11.00 years as shown in Figure 9b. Furthermore, the PDF associated with the time interval between damage occurrence (i.e. crack size $a = a_{min}$) and full damage (i.e. crack size $a = a_{max}$) is shown in Figure 9b. In general, damage should be detected and repaired before the time when the crack size reaches a_{max}. Since crack size will increase from a_{min} to a (see Equation (8b)) during the damage detection delay, the damage detection delay has to be less than the time associated with $a_{max} - a_{min}$. Therefore, the time interval between damage occurrence and full damage in Figure 9b can provide an upper bound of the damage detection delay.

Optimum balance of cost and expected damage detection delay

The general formulation of the bicriterion optimisation problem for a given number of inspections and/or monitorings N is

$$\begin{aligned} \text{Find} \quad & \boldsymbol{t}_{ins} = \{t_{ins,1}, t_{ins,2}, \ldots, t_{ins,N_i}\}; \\ & \boldsymbol{t}_{mon} = \{t_{mon,1}, t_{mon,2}, \ldots, t_{mon,N_m}\}; \\ & \boldsymbol{t}_{md} = \{t_{md,1}, t_{md,2}, \ldots, t_{md,N_m}\} \text{ and} \\ & \boldsymbol{\delta}_{0.5} = \{\delta_{0.5,1}, \delta_{0.5,2}, \ldots, \delta_{0.5,N_i}\} \end{aligned} \qquad (25)$$

$$\text{to minimise both} \quad E(t_{del}) \text{ and } C_{total} \qquad (26)$$

$$\begin{aligned} \text{such that } & t_{ins,j} - t_{ins,j-1} \geq 1.0 \text{ year}; \\ & 0.01 \leq \delta_{0.5,j} \leq 0.1; \; t_{mon,j} - t_{mon,j-1} \\ & \geq 1.0 \text{ year}; 0.3 \text{ year} \leq t_{md,j} \leq 1.0 \text{ year and} \\ & |\boldsymbol{t}_{mon} - \boldsymbol{t}_{ins}| \geq 1.0 \text{ year} \end{aligned} \qquad (27)$$

$$\text{given} \quad N = N_i + N_m; \text{ and } f_T(t) \qquad (28)$$

The design variables are the vectors of inspection times $\boldsymbol{t}_{ins}$, monitoring times $\boldsymbol{t}_{mon}$, monitoring durations $\boldsymbol{t}_{md}$ and quality of inspections $\boldsymbol{\delta}_{0.5}$. The time intervals between inspections and/or monitorings have to be at

Table 5. Pareto optimum solutions in Figure 10(a): values of objectives and design variables.

Pareto optimum solution	Objectives		Design variables										
	$E(t_{del})$ (years)	C_{total}	N	Optimum inspection and/or monitoring times (years)					$\delta_{0.5}$ and/or monitoring duration t_{md} (years)				
C_1	2.40	10.41	3	$t_{ins,1}$ 4.42	$t_{ins,2}$ 7.01	$t_{ins,3}$ 10.97			$\delta_{0.5,1}$ 0.01	$\delta_{0.5,2}$ 0.01	$\delta_{0.5,3}$ 0.01		
C_2	2.00	17.95	5	$t_{ins,1}$ 3.73	$t_{ins,2}$ 5.17	$t_{ins,3}$ 7.31	$t_{ins,4}$ 11.40	$t_{ins,5}$ 16.81	$\delta_{0.5,1}$ 0.01	$\delta_{0.5,2}$ 0.01	$\delta_{0.5,3}$ 0.01	$\delta_{0.5,4}$ 0.02	$\delta_{0.5,5}$ 0.10
C_3	1.64	21.61	3	$t_{mon,1}$ 3.45	$t_{mon,2}$ 6.56	$t_{ins,1}$ 14.83			$t_{md,1}$ 0.32	$t_{md,2}$ 0.30	$\delta_{0.5,1}$ 0.08		
C_4	1.22	26.02	4	$t_{mon,1}$ 3.03	$t_{mon,2}$ 5.23	$t_{ins,1}$ 9.31	$t_{ins,2}$ 16.09		$t_{md,1}$ 0.36	$t_{md,2}$ 0.30	$\delta_{0.5,1}$ 0.01	$\delta_{0.5,2}$ 0.07	
C_5	0.60	17.95	5	$t_{mon,1}$ 2.14	$t_{mon,2}$ 3.65	$t_{mon,3}$ 4.99	$t_{mon,4}$ 6.90	$t_{mon,5}$ 10.78	$t_{md,1}$ 0.51	$t_{md,2}$ 0.30	$t_{md,3}$ 0.30	$t_{md,4}$ 0.30	$t_{md,5}$ 0.30
C_6	0.40	68.70	5	$t_{mon,1}$ 1.93	$t_{mon,2}$ 3.93	$t_{mon,3}$ 6.02	$t_{mon,4}$ 7.98	$t_{mon,5}$ 11.60	$t_{md,1}$ 1.00	$t_{md,2}$ 0.98	$t_{md,3}$ 0.34	$t_{md,4}$ 0.30	$t_{md,5}$ 0.31

Note: N, total number of inspections and/or monitorings.

least 1 year. Constraints for t_{md} and $\delta_{0.5}$ are indicated in Equation (27). The GEV PDF $f_T(t)$ in Figure 9a is used to formulate $E(t_{del})$. For given N, the total number 2^N of Pareto sets $S_{N,n}$ can be obtained by solving the bicriterion optimisation problems in Equations (25)–(28). Finally, the Pareto solution set S can be obtained through the procedure given in Figure 4. Figure 10a shows this final Pareto set S and six representative solutions C_1–C_6. Values of design variables (i.e. N, t_{ins}, t_{mon}, t_{md} and $\delta_{0.5}$) and objective functions (i.e. $E(t_{del})$ and C_{total}) are given in Table 5. It should be noted that the annual discount rate r is assumed 3%. The combined inspection/monitoring plans corresponding to solutions C_1–C_6 are illustrated in Figure 10b.

Conclusions

This article presented a probabilistic approach to establish an optimum combined inspection/monitoring planning for ship and bridge structures subjected to fatigue based on bicriterion approach. For given number of inspections and monitorings, all possible combinations of inspection and monitoring were considered. Each combination was associated with a bicriterion optimisation formulation consisting of two conflicting objectives by simultaneously minimising both the expected damage detection delay and the total inspection and monitoring cost. Based on the Pareto solution sets of all combinations of inspection and monitoring for the given number of inspections and monitorings, the final Pareto set was obtained. Finally, this procedure was extended to determine the optimum number of inspections and monitorings. The following conclusions can be drawn from this study:

(1) Due to the scarcity of financial resources allocated for maintaining and/or improving the reliability of the deteriorating civil and marine infrastructure systems, an optimisation considering damage detection delay and inspection/monitoring is crucial. Along these lines, the proposed bicriterion approach provides powerful means to optimise inspection/monitoring planning for fatigue-sensitive structures under uncertainty.

(2) In addition, performance measures such as system reliability, robustness and redundancy may be integrated in the proposed approach, by extending it to a multicriterion optimisation formulation under uncertainty (Frangopol and Liu 2007, Frangopol 2011). Moreover, the optimum combined inspection/monitoring planning approach proposed in this article can be extended to life-cycle cost design of fatigue-sensitive structures including bridges and naval ships by considering initial, inspection, monitoring, maintenance, repair and failure costs.

(3) In general, fatigue damage can be detected with less delay by using monitoring than inspection. However, monitoring is usually more expensive than inspection. Therefore, combined inspection/monitoring planning provides an optimal-balanced solution. Damage detection delay leads to repair delay. This delay increases the probability of failure.

(4) The fatigue damage occurrence and propagation are random processes involving intermittent growths and dormant periods. In order to consider these evolutionary features, Markov chains, jump process models and stochastic differential equations have been developed (Sobczyk 1987). The scheduling of inspection and monitoring can be affected by the time evolution model of fatigue cracks. Therefore, further studies are needed to incorporate such advanced stochastic modellings into the approach proposed in this article.

Acknowledgements

The support from grants by (a) the National Science Foundation through CMS-0639428, (b) the Commonwealth of Pennsylvania, Department of Community and Economic Development, through the Pennsylvania Infrastructure Technology Alliance (PITA), (c) the US Federal Highway Administration Cooperative Agreement Award DTFH61-07-H-00040 and (d) the US Office of Naval Research Contract Number N00014–08–1–0188 is gratefully acknowledged. The opinions and conclusions presented in this article are those of the authors, and do not necessarily reflect the views of the sponsoring organisations.

References

Akpan, U.O., *et al.*, 2002. Risk assessment of aging ship hull structures in the presence of corrosion and fatigue. *Marine Structures*, 15 (3), 211–231.

Ayyub, B.M., *et al.*, 2002. Reliability-based design guidelines for fatigue of ship structures. *Naval Engineers Journal*, 114 (2), 113–138.

Berens, A.P. and Hovey, P.W., 1981. *Evaluation of NDE reliability characterization*. Dayton: Air Force Wright-Aeronautical Laboratory, Wright-Patterson Air Force Base.

Chung, H.-Y., Manuel, L., and Frank, K.H., 2006. Optimal inspection scheduling of steel bridges using nondestructive testing techniques. *Journal of Bridge Engineering*, 11 (3), 305–319.

Deb, K., *et al.*, 2002. A fast and elitist multiobjective genetic algorithm: NSGA-II. *IEEE Transactions on Evolutionary Computation*, 6 (2), 182–197.

Dobson, W.G., *et al.*, 1983. *Fatigue considerations in view of measured load spectra*. Washington, DC: SSC-315, Ship Structure Committee.

Fatemi, A. and Yang, L., 1998. Cumulative fatigue damage and life prediction theories: a survey of the state of the art for homogeneous materials. *International Journal of Fatigue*, 20 (1), 9–34.

Fisher, J.W., 1984. *Fatigue and fracture in steel bridges*. New York, NY: John Willey & Sons.

Fisher, J.W., Kulak, G.L., and Smith, I.F., 1998. *A fatigue primer for structural engineers*. Chicago, IL: National Steel Bridge Alliance.

Frangopol, D.M., 2011. Life-cycle performance, management, and optimization of structural systems under uncertainty: accomplishments and challenges. *Structure and Infrastructure Engineering*, 7 (6), 389–413.

Frangopol, D.M., Lin, K.Y., and Estes, A.C., 1997. Life-cycle cost design of deteriorating structures. *Journal of Structural Engineering*, 123 (10), 1390–1401.

Frangopol, D.M. and Liu, M., 2007. Maintenance and management of civil infrastructure based on condition, safety, optimization, and life-cycle cost. *Structure & Infrastructure Engineering: Maintenance, Management, Life-Cycle*, 3 (1), 29–41.

Frangopol, D.M. and Messervey, T.B., 2009. Life-cycle cost and performance prediction: role of structural health monitoring [Chapter 16]. *In*: S.-S. Chen and A.H.-S. Ang, eds. *Frontier technologies for infrastructures engineering*. Leiden, The Netherlands: CRC Press-Balkema-Taylor & Francis Group, 361–381.

Garbatov, Y. and Soares, C.G., 2001. Cost and reliability based strategies for fatigue maintenance planning of floating structures. *Reliability Engineering and System Safety*, 73 (3), 293–301.

Haimes, Y.Y., Lasdon, L.S., and Wismer, D.A., 1971. On a bicriterion formulation of the problems of integrated system identification and system optimization. *IEEE Transactions on Systems, Man, and Cybernetics*, 1 (3), 296–297.

Huang, B.-S. and Chiu, H.-N., 1995. The quality management of the imperfect production process under two monitoring policies. *International Journal of Quality & Reliability Management*, 12 (3), 19–31.

Irwin, G.R., 1958. *The crack-extension-force for a crack at a free surface boundary*. NRL report 5120. Washington, DC: Naval Research Laboratory.

Kim, S. and Frangopol, D.M., 2011a. Inspection and monitoring planning for RC structures based on minimization of expected damage detection delay. *Probabilistic Engineering Mechanics*, 26 (2), 308–320.

Kim, S. and Frangopol, D.M., 2011b. Optimum inspection planning for minimizing fatigue damage detection delay of ship hull structures. *International Journal of Fatigue*, 33 (3), 448–459.

Kwon, K. and Frangopol, D.M., 2010. Bridge fatigue reliability assessment using probability density functions of equivalent stress range based on field monitoring data. *International Journal of Fatigue*, 32 (8), 1221–1232.

Madsen, H.O., *et al.*, 1987. Probabilistic fatigue crack growth analysis of offshore structures, with reliability updating through inspection. *In*: *Proceedings of the marine structural reliability symposium*, 5–8 October 1987. Arlington, VA: SSC/SNAME, 45–55.

Madsen, H.O. and Sørensen, J.D., 1990. Probability-based optimization of fatigue design, inspection and maintenance. *In*: *Proceedings of the 4th international symposium on integrity of offshore structures*, 2–3 July 1990. London: Elsevier, 421–432.

Madsen, H.O., Torhaug, R., and Cramer, E.H., 1991. Probability-based cost benefit analysis of fatigue design, inspection and maintenance. *In*: *Proceedings of the marine structural inspection, maintenance and monitoring symposium*, 18–19 March 1991. Arlington, VA: SSC/SNAME, II.E.1–II.E.12.

Moan, T., 2005. Reliability-based management of inspection, maintenance and repair of offshore structures. *Structure and Infrastructure Engineering*, 1 (1), 33–62.

Moan, T., 2011. Life-cycle assessment of marine civil engineering structures. *Structure and Infrastructure Engineering*, 7 (1–2), 11–32.

Mohanty, J.R., Verma, B.B., and Ray, P.K., 2009. Prediction of fatigue crack growth and residual life using an exponential model: part I (constant amplitude loading). *International Journal of Fatigue*, 31 (3), 418–424.

Mori, Y. and Ellingwood, B.R., 1994a. Maintaining reliability of concrete structures. I: role of inspection/repair. *Journal of Structural Engineering*, 120 (3), 824–845.

Mori, Y. and Ellingwood, B.R., 1994b. Maintaining reliability of concrete structures. II: optimum inspection/repair. *Journal of Structural Engineering*, 120 (3), 846–862.

Packman, P.F., *et al.*, 1969. Definition of fatigue cracks through nondestructive testing. *Journal of Materials*, 4 (3), 666–700.

Paris, P.C. and Erdogan, F.A., 1963. Critical analysis of crack propagation laws. *Journal of Basic Engineering*, 85 (4), 528–534.

Schijve, J., 2003. Fatigue of structures and materials in the 20th century and the state of the art. *International Journal of Fatigue*, 25 (8), 679–702.

Shetty, N.K. and Baker, M.J., 1990. Fatigue reliability of tubular joints in offshore structures: reliability analysis. *In*: *Proceedings of the 9th international conference on offshore mechanics and arctic engineering*, 18–23 February 1990. Vol. 2. Houston, USA: ASME, 231–239.

Sobczyk, K., 1987. Stochastic models for fatigue damage of materials. *Advances in Applied Probability*, 19 (3), 652–673.

Appendix VIII

Dan M. Frangopol, Paolo Bocchini, Alberto Decò, Sunyong Kim, Kihon Kwon, Nader M. Okasha, Duygu Saydam, Integrated life-cycle framework for maintenance, monitoring, and reliability of naval ship structures, *Naval Engineering Journal*, 124(1): 89-99, 2012.

Dr. Dan M. Frangopol, Dr. Paolo Bocchini, Alberto Decò, Dr. Sunyong Kim, Dr. Kihyon Kwon, Dr. Nader M. Okasha, Duygu Saydam
Department of Civil and Environmental Engineering, Lehigh University

Integrated Life-Cycle Framework for Maintenance, Monitoring, and Reliability of Naval Ship Structures

ABSTRACT

In the field of Naval Engineering, the use of life-cycle analyses associated with the concept of aging and time-dependent reliability has recently gained momentum. In this regard, the U.S. Office of Naval Research supports a project at Lehigh University focused on the development of an integrated life-cycle framework for ship reliability assessment, redundancy estimation, damage detection, and optimum inspection planning.

This paper presents some of the results obtained at Lehigh University within this project, with emphasis on structural health monitoring and life-cycle analysis under uncertainty.

KEYWORDS

Life-Cycle
Reliability
Redundancy
Maintenance
Monitoring
Ships
Damage Detection
Optimization

Introduction

The modeling, assessment, and performance prediction of ship structures over time is, by its very nature, complex and uncertain. Uncertainty in modeling of structures and randomness in loading phenomena dictate the use of probabilistic methods in life-cycle analysis. Since models that treat this issue are very sensitive to changes in their input parameters, structural health monitoring (SHM) provides a powerful and necessary mechanism to reduce uncertainty, calibrate, and improve structural assessment and performance prediction models. Ultimately, optimal decisions are to be made that ensure the continuous safety during lifetime of naval ships with minimum associated expected life-cycle cost. Only a properly integrated probabilistic framework can yield such optimum decisions.

Figure 1 shows the typical time-dependent profile of a structural performance index of a ship (or any other structure) along the life-cycle. After an initial period during which the performance index (e.g., the reliability index) is approximately constant, the effects of material aging, deterioration, corrosion, fatigue, and other stressors begin to negatively affect the performance. If no actions are taken, this trend eventually brings the performance index below a minimum acceptable threshold. To avoid this event, preventive (i.e., before reaching the threshold) or essential (i.e., when reaching the threshold) maintenance actions should be applied. Unfortunately, the parameters of the performance model (e.g., initial value), of the deterioration model (e.g., time of initiation and deterioration rate), and of the maintenance effects (e.g., improvement in the performance, temporary reduction of the deterioration rate) are uncertain. These uncertainties propagate during the service life of the investigated ship. Therefore, the service life itself is uncertain.

Along this line, the U.S. Office of Naval Research supports a project at Lehigh University focused on the development of an integrated life-cycle framework for maintenance, monitoring, and reliability of naval ship structures. Several results have been obtained and published in international peer-reviewed journals [1-6]. Even though each paper can be seen as an individual contribution to the advancement of the research, they collectively belong to the same framework. Frangopol et al. [7] presented a qualitative overview of the proposed approach where each of the individual contributions is contextualized. The matrix represented in Figure 2 is meant to fulfill the same task.

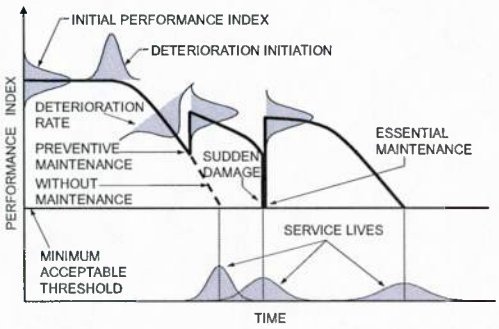

FIGURE 1 Time-dependent profile of a performance index (e.g., reliability index) along the life-cycle.

The papers indicated in Figure 2 collectively deal with four applications. The first one is the HSV-2 high speed naval craft, wave piercing catamaran [1, 8]. The second application is a joint high-speed sealift ship (JHSS) [4, 5]. Data for this application were collected on a scaled down model [9]. The third application is a typical mono-hull tanker section [3, 6, 10]. Finally, a sample hull was used to demonstrate the methodology presented in paper [2]. The main research topics that have been addressed are reliability, redundancy, structural health monitoring, fatigue, damage detection, and optimization.

The matrix in Figure 2 provides a graphical representation of the topics covered and applications presented by each article developed within the previously mentioned research project. In the reminder of this paper, some of the results that have been obtained are summarized not only from a qualitative point of view, but also with the numerical results obtained for each application.

SHM DATA PROCESSING

Reliability of naval structures can be assessed at key locations using monitoring data. These locations should be identified based on finite element analysis and engineering judgment. A high speed naval craft, HSV-2, was instrumented with various types of sensors, placed throughout the ship, to monitor and evaluate its response and performance [8]. The HSV-2 is a high speed, wave-piercing catamaran. During sea trials, the ship was operated in a manner such that data were collected at specific speed, heading, and sea state combinations. A total of 16 strain gages were dedicated to measure responses due to primary (global) wave loads. Okasha et al. [1] performed reliability analysis and damage detection of HSV-2 using the monitoring data collected by six of these sensors (T1-5 and T1-8 on Frame 24; T1-6 and T1-9 on Frame 46; T1-7 and T1-10 on Frame 61).

	HSV-2	JHSS	TANKER	SAMPLE HULL
RELIABILITY	[1]	[4, 5]	[3]	[2]
REDUNDANCY		[4]	[3]	
SHM	[1]	[4, 5]	[6]	
FATIGUE		[5]	[6]	
DAMAGE DETECTION	[1]		[6]	
OPTIMIZATION			[6]	[2]

FIGURE 2 Matrix of paper topics and applications.

The reliability of HSV-2 was quantified in terms of the strains induced by the global longitudinal bending moments recorded during the rough sea trials. Due to the speed of the ship, whipping strains caused by slamming impacts were also considered. The limit state equation at a predetermined key location in terms of the strain can be expressed as

$$g = x_R \varepsilon_R - x_w (\varepsilon_w + k_d \varepsilon_d) = 0 \quad (1)$$

where g is the performance function; ε_R is the resisting strain; ε_w and ε_d are the strains produced by the wave-induced bending moment and the dynamic load effects, respectively; x_R is the model uncertainty associated with the resisting strain; x_w is the model uncertainty associated with the wave-induced load effect prediction; and k_d is the correlation coefficient between wave-induced moment and dynamic load effects.

The recorded monitoring signals include the combined effects of the high-frequency waves due to slamming and the low-frequency waves. In order to perform the reliability analysis using the limit state in Eq. (1), the low-frequency and high-frequency strains need to be filtered. Figure 3(a) and (b) illustrate the hypothetical time history of the combined strains and filtered low-frequency and high-frequency strains, respectively.

The peak strains from filtered low-frequency and high-frequency signals in both sagging and hogging were extracted using a peak extraction algorithm. Kolmogorov– Smirnov tests were performed in order to find the best statistical distributions that fit these peak strain values. It

was concluded that the Rayleigh distribution and the exponential distribution provide a good fit for the low-frequency and high-frequency peaks, respectively.

For the reliability analysis, the maxima among the peak values — in other words, the upper tail behavior of these distributions — is of interest. Therefore, the obtained results were extrapolated using extreme value statistics. The largest values of both the Rayleigh and exponential distributions asymptotically converge to the Type I extreme value distribution

$$f_{L_n}(l)=\alpha_n e^{-\alpha_n(l-u_n)}\exp\left[-e^{-\alpha_n(l-u_n)}\right] \qquad (2)$$

where u_n is the characteristic largest value of the initial variate L, and α_n is an inverse measure of the dispersion of L_n. The parameters of the Type I extreme value for the Rayleigh distribution (low-frequency peak strains in sagging and hogging) and exponential distribution (high-frequency peak strains in sagging and hogging) were obtained. The resisting strain, ε_R, was assumed to follow a lognormal distribution with a mean value of 870 μ in/in [8] and coefficient of variation of 0.10.

The reliability analyses of the ship structure at various speeds, heading angles, sea states, and locations were carried out using the second order reliability method. Figure 4(a) presents the variation of the probability of failure with respect to speed and sea state with heading angle of 0° at frame 24 in sagging. The margin between the probabilities of failure in different sea states tends to increase with the higher vessel speed. Figure 4(b) illustrates the variation of probability of failure with respect to heading angle and sea state with speed of 20 knots at frame 24 in sagging. The lowest probability of failure is obtained for a heading angle of 90°, where the vessel is parallel to the waves, since the effects of longitudinal bending moments are less significant in this case. Figure 4(c) shows the variation of probability of failure with respect to frame position for speed of 20 knots, sea state 5, and heading angle 0° in sagging. Probability of failure increases when the key location is closer to the mid-hull region (around frames 25-45). This is expected since the limit state considered is in terms of strains due to longitudinal bending moments.

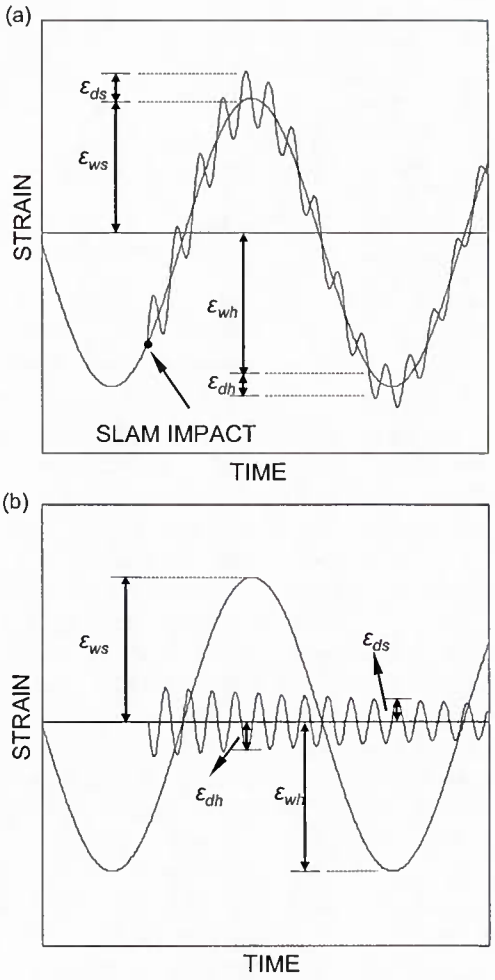

FIGURE 3
(a) Hypothetical time history of the combined strains, and (b) filtered low-frequency and high-frequency signals, adapted from [1].

PROBABILISTIC HULL STRENGTH

Classical incremental-curvature method based on the International Association of Classification Societies (IACS) guidelines or simple progressive collapse method developed by Hughes [11] (in which failed stiffened panels do not carry any loads and are progressively removed), can be adopted for the probabilistic assessment of the hull strength. However, these techniques are computationally demanding. Indeed, these approaches lead to a high computational time, especially when dealing with a large number of generated samples associated with the basic random variables. For this reason, Okasha and Frangopol [2] proposed a new optimization-based technique able to significantly reduce the computational time and to provide results that

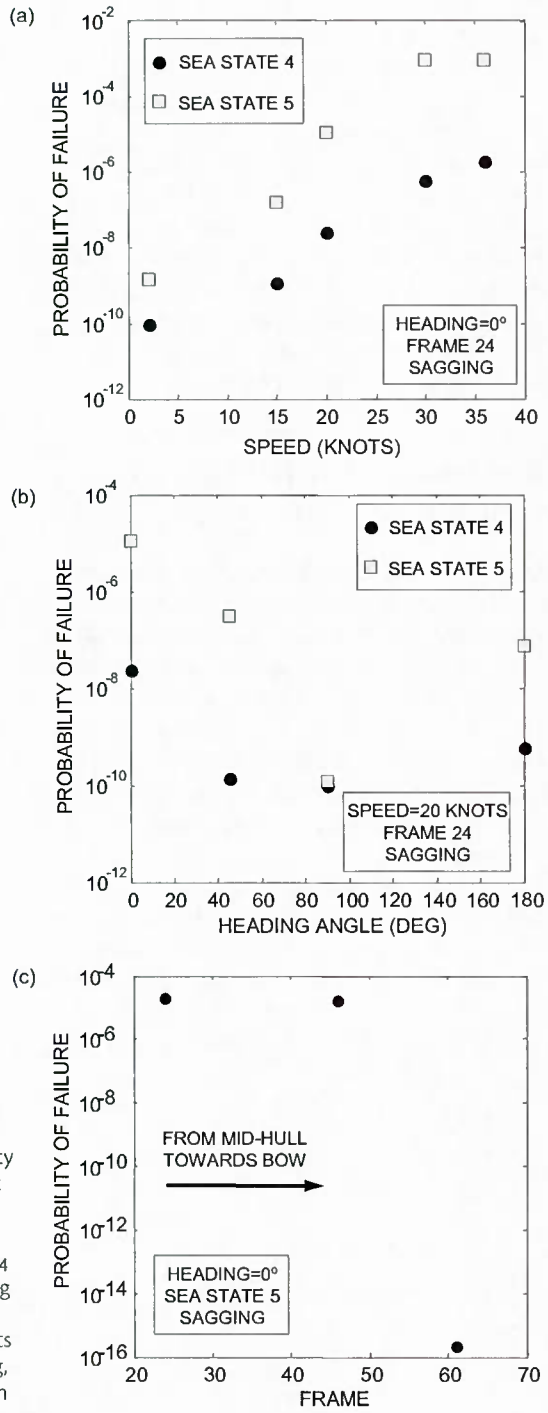

FIGURE 4
Variation of probability of failure with respect to (a) speed and sea state with heading angle of 0° at frame 24 in sagging, (b) heading angle and sea state with speed of 20 knots at frame 24 in sagging, and (c) frame position for speed of 20 knots, sea state 5 and heading angle 0° in sagging.

are as accurate as the ones of the incremental-curvature method.

In summary, the proposed approach treats the moment-curvature relationship as a non-linear implicit function to be optimized. Any given curvature κ is associated with a corresponding flexural capacity $M(\kappa)$ that is evaluated by applying the method recommended by IACS. Hence, the value of the curvature, that maximizes its associated bending moment, is found by applying an optimization search algorithm. Indeed, among a large number of discrete values of curvature, in few steps, $M(\kappa)$ is evaluated in order to determine which of such discrete values provides the maximum bending moment. The clear difference is that instead of obtaining a complete moment-curvature curve, only few values are evaluated and the procedure ends when the maximum moment is found.

The method proposed by Okasha and Frangopol [2] has been validated by investigating the ultimate flexural capacity of a box girder analyzed by considering both the incremental-curvature method and the optimization approach. Figure 5 shows the complete moment-curvature relationship for the box girder and the steps required to find the ultimate flexural capacity by the optimization technique. It was demonstrated that the great reduction in time fully justified the use of this advanced technique for the probabilistic strength assessment. More detailed explanations about this topic can be found in [2]. Subsequent studies successfully applied such technique to existing ship cross-sections [3, 4].

LIFE-CYCLE RELIABILITY AND REDUNDANCY

Safety of ship structures must be ensured over their entire life. In this context, life-cycle analyses must account for the evaluation of ship performance over time. Maintaining an adequate level of ship reliability and structural redundancy becomes the main issue in order to ensure satisfactory ship performance over its operational lifetime.

Reliability of ship structures is a topic that has been extensively investigated over the last decades. Generally, reliability is investigated with regard to ultimate flexural failure of the midship section [12, 13].

The ultimate collapse of a ship hull occurs only when its ultimate flexural capacity has been reached. This usually involves the failure of multiple components. However, collapse of redundant ship structures is preceded by the failure of a sequence of stiffened panels. In this context, the evaluation of the reliability associated with the occurrence of the first failure within the box girder becomes of critical importance in order to evaluate redundancy [3]. Indeed, the range between the capacity at which the first failure occurs and the ultimate capacity can be used to quantify structural redundancy [14], which provides warnings before failure. Moreover, a high level of redundancy can prevent sudden failure and mitigate the effects generated by unpredictable events.

Performance prediction requires the time-dependent assessment of reliability and redundancy [3]. Over time, the hull flexural capacity decay is mainly due to corrosion effects that reduce the thickness of plates throughout the hull girder. The corrosion model used is [12]

$$r(t)=C_1(t-t_o)^{C_2} \tag{3}$$

where $r(t)$ is the thickness loss (mm); t_o is the initiation time depending on coating life (years); C_1 is the annual corrosion rate (mm/years); C_2 is a constant; and t is the time expressed in years.

Time-variant reliabilities with respect to the first and ultimate failures have been assessed. The limit state function associated with the flexural failure mode is [15]

$$g(t)=x_R M(t)-x_{sw}M_{sw}-x_w M_w=0 \tag{4}$$

where $g(t)$ is the time-variant performance function; $M(t)$ is the time-variant resisting bending moment (associated with first or ultimate failure for sagging or hogging); M_{sw} is the still water bending moment; M_w is the wave-induced bending moment; x_R is the model uncertainty associated with the resistance determination; x_{sw} is the model uncertainty related to the still water bending moment prediction; and x_w is the model uncertainty associated with the wave-induced bending moment prediction.

Time-variant redundancy index $RI(t)$ was previously investigated for civil structures [16], and its definition has been extended to the case of ship structures [3]

$$RI(t)=\frac{P_{f,FFM}(t)-P_{f,UFM}(t)}{P_{f,UFM}(t)} \tag{5}$$

where $P_{f,UFM}(t)$ is the probability of the ultimate failure moment of the whole hull and $P_{f,FFM}(t)$ is the probability associated with the occurrence of first failure in the hull.

The time-variant reliability and redundancy have been assessed for an existing ship structure [3]. The results obtained are summarized in Figure 6. Time-variant failure probabilities with respect to first and ultimate failure for sagging are shown in Figures 6(a), while Figure 6(b) shows the profile of the redundancy index for both sagging and hogging bending moments.

SHM FOR RELIABILITY AND REDUNDANCY UPDATING

During its lifetime, a ship structure experiences loads of different magnitudes depending on the incurred sea state, ship speed, and heading angle. In order to provide an accurate assessment of the ship structural performance, SHM plays a role of crucial relevance. SHM provides an efficient tool for the collection of accurate field information regarding the operational loads and detects potential structural damage once it occurs.

In general, useful information, such as measured strains, may be converted to global ship responses. In this way, time-variant structural performance indicators, such as reliability and redundancy, can be updated by using the collected new information provided by the installed sensors [4].

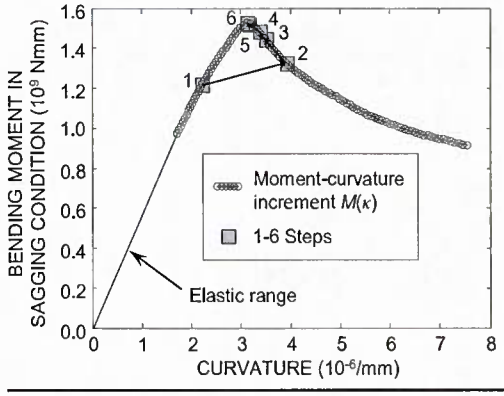

FIGURE 5
Ultimate flexural capacity evaluated with both incremental-curvature method and optimization approach, adapted from [2].

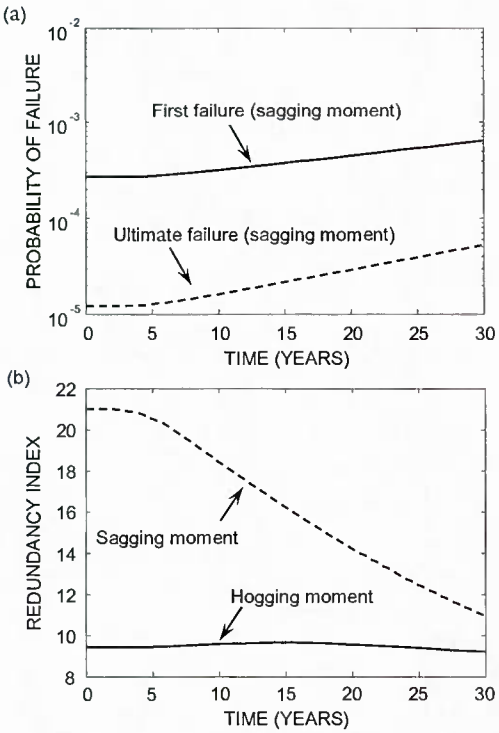

FIGURE 6
Time-variant (a) first failure and ultimate failure probability for sagging; (b) redundancy index for sagging and hogging, adapted from [3].

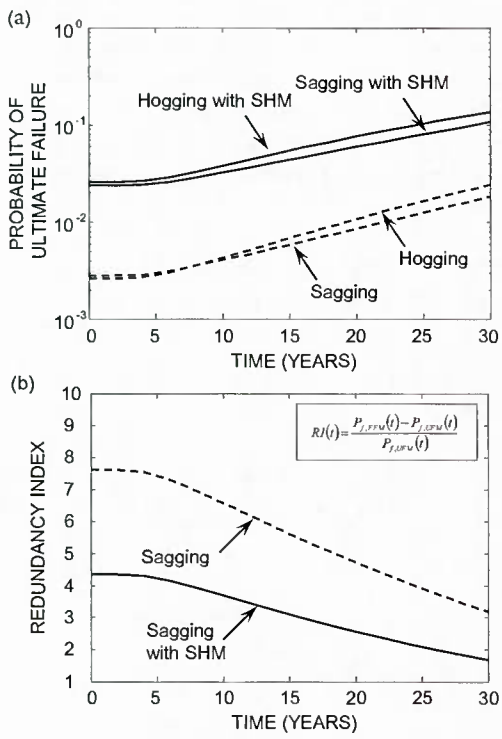

FIGURE 7
(a) Time-variant ultimate failure probability for sagging and hogging with and without SHM; (b) time-variant redundancy index for sagging with and without SHM, adapted from [4].

If monitoring information is not available, design code equations provide conservative estimations of the wave-induced load effects. This analysis leads to the evaluation of code-based reliability and redundancy, forming the so-called "prior information". Following the collection of new data, prior information is updated by using Bayesian inference [4].

This specific implementation of the Bayesian updating procedure is presented in [4], where the performance of the JHSS has been investigated. The model consists of a continuous aluminum backspline beam connected with shell sections in order to guarantee realistic vibrational responses including primary and secondary load effects (such as slam-induced whipping). The obtained signal has been filtered in order to evaluate the separate effects of low and high frequency waves. The collected data, used for the updating of the low frequency wave-induced loads, refer to sea state 7, 35 knot speed, and head seas, which correspond to the worst operational conditions that the ship is expected to encounter. With the use of SHM data, the limit state equation associated with the flexural failure mode becomes

$$g(t)=x_R M(t)-x_{SW} M_{SW}-x_W(M_W+k_d M_d)=0 \quad (6)$$

where M_d is the dynamic bending moment and k_d is the correlation coefficient between wave-induced and dynamic bending moments.

The results obtained by the prior analysis and the mentioned updating process are expressed in terms of time-variant failure probability and redundancy index. Figure 7(a) shows the time-variant profiles of the probability of ultimate failure associated with sagging and hogging with and without SHM. Figure 7(b) shows the time-variant profiles of the redundancy index.

A detailed explanation of the updating procedure and further explanation about the obtained results can be found in [4, 17].

FATIGUE RELIABILITY ASSESSMENT

The structural deterioration process due to fatigue significantly diminishes the service life of ship structures. Assessment and prediction of the structural performance of ships subjected

to fatigue generally include high uncertainties associated with sea loadings and fatigue. Hence, a probabilistic approach is well suited for fatigue reliability assessment and performance prediction of ship structures.

The steps for the fatigue reliability evaluation are: (a) classify the details of structural members for the S-N approach; (b) estimate the wave-induced and slamming-induced whipping responses by filtering at low and high frequency levels; (c) establish stress range histograms and probability density functions (PDF) by using a peak counting method from the unfiltered or filtered data at selected locations; (d) predict the probabilistic lifetime sea loads and estimate the cumulative number of cycles; and (e) perform a fatigue reliability analysis [5].

The histogram and the best-fitted PDF of stress range for a ship structural member under the hurricane loading state are shown in Figure 8. Based on this histogram, individual effective stress ranges according to given wave conditions (which are related to ship characteristics, ship speeds, relative wave headings, and sea states) can be computed and used to estimate the predicted effective stress range, considering all possible ship operational conditions. Figure 9 shows the number of cycles averaged daily for each test run under the hurricane loading state. The results from Figures 8 and 9 are used to estimate the effective stress range and the cumulative number of cycles for fatigue analysis.

The fatigue reliability index is shown in Figure 10. From this figure, it can be seen that the fatigue life of the ship decreases significantly when the ship operation rate α increases. Furthermore, the effect of low and high frequency loadings on lifetime fatigue reliability can be found [5].

Based on the probabilistic approach proposed in [5, 18], fatigue performance assessment and service life prediction of ship structures can be rationally estimated using monitoring data.

OPTIMAL INSPECTION PLANNING

Repair actions are affected by inspection results. In order to apply timely and effective repair actions, the expected damage detection delay should be minimized. A rational probabilistic approach for optimum inspection planning was presented in [6]. This planning is a solution of an optimization problem with the objective of minimizing the expected damage detection delay. Formulation of the expected damage detection delay includes uncertainties associated with damage initiation and propagation, and inspection method.

As previously mentioned, fatigue is one of the main deterioration mechanisms for ship structures. The fatigue crack can be affected by several factors such as location and length of

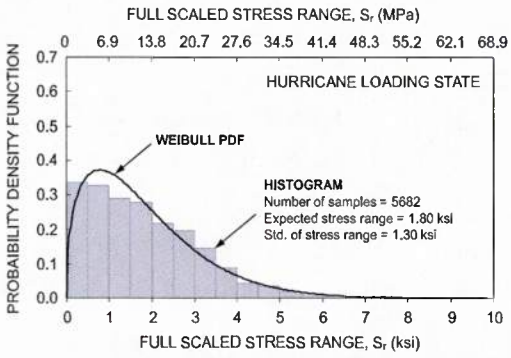

FIGURE 8
Histogram and Weibull PDF of stress range, adapted from [5].

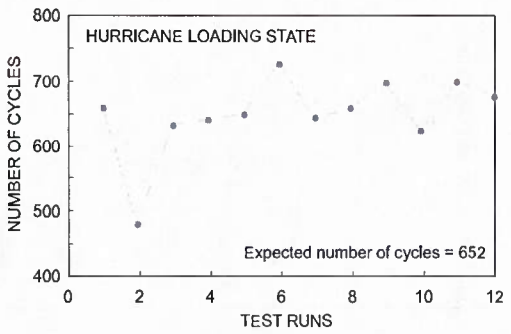

FIGURE 9
Number of cycles associated with hurricane loading, adapted from [5].

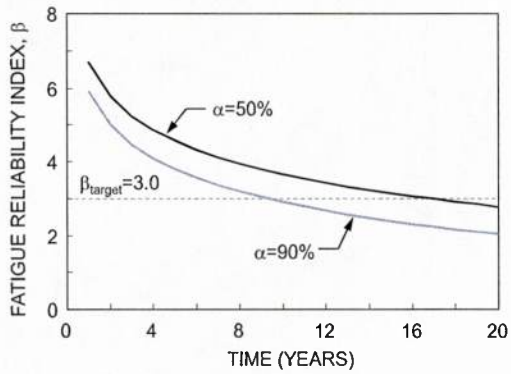

FIGURE 10
Time-dependent reliability index when operation rate α = 50% and 90%, adapted from [5].

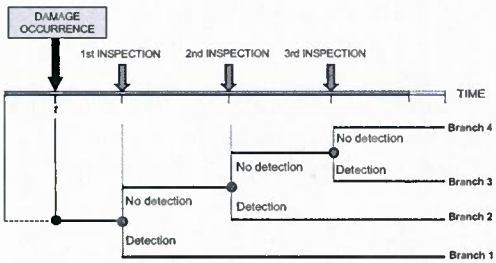

FIGURE 11 Event tree model for the expected damage detection delay, adapted from [6].

initial crack, stress range near the initial crack, number of cycles associated with the stress range, and material and geometrical properties. Among these factors, the selection of material types (e.g., aluminum, high strength, or mild steels) and frame spacing can be considered as the two primary decisions associated with fatigue life expectancy of the hull. This is because aluminum, used to improve the ship operational capabilities, can be more susceptible to fatigue cracking than steel [19], and fatigue cracking is very common in the connections between the transverse web frames and the longitudinal stiffeners [20]. Due to the mentioned sources of uncertainty, a probabilistic approach should be used to predict fatigue crack damage.

The probability of detection is determined by the quality of the inspection method. The relation between probability of detection and fatigue crack size can be expressed by a detectability function. This function has several representative forms, such as shifted exponential distribution, logistic curve, and normal cumulative distribution.

Figure 11 shows the event tree model when the damage occurs before the first inspection. This event tree includes the probability of damage detection. Furthermore, damage occurrence time can be treated as a continuous random variable described by its PDF. Finally, the expected damage detection delay can be formulated as indicated in [6]. The inspection planning is obtained from an optimization problem by minimizing the expected damage detection delay.

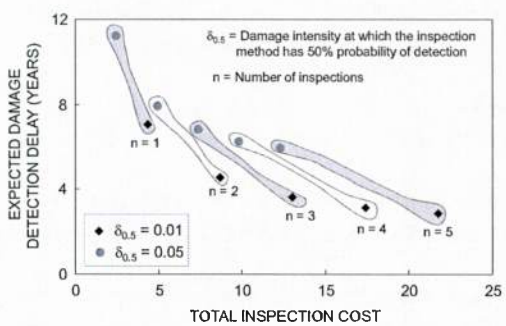

FIGURE 12 Relation between expected damage detection delay and total inspection cost, adapted from [6].

The relation between expected damage detection delay and total inspection cost is presented in Figure 12. In order to find a well-balanced solution associated with the conflicting objectives of minimizing both expected damage detection delay and inspection cost, a bi-objective optimization can be performed. Decision makers have much flexibility to select the best compromise among the solutions provided by the Pareto set. Such a set is presented in Figure 13.

The approach provided in [6, 21] can be extended to optimum monitoring planning and combined inspection / monitoring planning for ship structures.

Conclusions

This paper has collected and summarized a set of recent research results and applications. Their individual use leads to enhancements in the assessment of the conditions and planning of maintenance for naval ship structures. More importantly, their combination provides most of the necessary components of a comprehensive probabilistic life-cycle framework for maintenance, monitoring, and reliability assessment.

The first contribution consists of a technique for the effective post-processing of structural health monitoring data to be used in reliability analysis and damage detection of ship structures. The second contribution is a computationally efficient technique for the assessment of the hull strength probability distribution. The third original result is a methodology able to perform the ship reliability and redundancy assessment. Similarly, the fourth contribution exploits SHM to update the life-cycle structural reliability and redundancy prediction for the ship. The fifth contribution focuses on fatigue reliability assessment and residual fatigue life prediction. Finally, a technique for the optimal planning of inspections and monitoring has been described.

Among the further possible developments of these methodologies and their combination is a tool for the near real-time reliability assessment of ship structures as a function of the current

operating conditions (i.e., ship speed, sea state, relative heading angle). Such a tool can continuously collect information from sensors located on the ship and associate it with the ship operating conditions. By combining this information with the methodologies previously presented, it is possible to constantly update the reliability estimation, and to provide the crew with plots of the reliability as a function of the operating conditions. Moreover, such a system can alert the crew if the reliability index down-crosses a minimum acceptable threshold for a certain cross-section of the hull and set of operating conditions. Depending on the reliability level, the crew members can decide to avoid some particularly dangerous operating conditions indicated by the tool (e.g., reducing the speed or avoiding a range of heading angles) and either continue the mission or abort it.

Besides the future plans of the life-cycle reliability and optimization research group at Lehigh University that developed all the presented tools, further integrated use is likely to lead to other scientific advancements and practical applications that are not possible to foresee.

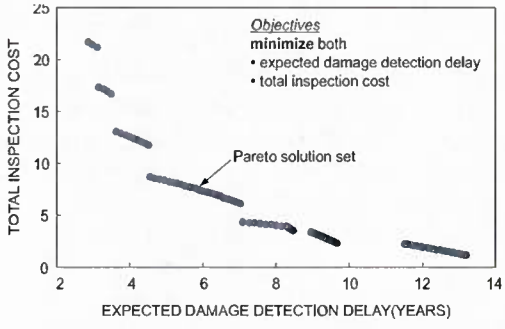

FIGURE 13
Pareto solution set for optimum inspection plan, adapted from [6].

REFERENCES

[1] Nader M. Okasha, Dan M. Frangopol, Duygu Saydam, and Liming W. Salvino. Reliability analysis and damage detection in high-speed naval craft based on structural health monitoring data. *Structural Health Monitoring*, 10(4): 361-379, 2011.

[2] Nader M. Okasha and Dan M. Frangopol. "Efficient Method Based on Optimization and Simulation for the Probabilistic Strength Computation of the Ship Hull". *Journal of Ship Research*, 54(4): 244–256, 2010.

[3] Alberto Decò, Dan M. Frangopol, and Nader M. Okasha. Time-variant Redundancy of Ship Structures. *Journal of Ship Research*, 55(3): 208-219, 2011.

[4] Nader M. Okasha, Dan M. Frangopol, and Alberto Decò. Integration of structural health monitoring in life-cycle performance assessment of ship structures under uncertainty. *Marine Structures*, 23(3): 303–321, 2010.

[5] Kihyon Kwon, Dan M. Frangopol, and Sunyong Kim. Fatigue performance assessment and service life prediction of high-speed ship structures based on probabilistic lifetime sea loads. *Structure and Infrastructure Engineering*, in press and already available online, DOI: 10.1080/15732479.2010.524984.

[6] Sunyong Kim and Dan M. Frangopol. Optimum inspection planning for minimizing fatigue damage detection delay of ship hull structures. *International Journal of Fatigue*, 33(3): 448–459, 2011.

[7] Dan M. Frangopol, Paolo Bocchini, Alberto Decò, Sunyong Kim, Kihon Kwon, Nader M. Okasha, Duygu Saydam, and Liming W. Salvino. Life-cycle ship reliability assessment, damage detection, and optimization. In *Proceedings of the 11th International Conference on Fast Sea Transportation - FAST 2011*, Honolulu, HI, USA, September 26-29, 2011.

[8] Thomas F. Brady. Global Structural Response Measurement of SWIFT (HSV-2) from JLOTS and Blue Game Rough Water Trials. NSWCCD-65-TR-2004/33, Naval Surface Warfare Center, Carderock Division, West Bethesda, MD, 2004.

[9] Edward A. Devine. An overview of the recently-completed JHSS monohull and trimaran structural seaways loads test program. Naval Surface Warfare Center, Carderock Division (NSWCCD), PowerPoint Briefing, 30 October, 2009.

[10] Carlos Guedes Soares and Yordan Garbatov. Fatigue reliability of the ship hull girder. *Marine Structures*, 9(3-4): 495-516, 1996.

[11] Owen F. Hughes. *Ship structural design: a rationally-based, computer-aided, optimization approach*. Wiley and Sons, New York, 1983.

[12] Unyime O. Akpan, Tamunoiyala S. Koko, Bilal M. Ayyub, and Timothy E. Dunbar. Risk assessment of aging ship hull structures in the presence of corrosion and fatigue. *Marine Structures*, 15(3): 211-231, 2002.

[13] Bilal M. Ayyub, Ibrahim A. Assakkaf, Jerome P. Sikora, John C. Adamchak, Khaled Atua, William Melton, and Paul E. Hess. Reliability-based load and resistance factor design (LRFD) guidelines for hull girder bending. *Naval Engineers Journal*, 114(2): 43-68, 2002.

[14] Samer Hendawi and Dan M. Frangopol. System reliability and redundancy in structural design and evaluation. *Structural Safety*, 16(1-2): 47-71, 1994.

[15] Jeom K. Paik and Paul A. Frieze. Ship structural safety and reliability. *Progress in Structural Engineering and Materials*, 3(2): 198-210, 2001.

[16] Nader M. Okasha and Dan M. Frangopol. Time-variant redundancy of structural systems. *Structure and Infrastructure Engineering*, 6(1-2): 279-301, 2010.

[17] Nader M. Okasha. Integration of system-based performance measures and structural health monitoring for optimized structural management under uncertainty. Ph.D. Thesis, Lehigh University, September 2010.

[18] Kihyon Kwon. Reliability assessment, performance prediction and life-cycle management of fatigue sensitive structures based on field test data. Ph.D. Thesis, Lehigh University, May 2011.

[19] Robert A. Sielski. Research needs in aluminum structure. *Proceedings of the 10th International Symposium on Practical Design of Ships and Other Floating Structures*, Houston, Texas, USA, October 2007.

[20] Michael R. Andersen. Fatigue crack initiation and growth in ship structures. Department of Naval Architecture and Offshore Engineering, Technical University of Denmark, 1998.

[21] Sunyong Kim. Integrated life-cycle framework for optimal inspection, monitoring and maintenance under uncertainty: applications to highway bridges and naval ship structures. Ph.D. Thesis, Lehigh University, May 2011.

ACKNOWLEDGMENTS

The support of the U.S. Office of Naval Research (contract number N-00014-08-0188, Structural Reliability Program, Director Dr. Paul E. Hess III, ONR, Code 331) is gratefully acknowledged.

The authors wish to thank Mr. Edward A. Devine and Dr. Liming W. Salvino for the data they provided.

The opinions and conclusions presented in this paper are those of the writers and do not necessarily reflect the views of the sponsoring organization.

AUTHOR BIOGRAPHIES

DR. DAN M. FRANGOPOL *is the Fazlur R. Khan Endowed Chair of Structural Engineering and Architecture at Lehigh University. He coordinates a research group of more than ten people including Ph.D. students and other researchers. He received his bachelor's degree from the Institute of Civil Engineering, Bucharest, Romania, and his doctoral degree from the University of Liège, Belgium.*

DR. PAOLO BOCCHINI *is an Assistant Professor at the Department of Civil and Environmental Engineering at Lehigh University. His research interests deal with probabilistic concepts applied to Mechanics and Civil Engineering. He received his degrees (B.Sc., M.Sc., and Ph.D.) from the University of Bologna, Italy.*

ALBERTO DECÒ *is a Research Assistant and Ph.D. candidate at Lehigh University. His research focuses on performance assessment and risk analysis of structural systems. He received his B.Sc. and M.Sc. from the University of Bologna, Italy.*

DR. SUNYONG KIM *is a former Research Assistant and Research Associate at Lehigh University. His research focuses on fracture mechanics, fatigue, and optimization. He received his B.Sc. degree from Yonsei University, Seoul, South Korea, his M.Sc. from KAIST (Korea Advanced Institute of Science and Technology), Daejon, South Korea, and his Ph.D. from Lehigh University.*

DR. KIHYON KWON *is a former Research Assistant at Lehigh University. Dr. Kwon is a specialist in fatigue reliability and residual life estimation of ships and bridges. He received his B.Sc. degree from Ajou University, Suwon, South Korea, and his M.Sc. and Ph.D. from Lehigh University.*

DR. NADER M. OKASHA *is a former Research Assistant at Lehigh University. He works in the field of life-cycle reliability assessment of naval and civil structures. He received his B.Sc. degree from Birzeit University, Ramallah, Palestine, and his M.Sc. and Ph.D. from Lehigh University.*

DUYGU SAYDAM *is a Research Assistant and Ph.D. candidate at Lehigh University. He studies performance indicators applied to various types of systems, including civil and naval structures. He received his B.Sc. degree from the Istanbul Technical University, Turkey, and his M.Sc. from Bogazici University, Istanbul, Turkey.*

Appendix IX

Dan M. Frangopol, Paolo Bocchini, Alberto Decò, Sunyong Kim, Kihon Kwon, Nader M. Okasha, Duygu Saydam, and Liming W. Salvino. Life-cycle ship reliability assessment, damage detection, and optimization. In *Proceedings of the 11th International Conference on Fast Sea Transportation - FAST 2011*, Honolulu, HI, USA, September 26-29, 2011.

11th International Conference on Fast Sea Transportation
FAST 2011, Honolulu, Hawaii, USA, September 2011

Life-Cycle Ship Reliability Assessment, Damage Detection, and Optimization

Dan M. Frangopol[1], Paolo Bocchini[1], Alberto Decò[1], Sunyong Kim[1], Kihyon Kwon[1], Nader M. Okasha[2], Duygu Saydam[1], and Liming W. Salvino[3]

[1]Engineering Research Center for Advanced Technology for Large Structural Systems (ATLSS), Department of Civil and Environmental Engineering, Lehigh University, Bethlehem, PA 18015, USA
[2]Formerly, Engineering Research Center for Advanced Technology for Large Structural Systems (ATLSS), Department of Civil and Environmental Engineering, Lehigh University, Bethlehem, PA 18015, USA
[3]Structures and Composite (Code 652), Naval Surface Warfare Center, Carderock Division, 9500 MacArthur Boulevard, West Bethesda, MD 20817-5700, USA

ABSTRACT

The present paper collects a body of scientific results obtained at Lehigh University, under the sponsorship of the U.S. Office of Naval Research. The aim of the entire research project was to build a general framework for the probabilistic analysis of ship structures in terms of reliability, redundancy, fatigue, material deterioration, damage detection, monitoring, and inspection optimization. Several articles published in international peer-reviewed journals by the first author and his co-workers address the previously mentioned sub-topics. This paper provides an overview of the results, presents the integrated approach that is being developed, and suggests future lines of research.

KEY WORDS

Life-cycle, reliability, monitoring, fatigue, damage detection, optimization.

1.0 INTRODUCTION

In 2008, a research team led by Dan M. Frangopol at Lehigh University started a research project aimed at developing an integrated life-cycle framework (ILF) for maintenance-monitoring-management of naval ship structures under uncertainty considering multiple and conflicting objectives. After a couple of years, several modules of the ILF have been completed and the most interesting results have been published in international journals.

The first part of this paper summarizes the general framework and the approach that all the proposed techniques share. Next, some results on fatigue reliability assessment and residual life estimation are presented. Then, a novel approach for the integration of structural health monitoring in reliability and redundancy assessment is described. Using monitoring data on strains under operation at selected locations, it is possible to assess the reliability of the ship for different speeds, sea states, and heading angles, for both sagging and hogging. Finally, a technique for the optimal planning of inspections is described.

Numerical applications on three existing ships are used to present and validate the proposed techniques.

In the concluding section, some future lines of research are also suggested.

2.0 INTEGRATED LIFE-CYCLE FRAMEWORK

The ILF for ships is represented in Fig. 1. The starting point is always a real application, such as a ship component or an entire ship structure. By means of appropriate analyses, it is possible to estimate the current reliability levels and predict the residual life of the investigated ship or component.

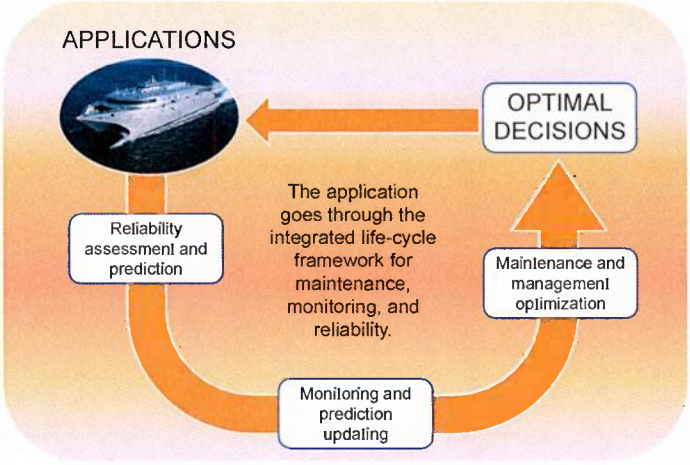

Fig. 1. General scheme of the integrated life-cycle framework for ships.

Then, the results based only on the ship design and the deterioration models (that include aging, corrosion, and fatigue) are combined with the information provided by structural monitoring, whenever available. This allows updating the initial assessment of the residual life and obtaining a more accurate prediction. In fact, generic deterioration models have proved to be adequate for structures and components that do not differ too much from those that have been used for the calibration of the model. A much more accurate assessment can be obtained by recalibrating the parameters of the model using data obtained directly from the investigated structure or component.

Next, optimization techniques can be applied to maximize the life-cycle performance and minimize the life-cycle cost. Decision makers can take advantage of their experience to select maintenance and management strategies, but when the analyzed application is very complex (such as the life-time analysis of a ship) and multiple objectives are involved (e.g. maximization of reliability, maximization of redundancy, minimization of the damage detection delay, minimization of the maintenance, inspection, and monitoring costs), an automatic tool is necessary to have an overall view and accurate comparison of the alternatives. In the proposed ILF, the multi-objective optimization provides a Pareto front (Deb 2001) of optimal solutions. Each solution belonging to the front represents a maintenance-monitoring-management strategy that satisfies all the constraints of the analysis (e.g. total cost lower than the available budget) and for which it is not possible to find a solution that improves one of the objectives without worsening at least another. Based on their expertise and engineering judgement, decision makers will choose the solution that best fits the specific application, among the various optimal ones.

Finally, the optimal decisions are applied to the investigated ship or component, so that the ILF can actually be effective and improve the quality of management and the performance of the fleet substantially. Fig. 1 represents the framework as a loop that starts and ends with a realistic application. The loop can be repeated multiple times across the life-cycle of a ship, updating the previous decisions based on the new information obtained through subsequent monitoring sessions.

The following sections present some of the results that have been obtained for individual modules of the described ILF.

3.0 RELIABILITY AND REDUNDANCY ASSESSMENT AND PREDICTION UPDATING BY MEANS OF STRUCTURAL HEALTH MONITORING

Okasha & Frangopol (2010) proposed a technique for the assessment of the ultimate capacity of a ship hull section subject to sagging and hogging moments. With respect to previous approaches based on the incremental curvature method (IACS 2008), the proposed technique produces a significant improvement of the computational efficiency. In fact, the incremental curvature method is based on repeated structural analyses for many values of the curvature to find the one that yields the highest bending moment. This is intrinsically an optimization problem and can be solved proficiently using techniques from operational research. In this way, rather than evaluating the bending moment of the cross-section for all the curvatures, it is evaluated at a very limited subset of values. In the case of complex ship hulls with many stiffeners and for analyses that include also the instability of the individual stiffeners, each moment-curvature computation is a demanding task. Therefore, the reduction of the number of moment computations from several hundreds to a few units results in a dramatic reduction of the CPU time.

This increase in the computational efficiency has enabled the use of simulation-based techniques for probabilistic analysis and reliability assessment. Otherwise, these techniques would have been computationally too demanding and impractical for real applications.

In particular, this technique was used by Okasha et al. (2010) and Decò et al. (2011) for the probabilistic characterization of the ultimate failure moment. In Okasha et al. (2010), a technique used Bayesian updating to combine the prior information on lifetime loading effects provided by IACS (2008) with structural health monitoring (SHM) data. Raw strain data measured in sea state 7 conditions by several sensors on the ship were processed to extract the information. First of all, the strain signal is decomposed into a high frequency component (that is associated with the slam impacts) and a low frequency component (associated with the wave induced moment). Then a peak extraction algorithm determines the number of cycles and the maximum values of the moments due to sagging and hogging, for both the low frequency and high frequency components. With these data, the probability density function (PDF) of the bending moments can be used to update the prior information. Once the PDFs of the external loads and of the capacity (e.g. ultimate moment, first yielding moment) are available, it is possible to perform a reliability analysis. Okasha et al. (2010) computed the reliability indices associated with first yielding and ultimate failure for a Joint High-Speed Sealift Ship (JHSS), based on SHM data collected on a scaled down model (Devine 2009) and using the second order reliability method (Liu et al. 1983) combined with Latin hypercube sampling (McKay et al. 1979).

In addition, by computing the probability of first yielding P_{fy} and ultimate failure P_{uf} along the life-cycle of the ship, it is possible to compute also the time-dependent redundancy index RI, defined as

$$RI(t) = \frac{P_{fy}(t) - P_{uf}(t)}{P_{uf}(t)} \quad (1)$$

where parameter t indicates time.

Plots over time of the reliability index and redundancy index of the ship structure are very useful to plan inspections, maintenance, SHM sessions, and, in general for the allocation of the available management budget. For

instance, Fig. 2 shows how redundancy varies over time differently for sagging and hogging bending moments. It was found that, depending on the ship geometry and accounting for the effects due to corrosion, redundancy may degrade, remain the same or even increase over time (Decò et al. 2011). The use of periodic prediction updating based on SHM data ensures that the deterioration models are constantly recalibrated to accurately represent the actual condition of the ship.

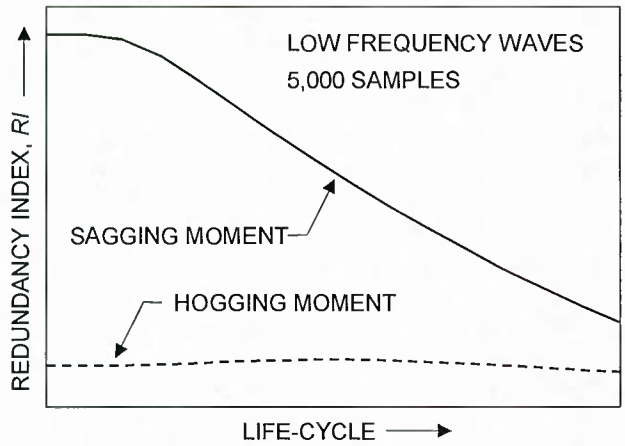

Fig. 2. Time-dependent redundancy index.

4.0 RESIDUAL-LIFE PREDICTION BASED ON FATIGUE AND RELIABILITY

The studies presented in the previous section dealt with the first two modules of the framework shown in Fig. 1 (i.e. reliability assessment and prediction; monitoring and prediction updating). Similarly, Kwon et al. (2011) provided a technique that covers the same two modules, but with a deeper insight on the effect of fatigue. In particular, a methodology for fatigue reliability assessment and service life prediction of high-speed ship structures based on the probabilistic lifetime sea loads estimated from model test data has been developed.

The classic S–N approach applied to selected structural details is used to estimate the structural capacity of the ship in terms of fatigue.

Then, model test SHM data are used to determine the stress range bin histogram by means of a peak counting method. A theoretical PDF is fitted to the stress range bin histogram by using the maximum likelihood method (the PDF family is selected by using the Kolmogorov-Smirnov goodness of fit test). Also in this case, the effects of low frequency wave-induced and high frequency slam-induced whipping loadings are investigated separately by using a signal filtering technique applied to the raw data. Ultimately, SHM data provide a probabilistic estimate of the lifetime sea loads in terms of load effects.

The approach is illustrated using data collected on the scaled JHSS monohull that was mentioned previously (Devine 2009). Several numerical results and sensitivity analyses have been performed and are presented in Kwon et al. (2011). For instance, Fig. 3 shows the evolution over a 20 year long life-cycle of the fatigue reliability index. As expected, if the annual operation rate α increases, the reliability index decreases. In any case, after a certain amount of years, that is accurately assessed by the proposed methodology, the reliability index down crosses a threshold that represents the minimum acceptable level. Before the occurrence of this event, maintenance actions should be applied to avoid failures. Fig. 4 shows the importance of combining low frequency wave-induced and high frequency slam-induced whipping loadings. In fact, if only one of the two load components is considered, the reliability index can be overestimated, thus being on the unconservative side.

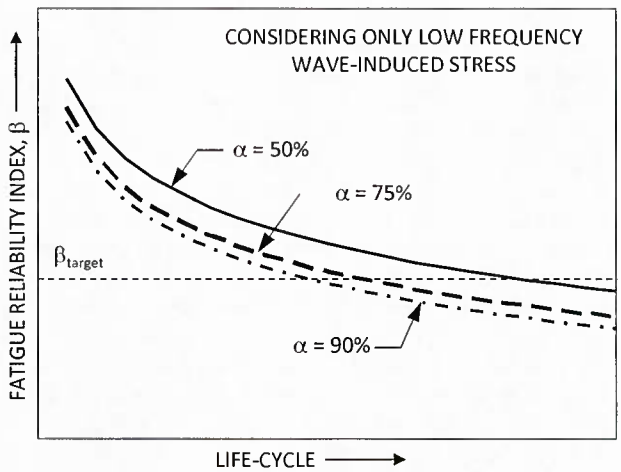

Fig. 3. Fatigue reliability index evolution along the life-cycle of the ship. For different annual operation rates α, the value of the reliability index and the time when the minimum acceptable reliability β_{target} is down crossed are different.

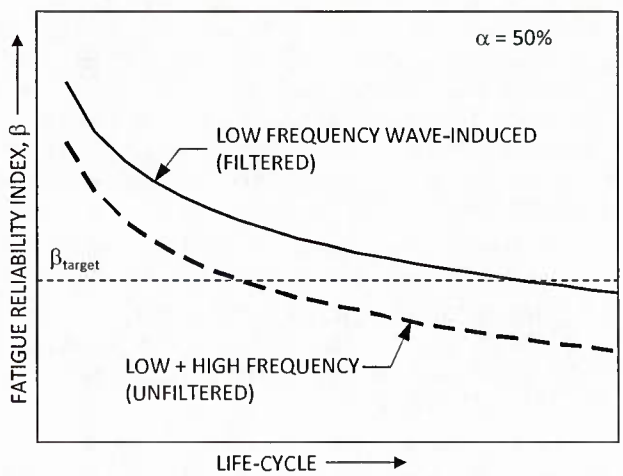

Fig. 4. Fatigue reliability index evolution along the life-cycle of the ship. Different effects induced by the low frequency waves alone and the combined low and high frequency stressors, for a fixed annual operation rate $\alpha = 50\%$.

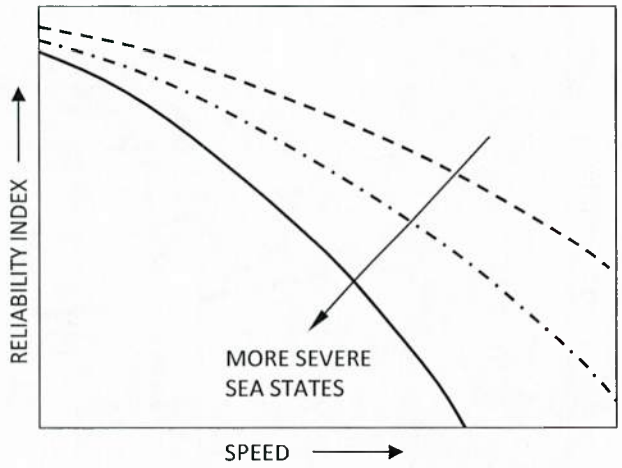

Fig. 5. Variation of reliability index at a point with respect to ship speed at different sea states at constant heading angle.

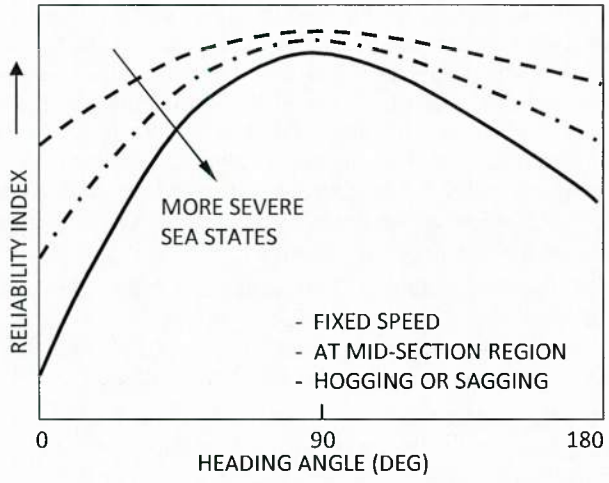

Fig. 6. Variation of reliability index at a point around mid-section with respect to heading at constant speed.

This detailed analysis on fatigue reliability can be repeated along the life-cycle of the ship to recalibrate the model using new SHM data. Moreover, it can be combined with the more general reliability study presented in the previous section to plan maintenance and inspection.

5.0 DATA PROCESSING AND DAMAGE DETECTION

The raw data processing and filtering technique that has been mentioned previously, is described in more detail in Okasha et al. (2011). In that paper, SHM data collected on the high speed naval craft HSV-2 during rough water trials (Brady 2004) has been used to assess the reliability of the ship structure and present a damage detection technique.

The results of the application on the HSV-2 reinforce the pre-existing belief that the probabilistic approach for analysis of structural safety is far superior to any deterministic approach. In fact, neglecting uncertainties could lead to inconsistent and misleading results.

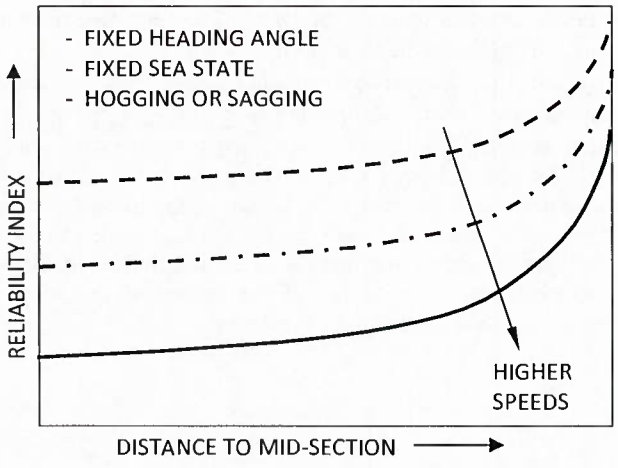

Fig. 7. Variation of reliability index with respect to the distance from mid-section of the ship at constant heading angle and sea state.

Sensitivity analyses to several operational condition parameters (e.g. sea state, ship speed, heading angle) have provided quantitative validations of what was qualitatively expected. Fig. 5 shows the variation of reliability index at a point with respect to ship speed at different sea states while the heading angle is kept constant. For instance, for a given sea state (i.e. 4) and a heading angle (i.e. 0°) the reliability is strongly affected by the ship speed, with the reliability index that drops from 9.2 for a speed of 15 knots to 8.4 for a speed of 30 knots. Fig. 6 illustrates the variation of reliability index at a point around mid-section with respect to heading angle, while the speed is kept constant. For heading angle equal to 90° (waves orthogonal to the ship) the ship operating speed does not affect the relative velocity of ship and waves. Therefore, in this case the reliabilities associated with different sea states are very close to each other. Fig. 7 represents the variation of reliability index with respect to the distance from mid-section of the ship while the heading angle and sea state are kept constant. It is verified, by means of a probabilistic approach, that mid-section is the most critical cross-section along the ship.

In addition, a damage detection technique based on a vector autoregressive model has been proposed. The same strain measurements have been used to assess the probability of having structural damage in the ship structures. Moreover, knowing the locations of the strain gauges, it is possible to locate the area of the ship that is most likely to be damaged. To this purpose, a damage sensitivity factor was introduced, that provides an easy to use and interpret metric to the analysts and the crew.

6.0 OPTIMIZATION OF INSPECTION AND MONITORING STRATEGIES

Kim & Frangopol (2011) provided an automated methodology for the assisted decision making process in

terms of inspection and monitoring. This module covers the last step of the framework in Fig. 1.

Kim & Frangopol (2011) proposed a multi-criteria optimization technique based on the concept of damage detection delay, which can be defined as the time-lapse from the damage occurrence to the time for the damage to be detected by inspection. The value of the time laps is a random variable affected by uncertainties associated with the damage occurrence and propagation and uncertainties associated with the quality of the inspection that may or may not detect an existing damage (see Fig. 8).

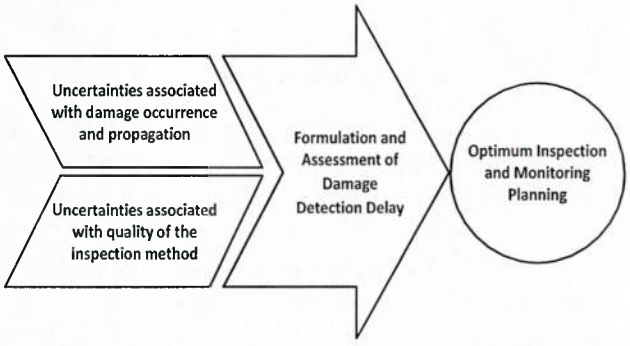

Fig. 8. Flowchart of the proposed approach for damage detection delay minimization.

A fully probabilistic methodology has been developed to address this issue. Uncertainties associated with damage occurrence and propagation are modelled using the classic fatigue crack growth approach, but with initial crack size, annual number of cycle, stress range, and material crack growth parameter described by probability distributions, rather than deterministic values.

Combining all the uncertainties with a comprehensive event tree Monte Carlo simulation, Kim & Frangopol (2011) assessed in a probabilistic sense, the damage detection delay associated with a given inspection strategy (i.e. schedule and type of inspections along the life-cycle of the ship). As expected, more frequent and accurate inspections provide lower damage detection delays. However, these inspections are also associated with higher costs. To assist the decision making process, a bi-objective optimization can be performed, aimed at minimizing the inspection cost and the expected damage detection delay. In this way, it is possible to determine the Pareto fronts of optimal schedules and accuracies for given numbers of inspections. Then, combining the front for several numbers of inspections, a general front of Pareto optimal inspection strategies is generated as shown in Fig. 9. Decision makers will select the strategy to be implemented based on the available budget and the desired level of expected damage detection delay.

Further studies are being performed to include also monitoring sessions in the framework proposed for inspection planning.

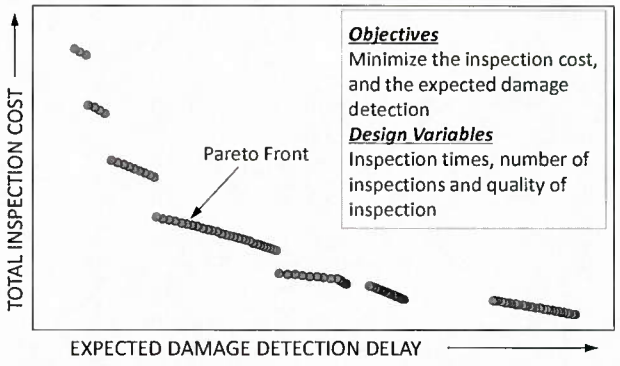

Fig. 9. General front of Pareto optimal inspection strategies.

7.0 CONCLUSIONS AND FUTURE WORK

Several modules belonging to an overall framework for the integrated life-cycle maintenance-monitoring-management of naval ship structures under uncertainty considering multiple and conflicting objectives have been presented. Even though each module can be considered as a separate methodology that can be employed as standalone technique, these modules have been developed to eventually converge into the described ILF. One of the most important future steps for the research along this line will be to make the integrated use of these modules automatic. In this way, a self-contained software package will be made available to analysts and crews for the assessment of the fleet condition and the optimal decision making.

Simultaneously, further enhancements of the individual modules are investigated. For instance, as previously mentioned, the technique for optimal inspection planning is being extended to account also for SHM sessions.

Finally, based on the results obtained, a tool for the near-real time reliability assessment of a ship based on the operating conditions can be developed. This tool will be able to collect monitoring data from strain sensors on the ship, combine these data with the information on the operating condition of the ship provided by the navigation system (e.g. speed) and constantly update the reliability assessment for the ship. Moreover, it will be able to alert the crew in near real-time whenever the reliability index associated with any operating condition down crosses an acceptable threshold. Therefore, the crew will be able to safely take the ship to a harbour using the operating conditions (e.g. speed and heading angle) that are still reliable and have the ship repaired.

REFERENCES

Brady, T.F. (2004). Global structural response measurement of SWIFT (HSV-2) from JLOTS and blue game rough water trials. West Bethesda, MD: NSWCCD-65-TR-2004/33, Naval Surface Warfare Center, Carderock Division.

Deb, K. (2001). Multi-objective optimization using evolutionary algorithms. John Wiley and Sons.

Decò, A., Frangopol, D.M. & Okasha, N.M. (2011). "Time-variant redundancy of ship structures." Journal of Ship Research, in press.

Devine, E.A. (2009). An overview of the recently-completed JHSS Monohull and Trimaran structural seaways loads test program. Naval Surface Warfare Center, Carderock Division (NSWCCD), PowerPoint Briefing, 30 October, 2009.

Goldberg, D.E. (1989). Genetic Algorithms in Search, Optimization, and Machine Learning. Addison-Wesley Professional.

IACS (2008). Common structural rules for double hull oil tankers, International Association of Classification Societies. Available at: http://www.iacs.org.uk (visited on March 14, 2011).

Kim, S. & Frangopol, D.M. (2011). "Optimum inspection planning for minimizing fatigue damage detection delay of ship hull structures." International Journal of Fatigue **33**(3), pp. 448-459.

Kwon, K., Frangopol, D.M. & Kim, S. (2011). "Fatigue performance assessment and service life prediction of high-speed ship structures based on probabilistic lifetime sea loads." Structure and Infrastructure Engineering, in press, doi: 10.1080/15732479.2010.524984.

Liu, P.L., Lin, H.Z. & Der Kiureghian A. (1983). CALREL User Manual. Department of Civil Engineering, University of California, Berkeley.

McKay, M.D., Beckman, R.J. & Conover, W.J. (1979). "A comparison of three methods for selecting values of input variables in the analysis of output from a computer code." Technometrics **21**(2), pp. 239–245.

Okasha, N.M. & Frangopol, D.M. (2010). "Efficient method based on optimization and simulation for the probabilistic strength computation of the ship hull." Journal of Ship Research **54**(4), pp. 244-256.

Okasha, N.M., Frangopol, D.M. & Decò, A. (2010). "Integration of structural health monitoring in life-cycle performance assessment of ship structures under uncertainty." Marine Structures, **23**(3), pp. 303-321.

Okasha, N.M., Frangopol, D.M., Saydam, D. & Salvino, L.W. (2011). "Reliability analysis and damage detection in high-speed naval craft based on structural health monitoring data." Structural Health Monitoring, in press, doi: 10.1177/145921710379516.

ACKNOWLEDGEMENTS

The support of the U.S. Office of Naval Research (contract number N-00014-08-0188, Structural Reliability Program, Director Dr. Paul E. Hess III, ONR, Code 331) is gratefully acknowledged.

The opinions and conclusions presented in this paper are those of the writers and do not necessarily reflect the views of the sponsoring organization.